ISSN 2007-2422

Tecnología y Ciencias del Agua

• Índice de revistas mexicanas de investigación científica y tecnológica del Consejo Nacional de Ciencia y Tecnología (Conacyt)

Incluida en Thomson Reuters Science Citation Index® (ISI) • Expanded Thomson Reuters Research Alert® (ISI) • EBSCO • ProQuest • Elsevier • Redalyc

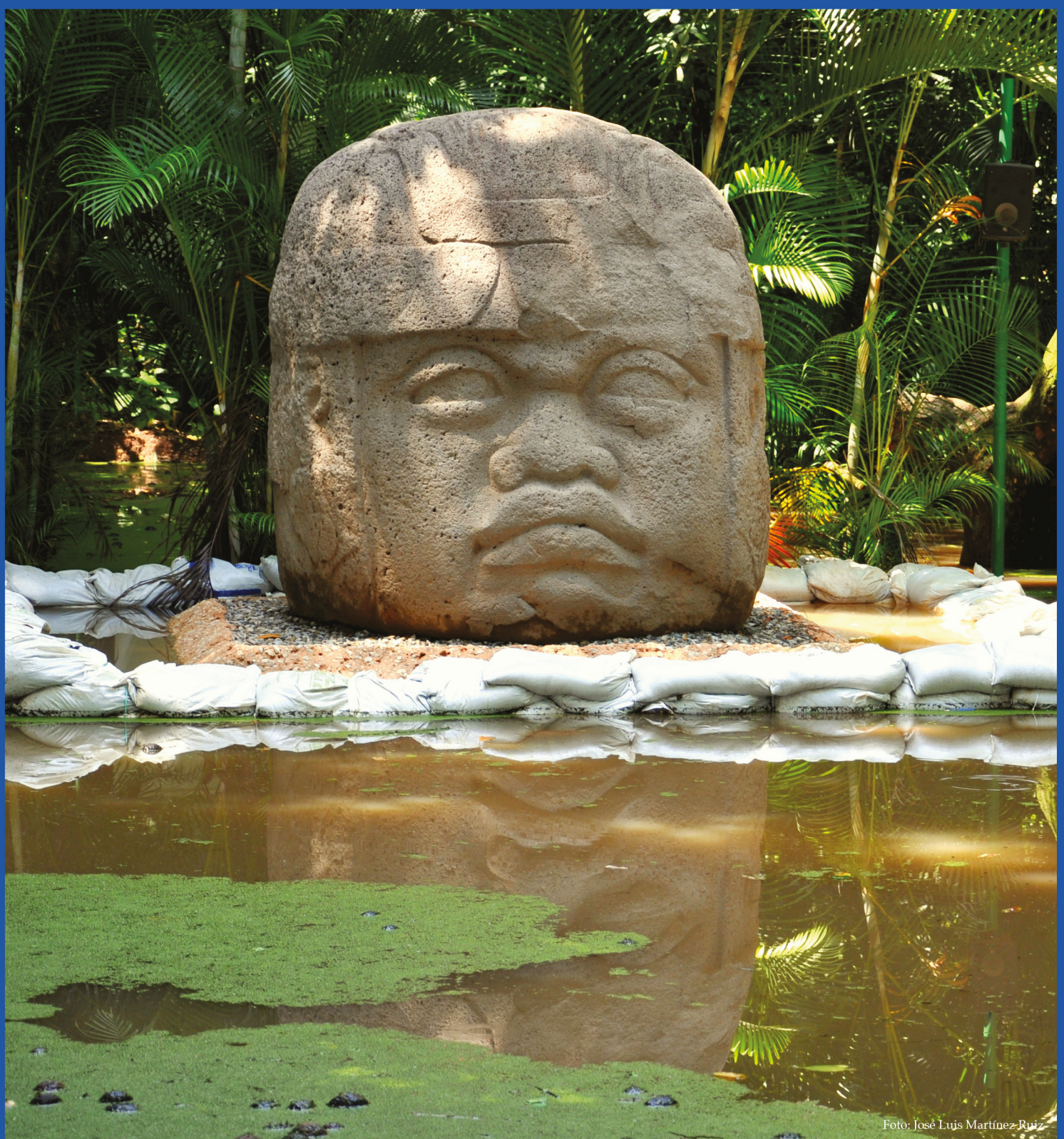

Foto: José Luis Martínez Ruiz

Vol. 10, núm. 4, julio-agosto de 2019

Tecnología y Ciencias del Agua

Consejo Editorial

Comité Editorial

© ***TECNOLOGÍA Y CIENCIAS DEL AGUA***, vol. 10, núm. 4, julio-agosto de 2019, es una publicación bimestral, editada y distribuida por el Instituto Mexicano de Tecnología del Agua, Paseo Cuauhnáhuac núm. 8532, Progreso, Jiutepec, Morelos, C.P. 62550, México, teléfono: +(52) (777) 3293670 o 3293600, extensiones 474 y 342, fax: + (52) (777) 3293670. Reserva de Derechos al Uso Exclusivo No. 04-2011-091215154300-102, ISSN, 2007-2422, ambos otorgados por el Instituto Nacional de Derechos de Autor. Número de Certificado de Licitud de Título y Contenido 16200.

Tecnología y ciencias del agua constituye la continuidad de las revistas *Irrigación en México* (1930-1946); *Ingeniería hidráulica en México* (1947-1971); *Recursos hidráulicos* (1972-1978); *Ingeniería hidráulica en México*, segunda época (1985-2009), y *Tecnología y Ciencias del Agua*, Antes *Ingeniería Hidráulica en México* (2010-2011).

Contenido

Artículos

Contents

Articles

Contenido

Artículos

Contents

Articles

DOI: 10.24850/j-tyca-2019-04-01

Special Article

Analysis of Rainfall Features and Calculation of Rainfall Pattern of Short Duration Rainstorm in Wuhan, China

Análisis de las características de precipitación y cálculo del modelo de precipitación de tormenta de corta duración en Wuhan, China

T. Peng[1]

J. Wang[2]*

Z. Huang[3]

[1]Hubei Key Laboratory for Heavy Rain Monitoring and Warning Research, Institute of Heavy Rain, Wuhan, China, email: 28834608@qq.com, ORCID 0000-0003-3014-1085

[2]Hubei Key Laboratory for Heavy Rain Monitoring and Warning Research, Institute of Heavy Rain, Wuhan, China, email: nanxingong@163.com, ORCID 0000-0002-2171-661X

[3]Hubei Key Laboratory for Heavy Rain Monitoring and Warning Research, Institute of Heavy Rain, Wuhan, China, email: hzyqxj@126.com, ORCID 0000-0003-4950-611X

*Corresponding author: Wang Jun-chao, email: nanxingong@163.com

Abstract

Based on data of daily rainfall in the 66 years from 1951 to 2016 and precipitation minute data of the heavy rainfall event (daily rainfall > 50 mm) in Wuhan, China, several methods such as linear tendency, cumulative distance, and statistical analysis were used to analyze the rainfall features and to calculate the Rainfall Pattern of Short Duration Storm. It is found that: 1) The average rainfall precipitation in Wuhan was 1260.9 mm from 1951 to 2016, the change trend of annual precipitation in the past 66 years existed two rises and falls. The obvious change happened in 1979. The rainfall mainly concentrated in between April and August, accounting for about 65.8%. 2) In Wuhan city 309 rainstorm days and 65 heavy rainstorm days happened in the past 66 years, each year 4.69 rainstorm days and 0.98 heavy rainstorm days happened, and

among average five rainstorm days 1 day was heavy rain. The most number of 12 rainstorm days happened in 1991. The trend of maximum daily rainfall firstly descended from 1951 to 1983, and then it increased up to 2016. 3) The daily rainstorm variation since 2000 shows that the average precipitation of 80 rainstorms was 83.28 mm, the max hour rainfall peak happened at 11:00 am BJT, the maximum average 3-hours rainfall occurred between 10:00 am and 12:00 pm BJT, and the max of average 6-hours rainfall occurred between 07:00 am and 12:00 pm BJT. 4) The coefficient of rainfall peaks for 1-hour rainfall, RP3-1, was about 0.439, and coefficient of rainfall peaks for 2-hour rainfall, RP3-2 was about 0.481.

Keywords: Wuhan City, Rainfall Features, Short Duration Storm, Rainfall Pattern, Coefficient of Rainfall Peaks.

Received: 18/12/2018

Accepted: 19/03/2019

Introduction

According to the latest National Bureau of statistics data, the rate of urbanization of China has reached 52.6% with the rapid development of China's Urbanization. Most of the population, wealth and infrastructure concentrate in large cities, and therefore, flood disaster losses in cities, caused by torrential rains, increase. The observation data of city flood show that its peak flow is several times or even ten times higher than the natural river basin flood in the same area. Floods constitute a serious threat to cities with a dense population, developed industry and commerce, and many buildings. At the same time, the continuous development of underground space tremendously changes the city environment and brings huge risks to the safety of flood control. In recent years, Beijing, Shanghai, Wuhan and other big cities have hit by rainstorms, causing great losses of people's lives and property (Wang, 2014).

Wuhan city has a special geographical position and obvious rainfall features. Four extraordinary floods occurred in Wuhan in 1931, 1954, 1998, and 2016. In particular, during the week of June 30th to July 6th, 2016, a continuous rainfall level exceeded the city's highest value since meteorological records began (up to 560.5 mm). This flood disaster in Wuhan led to the 740,000 acres of crops being damaged, 9758 houses collapsed or being damaged, and significant damage to the road

infrastructure. The direct economic cost of the flood was 4.8 billion RMB. In order to prevent the rainstorm, some researches on rainfall features and rule and rainfall pattern have made. Chen, Yang and Tu (1999) given the daily variation feature of the last 100 Rainstorm and large Rainstorm in Wuhan. Yang *et al.* (2001) analyzed the change trends of heavy rainfall events for last 40 years in the Chang Jiang valley. Liu, Chen, and Zhang (2007) analyzed the precipitation characteristics in Hubei Province and their influence on flood/drought. Zhang, Qin and Chen (2008) analyzed the change Characteristics of precipitation in the Latest 56 Years in Wuhan. Wang, Zhang and Wang (2010) analyzed characteristics of short-duration precipitation extremes of Badong and Yichang in the Yangtze Three Gorges Area. Fischer *et al.* (2012) give the probability distribution of precipitation extremes in the Zhujiang River Basin, South China. In order to update the knowledge on Wuhan city drainage system, this paper analyzed the in Wuhan and calculates the rainfall pattern of short-duration storms based on previous studies. It has important practical significance for city waterlogging prevention, rational use of rainwater resources and the construction of sponge city.

Materials and Methods

Rainfall Data

With the improvement of modern meteorological service system, 50 automatic rain-gauges there installed in Wuhan. According to the requirements of the study and the history of rainfall rain-gauge, we selected the rain-gauge located in the East and West Lake District of Wuhan for analysis. The data were collected from a total of 66 years in Wuhan during 1951-2016. The precipitation level is divided into 10.0 mm from now on referred to as light rain, 10.0-24.9 mm for moderate rain, 25.0-49.9 mm for heavy rain, greater than or equal to 50.0 mm is called a rainstorm, and greater than or equal to 100.0 mm heavy rainstorm. Based on the selected in 1980-1999 single day rainfall greater than 100 mm and the daily precipitation more than 50 mm in 2000-2016, we performed Rainfall Calculation analysis of 80 rainstorms and short duration heavy rainfalls.

Analysis Method

Calculation Method for Frequency of Annual Rainfalls. The rainfall data over the years, a total of N, in the order from large to small, got the rank number of each rainfall (i), and then the frequency of annual rainfalls (F) can be obtained by equation (1).

$$F_i = i/(N+1) \times 100\% \quad (1)$$

Linear Trend Method. Linear trend calculation values of meteorological elements with the correlation coefficient r between the time sequence and the natural number sequence B, and the meteorological elements (called trend coefficient) X_i, sample n climate variables, denoted by t_i corresponding to the time, reveal a linear regression of X_i over t_i, that is:

$$X_i = a + b\ x\ t_i \quad (2)$$

i = 1, 2, 3, 4…n

Cumulative Anomaly Method. During the study, the cumulative precipitation method (equation 3) was used to analyze the change trend of annual precipitation in Wuhan (Zhang *et al.*, 2008):

$$CA_j = \sum_{i-1}^{j}(xi - \overline{x}) \quad (3)$$

（j ≤ n, n is the Sequence length）

Where CA_j varies from the cumulative first year to j years of an anomaly, the average value for the entire sequence, positive and negative values of CA_j are possible. In this article, we extract only 1-3 extreme points of each sequence, namely extracting only the strongest signal, and continue for 4 years after the extraction.

Calculation Method of the Rainfall Pattern of a Short Duration Rainstorm. Keifer and Chu (1957) given the synthetic storm pattern for

drainage design. Wang, Zhao and Gong (2015) performed the classification of short-duration rainfall pattern of Beijing with fuzzy identification method and statistical analysis method based on 1-minute interval rain record. Bi, Chen and Yao (2015) analyzed Urban Rainstorm Pattern of Xi'an and calculated the position coefficients of rainfall peaks of 24-h rain. Tang *et al.* (2018) analyzed the spatial and temporal variations of short-duration heavy precipitation through the rain data in Jiangxi during 1961-2015. Here, with the position coefficients of rainfall peaks can calculate the rainfall pattern of short duration rainstorm based on 3-h Rainstorm data. Firstly, the strongest 3-h rainfall must be found out from the rainstorms, and the maximum 1-h and 2-h rainfalls must be found out also from the strongest 3-h rainfall; and then the position coefficients of 1-h and 2-h rainfall peaks will be determined. Finally, the Rainfall Pattern of 3-h Rainstorm will be obtained.

Rainfall Feature Analysis

Annual Rainfall Feature

Frequency Analysis of Annual Rainfalls. According to the observation data in Wuhan Rain-gauge from 1951 to 2016, we found that the average rainfall was 1260.9 mm, the maximum rainfall was 2056.9 mm in 1954, the minimum was 726.7mm in 1966. Frequency analysis of annual rainfalls is adopted in Zhejiang Province (Liu *et al.*, 2009), in Beijing Area (Li *et al.*, 2011), in Hunan Province (Kuang *et al.*, 2013), in main river basin in China (Wang, Wang and Zhang, 2018). Based on other studies, if the frequency of rainfalls is less than or equal to 25 percent, the year can be defined as a wet year. If the rainfall frequency is greater than 25 percent and is less than 75 percent, such a year can be defined as a normal water year. If the rainfall frequency is greater than or equal to 75 percent, the rainfall year can be defined as a dry year. From Table 1, it is found that there were 16 wet years with the average rainfall of 1671.5 mm, there were 34 normal water years with the average rainfall of 1217.7 mm, and there were 16 dry years with the average rainfall of 942.1 mm (Table 1 and Figure 1).

Table 1. The Calculation results of Annual Rainfall frequency in Wuhan from 1952 to 2016.

No	Year	R (mm)	F (%)	No	Year	R (mm)	F (%)	No	Year	R (mm)	F (%)
1	1954	2056.9	1.49	23	2010	1337.9	34.33	45	2013	1079.8	67.16
2	1983	1894.9	2.99	24	1988	1332.3	35.82	46	1972	1075.2	68.66
3	2016	1834.8	4.48	25	1975	1320.2	37.31	47	1961	1061.1	70.15
4	1991	1795.2	5.97	26	1996	1319.5	38.81	48	1952	1052.8	71.64
5	1969	1744.2	7.46	27	1951	1303.3	40.30	49	1986	1050	73.13
6	1998	1729.2	8.96	28	1995	1296.3	41.79	50	2006	1047.1	74.63
7	1989	1654.9	10.45	29	2008	1266.8	43.28	51	1994	1045.5	76.12
8	1962	1645.3	11.94	30	1970	1235.7	44.78	52	1960	1041.9	77.61
9	1982	1632.4	13.43	31	1973	1229.5	46.27	53	1985	1029.7	79.10
10	1980	1623.6	14.93	32	1955	1220.8	47.76	54	2007	1023.2	80.60
11	1993	1584.6	16.42	33	2014	1215.7	49.25	55	1979	1001.9	82.09
12	1959	1575.8	17.91	34	1984	1209	50.75	56	1956	992.9	83.58
13	2004	1572.2	19.40	35	1977	1195	52.24	57	1968	990.6	85.07
14	2002	1516.1	20.90	36	2000	1179.8	53.73	58	2011	987.2	86.57
15	1987	1449.4	22.39	37	1967	1179.2	55.22	59	1974	965.5	88.06
16	1958	1434.5	23.88	38	2009	1158	56.72	60	1997	946.6	89.55
17	2015	1432.8	25.37	39	1981	1154	58.21	61	1965	920.2	91.04
18	2012	1400.1	26.87	40	1953	1132.7	59.70	62	2001	899.8	92.54
19	2003	1386.1	28.36	41	1963	1125.6	61.19	63	1976	890.7	94.03
20	1999	1380.6	29.85	42	2005	1116.6	62.69	64	1978	811.7	95.52
21	1990	1355	31.34	43	1992	1116.4	64.18	65	1971	800.2	97.01
22	1957	1344.8	32.84	44	1964	1091.9	65.67	66	1966	726.7	98.51

Notes: R is the annual rainfall precipitation value; F - Frequency of annual rainfalls.

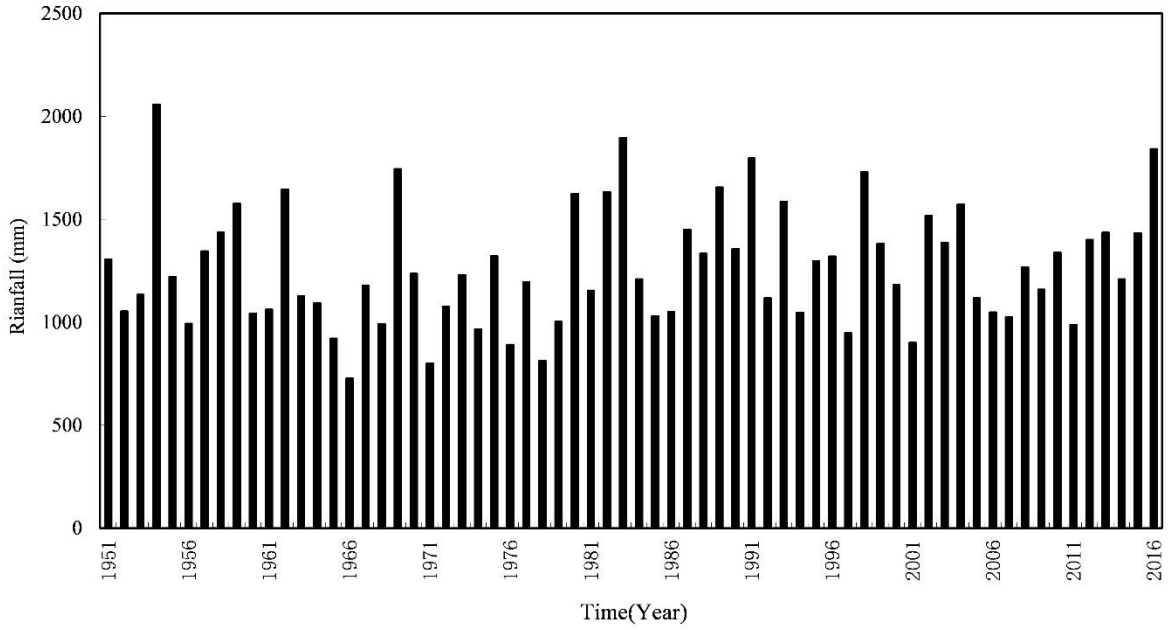

Figure 1. The Annual Rainfall Distribution in Wuhan from 1951 to 2016.

Trend Analysis of Annual Rainfalls. During the studies, the accumulation anomaly method was used to analyze the change trend of annual rainfalls in Wuhan. From Figure 2, one can see that the change trend of annual precipitation in Wuhan in the past 66 years displays two rises and falls overall. Namely, the annual rainfall possessed the rising trend from 1951 to 1960's beginning, when reached the maximum value. Then the annual rainfall precipitation began to reduce gradually to the lowest value from 1960's to 1970's. At the beginning of 1980's, the annual rainfall began to rise from 1980's to 2004. Then the annual rainfall began to fell again until 2011 and rose from 2012. It is evident from Figure 2 that an obvious change happened in 1979.

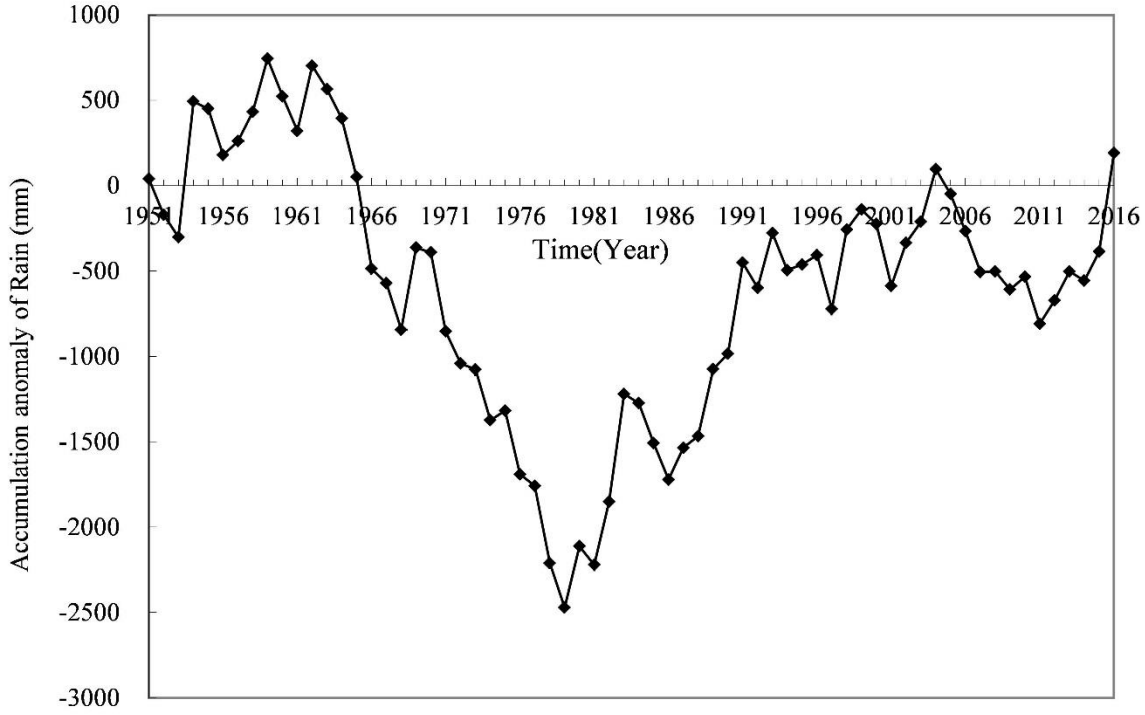

Figure 2. The Accumulation anomaly of Annual Rainfall Distribution in Wuhan from 1951 to 2016.

Monthly Rainfall Feature

Based on the statistics and analysis of rainfall data from 1951 to 2016 in Wuhan rain-gauge, the average, maximum and minimum rainfall precipitation of every month from 1951 to 2016 are given in Table 2. It was found that the rainfalls concentrated mainly in between April and August, accounting for about 65.8%. The mean monthly maximum rainfall occurred in June (217.9 mm), followed by July (189.7 mm), May (164.2 mm), April (135.9 mm), and August (118.9mm); the maximum monthly rainfall of 758.4 mm happened in July 1998 (See Table 2 and Figure 3).

Table 2. The statistics results of the Monthly Rainfall Feature in Wuhan from 1952 to 2016.

	Month	Jan	Feb	Mar	Apr	May	June	July	Aug	Sept	Oct	Nov	Dec

Rainfall (mm）	Ave	39.8	61.3	94.2	135.0	159.3	218.8	200.1	119.6	77.2	74.3	56.2	29.2
	Max	107.7	183.1	225	333.6	354.9	522.8	758.4	482.5	219.4	409.2	166.8	107.3
	Year	2000	1990	1992	2002	1954	1959	1998	1969	1973	1983	1967	1968
	Min	0	1.8	16.6	22.9	36.2	13.1	28.9	0.3	1	0	0.2	0
	Year	1963	1968	1962	2000	1981	1963	1978	1966	2001	1979	1995	1999

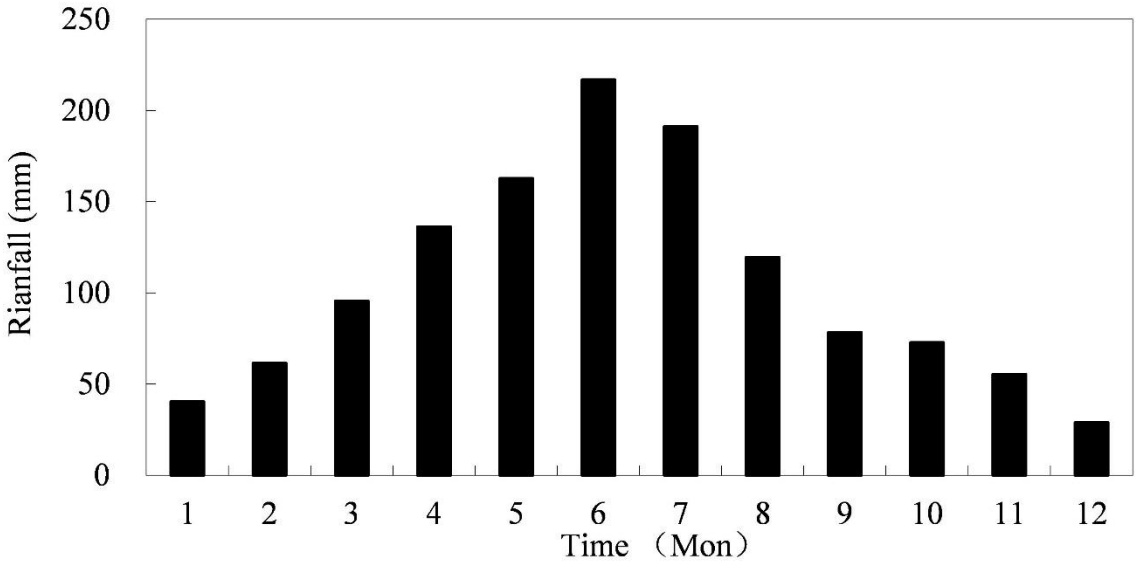

Figure 3. The Distribution Feature of Average Monthly Rainfall in Wuhan from 1951 to 2016.

Distribution and Trend analysis of Rainstorms

Based on the rainfall data in Wuhan from 1951 to 2016, the days of a rainstorm and heavy rainstorm are calculated and the results are shown in Figure 4 and Tables 3 and 4. It is found that in Wuhan city 309 rainstorm days happened in the past 66 years. The most rainstorm days happened in 1991, there were 12 days, followed by 1954 (11 days), and 2004 (10 days) (Figure 4). Among 309 rainstorm days, rainfalls between 50 mm and 100 mm appeared 244 days, accounted for 78.97%; rainfalls between 100 mm and 200 mm appeared 58 days, accounting for 18.77%; rainfalls between 200 mm and 300 mm happened 6 times, accounted for 1.94%, and the rainfall greater than 300 mm appeared 1 time only (see Table 3).

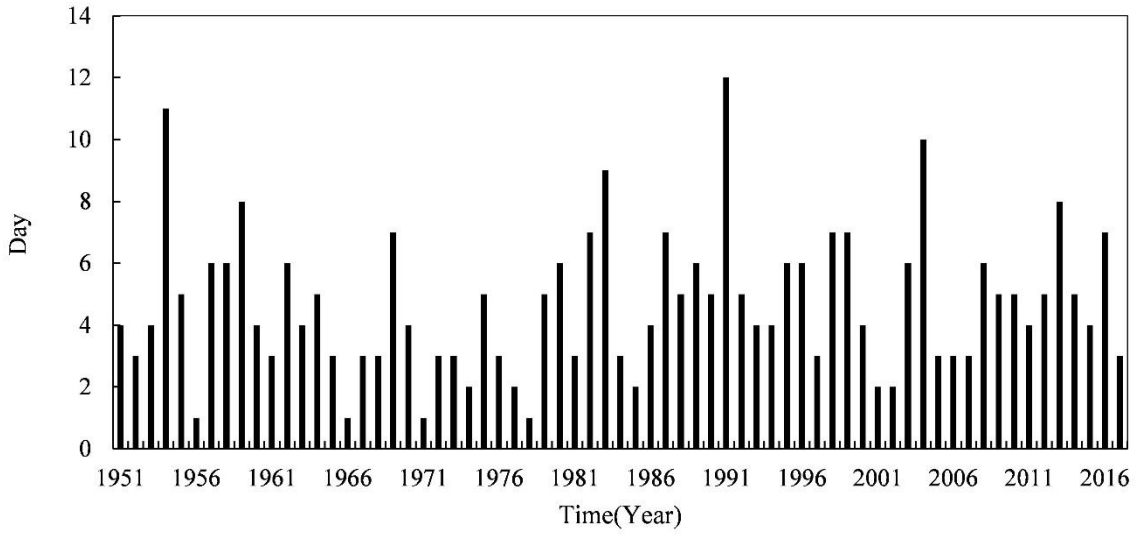

Figure 4. The rainstorm Days in each year from 1951 to 2016.

In Wuhan city, heavy rainstorms happened 65 days in the past 66 years. On average, each year happened 4.69 rainstorm days and 0.98 heavy rainstorm days. Namely, among five rainstorm days, one was a heavy rainstorm. Rainstorms and heavy rainstorms in Wuhan mostly happen in summer, followed by spring, autumn and winter. Among them, rainstorms in summer accounted for 65.05%; heavy rainstorms also concentrated mainly in summer, it accounted for 81.54%. Winter rainstorms in Wuhan only happened 3 days in the past 66 years, less than 1% of the total year (see Table 4).

Table 3. Distribution Feature of different grade rainstorms in Wuhan.

Rainfall range (mm)	50~100	100~200	200~ 300	>300	Total
Number of days	244	58	6	1	309
Percentage (%)	78.97	18.77	1.94	0.32	100

Table 4. Distribution Feature of rainstorm days and large rainstorm days in Wuhan.

Season	Spring	Summer	Autumn	Winter	Total
A	70	201	35	3	309
a	1.06	3.05	0.53	0.045	4.667
Pa(%)	22.73	65.05	11.36	0.97	100
B	9	53	3	0	65

b	0.14	0.80	0.045	0	0.985
P_b(%)	13.85	81.54	4.61	0	100

A, B are the numbers of rainstorms and heavy rainstorm days; a and b are the average of A and B in 66 years.

Pa and Pb are the percentages of A and B.

Based on maximum daily rainfall data in one year from 1951 to 2016, we found that the trend of maximum daily rainfall was similar to that of annual rainfalls: the maximum daily rainfall firstly descended from 1951 to 1983, then it rose up from 1984 to 2016 (Figure 5).

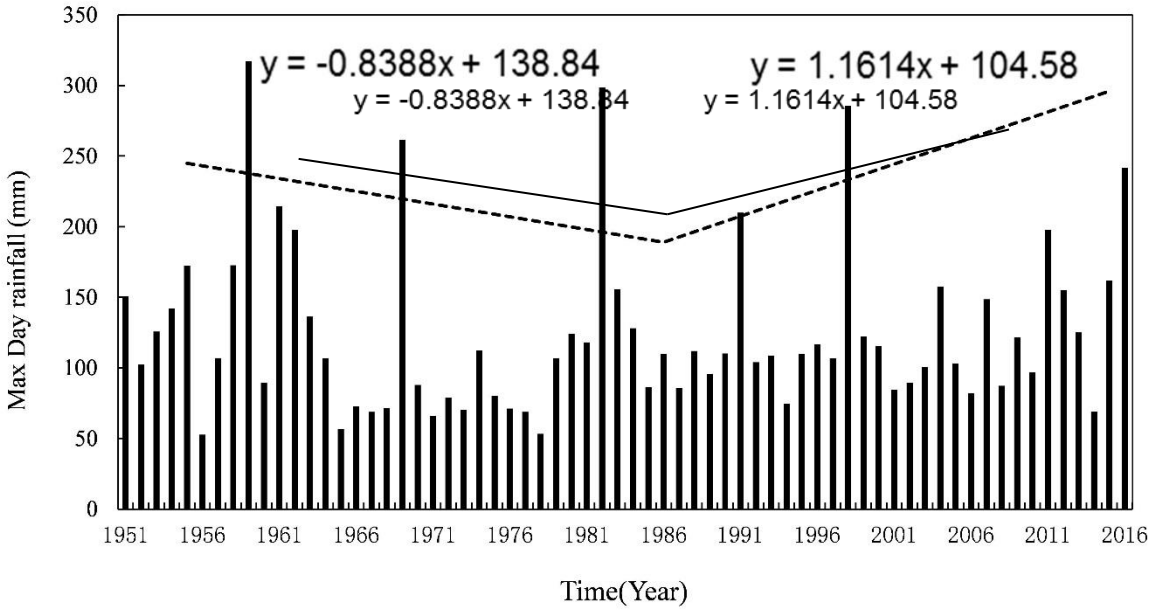

Figure 5. Maximum daily rainfall from 1951 to 2016 (y-axis is maximum daily rainfall; x-axis is the time in years).

Daily Variation of Rainstorms Since 2000

Within this study, we have analyzed 80 rainstorms since 2000, and selected daily rainfalls exceeding 50 mm, to analyze the feature of strong rainfall in a short duration. Among them, 18 daily rainstorms precipitation exceeded 100 mm. The maximum daily rainfall of 245.1 mm happened on July 6, 2016. The statistical results of the rainstorm daily variation since

2000 are presented in Table 5 and Figure 6. According to Table 5, the average precipitation of 80 rainstorms was 83.28 mm, the maximum 1-h rainfall precipitation of 86.1 mm occurred at 09 am on 19, June 2016. The maximum average 1-h rainfall was 5.74mm at 11:00 am BJT, the maximum average 3-hours rainfall was 15.93 mm in between 10:00 am and 12:00 pm BJT, and the maximum average 6-h rainfall of 29.01 mm occurred between 07:00 am and 12:00 pm BJT.

From Figure 7, we can see two peaks in the rainstorm daily variation feature since 2000, the maximum peak happened at 11:00 am BJT, another one happened at 04:00 am BJT This result differs from the study (Zhang Yin-lin et al,2008), in which the maximum peak was revealed at 05:00 am BJT, and the next one at 10:00 am BJT. The reason for such a deviation may be that the annual rainfall has increased since 2012.

Table 5. The statistical results of rainstorm daily variation from 2000 to 2016 (unit: mm).

Time	Ave1	Max1	Ave3	Ave6	Time	Ave1	Max1	Ave3	Ave6
21:00	3.18	35.60	7.71	17.01	09:00	4.85	33.85	15.90	28.34
22:00	2.76	40.90	7.86	18.17	10:00	5.31	42.10	15.93	27.04
23:00	1.76	19.60	8.31	20.01	11:00	5.74	86.10	14.71	24.60
00:00	3.33	32.00	9.30	22.16	12:00	4.88	49.10	12.44	20.82
01:00	3.22	50.00	10.32	23.18	13:00	4.09	34.70	11.12	17.58
02:00	2.75	29.60	11.70	24.29	14:00	3.47	31.70	9.90	14.44
03:00	4.35	34.58	12.85	25.44	15:00	3.56	33.68	8.38	12.49
04:00	4.60	40.10	12.86	25.95	16:00	2.87	41.40	6.47	
05:00	3.91	30.30	12.59	26.65	17:00	1.96	34.20	4.54	
06:00	4.35	31.65	12.59	28.49	18:00	1.64	36.30	4.11	
07:00	4.33	28.00	13.08	29.01	19:00	0.94	15.59		
08:00	3.91	25.90	14.06	28.77	20:00	1.53	29.15		
Total	83.28	Max of Ave1	5.74	Max of Ave3	15.93	Max of Ave6	29.01	Max of Max1	86.1

Notes: Ave1, Ave3, Ave6 are the average of 1-h rainfalls, 3-h rainfalls, and 6-h rainfalls for 80 rainstorms.

Max1 is the maximum rainfall precipitation averaged for 80 rainstorms.

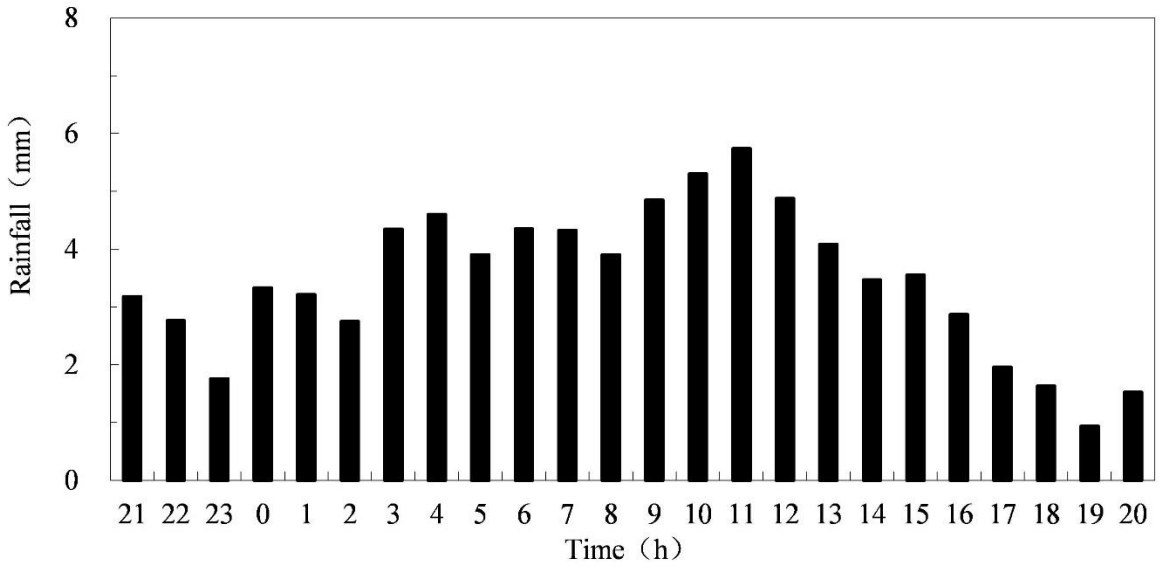

Figure 6. The rainstorm daily variation feature from 2000 to 2016.

Rainfall Pattern of Short Duration Rainstorm

The Rainfall Pattern (RP) of Short Duration Rainstorm is key knowledge for drainage planning in Wuhan city. Based on the drainage and waterlogging planning of downtown in Wuhan city, the rainfall patterns of short duration rainstorms were divided into the following four categories with the different position coefficients of rainfall peaks: RP1: 0< RP <=0.33; RP2: 0.33< RP <=0.5; RP3: 0.5< RP <=0.67; RP4: 0.67< RP <=1.

For this estimation, we selected the strongest 3-h rainfall out of the above-mentioned 80 rainstorms, and then the maximum 1-h and 2-h rainfalls were found within 3-h rainfalls. Thus, the position coefficients of rainfall peaks for 1-h and 2-h rainfalls were obtained as presented in Tables 6-7, and Figures 7- 8.

The position of 1-h rainfalls peaks (RP3-1) coefficients shows that among 80 rainstorms, RP1 appeared 35 times, accounted for 43.75%, RP2 appeared 15 times, accounted for 18.75%, RP3 appeared 14 times, accounted for 17.50%, RP4 appeared 16 times, accounted for 20.00%, and the average for RP3-1 of 80 rainstorms is 0.439 (Table 6, Figure 7).

The coefficients of rainfall peaks for 2-h rainfalls (RP3-2) show that among 80 rainstorms, RP1 appeared 20 times, accounted for 25%, RP2 appeared 29 times, accounted for 36.25%, RP3 appeared 31 times, accounted for

38.75%, RP4 not appeared, the average for RP3-2 of 80 rainstorms is 0.481 (Table 7, Figure 8).

Table 6. The results for Rainfall Pattern of RP3-1.

Rainfall Pattern	category	RP1	RP2	RP3	RP4	Total
	average	0.439				
Number		35	15	14	16	80
Percentage（%）		43.75	18.75	17.50	20.00	100

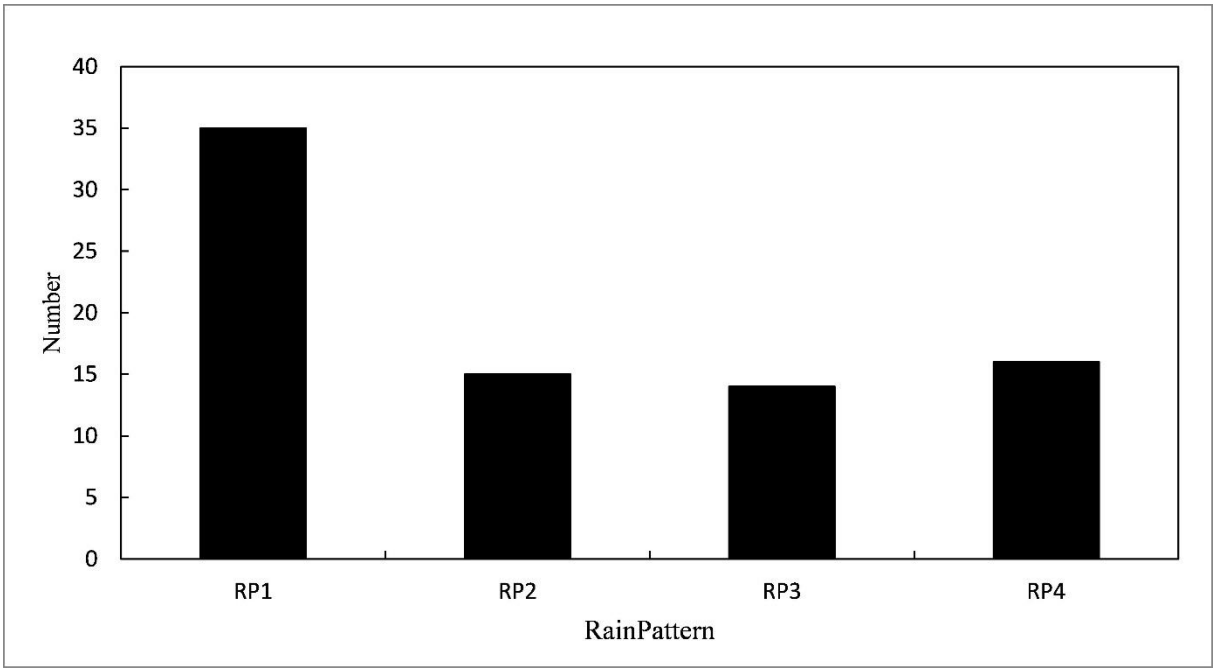

Figure 7. Coefficients of 1-h rainfalls peaks (RP3-1).

Table 7. The results for Rainfall Pattern of RP3-2.

Rainfall Pattern	Category	RP1	RP2	RP3	RP4	Total
	average	0.481				
Number		20	29	31	0	80
Percentage（%）		25	36.25	38.75	0	100

Tecnología y ciencias del agua, 10 (4), 1-17. DOI: 10.24850/j-tyca-2019-04-01

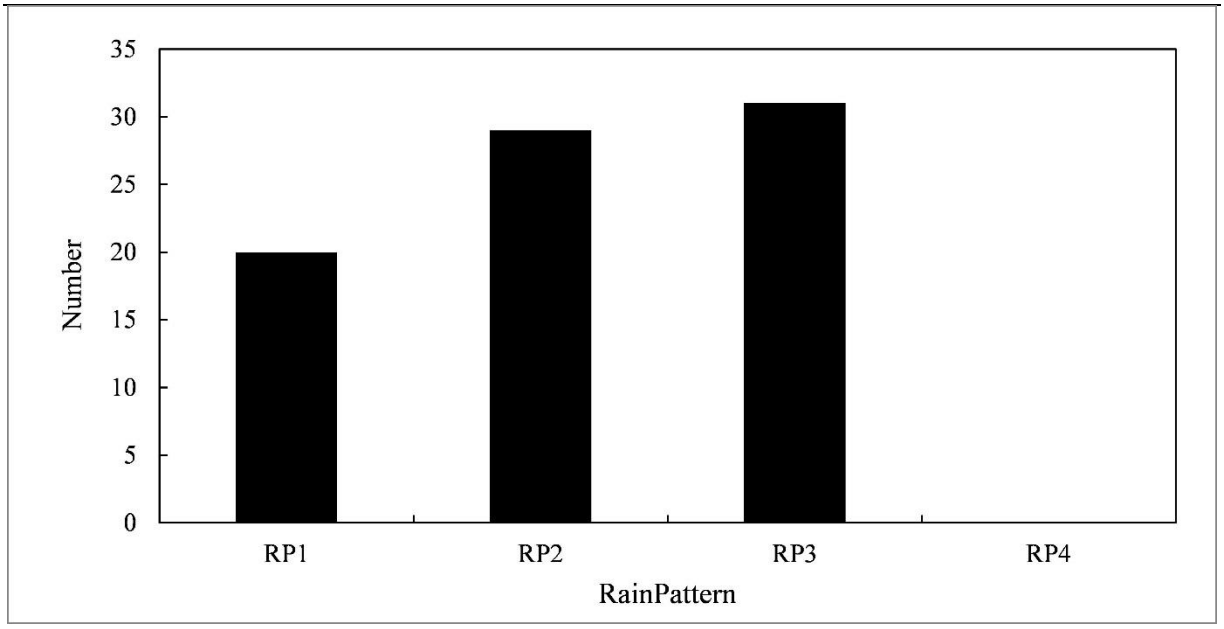

Figure 8. Coefficients of 2-h rainfalls peaks (RP3-2).

Conclusion

Studies of rainfall features and short duration rainfall patterns are of vital importance for many large cities in China to develop their drainage and waterlogging systems. We analyzed data of daily rainfall in 66 years from 1951 to 2016 and performed statistical calculations for precipitation data of 80 heavy rainfalls (daily rainfall >50 mm) from 2000 to 2016 in Wuhan city. Annual and monthly rainfall feature, distribution and trend analysis of rainstorms, daily variation of rainstorms since 2000 as well as short duration rainstorm patterns have been obtained. The conclusions are the following:

1) The average rainfall precipitation was 1260.9 mm from 1951 to 2016; the change trend of annual precipitation in Wuhan in the past 66 years displays two rises and falls. Namely, the annual rainfall had a rising trend from 1951 to at the beginning of 1960's and reached the maximum value. Then the annual rainfall precipitation began to reduce gradually from 1960's to 1970's. At the beginning of 1980's, the annual rainfall precipitation rose again from 1980's to 2004. After that, the annual rainfall decreased until 2011, and finally, it rises since 2012. The critical change in the trend happened in 1979.

2) Rainfalls concentrated mainly in between April and August, accounting for about 65.8%. The mean monthly maximum rainfall occurred in June

(217.9 mm), followed by July (189.7 mm), May (164.2 mm), April (135.9 mm), and August (118.9 mm).

3）In Wuhan city 309 rainstorm days and 65 large rainstorm days happened in the past 66 years; each year happened 4.69 rainstorm days and 0.98 large rainstorm days. The most number of 12 rainstorm days happened in 1991. The trend of maximum daily rainfall was similar to that of annual rainfalls, the maximum daily rainfalls firstly descended from 1951 to 1983, then increased up to 2016.

4) The daily rainstorm variation since 2000 shows that the average of 80 rainstorms was 83.28 mm, the maximum hour rainfall peak happened at 11:00 am BJT, the maximum average 2-h rainfall occurred between 10:00 am and 12:00 am BJT, and the maximum average 6-h rainfall took place between 07:00 am and 12:00 am BJT.

5) The coefficient of rainfall peaks for 1-hour rainfall, RP3-1, was about 0.439, and the coefficient of rainfall peaks for - hour rainfall, RP3-2, was about 0.481.

Acknowledgments

The study was supported by the National Natural Science Foundation of China (51379149) and the Research and Operation Project of the Institute of Heavy Rain, CMA, Wuhan (JK201704, JK201707) and the Research Project of Wuhan Planning Research Institute(ZD17-B-002).

References

Bi, X., Chen, L. Y. & Yao, D. S. (2015). Analysis on Urban Rainstorm Pattern of Xi'an. *Journal of Anhui Agri-Sci*, 43(35): 295-297, 325.

Chen, Z. H., Yang, H. Q. & Tu, S. Y. (1999). Daily variation Feature of last 100 Rainstorm and large Rainstorm in Wuhan and Yichang. *Torrential Rain and Disasters*, 18(3):11-14.

Keifer, C. J. & Chu, H. H. (1957). Synthetic storm pattern for drainage design. *Journal of Hydraulics Division ASCE*, 83(HY4): 1-25.

Liu, K. Q., Chen, Z. H. & Zhang, L. P. (2007). Analysis of Precipitation Characteristics in Hubei Province and Their Influence on Flood/Drought in the Last 45 Years. *Meteorological Monthly*, 33(11):58-64.

Liu, D. D., Li, M., Lou, Z. H. & Chen, X. H. (2009). Analysis of Rainfall Characteristics in Zhejiang Province in Recent 50 Years. *Journal of Natural Resources*, 24(11): 1973-1983.

Li, M., Xia, J., Chen, S. M. & Meng, D. J. (2011). Wavelet Analysis on Annual Precipitation around 300 Years in Beijing Area. *Journal of Natural Resources*, 26(6): 1001-1011.

Fischer, T., Su, B. D., Luo, Y. & Scholten, T. (2012). Probability distribution of precipitation extremes for weather index-based insurance in the Zhujiang River Basin, South China. *Journal of Hydrometeorology*, 13(3): 1023-1037.

Tang, C., Xu, A., Ma, F. & Dai, Z. (2018). Spatial and temporal variations of short-duration heavy precipitation in Jiangxi during 1961-2015. *Torrential Rain and Disasters*, 2018, 37(5): 421-427.

Wang, B. Y., Zhao, L. N. & Gong, Y. F. (2015). Characteristics of temporal pattern and return period of short-duration rainfall at Beijing Observatory. *Torrential Rain and Disasters*, 34(4): 302-308.

Wang, H. J., Zhang, J. & Wang, H. J. (2010). The Characteristics of Short-duration Precipitation Extremes of Badong and Yichang in the Yangtze Three Gorges Area. *Torrential Rain and Disasters*, 29(1): 38-43.

Wang, L. P., Wang, W. G. & Zhang, J. Z. (2018). Analysis on spatial and temporal distribution characteristics of precipitation processes over main river basin in China. *Journal of Natural Disasters*, (2): 161-173.

Wang, Q. (2014). Analysis for Causes and Countermeasures of urban rainstorm waterlogging in Beijing. *Water & Wastewater Engineering*. (s1): 127-130.

Kuang, M. J., Xie, H. X., Sui, B., Wang, C. H., Song, D. S. & Li, D. (2013). Analysis on Spatiotemporal Characteristics of Precipitation in Hunan Province from 1961 to 2010. *Research of Soil and Water Conservation*, 20(5): 145-149.

Yang, H. Q., Chen, Z. H., Shi, Y. & Ren, G. Y. (2001). Change Trends of Heavy Rainfall Events for last 40 years in the Chang Jiang valley. *Meteorological Monthly*, 31(3): 66-68.

Zhang, Y. L., Qin, J. & Chen, Z. H. (2008). Analysis on the Change Characteristics of Precipitation in the Latest 56 Years in Wuhan. *Torrential Rain and Disasters*, 27(3): 63-67.

DOI: 10.24850/j-tyca-2019-04-02

Special Article

Temporal and Spatial Signatures of Sediment Transport at the Watershed Scale: An Approach to Understand the Behavior of the Watershed

Huellas temporales y espaciales del transporte de sedimentos en la escala de la cuenca hidrográfica: una aproximación para entender el comportamiento de la cuenca hidrográfica

D. Liu[1]

F. Tian[2]*

H. Li[3]

H. Lu[4]

M. Lin[5]

M. Sivapalan[6]

[1]State Key Laboratory of Eco-hydraulics in Northwest Arid Region of China, Xi'an University of Technology, China

Department of Land Resources and Environmental Sciences, Montana State University, United States of America, email: ldfchn@126.com, ORCID 0000-0003-3831-3865

[2]State Key Laboratory of Hydroscience and Engineering, Department of Hydraulic Engineering, Tsinghua University, China, email: tianfq@tsinghua.edu.cn, ORCID 0000-0001-9414-7019

[3]Department of Land Resources and Environmental Sciences, Montana State University, United States of America, email: hongyili.jadison@gmail.com, ORCID 0000-0002-9807-3851

[4]Ministry of Education Key Laboratory for Earth System Modeling, Department of Earth System Science, Tsinghua University, China

The Joint Center for Global Change Studies, Beijing, China, email: luhui@tsinghua.edu.cn, ORCID 0000-0003-1640-239X

[5]School of Statistics and Mathematics, Central University of Finance and Economics, Beijing, China, email: mlin@cufe.edu.cn, ORCID 0000-0002-2791-5476

[6]Department of Geography, University of Illinois, USA

Department of Civil and Environmental Engineering, University of Illinois, United States of America, email: sivapala@illinois.edu, ORCID 0000-0003-3004-3530

*Corresponding author: Fuqiang Tian, email: tianfq@tsinghua.edu.cn

Abstract

Sediment yield is affected by many factors, such as climate, geology, geomorphology, land use and human activities. Sediment signatures are the statistic indices or curves that are able to effectively describe the temporal and spatial characteristics of sediment transport and evaluate the ability of the streamflow to deliver the sediment. In this study, the sediment signatures of Upper Sangamon River Basin, which is an intensively managed watershed for agriculture development, are analyzed. Firstly, a semi-distributed model of sediment transport is built up based on the Tsinghua Representative Elementary Watershed (THREW) model, and it is applied to the Upper Sangamon River Basin. The result of sediment simulation is analyzed by four sediment signatures, i.e. specific sediment yield, sediment delivery ratio, cumulative sediment curve and effective discharge. The sediment signatures are consistent with each other and accord with the fact of the agricultural production in Upper Sangamon River Basin.

Keywords: Sediment, soil erosion, effective discharge, sediment delivery ratio, hydrological model.

Received: 18/12/2018

Accepted: 20/03/2019

Introduction

Sediment transport is a key issue in the river basin management all over the world and the research of sediment transport is essential for better management practices including the land use management, river restoration, pollution control, water supply and so on. The relations of the magnitude and the frequency of sediment transport were discussed by Wolman and Miller (1960) and the important concept of effective discharge was introduced. Walling (1983) reviewed the limitation of the sediment delivery ratio concept and considered the problems of

temporal and spatial lumping and its black nature. Many research has been done to analyze effective discharge (Crowder and Knapp, 2002), magnitude-frequency of bed load transport (Torizzo *et al.*, 2004), sediment delivery ratio (Lu *et al.*, 2005, Parsons *et al.*, 2006), sediment yield (Hassan *et al.*, 2008) and other indices or relations. Meanwhile, many sediment simulation models were proposed based on different methods (Arnold *et al*., 1990, Viney *et al*., 1999, Singh *et al*., 2008). However, the temporal and spatial characteristic of sediment transport within the river basin is still a complex issue and the knowledge of the associated processes of sediment transport still represents an important research need (Walling, 1983).

Over the last few decades, global climate change has been reported by many researchers and regional climate change is also an important topic because regional climate change has a more direct effect on the regional water resources, agriculture, forest and others (Dvorak *et al.*, 1997, Christensen *et al.*, 2004). In order to deal with the effect of the climate change on the watershed management, especially on the land use and management, some indices or signatures are needed to estimate the soil erosion on the hillslope and sediment delivery in the stream network quantitively.

The Upper Sangamon River Basin (USRB) in the center of Illinois State of USA is intensively managed, following conversion to intensive agricultural production during the late 19th Century through the formation of drainage districts, excavation of drainage ditches and installation of subsurface drainage tiles and is dominant by agricultural production nowadays. The suspended sediment data in USRB were gauged by the US Geological Survey and Illinois State Water Survey separately. As one of the streams in Illinois State, the effective discharges in USRB have been estimated with available data (Crowder and Knapp, 2002) and further analysis is required. In this paper, a semi-distributed model of sediment transport is built up based on a hydrological model, Tsinghua Representative Elementary Watershed (THREW) model, and then the model is applied to Upper Sangamon River Basin. The effects of crop transpiration and tile drainage are involved in the model. The modeling of evapotranspiration is improved by introducing the Leaf Area Index (LAI) and the tile drainage as an important type of interflow is introduced into the model. The result of sediment simulation is analyzed by the sediment signatures due to the poor observed sediment data. The study aims to reveal the characteristics of sediment transport of the watershed scale in terms of the temporal and spatial signatures, i.e. specific sediment yield, sediment delivery ratio, cumulative sediment curve and effective discharge.

Study Area

The Upper Sangamon River Basin (USRB) is 3150 km^2 at the confluence of the Illinois River in the center of Illinois State, USA. Average annual precipitation (1984-2007) is approximately 870 mm/year, while snow represents approximately 5% of it. Average annual potential evaporation (1984-2007) is approximately 1630 mm/year. The annual average temperature in the basin is 11℃, and the monthly average temperature is from −5℃ in January to 24℃ in July. Average annual water yield measured at the USGS stream gauging station at Monticello (Drainage area of 1425 km^2, Figure 1) during 1971-2000 is approximately 300 mm/year.

The USRB is intensively managed, following conversion to intensive agricultural production during the late 19th Century through the construction of railroads, the formation of drainage districts, excavation of drainage ditches and installation of subsurface drainage tiles. Poorly drained soils and ephemeral wetlands used to be common, but have been significantly modified through the construction of tile drains. Native vegetation used to be tallgrass prairie but has since been replaced by row crops (Alexander and Darmody, 1991). Approximately 84% of the land in the basin is currently devoted to agricultural production, while land in the Conservation Reserve Program covers 7.2% of the basin, urban land 4.5% and wetlands cover 2.4%.

Tecnología y ciencias del agua, 10 (4), 18-45. DOI: 10.24850/j-tyca-2019-04-02

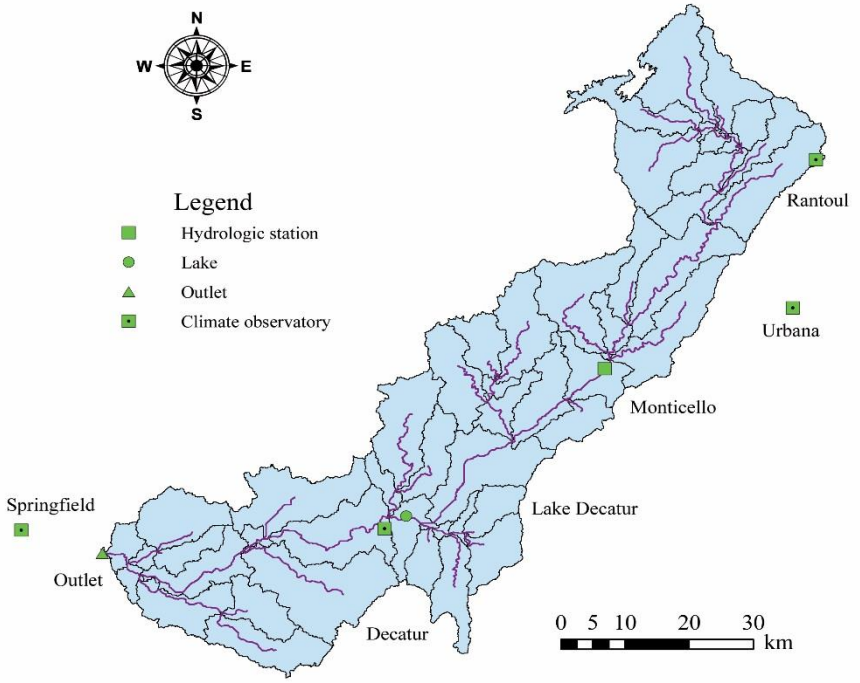

Figure 1. Map of USRB and distribution of ground stations.

Lake Decatur locates at the middle stream of USRB with the watershed area of 2400 km^2, and it is a water supply reservoir that supplies water to the City of Decatur with a population of 86,000. The dam of the reservoir was modified in 1956 and the maximum capacity of the lake increased to 34.56 million m^3 (Keefer and Bauer, 2005). The operation regime of the reservoir is unknown, so the USGS stream gauging station at Monticello (as shown in Figure 1) is selected for the calibration and validation of the model, which is at the upstream of the reservoir with the drainage area of 1425 km^2.

Data

The data used in the modeling include Digital Elevation Model (DEM), soil class, LAI, Normalized Difference Vegetation Index (NDVI), land cover, precipitation, potential evaporation, observed stream flow, observed sediment concentration and discharge. The geographic data are extracted from a DEM with the resolution of 1 arc second. The soil class is mainly extracted from the STATSGO database. The LAI is extracted from the product of "MODIS/Terra Leaf Area Index/FPAR 8-Day L4 Global 1km SIN Grid V004", NDVI from "MODIS/Terra

Tecnología y ciencias del agua, 10 (4), 18-45. DOI: 10.24850/j-tyca-2019-04-02

Vegetation Indices Monthly L3 Global 1km SIN Grid V004", and land cover from "MODIS/Terra Land Cover Type Yearly L3 Global 1km SIN Grid V004". The hourly precipitation data from DS3240 dataset of the National Climatic Data Center (NCDC) of NOAA are used in the model. The potential evaporation is extracted from North American Regional Reanalysis (NARR) of NOAA. Observed streamflow at Monticello is downloaded from the website of USGS. The observed sediment concentration and discharge at Monticello comes from the Benchmark Sediment Monitoring Program by Illinois State Water Survey. The air temperature and snow data at Urbana used in the discussion are obtained from the Illinois State Climatologist's Office, Illinois State Water Survey.

Model

Tsinghua Representative Elementary Watershed (THREW) model (Tian, 2006, Tian *et al*., 2008) is applied to the Upper Sangamon River Basin in the USA. THREW model is a semi-distributed hydrological model based on the Representative Elementary Watershed (REW) approach, and the model has been successfully applied to many watersheds in China, USA and Austria(Tian, 2006; Tian *et al.,* 2008; Liu *et al.*, 2009; Li *et al.*, 2010; Li *et al.*, 2012; Tian *et al.*, 2012; Liu *et al.*, 2012; Sun *et al.*, 2014; He *et al.*, 2014; He *et al.*, 2015; Liu *et al.*, 2015). The soil erosion and suspended sediment delivery are simulated based on the THREW model, which is named Tsinghua Representative Elementary Watershed model including Sediment (THREWS).

Hydrological Process

Tian *et al.* (2006) have extended the Representative Elementary Watershed approach for cold regions. The details are shown in Tian *et al.* (2006) and Mou *et al.* (2008). In the THREW model, each REW is partitioned into six surface sub-regions and two subsurface sub-regions. The hydrological processes of each sub-region in THREW model are described in Lee *et al.* (2007) and Tian *et al.* (2008).

In USRB, the river basin is divided into 51 REWs as shown in Figure 1. In each REW, there are four sub-regions (or zones) in the surface layer,

and they are a bare soil zone, a vegetated zone, a sub-stream-network zone, and the main channel reach zone. There are three sub-regions in the sub-surface layer, which are an upper unsaturated zone, a lower unsaturated zone and a saturated zone. The hydrological processes including ground surface depression, canopy interception, saturation and infiltration excess runoff, overland and channel routing are modeled as described in THREW model.

After the initial calibration of the THREW model, it is supposed that the dominant factors in the evapotranspiration and runoff generation in USRB are different from them in the other study areas where the THREW model has been applied (Tian, 2006; Mou *et al.*, 2008). Through the investigation and diagnosing, crop transpiration and tile drainage are supposed to be important in the rainfall-runoff process. The effects of crop transpiration and tile drainage are involved into THREW model.

As introduced previously, approximately 84% of the land in USRB is currently devoted to agricultural production, while land in the Conservation Reserve Program covers 7.2% of the basin, urban land 4.5% and wetlands cover 2.4%. Especially, in the Lake Decatur watershed, the row crops of corn and soybean in 1994 covered 85.3% of the land. The grassy crops of small grains and hay covered only 2.4% and nonagricultural land uses 12.3% of the land. Corn and soybeans nearly equally cover the cropland area at 42.0% and 43.3%, respectively (Demissie and Keefer, 1996). The 1995 Illinois land cover/land-use database indicates that 80% of the Lake Decatur watershed area was agricultural land. The remaining acreage is grassland (11.8%), forest (2.8%), wetlands/marsh (1.4%), urban/transportation (2.9%), and water (0.7%). Corn and soybeans, the dominant crops, comprised 82% of the Lake Decatur watershed in 2002 (Keefer and Bauer, 2005).

As the crop transpiration is significant in the evapotranspiration due to the high fraction of vegetation cover in USRB, the modeling of evapotranspiration (E_T, m/s) is improved by introducing LAI (Allen *et al*., 1998, Amenu and Kumar, 2008), as shown in Equation (1).

$$E_T = \alpha \cdot E_P \cdot F_{root} \cdot LAI \cdot S_u \quad (1)$$

Where α is empirical parameter depending on crop type and is typically 0.5, E_p is potential evaporation (m/s), F_{root} is the fraction of the root distribution, *LAI* is the leaf area index, and S_u is soil moisture saturation degree.

As reported by Demissie and Keefer (1996), interflow is the relatively quick movement of water in the shallow soil layers, and baseflow

sustains the flow in the stream during late summer and fall as well as during drought years in Sangamon River. The investigation of soil water balance in the Sangamon River basin indicates that more water contributes the stream through the combined effects of interflow and baseflow than from surface runoff (Demissie and Keefer, 1996). So the contribution of interflow and baseflow to the stream flow in USRB is very important.

Because of the extensive installation of subsurface drainage tiles in USRB to lower the groundwater table, the tile drainage as an important type of interflow is introduced into the model. While estimating saturated hydraulic conductivity in a tile-drained field, Rupp (2004) derived an analytical solution of tile drainage for an initial saturated unconfined rectangular aquifer. Green *et al.* (2006) proposed a formula of tile drainage on the daily scale for SWAT when they used SWAT2005 to evaluate streamflow in tile-drained regions. As the initial states of the aquifer and the distribution of the tiles in USRB are unknown and the time step in the THREW model is usually less than a day, a formula called linear reservoir model from conceptual model, especially Xin'anjiang Model, is used in the model, as shown in Equation (2) and Figure 2.

$$Qtile = \begin{cases} 0 \\ KD \cdot KSs \left(\frac{y_s-(Z-Ztile)}{Ztile}\right)^{KA} \end{cases} \quad (2)$$

$$if\ y_s \leq Z - Ztile,\ if\ y_s > Z - Ztile$$

where *Qtile* is the discharge per unit area of tile drainage (m/s), y_s is the average thickness of the saturated zone (m), *Z* is total soil thickness in the modeling (m), *Ztile* is depth of tile drainage (m), *KSs* is saturated hydraulic conductivity in saturated zone (m/s), *KD* is a linear parameter for tile discharge, and *KA* is an exponential parameter for tile discharge.

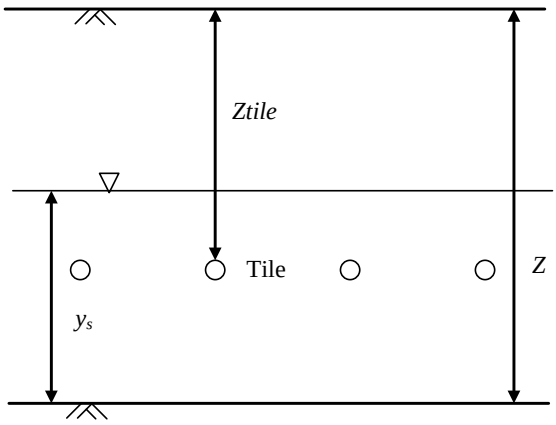

Tecnología y ciencias del agua, 10 (4), 18-45. DOI: 10.24850/j-tyca-2019-04-02

Figure 2. Schematic of tile drainage.

Sediment Process

The sediment processes in the model include sediment erosion from the hillslope, deposition, re-entrainment and bed degradation in the main channel. The sediment is generated from the hillslope and is transported to the main channel by surface runoff. In the main channel, the sediment in the water is allowed to deposit to channel floor while the loose sediment would be removed by the stream flow. If all of the loose sediment on the channel is removed, the degradation of the channel bed will happen. In the main channel, the sediment is transported together with water flux from the upstream by the stream flow and then to downstream.

In the model, sediment erosion from the hillslope to the main channel is assumed to associate with surface runoff from sub-stream-network zone to the main channel reach zone, and the formula of sediment erosion rate ($Q_{st,}$ kg/s) is a further conceptualization of the Modified Universal Soil Loss Equation (Neitsch *et al*., 2005; Viney *et al*., 1999), as shown in Equation (3).

$$Q_{st} = C \cdot s_t \cdot (Q_t \cdot A)^{\delta} \tag{3}$$

where C and δ are the empirical parameters, s_t is the slope of the sub-stream-network zone, and Q_t is the water discharge from sub-stream network to the main channel (m^3/s), A is the area of the REW(km^2).

The modeling of deposition, re-entrainment and bed degradation in the main channel followed the SWRRB model (Simulator for Water Resources in Rural Basins) (Arnold *et al*., 1990), i.e. the original of SWAT. A new zone for the sediment storage on main channel floor (sf-zone) is added to THREW model to model the sediment exchange between the water and the channel floor.

The sediment deposition in the main channel depends on the falling velocity of the sediment particles. The falling velocity formula ($v_{f,}$ m/s) used in this study is an approximate form widely used in practice (Shao and Wang, 2005), as shown in Equation (4).

$$v_f = -9\frac{v}{d} + \sqrt{(9\frac{v}{d})^2 + \frac{\gamma_s - \gamma}{\gamma} g d} \quad (4)$$

where γ_s is the density of sediment (kg/m^3) and γ is the density of water (kg/m^3), g is the gravity acceleration (m/s^2), d is the sediment particle diameter (m), and ν is the kinematic viscosity coefficient of water (m^2/s).

Travel time in the main channel of each REW (t, s) is

$$t = L_c / v \quad (5)$$

where L_c is the length of the channel (m), and v is the velocity (m/s).

The height that sediment of particle will fall during travel time (y_f, m) is

$$y_f = v_f \cdot t \quad (6)$$

The instantaneous sediment delivery ratio in each main channel (DR) is

$$DR = \begin{cases} 1 - 0.5 y_f / y_r \\ 0.5 y_r / y_f \end{cases} \quad (7)$$

if $y_f \leq y_r$, *if* $y_f > y_r$

where y_r is water depth in the main channel (m).

The deposition rate in the main channel (dep, kg/s) is

$$dep = \frac{S_{sr}}{t}(1 - DR) \quad (8)$$

where S_{sr} is the sediment storage in the water of the main channel (kg).

If there is loose sediment on the channel floor, i.e., the sediment storage in sf-zone (S_{sf}, kg) is positive, the sediment re-entrainment occurs. Otherwise, the degradation of the channel floor begins. The riverbed degradation (deg, kg/s) is the sum of the sediment re-entrainment and channel floor degradation, as shown in Equation (9).

$$deg = \begin{cases} k_1 \cdot \gamma \cdot Q_r \cdot s_r \\ k_1 \cdot k_2 \cdot \gamma \cdot Q_r \cdot s_r \end{cases} \quad (9)$$

$$if\ S_{sf} > 0,\ if\ S_{sf} \leq 0$$

where k_1 and k_2 are parameters, Q_r is the stream flow in the main channel (m^3/s), and s_r is the slope of the main channel.

Simulation Results

In the simulation, the water year is from October to September of next year. The period from Oct. 1993 to Sep. 1994 is selected for the model's warming up to eliminate the impact of the initial conditions. The period for the calibration is from Oct. 1994 to Sep. 1997 and the period for the validation is from Oct. 1997 to Sep. 2007. The simulated stream flow with the hourly time step at Monticello is used in the calibration and validation. Two standard indices, i.e. Nash-Sutcliffe efficiency coefficient (*NSEC*), and the coefficient of determination (R^2), and two signature curves, i.e. the regime curve and the hydrograph, are used to guide manual calibration of the hydrological model.

During the 3-year calibration period, we obtained *NSEC* within 0.69~0.86, and R^2 within 0.70~0.87 as shown in

Figure **3**. For the whole calibration period, *NSEC* is 0.72 and R^2 is 0.74. Figure 4 presents the seasonality of the water balance in the whole simulation period. After the calibration, the simulated runoff curve, i.e. the regime curve, shows good consistency with the observed runoff curve in the simulation period.

Using the parameters obtained by calibration, the model is then validated from Oct. 1997–Sep. 2007. During the 10-year validation period, we obtain *NSEC* within 0.12~0.79, and R^2 within 0.48~0.82 as shown in

Figure **3**. For the whole validation period, *NSEC* is 0.69 and R^2 is 0.70. The maximum *NSEC* and R^2 are obtained simultaneously in the year Oct. 2004-Sep. 2005, while the minimum *NSEC* in the year Oct. 1999-Sep. 2000 and minimum R^2 in the year Oct. 2000-Sep. 2001. Because the

annual precipitation from Oct. 1999 to Sep. 2000 is 689mm and that from Oct. 2000 to Sep. 2001 is 701mm, which is 20.8% and 19.4% less than the average annual precipitation (870mm) respectively, the model's performance from Oct. 1999 to Sep. 2001 is unexpected as shown in
Figure **3**.

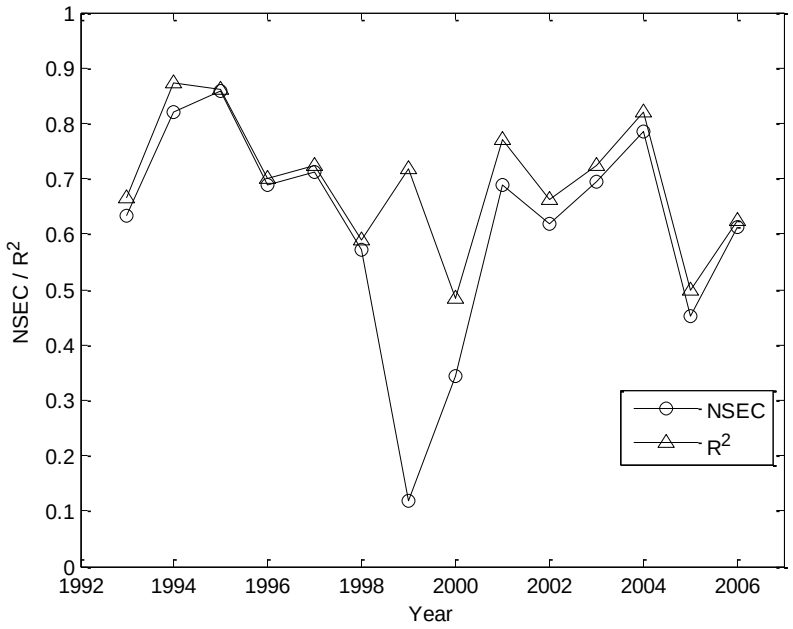

Figure 3. The evaluation indices of the simulation.

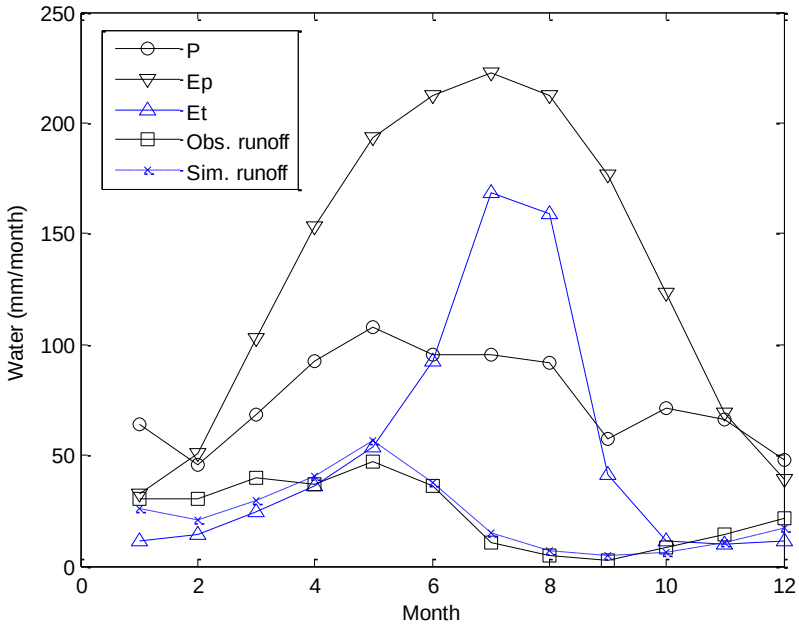

Figure 4. The seasonality of the water balance.

The observation of sediment discharges at Monticello isn't regularly daily and sometimes there are several sediment discharges in one day. On the other hand, the sediment discharge is not observed on some days. In the simulation period from Oct. 1, 1993, to Sep. 30, 2007, there are only 615 data, so the sediment model is not calibrated. The calibration of the sediment model is just used to confirm that the simulated sediment discharges are reasonable as shown in Figure 5.

Tecnología y ciencias del agua, 10 (4), 18-45. DOI: 10.24850/j-tyca-2019-04-02

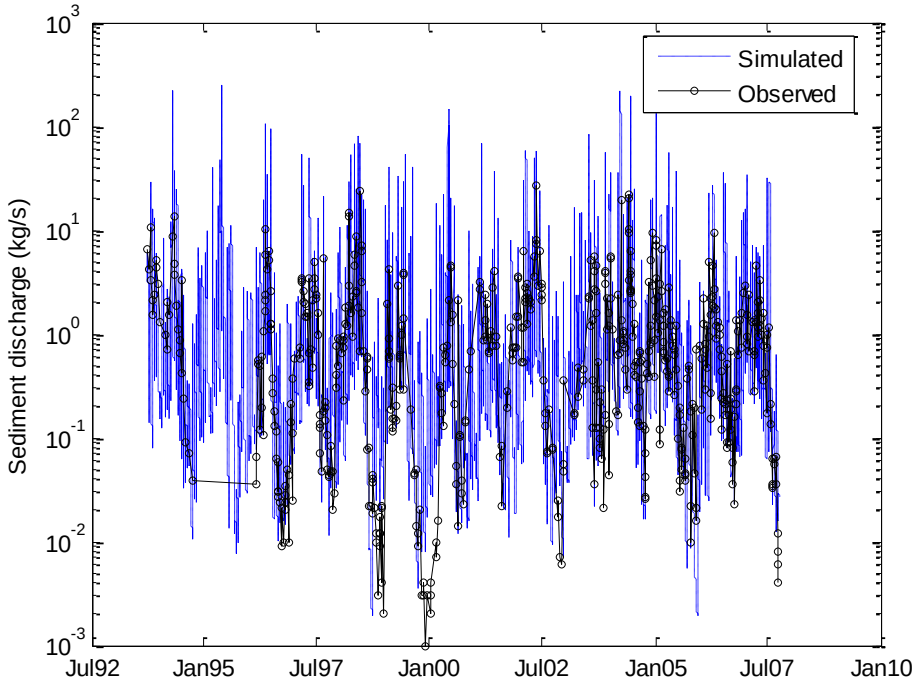

Figure 5. Simulated and observed sediment discharge at Monticello.

Sediment Signatures

There have been many statistic indices and curves for the analysis of sediment erosion and transport in the river basin, such as specific sediment yield, sediment delivery ratio (Walling, 1983), water-sediment cumulative percentage curve (Torizzo *et al.*, 2004) and effective discharge (Wolman and Miller, 1960). They are useful to analyze the temporal and spatial characteristics of sediment and evaluate the ability of the streamflow to deliver the sediment, which can be named as sediment signatures. However, the application of sediment signatures is limited by the available observed sediment data in the river basin.

The specific sediment yield, sediment delivery ratio, cumulative sediment curve and effective discharge, as the sediment signatures, are discussed in this section. Because of the small amount of observed sediment data, only simulated sediment discharges are used in the analysis of the sediment signatures.

Specific Sediment Yield

Sediment yield from a basin is a portion of soil eroded from the hillslope and it's the result of the combination of sediment erosion, deposition, re-entrainment and river bed degradation. To depict the scale property of sediment at the river basin scale, a lot of observed data will be required (Hassan *et al.*, 2008). And then problems will come, including limited length and irregular frequency of the data, the poor spatial distribution of the stations. However, with the simulation of sediment process in USRB, long-term regular, well-distributed sediment discharges are available to analyze the relationship of specific sediment yield and drainage area.

In THREWS model, one REW and all of its upstream REWs make up of a subbasin and the annual sediment yield and specific sediment yield of all subbasins are calculated as shown in Figure 6 and Figure 7.

Figure 6 shows that sediment yield increases with drainage area, but there is no significant trend for the relation of specific sediment yield and drainage area as shown in Figure 7. In USRB most of the land is farmland with corn and soybean, so the status of sediment erosion is nearly uniform all over the basin. The variability of specific sediment yield mainly comes from the heterogeneity of the river channel.

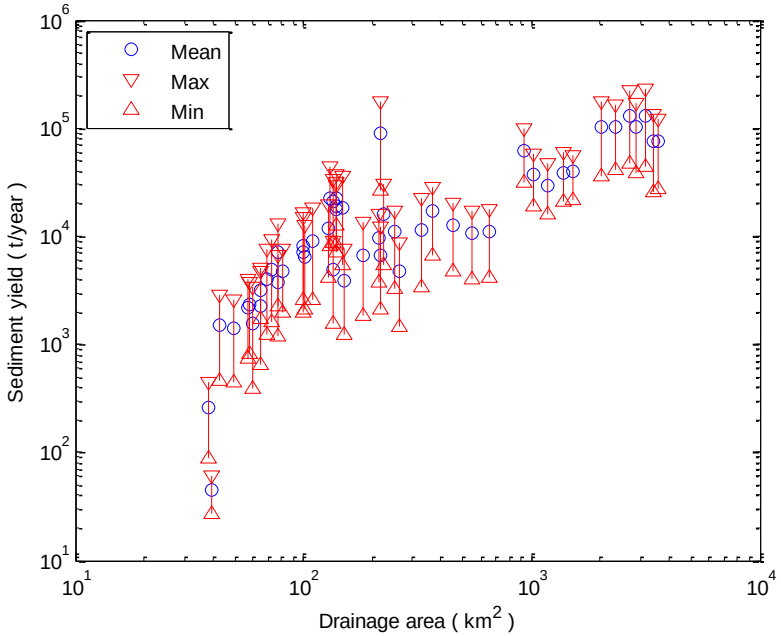

Figure 6. Sediment yield of all subbasins in USRB.

Tecnología y ciencias del agua, 10 (4), 18-45. DOI: 10.24850/j-tyca-2019-04-02

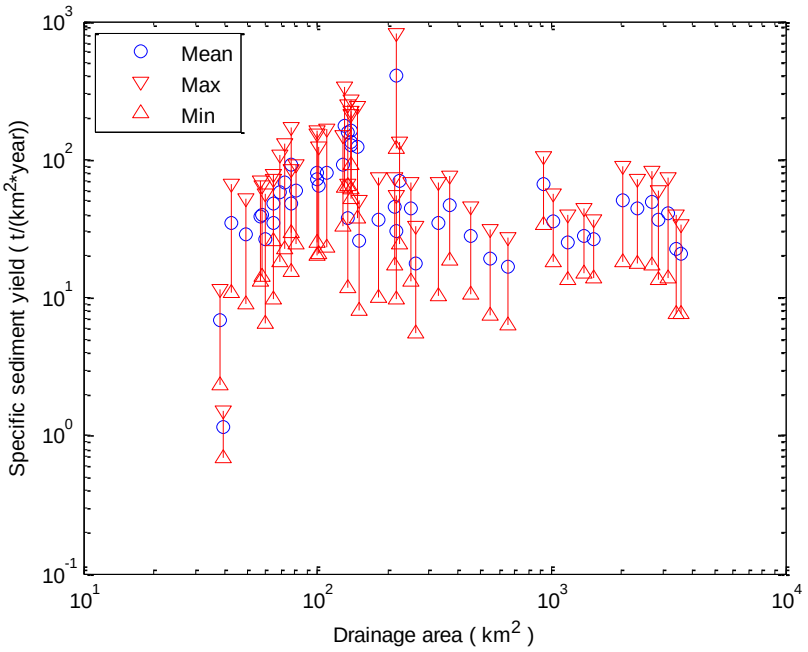

Figure 7. Specific sediment yield of all subbasins in USRB.

Sediment Delivery Ratio

Sediment delivery ratio (SDR) is used to estimate the quantity of sediment erosion on the hillslope by many researchers (Walling, 1983, Lu *et al.*, 2005), while some researchers think that the concept of sediment delivery ratio is a fallacy (Parsons *et al.*, 2006). However, at a proper temporal and spatial scale, the SDR concept is still a useful tool to describe the characteristics of a watershed. In this study, the SDR is defined as the ratio of annual sediment yield to annual sediment erosion in the watershed. In the modeling, sediment delivery ratio can be calculated with the annual sediment yield and annual sediment erosion. So the annual sediment delivery ratios of all subbasins in the simulation period are got, and the mean, the maximum and the minimum for each subbasin are shown in Figure 8.

In the simulation period, the sediment delivery ratio for each subbasin didn't vary too much. Figure 8 shows a relation that sediment delivery ratio decrease as the area of the subbasin increase and the result is consistent with the other research (Lu *et al.*, 2005).

However, there are some unexpected points which are larger than 1 or

smaller than 0.01. There are 6 SDR which are larger than 1 for REW 47 (REW 47 is a subbasin) in the simulation period and the mean is 0.97. The SDR larger than 1 suggests that the riverbank and riverbed are degraded by the streamflow and the river channel is a source of sediment. For subbasin 18 (drainage area is 1168km^2) corresponding to REW 18, the mean SDR is 0.119, so in comparison with the SDR of upstream subbasin the river channel of REW 18 is a sink of sediment and most of the sediment is deposited on the riverbed. This is in accordance with the small specific sediment yield as shown in Figure 7.

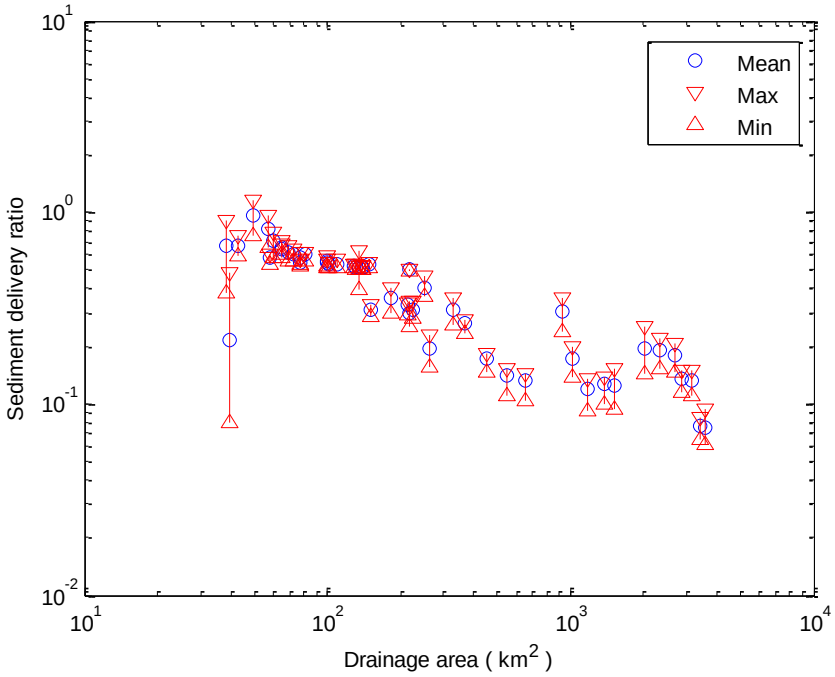

Figure 8. Sediment delivery ratio of all subbasins in USRB.

Cumulative Sediment Curve

Torizzo *et al.* (2004) used the water-sediment cumulative percentage curve to attempt to show the ability of the different magnitude streamflow (i.e. water discharge) to transport the sediment. Because the water-sediment cumulative percentage curve doesn't show the contribution of the different magnitude of streamflow clearly, the cumulative sediment curve is introduced.

To plot the cumulative sediment curve, both of the streamflow data and the sediment discharge data of one year are arranged by the ascending

order of the streamflow, the sediment discharge data are cumulated ascendingly only, and then the cumulative sediment discharge data are normalized by the total sediment. The ascending streamflow data and the normalized cumulative sediment data are plotted in the figure. The cumulative sediment curve at Monticello is shown in Figure 9. Although the annual maximum streamflow changed from 48.2m^3/s to 222.3m^3/s in the simulation period, the streamflows corresponding to the 50% sediment always were not larger than 46.6m^3/s as shown in Figure 9. So the main contributor of the sediment transport is the small streamflows and all of the curves are upward concave curves. Otherwise, if the main contributor is the large streamflows, the curve will be downward concave curves.

The critical streamflows, which are corresponding to 25%, 50% and 75% of cumulative sediment, are named as Q_{25}, Q_{50} and Q_{75} as shown in Figure 10. Although Q_{75} changed from 26.5m^3/s to 114.8m^3/s, Q_{25} and Q_{50} didn't change too much and the ranges were from 7.8m^3/s to 27.0m^3/s, and from 12.6m^3/s to 46.6m^3/s, respectively.

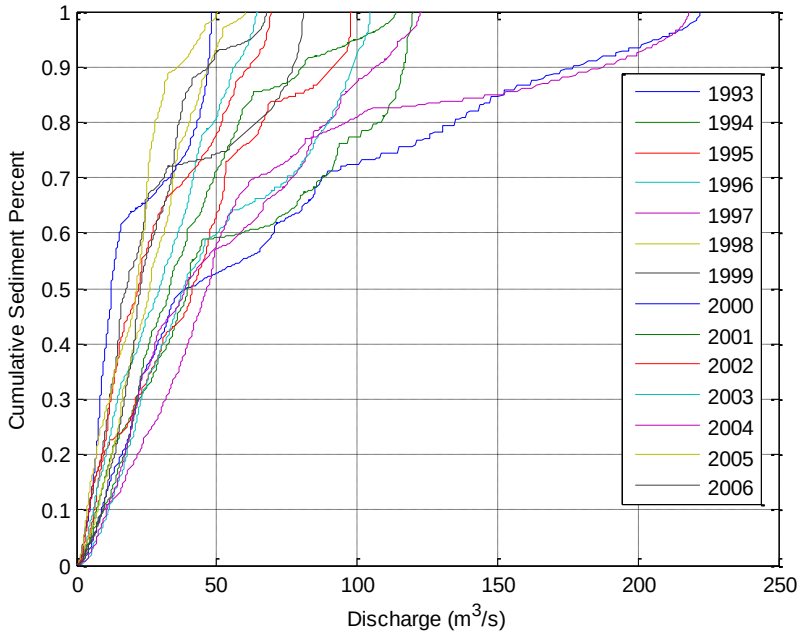

Figure 9. Cumulative sediment curve at Monticello in USRB.

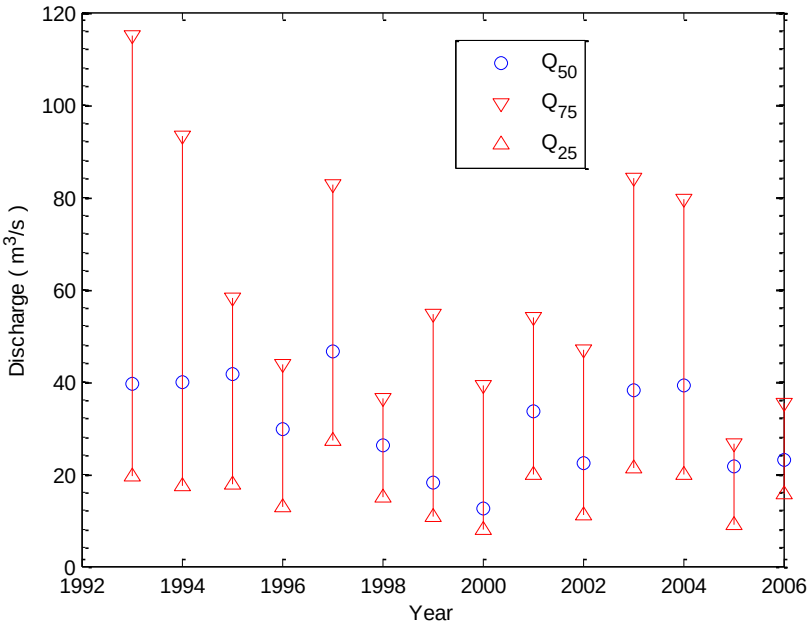

Figure 10. Critical streamflows of sediment transport at Monticello in USRB.

Effective Discharge

The effective discharge is a concept introduced by Wolman and Miller (1960) and widely used in the research of sediment transport (Torizzo *et al.*, 2004). The effective discharge is defined as the range of water discharges which transports the largest portion of the annual sediment yield. In the study, the length of the discharge intervals used to subdivide the entire streamflow series chooses to be 20m^3/s after it is tried several times and the central value represents the range after here. The absolute quantity of suspended sediment load, which is carried by each discharge interval within one year, is computed to graph sediment load histogram and the effective discharge is the central value of the discharge interval carrying the most sediment load.

The effective discharges of the outlets of all subbasins in USRB are calculated and are shown in Figure 11. For all subbasins, the minimum effective discharge in the simulation period is 10m^3/s and the mean and maximum effective discharge increase with the area of the subbasin slightly. But the largest mean effective discharge is only 57.1m^3/s, which is quite small. The effective discharge with the observed suspended sediment data from 1981 to 2000 at Monticello is 16.5m^3/s

(Crowder and Knapp, 2002). The mean effective discharge of REW 16 corresponding to Monticello is 21.4m^3/s, which is near to observed effective discharge. In USRB, the small streamflows transport the largest portion of sediment yield and the conclusion is consistent with the result of cumulative sediment curve.

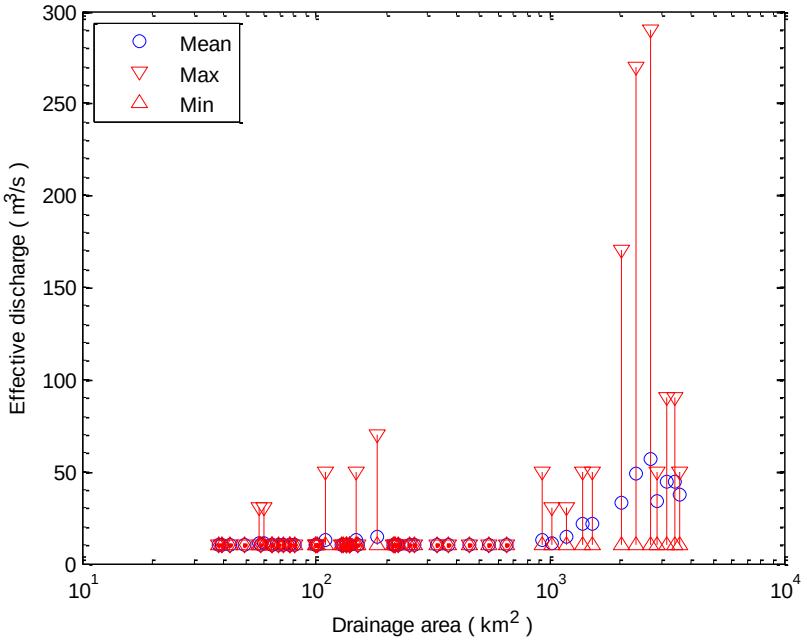

Figure 11. Effective discharges of all subbasins in USRB.

Discussion

Precipitation Data

In the modeling, all of the precipitation is assumed to be rainfall and the freeze of the soil moisture is neglected in the model. However, the snow depth on the ground as shown in Figure 12 is notable at Urbana, one of the main climate observatories used in the modeling (Figure 1), and the duration when there is snow on the ground continuously is quite long in some winters, as shown in Figure 13.

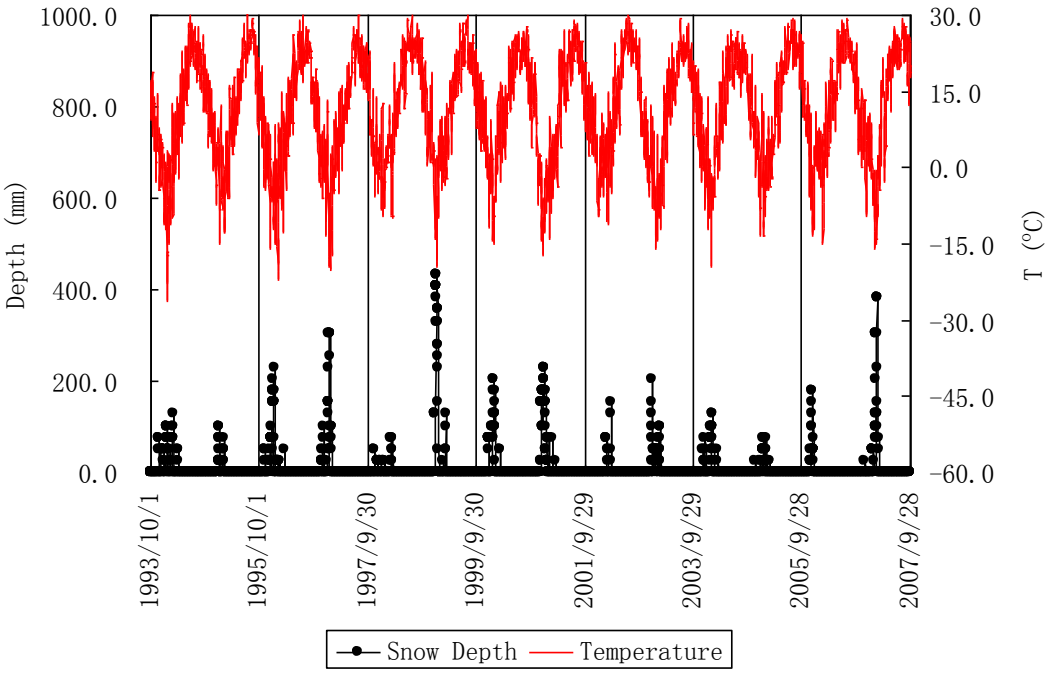

Figure 12. Snow depth and air temperature at Urbana.

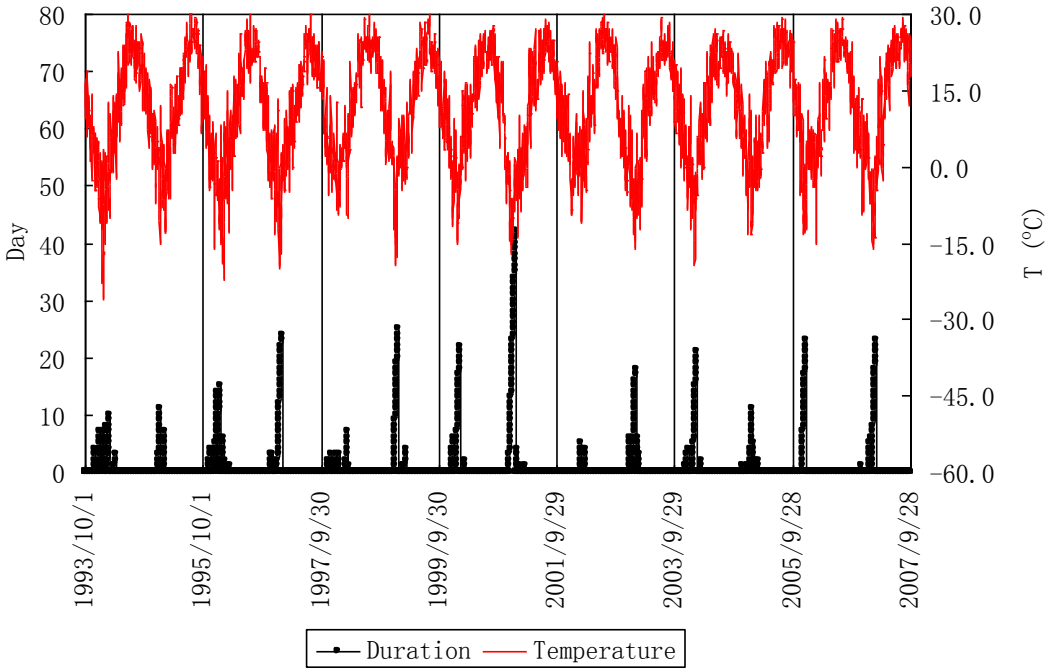

Figure 13. Duration and air temperature at Urbana.

Especially in Dec. 2000 and Jan. 2001, the daily mean temperatures of 53 days were below 0 ℃, and the precipitation was mainly in the form of

Tecnología y ciencias del agua, 10 (4), 18-45. DOI: 10.24850/j-tyca-2019-04-02

snow and stored on the ground. The period when there is snow on the ground continuously is 42 days, from Dec. 12, 2000, to Jan. 22 2001, as shown in Figure 14. In Feb. 2001, the air temperature fluctuated around 0 ℃ and the freezing soil started to melt. So the saturation of the soil should be very high. On Feb. 24, 2001, the rainfall at Urbana is 47mm and a large flood peak of 168.5 m^3/s appeared in the next several days.

Therefore, the model which neglects snow and freeze of the soil moisture should be unable to capture the rainfall-runoff process due to snow and freeze of the soil moisture and in the future modeling of the area, the snow and freeze of soil moisture should be brought into the model.

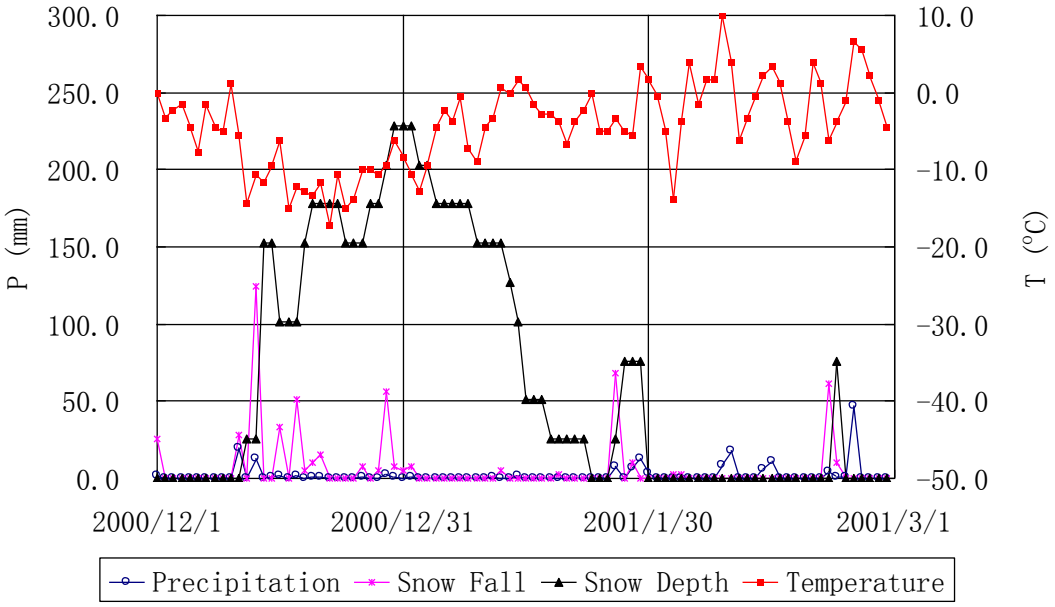

Figure 14. Precipitation and air temperature at Urbana from Dec. 2000 to Feb. 2001.

Strange Years

NSEC of simulated discharges in the water years of 1999-2000 and 2000-2001 are quite low and they are strange years due to the larruping precipitation and runoff regimes as shown in Figure 15. The annual precipitation of the water years of 1999-2000 and 2000-2001 is 689mm and 701mm, respectively, but the average annual precipitation of the basin is 870mm. It seems that the poor performance of the model

Tecnología y ciencias del agua, 10 (4), 18-45. DOI: 10.24850/j-tyca-2019-04-02

in the two water years is due to the weak ability of the model to simulate the hydrological process in dry years, but in fact, the rainfall-runoff processes in the two years are absolutely different. The observed runoff coefficient at Monticello of the two years is 0.11 and 0.31, respectively, and then the water year of 1999-2000 is a dry year indeed as well as in name, as shown in Figure 15. However, the observed runoff coefficient in Feb. and Mar. 2001 is 0.96 and 1.81, respectively, which are unconventionally high, near or larger than 1. The high observed runoff coefficient is mainly due to the snow and freeze of the soil moisture in winter and spring, which should be the main cause of the model's poor performance. The high runoff coefficient, which is near or larger than 1, also appears in the other years in the simulation period.

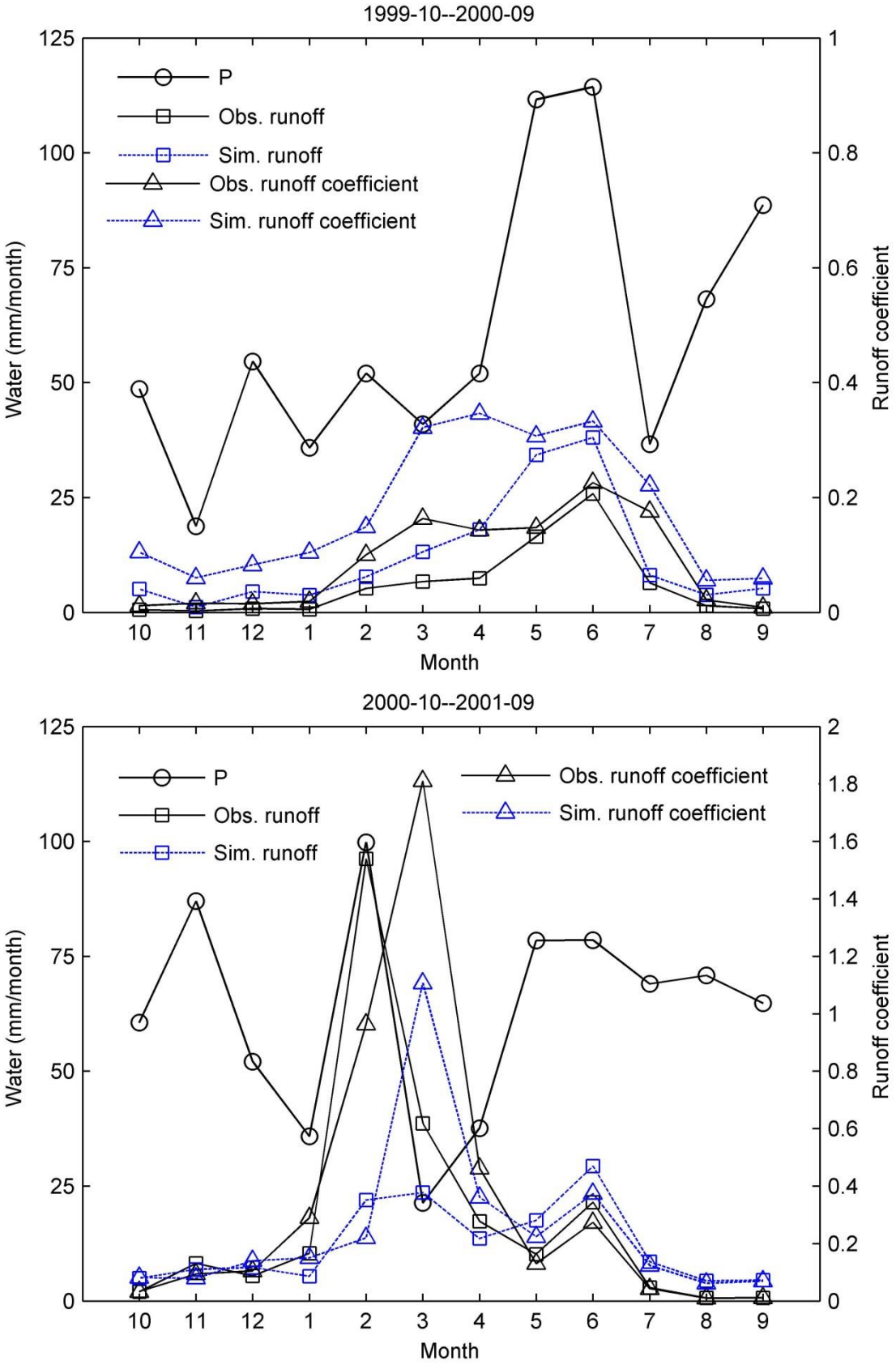

Figure 15. Monthly precipitation and runoff from Oct. 1999 to Sep. 2001.

Sediment Observation

From Oct. 1, 1993, to Sep. 30, 2007, there are only 615 observed data of sediment discharges, so the observed data can't be used in the analysis of the sediment signatures. In order to understand the temporal and spatial characteristics of sediment delivery in USRB, the observation of sediment discharge should be improved to be regular and it's suggested that the regular daily observation of sediment concentration is required at least. In the next step, the analysis of sediment signatures will be applied in a well-gauged basin and new signatures will be brought in.

Conclusion

Through the investigation and diagnosing in Upper Sangamon River Basin, the closure relationships in THREW model are improved in this paper. Crop transpiration and tile drainage are found to play important roles in the hydrological process due to agricultural activities in USRB. So the modeling of evapotranspiration is improved by introducing LAI and the tile drainage as an important type of interflow is brought into the THREW model. Although THREW model with the improvement performs quite well in the moderate years, the closure relationships will be improved further due to the poor performance in the extremely dry years and cold months.

A semi-distributed sediment simulation model, THREWS, is built up based on the modeling framework of THREW model by introducing the sediment processes in the watershed, which include sediment erosion from the hillslope, deposition, re-entrainment and bed degradation in the main channel. The result of the simulation is used in the analysis of the sediment signatures in the paper.

Four sediment signatures, i.e. specific sediment yield, sediment delivery ratio, cumulative sediment curve and effective discharge, are applied in the analysis of the sediment simulation in USRB. The characteristics of the sediment transport in USRB which are represented by the sediment signatures are consistent with each other and accord with the fact of the agricultural production in USRB.

Tecnología y ciencias del agua, 10 (4), 18-45. DOI: 10.24850/j-tyca-2019-04-02

Acknowledgment

This work was partially supported by the National Natural Science Foundation of China (NSFC) (Grant No. 51779203, 51609270, 41330858). Funding was also provided by the Basic Research Plan of Natural Science of Shaanxi Province (2016JQ5105), SRFDP (20136118120021) and National Department Public Benefit Research Foundation of Ministry of Water Resources (201501058). With the financial support of China Scholarship Council, Dengfeng Liu has been studied in the University of Illinois, USA and part of the work was done during this period.

Reference

Alexander, J. D. & Darmody, R. G. (1991). Extent and organic matter content soils in Illinois soil associations and Counties [R]. Agronomy Special Report, University of Illinois, USA.

Allen, R. G., Pereira, L. S., Raes, D., & Smith, M. (1998). FAO Irrigation and Drainage Paper No. 56 Crop evapotranspiration: guidelines for computing crop water requirements [M], 290 pp.

Amenu, G. G. & Kumar, P. (2008). A model for hydraulic redistribution incorporating coupled soil-root moisture transport [J]. Hydrology and Earth System Science Discussion, 12(1): 3719-3769.

Arnold, J.G., Williams, J.R., Nicks A.D., & Sammons, N.B. (1990). SWRRB: A basin scale simulation model for soil and water resources management[M]. Texas A&M Univ. Press, College Station, TX, USA.

Christensen, N. S., Wood, A. W., Voisin, N. et al. (2004). The Effects of Climate Change on the Hydrology and Water Resources of the Colorado River Basin [J]. Climatic Change, 62(1): 337-363.

Crowder, D. W. & Knapp, H. V. (2002). Effective Discharges of Illinois Streams [R]. Illinois State Water Survey Contract Report 2002-10, Champaign, IL, USA.

Demissie, M. & Keefer, L. (1996). Watershed Monitoring and Land Use Evaluation for the Lake Decatur Watershed [R]. Illinois State Water Survey Miscellaneous Publication 169, Champaign, IL, USA.

Dvorak, V., Hladny, J. & Kasparek, L. (1997). Climate change hydrology and water resources impact and adaptation for selected river basins in the Czech Republic [J]. Climatic Change, 36(1): 93-106.

Green, C. H., Tomer, M. D., Di Luzio, M. & Arnold, J. G. (2006). Hydrologic evaluation of the soil and water assessment tool for a large tile-drained watershed in Iowa [J]. Transactions of the ASABE, 49(2): 413-422.

Hassan, M. A., Church, M. Xu, J. et al. (2008). Spatial and temporal variation of sediment yield in the landscape: Example of Huanghe (Yellow River) [J]. Geophysical Research Letters, 35(6), L06401, doi:10.1029/2008GL033428.

He, Z., Parajka, J., Tian, F. & Blöschl, G. (2014). Estimating degree-day factors from MODIS for snowmelt runoff modeling [J]. Hydrology and Earth System Sciences, 18(12): 4773-4789.

He, Z., Tian, F., Gupta, H. & Hu, H. (2015). Diagnostic calibration of a hydrological model in a mountain area by hydrograph partitioning [J]. Hydrology and Earth System Sciences, 19(4): 1807-1826.

Keefer, L. & Bauer, E. (2005). Watershed Monitoring for the Lake Decatur Watershed 2000-2003 [R]. Illinois State Water Survey Contract Report 2005-09, Champaign, IL, USA.

Lee, H., Zehe, E. & Sivapalan, M. (2007). Predictions of rainfall-runoff response and soil moisture dynamics in a microscale catchment using the CREW model [J]. Hydrology and Earth System Sciences, 11(2): 819-849.

Li, H., Sivapalan, M. & Tian, F. (2012). Comparative diagnostic analysis of runoff generation processes in Oklahoma DMIP2 basins: The Blue River and the Illinois River [J]. Journal of Hydrology, 418–419: 90-109.

Li, H., Sivapalan, M., Tian, F. & Liu, D. (2010). Water and nutrient balances in a large tile-drained agricultural catchment: a distributed modeling study [J]. Hydrology and Earth System Sciences, 14(11): 2259-2275.

Liu, D., Chang, J., Tian, F., Huang, Q. & Meng, X. (2015). Analysis of baseflow index based hydrological model in Upper Wei River basin on the Loess Plateau in China [J]. Proc. IAHS, 368: 403-408.

Liu, D., Tian, F. & Hu, H. (2009). Sediment simulation at Upper Sangamon River basin using THREW model [J]. IAHS Publication 335: 187-195.

Liu, D., Tian, F. & Hu, H. (2012). The role of run-on for overland flow and the characteristics of runoff generation in the Loess Plateau, China [J]. Hydrological Sciences Journal, 57(6): 1-11.

Lu, H., Moran, C. J. & Sivapalan, M. (2005). A theoretical exploration of catchment-scale sediment delivery [J]. Water Resources Research, 41(9), W09415, doi:10.1029/2005WR004018.

Mou, L., Tian, F., Hu, H. & Sivapalan, M. (2008). Extension of the Representative Elementary Watershed approach for cold regions: constitutive relationships and an application [J]. Hydrology and Earth System Science, 12(2): 565-585.

Neitsch, S. L., Arnold, J. G., Kiniry, J. R. & Williams, J. R. (2005). Soil

and Water Assessment Tool theoretical Documentation Version 2005 [R]. Texas Water Resources Institute, College Station, Texas, USA.

Parsons, A. J., Wainwright, J., Brazier, R. E. & Powell, D. M. (2006). Is sediment delivery a fallacy? [J]. Earth Surface Processes and Landforms. 31(10): 1325–1328.

Rupp, D. E., Owens, J. M., Warren, K. L. & Selker, J. S. (2004). Analytical methods for estimating saturated hydraulic conductivity in a tile-drained field [J]. Journal of Hydrology, 289(1-4): 111–127.

Shao, X. & Wang, X. (2005). Introduction to river mechanics [M]. Beijing: Tsinghua University Press.

Singh, P. K., Bhunya, P. K., Mishra, S. K. et al. (2008). A sediment graph model based on SCS-CN method [J]. Journal of Hydrology, 349(1-2): 244-255.

Sun, Y., Tian, F., Yang, L. & Hu, H. (2014). Exploring the spatial variability of contributions from climate variation and change in catchment properties to streamflow decrease in a mesoscale basin by three different methods [J]. Journal of Hydrology, 508: 170-180.

Tian, F., Hu, H., Lei, Z. & M. Sivapalan (2006). Extension of the representative elementary watershed approach for cold regions via explicit treatment of energy related processes [J]. Hydrology and Earth System Science, 10(5): 619-644.

Tian, F. (2006). Study on thermodynamic watershed hydrological modeling [D], Tsinghua University, Beijing. China.

Tian, F., Hu, H. & Lei, Z. (2008). Thermodynamic watershed hydrological model (THModel): constitutive relationship [J]. Science in China, Series E, 51(9): 1353-1369.

Tian, F., H. Li & M. Sivapalan (2012). Model diagnostic analysis of seasonal switching of runoff generation mechanisms in the Blue River basin, Oklahoma [J]. Journal of Hydrology, 418–419: 136-149.

Torizzo, M. & Pitlick, J. (2004). Magnitude-frequency of bed load transport in mountain streams in Colorado [J]. Journal of Hydrology, 290(1-2): 137-151.

Viney, N. R. & Sivapalan, M. (1999). A conceptual model of sediment transport: application to the Avon River Basin in Western Australia [J]. Hydrological Processes, 13(05): 727-743.

Walling, D. E. (1983). The sediment delivery problem [J]. Journal of Hydrology, 65(1-3): 209-237.

Wolman M. G., Miller, J.P. (1960). Magnitude and frequency of forces in geomorphic processes [J]. Journal of Geology, 68(1): 54-74.

DOI: 10.24850/j-tyca-2019-04-03
Special Article

Brominated Flame Retardants in Edible Fishes from Three Gorges Reservoir, China

Retardantes de llama bromados en peces comestibles del embalse de las Tres Gargantas, China

X. Ding[1]
J. Liu[2]*
W. Wen[3]

[1]State Key Laboratory of Simulation and Regulation of the River Basin Water Cycle, China Institute of Water Resources and Hydropower Research (IWHR), Beijing, China

Department of Water Resources, China Institute of Water Resources and Hydropower Research (IWHR), Beijing, China, email: dingxiangyi840318@163.com, ORCID 0000-0002-2802-0412

[2]State Key Laboratory of Simulation and Regulation of the River Basin Water Cycle, China Institute of Water Resources and Hydropower Research (IWHR), Beijing, China

Department of Water Resources, China Institute of Water Resources and Hydropower Research (IWHR), Beijing, China, email: liujiahong00@sohu.com, ORCID 0000-0003-2611-6100

[3]School of Environment, Beijing Normal University, Beijing, China, email: wenwuliwen@163.com, ORCID 0000-0002-6665-5451

*Corresponding author: Jiahong Liu, email: liujiahong00@sohu.com

Abstract

Brominated flame retardants (BFRs) have attracted increasing attention in recent decades because of their persistence, distribution, bioaccumulation, and biotoxicity in the environment. In the present study, the levels and distribution of polybrominated diphenyl ethers (PBDEs) and polybrominated biphenyl (PBBs) in twenty-four samples of twelve fish species collected from the Three Gorges Reservoir (TGR) were analyzed. The results indicated that ∑PBDE concentrations in fish muscle ranged from 22.62 pg g^{-1} by wet weight

(ww) (yellowcheek carp) to 217.75 pg g^{-1} ww (yellow catfish). BDE47 and BDE209 were the most predominant congeners, with their sum accounted for 23.62–68.16% of ∑PBDEs. ∑PBB concentrations ranged from 27.83 pg g^{-1} ww (silver carp) to 155.75 pg g^{-1} ww (topmouth culter); BB49 and BB209 were detected in all samples, with concentrations ranging from 4.62 to 47.10 pg g^{-1} ww and 1.29 to 80.95 pg g^{-1} ww, respectively. There are no significant correlations between the BFRs levels and fish length (or weight) in these samples. Compared to other areas, the level of BFRs in edible fishes from TGR was low.

Keywords: BFRs, PBDEs, PBBs, Fish muscle, Three Gorges Reservoir.

Received: 18/12/2018

Accepted: 20/03/2019

Introduction

Polybrominated diphenyl ethers (PBDEs) and polybrominated biphenyls (PBBs) are a class of brominated flame retardants (BFRs). They are widely applied in various domestic products, such as carpet pads, castings, foam cushions in chairs, and couches (De Wit, 2002; Alaee, Arias, Sjodin, & Bergman, 2003). Because of their lack of chemical binding and migratory aptitudes, PBDEs and PBBs may enter the environment during production and use as well as dismantling of these products (Osako, Kim, & Sakai, 2004; Wang, Ma, Lin, Na, & Yao, 2009). Accordingly, PBDEs and PBBs have been extensively detected in water as well as in sediment (Law et al., 2014; Wang et al., 2015; Zhang et al., 2015; Yu et al., 2016). Owing to their lipophilicity and bioaccumulative properties, they had been detected in various aquatic species. Because of their biotoxicity, some congeners of PBDEs (tetra-, penta-, hexa-, and hepta-bromodiphenyl ether) and PBBs (hexabromobiphenyl) were labeled as persistent organic pollutants (POPs) at the fifth meeting of the Conference of the Parties to the Stockholm Convention on POPs. Although some of these compounds were phased out in developed regions, their use has been increasing in some developing countries. In China, the production of deca-BDE increased 1.5 times in 2004 relative to 2000 (Xiang et al., 2007).

The Yangtze River, the longest river in China and the third longest in the world, descends 7,500 m from the Tibetan Plateau to the East China Sea with a journey of 6,300 km. The Three Gorges Dam (TGD), which is the largest dam in the world, has a length of 2,335 m and a height of 185 m. The Three Gorges Reservoir (TGR) located at the portion of the Yangtze river basin between Chongqing and Yichang, has an area of 1,080 km^2 and is the source of fresh drinking water and favorite fish for 16 million people (Wang et al., 2017). Some researchers investigated the level and distribution of PBDEs and PBBs in surface water and sediment in TGR (Zhao et al., 2013; Wang et al., 2017). Wang et al. (2017) detected some low molecular weight PBDEs in water and large molecular weight PBDEs in sediment. The concentration PBDEs was up to 811 pg g^{-1} lipid (dissolved bioavailable PBDEs) in water and 52,843 pg g^{-1} by dry weight (dw) in sediment. Zhao et al. (2013) measured the concentrations of PBDEs and PBBs as 22.41 and 35.24 pg g^{-1} dw, respectively. Given their high bioaccumulative abilities, PBDEs and PBBs are likely accumulated in fish in the TGR. However, no studies on BFRs in edible fishes from the TGR have been published to date and the accumulation of chemicals in edible fish has rarely been known by the public. Diet is the most common pathway for human exposure to PBDEs or PBBs. Since TGR is the main source of edible fish for local residents, it is crucial to investigate the levels as well as the distribution of PBDEs and PBBs in fishes in this area.

In this study, environmental concentrations of 49 BFRs in 24 fish specimens from 12 species were collected at the TGR. All of the sampling sites were located at a tributary of the Yangtze River. The monitored BFRs included 27 PBDE congeners and 22 PBB congeners. Twelve fish species included carp (*Cyprinus carpio*), grass carp (*Ctenopharyngodon idella*), brass gudgeon (*Coreius heterodon*), trout (*Squaliobarbus curriculus*), topmouth culter (*Erythroculter ilishaeformis*), catfish (*Silurus asotus*), yellow catfish (*Pelteobagrus fulvidraco*), silver carp (*Hypophthalmichehys molitrix*), mandarin fish (*Siniperca kneri Garman*), rock carp (*Spinibarbus sinensis*), yellowcheek carp (*Elopichthys bambusa*), and basilewsky (*Hemiculter leuciclus*). The main aim of this study was to examine the levels and distribution of PBDEs and PBBs in different fish species from the TGR and to evaluate the bioaccumulation of individual PBDE and PBB congeners in 12 fish species.

Materials and Methods

Tecnología y ciencias del agua, 10 (4), 46-65. DOI: 10.24850/j-tyca-2019-04-03

Sample Collection and Preparation

Twenty-four freshwater fish samples of 12 species were collected at the sampling locations shown in Fig. 1. The fish lengths were measured, fishes were dissected, and the muscle tissue was maintained at -20°C before use.

The fish samples were frozen, dried, ground into powder in a mortar, and passed through a 100-mesh sieve for follow-up analysis. Five grams of each sample was spiked with 10 ng of 2,4,5,6-tetrachloro-m-xylene, pentachloro-nitrobenzene and PCB209 as surrogate congener standards and placed into extraction cells together with 2 g activated copper powder and kieselguhr. The cells were extracted using ASE 300 (accelerated solvent extractor) (Dionex, CA, USA). The extracted solvents were n-hexane and methylene chloride (1:1, v/v).

Extracts were combined and concentrated to 6.0 mL under a nitrogen stream and 2.5 mL of each concentrated extract was cleaned by Gel Permeation Chromatography (GPC). The mobile phase for GPC was ethyl acetate and hexamethylene (1:1, v/v). The portion including the analyzed BFRs was collected between 8 and 16 min (total of 37.6 mL of eluent). The extract was concentrated to 1 mL by rotary evaporation (400 mbar, 40°C). The concentrated extract was further cleaned using a multilayer silica gel column that consisted of 4 g deactivated silica (3.3% organic-free reagent water w/w), 2 g anhydrous sodium sulfate, 4 g deactivated silica (3.3% organic-free reagent water w/w), 2 g anhydrous sodium sulfate, and 8 g acidic silica (44% concentrated sulfuric acid w/w). To protect the samples from debromination caused by UV light, the silica gel column was wrapped in aluminum foil and then pre-eluted with 80 mL hexane before use. To collect PBB and PBDE congeners, 100 mL *n*-hexane and 10% methylene chloride in 80 mL *n*-hexane were used (EPA, 1996). The eluents were concentrated to 1 mL individually through rotary evaporation and the solvent from each sample was evaporated to dryness at 25°C under a gentle nitrogen stream and finally re-dissolved in 100 µL *n*-hexane.

Tecnología y ciencias del agua, 10 (4), 46-65. DOI: 10.24850/j-tyca-2019-04-03

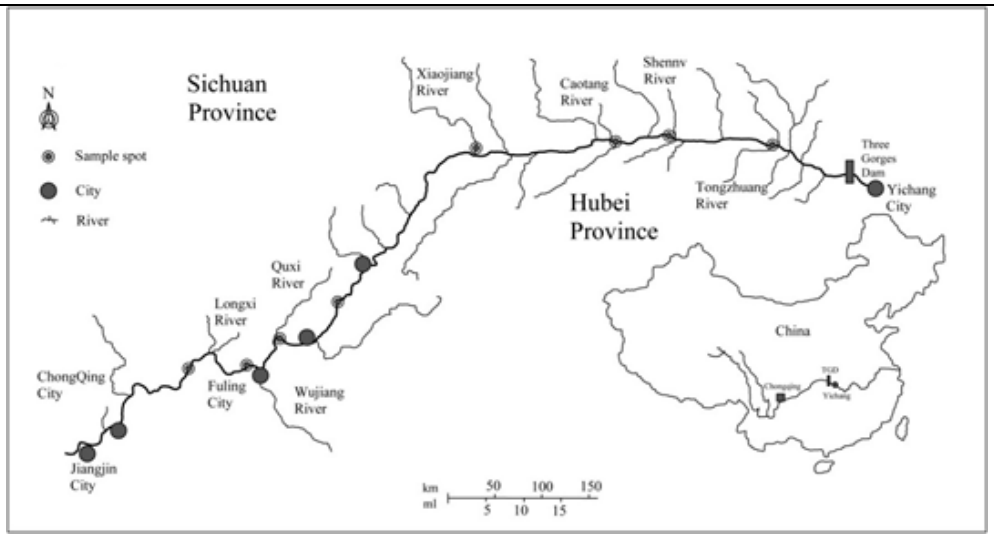

Figure 1. Map of sampling locations.

Instrumental Analysis

Target compounds were analyzed by Varian CP3800/300 triple-quadrupole system (GC-MS/MS) (Varian, USA). The capillary was VF-5-MS (Varian, USA). The temperature of the column oven was increased from 90°C (initial time: 1 min) to 250°C at a rate of 4°C/min, then increased at a rate of 25°C/min from 250°C to 300°C and it was maintained at 300°C for 5 min. The temperature of the GC injector, the MS ion source, and the transfer line was kept at 260°C, 230°C, and 250°C, respectively. Helium was the carrier gas with a flow rate of 1.5 mL/min and the injection volume of 1 μL. For the analysis of PBBs and PBDEs, the mass spectrometer was run in the negative chemical ionization (NCI) mode.

Quality Control and Statistical Analysis

To avoid contamination, a solvent blank and a procedural blank were operated for every ten samples. Limits of detection (LOD) for the analytes in the present study were defined as three times the signal-to-noise ratio (*S*/*N*) and were 0.1–0.6 pg g^{-1} ww for PBDEs, 0.1–0.3 pg g^{-1} ww for PBBs, and 0.8–1.0 pg g^{-1} ww for PBB209 and PBDE209, respectively. Spike-recoveries for $^{13}C_{12}$-labeled PBDEs (at 1 ng),

PCNB, TMX, and PCB209 were 73.5–94.6%, 80.4–105.3%, 70.2–91.7%, and 90.5–111.2%, respectively. Standard calibration curves were established for quantification and they fitted the data well (r^2 > 0.99).

Results

The values of ∑PBDEs and ∑PBBs refer to the sum of all targeted PBDE and PBB congeners, respectively. Information on the levels of ∑PBDEs and ∑PBBs in fish samples is summarized in Tables 1 and 2.

Table 1. Biometric information and concentrations of PBDEs (pg g^{-1} ww) in 12 fish species.

	Carp	Grass carp	Brass gudgeon	Trout	Top mouth culter	Cat-fish	Yellow catfish	Silver carp	Mandarin fish	Rock carp	Yellow-cheek carp	Basile-wsky
n	2	3	1	1	2	2	1	4	3	2	2	1
[a]Weight(kg)	2.4	2.7	1.2	0.4	0.44	0.2	0.33	1.51	0.25	0.53	0.22	0.2
[a]Length (cm)	36.8	41.5	24.5	21.6	31.15	30.35	29.2	40.05	24.7	26.42	33.25	17.7
BDE3	[b] -	8.21	-	-	-	-	-	-	-	-	-	-
BDE7	-	-	-	-	-	-	-	0.16	2.41	-	-	0.08
BDE15	4.78	2.27	-	-	3.58	-	-	-	4.65	-	-	-
BDE17	-	-	-	1.46	-	2.17	0.66	1.23	0.29	1.05	-	1.16
BDE28	4.21	2.92	1.67	13.47	7.77	18.21	14.67	14.79	9.69	15.38	1.89	22.02
BDE49	4.32	1.90	1.00	4.85	7.50	10.99	16.48	13.53	3.97	9.29	1.00	18.60
BDE71	2.76	1.98	1.15	4.72	7.21	10.44	15.68	12.79	4.49	8.81	1.09	18.61
BDE47	8.36	3.80	6.60	6.87	22.25	31.28	42.48	3.59	13.04	8.65	4.23	13.27
BDE66	0.21	0.55	1.27	1.24	1.17	0.57	6.19	-	1.57	0.83	-	-
BDE77	-	0.55	-	-	1.21	-	-	-	0.63	-	-	-
BDE10	0.13	0.19	0.28	-	2.79	4.0	4.33	-	0.61	-	-	-

0						1						
BDE119	0.55	0.37	0.20	-	2.59	3.99	4.46	1.62	0.47	0.23	0.62	1.38
BDE99	2.61	1.22	2.63	0.91	3.84	6.83	21.04	1.49	2.93	0.77	1.95	5.82
BDE85	0.89	1.23	-	0.92	5.03	7.51	6.07	-	1.07	-	-	-
BDE126	-	-	8.28	-	-	1.10	-	-	1.82	-	1.97	4.55
BDE154	1.25	0.53	1.59	0.66	8.23	11.55	11.36	0.85	4.00	2.07	0.71	0.65
BDE153	-	1.19	1.44	2.29	5.88	5.85	10.69	1.87	2.14	1.42	0.51	2.38
BDE138	-	-	-	-	-	-	-	-	-	-	-	-
BDE156	-	-	-	-	2.95	2.92	-	-	-	-	-	-
BDE184	-	-	-	-	-	-	-	-	-	-	-	-
BDE183	-	4.46	-	8.60	7.99	-	4.83	4.78	-	-	-	-
BDE191	-	4.82	-	-	-	-	-	6.84	-	-	-	-
BDE197	-	-	-	-	-	-	-	-	-	-	-	-
BDE196	-	-	-	-	-	-	-	-	-	-	-	-
BDE207	-	-	-	-	-	-	-	-	-	-	-	-
BDE206	-	-	-	-	-	-	-	3.85	3.36	-	-	-
BDE209	36.63	6.12	-	-	-	-	58.80	81.89	8.71	9.80	8.65	65.96
[c]ΣPBDEs	66.71	42.33	26.10	45.98	89.97	117.41	217.75	149.28	65.86	58.30	22.62	154.48

[a] average concentrations;

[b] "-": not detected;

[c] geometric mean.

Table 2. Biometric information and concentrations of PBBs (pg g^{-1} ww) in 12 fish species.

	Carp	Grass carp	Brass gudgeon	Trout	Top mouth culter	Catfish	Yellow catfish	Silver carp	Mandarin fish	Rock carp	Yellow-cheek carp	Basilewsky
n	2	3	1	1	2	2	1	4	3	2	2	1
[a] Weight(kg)	2.4	2.7	1.2	0.4	0.44	0.2	0.33	1.51	0.25	0.53	0.22	0.2
[a] Length(cm)	36.8	41.5	24.5	21.6	31.15	30.35	29.2	40.05	24.7	26.42	33.25	17.7
PBB1	1.25	3.05	1.49	1.33	2.67	0.80	2.32	0.81	2.36	3.18	-	-
PBB2	0.11	0.81	5.74	-	0.58	4.69	-	0.16	3.01	0.70	11.75	24.37
PBB3	-	-	2.54	-	-	2.09	-	-	-	-	-	-
PBB10	-	-	-	-	-	-	-	-	-	-	-	-
PBB4	-	-	-	-	-	-	-	-	-	-	-	-
PBB9	-	-	-	-	-	-	-	-	-	-	-	-
PBB7	2.98	1.13	-	-	2.56	-	-	-	7.07	-	-	-
PBB15	-	-	-	-	-	-	-	-	0.57	-	-	-
PBB30	-	-	-	-	-	-	-	-	0.40	0.94	-	-
PBB18	-	-	-	-	-	-	-	-	-	-	-	-
PBB29	-	-	-	-	-	-	-	-	1.68	-	-	-
PBB26	-	-	-	2.15	-	-	-	-	-	-	-	-
PBB31	1.96	1.23	1.02	5.10	2.60	9.41	4.45	8.21	4.73	11.27	3.40	16.20
PBB53	-	-	-	-	-	-	-	-	8.90	-	-	45.91
PBB38	0.61	0.34	-	1.72	0.45	2.68	1.84	0.45	1.28	1.29	1.09	4.63
PBB52	-	-	-	-	-	-	-	-	0.40	-	-	-
PBB49	10.13	4.62	7.51	7.62	24.35	40.91	47.10	6.41	12.84	9.60	8.61	25.19
PBB103	-	-	-	-	-	-	-	-	-	-	-	-

PBB101	-	0.51	-	-	1.42	-	2.82	-	0.84	3.96	-	-
PBB155	0.44	1.13	1.12	0.51	3.79	-	6.01	1.09	0.45	-	-	-
PBB153	2.43	1.29	3.24	1.12	12.17	18.04	14.10	2.52	4.87	3.86	0.99	3.59
PBB209	2.98	37.25	4.05	78.83	80.95	19.37	1.29	1.75	4.29	2.44	3.72	15.67
[c]ΣPBBs	33.02	56.08	34.30	106.06	155.75	138.51	126.64	27.83	59.40	46.83	38.19	123.98

[a] average values; [b] "-": not detected; [c] geometric mean.

The levels of PBDEs in muscle ranged from 22.62 (yellowcheek carp) to 217.75 (yellow catfish) pg g^{-1} ww (Table 1). BDE209 was the dominant BDE congener (contribution to PBDEs ranged from 26.97% to 54.59%) in five species (carp, yellow catfish, silver carp, yellowcheek carp, basilewsky); meanwhile, the level of BDE209 in these species ranged from 8.65 to 81.89 pg g^{-1} ww (Figure 2). BDE47 was the dominant congener in topmouth culter (22.25 pg g^{-1} ww, 24.74% of PBDEs), catfish (31.28 pg g^{-1} ww, 26.51% of PBDEs), and mandarin fish (13.04 pg g^{-1} ww, 19.76% of PBDEs). BDE28 was the main congener in trout (13.47 pg g^{-1} ww) and rock carp (15.38 pg g^{-1} ww) and the ratios of BDE28-to-PBDEs in these two species were 29.29% and 26.52%, respectively. The dominant BDE congener in grass carp was BDE3 (41.07 pg g^{-1} ww), with a BDE3/PBDEs ratio of 19.56%. The dominant BDE congener in brass gudgeon was BDE126 (41.38 pg g^{-1} ww), with a BDE126/PBDEs ratio of 31.83%. Furthermore, the sum of BDE47 and BDE209 in 11 fishes (except trout) accounted for 23.62% to 68.16% of total PBDEs.

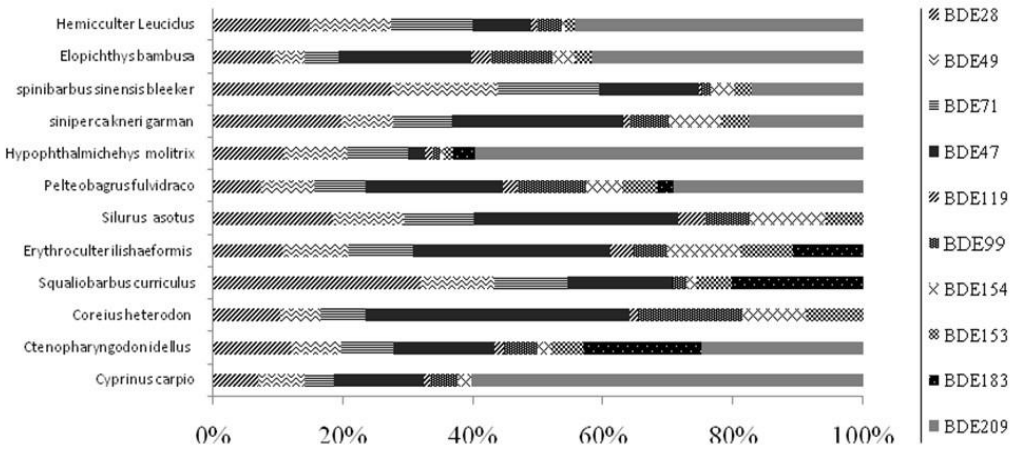

Figure 2. Relative abundances of individual PBDE congeners in fish samples.

For all samples, the levels of ∑PBBs in muscle ranged from 27.83 pg g^{-1} ww in silver carp to 155.75 pg g^{-1} ww in topmouth culter (Table 2). BB209 was the main congener in grass carp (186.26 pg g^{-1} ww), *Spualiobarbus curriculus* (394.13 pg g^{-1} ww), and topmouth culter (404.76 pg g^{-1} ww), with the BB209/PBBs ratios of 71.64%, 80.43%, and 61.33%, respectively (Figure 3). BB49 was the dominant BB congener (contribution to PBBs ranged from 25.71% to 58.87%) in six species (*Cyprinus carpio*, brass gudgeon, catfish, *Pelteobagrus fulvidraco*, *Siniperca kneri Garman*, basilewsky) with concentrations ranging from 37.54 to 235.49 pg g^{-1} ww. In addition, the dominant BB congener in the chub and *Spinibarbus sinensis* was BB31 (41.03 pg g^{-1} ww and 56.37 pg g^{-1} ww), which accounted for 37.30% and 29.67% of PBBs, respectively. The dominant BB congener in yellowcheek carp was BB2 (58.76 pg g^{-1} ww), with a ratio of 39.18% to PBDEs.

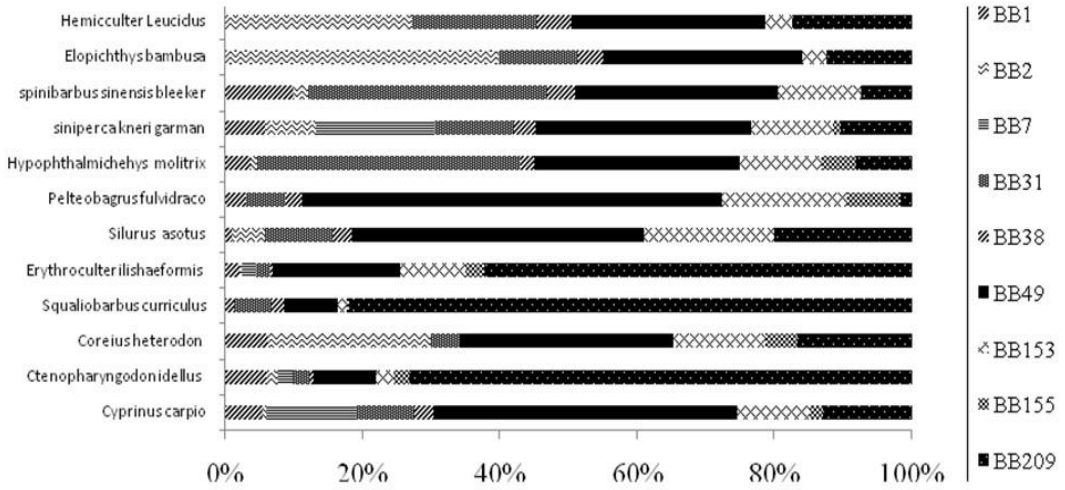

Figure 3. Relative abundances of individual PBB congeners in fishes.

Discussion

Concentrations of PBDEs in Fish

PBDE levels in muscle (22.62–217.75 pg g^{-1} ww) varied with the species type because of the bioaccumulative characteristics of

different species at different age groups. The concentrations of PBDEs in yellow catfish were higher (up to 217.75 pg g^{-1} ww) than those in other species (about 22.62 pg g^{-1} ww). The most frequently analyzed congener, BDE47, was used for comparison with other studies listed in Table 3. In the present study, mean PBDE concentrations in muscle were close to those from the Eastern China coastline (1.11 to 5.08 ng g^{-1} lipid weight) (Xia et al., 2011) and Bo Sea (0.31 to 2.73 ng g^{-1} dw), but lower than those from Europe (119 ng g^{-1} lipid weight) (Hayward, Wong, & Krynitsky, 2007), as well as from Taiwan (107 ng g^{-1} lipid weight) (Peng, Huang, Weng, & Yak, 2007).

Table 3. Levels of PBDEs and PBBs (ng g^{-1} ww) in fishes from other studies.

Location	Year	Units	PBDEs	BDE47	PBBs	BB153	References
TGR[a]	2010	Wet weight	0.11–1.09	0.02–0.21	0.14–0.78	0.01–0.09	Present study
Laurentian Great Lakes, Canada	1997	Wet weight	27–95	16-58	0.25–3.10	0.19–2.08	Luross et al. (2002)
Guangzhou, China[b]	2003–2004	Lipid weight	46.3	27.4	9.86	0.21	Jiang et al. (2005)
Zhoushan, China[c]	2003–2004	Lipid weight	6.72	2.87	2.09	0.02	Jiang et al. (2005)
Control site, Zhejiang, China	2007	Lipid weight	35.9	13.3	20.3	NA	Zhao et al. (2009)
Disassembly site, Zhejiang, China	2007	Lipid weight	43.3	17.2	79.9	5.2	Zhao et al. (2009)
Pearl River Estuary, China[d]	2004	Lipid weight	67.28–181.20	42.9–99.7	-	-	Xiang et al. (2007)
Yangtze River, China[e]	2006	Lipid weight	NA–1100	8.3–160	-	-	Xian et al. (2008)
Sir Dam Lake, Kahramanmaras, Turkey[f]	2003	Lipid weight	0.08–0.67	0.07–0.54	-	-	Perugini et al. (2004)
The Ross Sea, South of Italy[g]	2001–2002	Wet weight	0.09–0.44	-	-	-	Borghesi et al. (2009)
Mediterranean	2003	Wet	15.1	-	-	-	Borghesi et al.

Sea [h]		weight					(2009)
Wild caught, USA [i]	2004	Wet weight	0.04–38	-	-	-	Hayward, Wong, & Krynitsky (2007)
Farm-raised, USA [i]	2004	Wet weight	0.5–1.7	-	-	-	Hayward, Wong, & Krynitsky (2007)
Northeastern Pacific Ocean [j]	1993–1996	Lipid weight	203–1015	-	3.0–31	-	Rayne et al. (2004)
Ellasjøen and Øyangen [k]	1999 and 2001	Wet weight	-	<0.15–13.98	-	<0.09–0.59	Evenset, Christensen, & Kallenborn (2005)

[a] Including carp, grass carp, brass gudgeon, trout, topmouth culter, catfish, yellow catfish, silver carp, mandarin fish, rock carp, yellowcheek carp, and basilewsky

[b] White mouth croaker, belt fish, Japanese mackerel, silvery pomfret, and small yellow croaker

[c] Small yellow croaker, cinnamon flounder, white mouth croaker, conger pike, silvery pomfret

[d] Including silvery pomfret, robust tonguefish, large yellow croaker, and flathead fish

[e] Including carp, bream, perch

[f] Including native flounder, eel, native gray mullet, native horse mackerel, cultured flounder, native red sea bream, native sea bass, cultured yellowtail, and cultured red sea bream

[g] Including thynnus

[h] Including chinook, sockeye, and coho salmon

[i] Including Atlantic and Icelandic salmon fillets

[j] Including killer whales

[k] Including zooplankton, chironomid larvae, small Arctic char, and tadpole shrimps

"-" means not studied

PBDEs Congener Profiles

BDE209 was the dominant BDE congener in all samples, similar to the results from the Pearl River, Bo Sea, Dongguan, and Shunde (Zhang, Ni, Guan, & Zeng, 2010). Such a finding is not surprising because the annual global consumption of deca-BDE (i.e., PBDE209) is 28,000 ton, which accounts for as much as 70% of the total amount of PBDEs. These findings are in agreement with a previous study on PBDEs in sediments from the TGR (Zhao et al., 2013).

BDE47 was the main congener in three fish species, including topmouth culter, catfish, and mandarin fish, and the ratios of BDE47 to total PBDEs in these species were 24.74%, 26.51%, and 19.76%, respectively. This result is consistent with a previous study conducted in the Mediterranean Sea (Borghesi et al., 2009) and with the studies of different species in other parts of the world (Brown, Winkler, Visita, Dhaliwal, & Petreas, 2006; Aksoy et al., 2011; Liu et al., 2011). BDE47 and 99 were considered the dominant isomers in commercial penta-BDE products, accounting for 38.2% and 48.6% of the total product (DE-71) Evenset et al. (2005). The increasing use of the penta-BDE mixture in China may also lead to unwanted emissions of BDE47. The reasons for the abundance of BDE47 in fishes include source emissions and the debromination of PBDEs to BDE47 in organisms (Bezares-Crusz, Jafvert, & Hua, 2004; Stapleton, Letcher, & Baker, 2004; Zheng et al., 2016).

BDE28 was the main congener in trout (29.29%, 13.47 pg g^{-1} ww) and rock carp (26.52%, 15.38 pg g^{-1} ww). This result is on agreement with the findings for the Yangtse River (Xian et al., 2008) and Pearl River deltas (Guo et al., 2008). Past research demonstrated that BDE28 was the predominant photoproduct of BDE47 in surfactant micelles (Erdogrul, Covaci, & Schepens, 2005). Zhao et al. (2013) also detected high BDE28 concentrations in the study area. Therefore, the origin of high concentrations of BDE28 in fishes is the BDE28 in the environment.

The dominant BDE congener in grass carp and brass gudgeon was BDE3 (19.56%, 41.07 pg g^{-1} ww) and BDE126 (31.83%, 41.38 pg g^{-1} ww). The sum of BDE47 and BDE209 in 11 fish species (except trout) in the present study accounted for 23.62–68.16% of total PBDEs. BDE47 and BDE209 originated from penta-BDE and deca-BDE mixtures used in electrical or electronic products are the likely sources of BDE47 and BDE209 in fishes, respectively. The differences in species and sampling locations result in the differences in dominant BDE congeners (BDE47 or BDE209) in fish.

Ratio of BDE99/BDE100

The ratio of PBDE congeners is significant for exploring the mechanisms of bioaccumulation in organisms (Borghesi et al., 2009). In the present study, the ratio of BDE99 to BDE100 was different among species (varied from 42:58 to 5:95). It was 5:95 in carp, 13:87 in grass carp, 10:90 in brass gudgeon, 42:58 in topmouth culter, 37:63 in catfish, 17:83 in yellow catfish and mandarin fish (ratios were not calculated for trout, silver carp, rock carp, yellowcheek carp, and basilewsky because BDE100 or BDE99 was not detected in those samples). The average ratio of these congeners in fish was 30:70 (w/w) (Harris, Kiparississ, & Metcalfe, 1994) because BDE100 has a higher bioavailability or a lower biodegradability than BDE99.

The BDE99/BDE100 ratios in this study were less than 84:16 (ratio of BDE99 to BDE100 in the industrial product Bromkal70-5DE), indicating that the species used in this study had the ability to metabolize BDE99 or that BDE100 can pass through biota membranes more easily than BDE99 (Luross et al., 2002).

A relevant study reported the debromination of BDE99 to BDE47 in carp (Harris et al., 1994), which is considered a high metabolizer due to the lowest ratio of BDE99 to BDE100 (5:95). Both topmouth culter and catfish had higher BDE99/BDE100 ratios (42:58 and 37:63, respectively) and higher PBDE concentrations (89.97 and 117.14 pg g^{-1} ww, respectively). Although the BDE99/BDE100 ratio in carp was the lowest (5:95), the concentration of PBDE (66.71 pg g^{-1} ww) was higher. The differences in BDE99/BDE100 ratios and PBDE concentrations in different species suggested that, besides their living and feeding habits, the metabolization ability was important for the accumulation of PBDEs in biota. These results confirmed that the BDE99/BDE100 ratio depended on the species type as well as the location (Perugini et al., 2004).

Concentrations of PBBs in Fish

Tecnología y ciencias del agua, 10 (4), 46-65. DOI: 10.24850/j-tyca-2019-04-03

In all the samples, ∑PBBs ranged from 27.83 pg g^{-1} ww in silver carp to 155.75 pg g^{-1} ww in topmouth culter. These concentration levels were comparable to the results from other regions, such as Laurentian Great Lakes (Luross et al., 2002), Guangzhou, and Zhoushan (Jiang et al., 2005), but lower than those in fish samples collected from e-waste disassembly sites in Zhejiang (Zhao et al., 2009). This comparison might be confounding because of the differences in fish species and the amount of analyzed PBB congeners.

PBBs Congener Profiles

The relative abundance of each PBB congener in fish are shown in Fig. 3. BB49 and BB209 were the main congeners and detected in all fishes; however, the concentration of BB49 (4.62–47.10 pg g^{-1} ww) was similar to that in lake trout (6.8–125 pg g^{-1} ww) (Luross et al., 2002). In the present study, high concentrations (1.29–80.95 pg g^{-1} ww) and ratios (ratio of 100%) of BB209 were detected in most fishes, different from those detected in fish samples from Zhejiang (Zhao et al., 2009). The high proportion of BB209 in this study might be caused by the use of specific technical mixtures of PBBs in this area. Zhao et al. (2013) studied polyhalogenated aromatic hydrocarbons in surface sediments of the TGR and measured high concentrations of BB209. However, BB209 was not an important PBB congener reported in other studies. In other studies, BB153 was the most abundant congener in fishes (Rayne et al., 2004), while this study detected lower concentrations (1.29–18.04 pg g^{-1} ww) and smaller ratios of BB153-to-∑PBBs (2.30%–13.02%) (Table 2). These differences are likely caused by the differences in the study area and fish species. In addition, continual emissions of the hexa-BB mixture to the environment during the past few decades may lead to the high abundance of BB153 in the area (100%). Anaerobic debromination of commercial octa- and deca-BB mixtures is another factor that plays a role in the results.

PBDEs and PBBs in Different Fish Species

Topmouth culter, catfish, mandarin fish, and yellowcheek carp are carnivorous; grass carp that often feeds on phytoplankton, zooplankton, and bacteria is herbivorous; and carp, brass gudgeon, silver carp, rock carp, trout, yellow catfish, and basilewsky are omnivorous fish species. The concentration of ∑PBDEs was the highest in basilewsky and yellow catfish and the concentration of ∑PBBs was the highest in topmouth culter and catfish (Table 2). The levels of PBDEs and PBBs in carnivorous fish showed no significant difference from the levels in omnivorous or herbivorous fish ($P > 0.05$).

Relation of PBDE and PBB Concentrations with Fish Characteristics

We analyzed the relationship between PBDE and PBB concentrations and specific characteristics of fish. No significant correlation with the weight or length of the fish was observed in the TGR. This result is consistent with those of the previous studies conducted in the Hudson River, New York (Xia et al., 2008) and the Mediterranean Sea (Corsolini, Guerranti, Perra, & Focardi, 2008). However, some studies reported positive correlations between the concentrations of hydrophobic substances with fish length (Bordajandi, Martin, Abad, Rivera, & Gonzalez, 2006; Malakhova & Voronov, 2008).

Conclusion

This study is the first to investigate the concentrations and the distribution of PBBs and PBDEs in 12 edible fishes from the TGR. The results show that the levels of PBDEs and PBBs were, in general, low in fishes collected from the TGR. The relatively high levels of BDE209 and BB209 in fishes indicate that China is one of the major consumers of industrial compounds such as deca-BDE and deca-BB mixtures in Asia. The predominance of lower brominated PBDE and PBB congeners including BDE47 and BB49 in samples suggests that the debromination may play a key role in the fate of BFRs in the environment and more research

should be conducted in the transformation mechanisms of BFRs in biota. Furthermore, the levels and distribution of PBBs and PBDEs are related to the feeding habits of fishes.

Acknowledgments

This study is supported by the Research Fund of the State Key Laboratory of Simulation and Regulation of Water Cycle in River Basin, China Institute of Water Resources and Hydropower Research (No. 2016ZY02) and the Chinese National Natural Science Foundation (No. 51522907, No. 51279208).

References

Aksoy, A., Das, Y. K., Yavuz, O., Guvenc, D., Atmaca, E. & Agaoglu, S. (2011). Organochlorine Pesticide and Polychlorinated Biphenyls Levels in Fish and Mussel in Van Region, Turkey. *The Bulletin of Environmental Contamination and Toxicology,* 87(1), 65-69.

Alaee, M., Arias, P., Sjodin, A. & Bergman, A. (2003). An overview of commercially used brominated flame retardants, their applications, their use patterns in different countries/regions and possible modes of release. *Environment International*, 29 (6), 683-689.

Bezares-Cruz, J., Jafvert, C. T. & Hua, I. (2004). Solar photodecomposition of decabromodiphenyl ether: products and quantum yield. *Environmental Science and Technology*, 38(15), 4149-56.

Bordajandi, L. R., Martin, I., Abad, E., Rivera, J. & Gonzalez, M. J. (2006). Organochlorine compounds (PCBs, PCDDs and PCDFs) in seafish and seafood from the Spanish Atlantic southwest coast. *Chemosphere*, 64(9), 1450-1457.

Borghesi, N., Corsolini, S., Leonards, P., Brandsma, S., de Boer, J. & Focardi, S. (2009). Polybrominated diphenyl ether contamination levels in fish from the Antarctic and the Mediterranean Sea. *Chemosphere*, 77(5), 693-698.

Brown, F. R., Winkler, J., Visita, P., Dhaliwal, J. & Petreas, M. (2006). Levels of PBDEs. PCDDs, PCDFs, and coplanar PCBs in edible fish from California coastal waters. *Chemosphere*, 64(2), 276-286.

Corsolini, S., Guerranti, C., Perra, G. & Focardi, S. (2008). Polybrominated diphenyl ethers, perfluorinated compounds and chlorinated pesticides in swordfish (Xiphias gladius) from the Mediterranean Sea. *Environmental Science and Technology*, 42(12), 4344-4349.

De Wit, C. A. (2002). An overview of brominated flame retardants in

the environment. *Chemosphere,* 46(5), 583-624.

EPA. (1996). *Method 3630C-Silica Gel Cleanup, SW-846 Manual, 3rd Ed.* Environmental Protection Agency.

Erdogrul, O., Covaci, A. & Schepens, P. (2005). Levels of organochlorine pesticides, polychlorinated biphenyls and polybrominated diphenyl ethers in fish species from Kahramanmaras, Turkey. *Environment International*, 31(5), 703-711.

Evenset, A., Christensen, G. N. & Kallenborn, R. (2005). Selected chlorobornanes, polychlorinated naphthalenes and brominated flame retardants in Bjornoya (Bear Island) freshwater biota. *Environmental Pollution*, 136(3), 419-430.

Guo, L. L., Qiu, Y. W., Zhang, G., Zheng, G. J., Lam, P. K. S., & Li, X. D. (2008). Levels and bioaccumulation of organochlorine pesticides (OCPs) and polybrominated diphenyl ethers (PBDEs) in fishes from the Pearl River estuary and Daya Bay, South China. *Environmental Pollution*, 152(3), 604-611.

Harris, G. E., Kiparissis, Y. & Metcalfe, C. D. (1994). Assessment of the Toxic Potential of Pcb Congener-81 (3,4,4',5-Tetrachlorobiphenyl) to Fish in Relation to Other Non-Ortho-Substituted Pcb Congeners. *Environmental Toxicology and Chemistry*, 13(9), 1405-1413.

Hayward, D., Wong, J. & Krynitsky, A. J. (2007). Polybrominated diphenyl ethers and polychlorinated biphenyls in commercially wild caught and farm-raised fish fillets in the United States. *Environmental Research*, 103(1), 46-54.

Jiang, Q. T., Lee, T. K. M., Chen, K., Wong, H. L., Zheng, J. S., Giesy, J. P., Lo, K. K. W., Yamashita, N. & Lam, P. K. S. (2005). Human health risk assessment of organochlorines associated with fish consumption in a coastal city in China. *Environmental Pollution*, 136(1), 155-165.

Law, R. J., Covaci, A., Harrad, S., Herzke, D., Abdallah, M. A. E., Femie, K., Toms, L. M. L. & Takigami, H. (2014). Levels and trends of PBDEs and HBCDs in the global environment: Status at the end of 2012. *Environment International*, 65, 147-158.

Liu, Y. P., Li, J. G., Zhao, Y. F., Wen, S., Huang, F. F. & Wu, Y. N. (2011). Polybrominated diphenyl ethers (PBDEs) and indicator polychlorinated biphenyls (PCBs) in marine fish from four areas of China. *Chemosphere*, 83(2), 168-174.

Luross, J. M., Alaee, M., Sergeant, D. B., Cannon, C. M., Whittle, D. M., Solomon, K. R. & Muir, D. C. G. (2002). Spatial distribution of polybrominated diphenyl ethers and polybrominated biphenyls in lake trout from the Laurentian Great Lakes. *Chemosphere*, 46(5), 665-672.

Malakhova, L. & Voronov, V. (2008). Organochlorine pollution of mariculture objects of the Crimea coastal area (Black Sea). *The NATO Science for Peace and Security Programme*, 169-176.

Osako, M., Kim, Y. J. & Sakai, S. I. (2004). Leaching of brominated flame retardants in leachate from landfills in Japan. *Chemosphere,* 57(10), 1571-1579.

Peng, J. H., Huang, C. W., Weng, Y. M. & Yak, H. K. (2007). Determination of polybrominated diphenyl ethers (PBDEs) in fish samples from rivers and estuaries in Taiwan. *Chemosphere,* 66(10), 1990-1997.

Perugini, M., Cavaliere, M., Giammarino, A., Mazzone, P., Olivieri, V. & Amorena, M. (2004). Levels of polychlorinated biphenyls and organochlorine pesticides in some edible marine organisms from the Central Adriatic Sea. *Chemosphere*, 57(5), 391-400.

Rayne, S., Ikonomou, M. G., Ross, P. S., Ellis, G. M. & Barrett-Lennard, L. G. (2004). PBDEs, PBBs, and PCNs in three communities of free-ranging killer whales (Orcinus orca) from the northeastern Pacific Ocean. *Environmental Science and Technology*, 38(16), 4293-4299.

Stapleton, H. M., Letcher, R. J. & Baker, J. E. (2004). Debromination of polybrominated diphenyl ether congeners BDE 99 and BDE 183 in the intestinal tract of the common carp (Cyprinus carpio). *Environmental Science and Technology*, 38(4), 1054-61.

Wang, Z., Ma, X., Lin, Z., Na, G. & Yao, Z. (2009). Congener specific distributions of polybrominated diphenyl ethers (PBDEs) in sediment and mussel (Mytilus edulis) of the Bo Sea, China. *Chemosphere,* 74(7), 896-901.

Wang, X. T., Chen, L., Wang, X. K., Zhang, Y., Zhou, J., Xu, S. Y., Sun, Y. F. & Wu, M. H. (2015). Occurrence, profiles, and ecological risks of polybrominated diphenyl ethers (PBDEs) in river sediments of Shanghai, China. *Chemosphere,* 133, 22-30.

Wang, J., Bi, Y., Henkelmann, B., Wang, Z., Pfister, G. & Schramm, K.-W. (2017). Levels and distribution of polybrominated diphenyl ethers in Three Gorges Reservoir, China. *Emerging Contaminants*, 3(1).

Xia, K., Luo, M. B., Lusk, C., Armbrust, K., Skinner, L. & Sloan, R. (2008). Polybrominated diphenyl ethers (PBDEs) in biota representing different trophic levels of the Hudson River, New York: From 1999 to 2005. *Environmental Science and Technology*, 42(12), 4331-4337.

Xia, C. H., Lam, J. C. W., Wu, X. G., Sun, L. G., Xie, Z. Q. & Lam, P. K. S. (2011). Levels and distribution of polybrominated diphenyl ethers (PBDEs) in marine fishes from Chinese coastal waters.

Chemosphere, 82(1), 18-24.

Xian, Q. M., Ramu, K., Isobe, T., Sudaryanto, A., Liu, X. H., Gao, Z. S., Takahashi, S., Yu, H. X. & Tanabe, S. (2008). Levels and body distribution of polybrominated diphenyl ethers (PBDEs) and hexabromocyclododecanes (HBCDs) in freshwater fishes from the Yangtze River, China. *Chemosphere*, 71(2), 268-276.

Xiang, C. H., Luo, X. J., Chen, S. J., Yu, M., Mai, B. X. & Zeng, E. Y. (2007). Polybrominated diphenyl ethers in biota and sediments of the Pearl River Estuary, South China. *Environmental Toxicology and Chemistry*, 26(4), 616-623.

Yu, G., Bu, Q. W., Cao, Z. G., Du, X. M., Xia, J., Wu, M. & Huang, J. (2016). Brominated flame retardants (BFRs): A review on environmental contamination in China. *Chemosphere,* 150, 479-490.

Zhang, B. Z., Ni, H. G., Guan, Y. F. & Zeng, E. Y. (2010). Occurrence, bioaccumulation and potential sources of polybrominated diphenyl ethers in typical freshwater cultured fish ponds of South China. *Environmental Pollution*, 158(5), 1876-1882.

Zhang, W., Lu, Y., Gao, S., Jia, X., Yu, Z., Zeng, X., Sheng, G. & Fu, J. (2015). Determination of polybrominated diphenyl ethers in soils and sediment of Hanfeng Lake, Three Gorges. *Journal of Environmental Science and Health. Part A, Toxic/Hazardous Substances & Environmental Engineering*, 50(13), 1316-1323.

Zhao, G. F., Zhou, H. D., Wang, D. H., Zha, J. M., Xu, Y. P., Rao, K. F., Ma, M., Huang, S. B. & Wang, Z. J. (2009). PBBs, PBDEs, and PCBs in foods collected from e-waste disassembly sites and daily intake by local residents. *Science of the Total Environment*, 407(8), 2565-2575.

Zhao, G., Li, K., Zhou, H., Liu, X., Zhang, P., Wen, W., Yu, Y., & Yuan, H. (2013). Polyhalogenated aromatic hydrocarbons in surface sediments from Three Gorges Reservoir. *Journal of Environmental Science and Health, Part A*, 48(2), 136-144.

Zheng, B. H., Zhao, X. R., Ni, X. J., Ben, Y. J., Guo, R., & An, L. H. (2016). Bioaccumulation characteristics of polybrominated diphenyl ethers in the marine food web of Bohai Bay. *Chemosphere*, 150, 424-430.

DOI: 10.24850/j-tyca-2019-04-04
Special Article

Rationality Analysis of the Heihe River '97' Water Diversion Scheme under Changing Environment

Análisis de racionalidad del esquema '97' de desviación del agua del río Heihe bajo un entorno cambiante

M. Zhao[1]
X. Jiang[2]*
Q. Huang[3]
G. Dong[4]

[1]State Key Laboratory Base of Eco-Hydraulic Engineering in Arid Area, Xi'an University of Technology, Shaanxi, China, email: mlzhao1314@outlook.com, ORCID 0000-0003-0474-2637

[2]Northwest University, Shaanxi, China, email: xhjiang@nwu.edu.cn, ORCID 0000-0002-3805-5766

[3]State Key Laboratory Base of Eco-Hydraulic Engineering in Arid Area, Xi'an University of Technology, Shaanxi, China, email: syhuangqiang@163.com, ORCID 0000-0001-9183-9298

[4]Institute of Hydraulic Research, YRCC, Henan, China, email: dongguotao@hky.yrcc.gov.cn, ORCID 0000-0002-1292-2091

*Corresponding author: Xiaohui Jiang, email: xhjiang@nwu.edu.cn

Abstract

The environmental condition has changed after the implementation of the '97' water diversion scheme, and there are still queries regarding the rationality of the water diversion scheme due to the potential difficulty of completing the releasing goal of Zhengyixia section. This paper simulated the implementation of the scheme through a simulation model for water resources allocation in the Heihe River. Then, the rationality of the water diversion scheme was evaluated. Results indicated that, in the current water demand situation, the releasing indicator could not be completed. The releasing indicator could be accomplished under two returning farmland schemes in the midstream, but the irrigation guarantee rate is low and the groundwater is overused.

Therefore, there are some irrationalities between the '97' water diversion scheme based on economic, social and hydrologic conditions in the Heihe River in the mid-1980s and the current situation of the Heihe River Basin.

Keywords: Rationality, changing environment, ecological restoration, the Heihe River, water resources allocation, '97' water diversion scheme.

Received: 18/12/2018

Accepted: 21/03/2019

Introduction

The Heihe River is the second largest inland river in China. In recent decades, the water demand in the middle reaches of the Heihe River had increased dramatically (Huang et al. 2016c) with the rapid regional development of the economy and society. This has resulted in a significant decrease in the releasing water to the lower reaches, vegetation degeneration and the disappearance of lakes. One of the most severe challenges is sustainable management due to a shortage of water resources (Kharrazi et al. 2016; Huang et al. 2016a; Huang et al. 2016b). To curb the trend of ecological degradation in the lower reaches of the Heihe River, the Yellow River Conservancy Commission of the Ministry of Water Resources has developed a water diversion scheme for the middle and lower reaches of the Heihe River in different inflow years. After implementing the scheme, the utilization efficiency of water resources has been improved dramatically, and the domestic, productive and ecological water in the basin has been allocated reasonably (Jiang & Liu 2009; Tang & Jiang 2009; Zhang et al. 2011; Zhao & Huang 2015).

However, some increasingly severe problems about the water diversion scheme have been exposed. On the one hand, the middle reaches of the Heihe River faced critical water shortage constraints because of the intensive evapotranspiration, limited water inflow, minimal precipitation, and obligatory water discharge to downstream since 2000. As a result, the environment in the middle reaches has degenerated, and the restoration of the oasis in the lower reaches of the Heihe River has still not been reached (Jiang et al. 2009; Lu et al. 2011). On the other hand, under the demand of the '97' water diversion scheme, the releasing water of the Zhengyixia section is still not adequate. The

inadequate scheme showed that the higher the inflow was, the more difficult it was to achieve the mission. The problem of inadequate releasing water of the Zhengyixia section has become a major concern (Liu & Wang 2012; Wu et al. 2015). Gansu Province and Inner Mongolia Autonomous Region cannot reach an agreement on how to implement the '97' water diversion scheme. The economic and social conditions, as well as the hydrologic connectivity in the Heihe River, had changed significantly after the implementation of the water diversion scheme. Therefore, it is necessary to systematically analyze the implementation of the water diversion scheme through a quantitative manner under changing environment, and scientifically evaluate the rationality of the '97' water diversion scheme, thereby providing a solid basis for the scientific management of water resources in the Heihe River Basin.

Study Area

The Heihe River Basin covers the Inner Mongolia Autonomous Region, Qinghai and Gansu Provinces from upper reaches to lower reaches, whose area is about 134 000 km^2. The Heihe River is divided into three parts by Yingluoxia section and Zhengyixia section. Figure 1 shows the map of the Heihe River Basin.

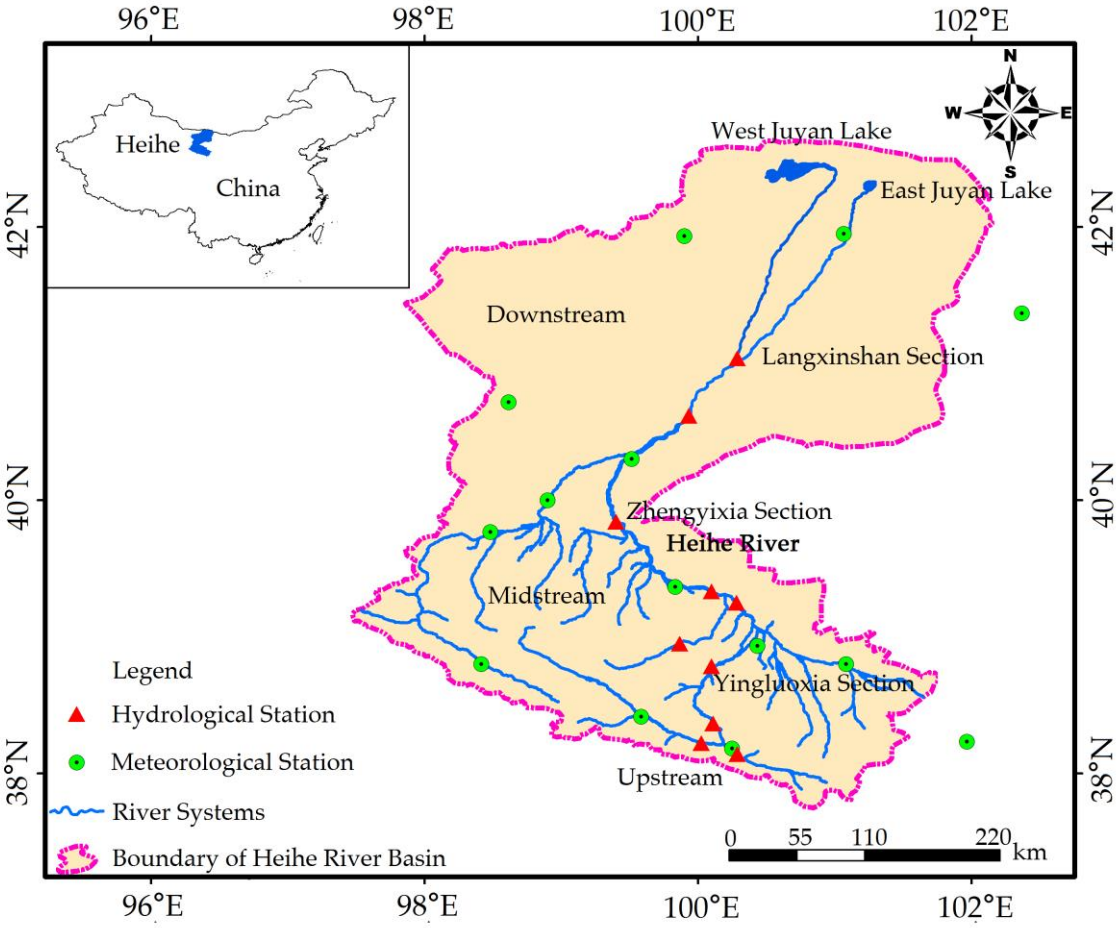

Figure 1. Map of the Heihe River Basin.

Change after the Establishment of the Water Diversion Scheme

The '97' water diversion scheme was made according to hydrological data and the economic and social conditions from 1955 to 1986.

Tecnología y ciencias del agua, 10 (4), 66-87. DOI: 10.24850/j-tyca-2019-04-04

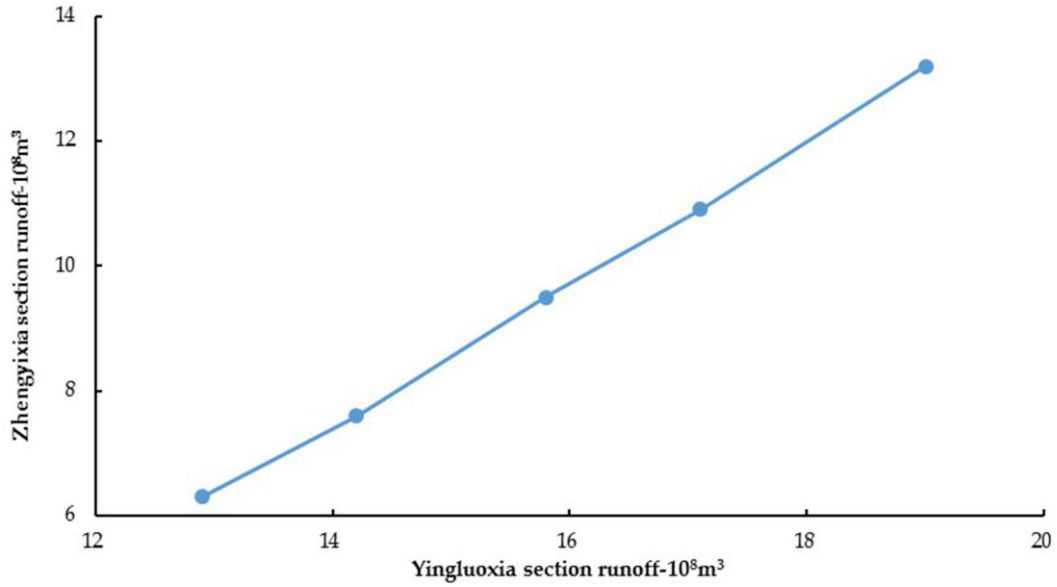

Figure 2. The '97' water diversion scheme.

Details of the '97' water diversion scheme are shown in Figure 2. The aim of the '97' water diversion scheme is to ensure water usage in the middle reaches in low flow years, and to allocate more water to the downstream in high flow years. The premise of implementing water diversion scheme is that water-saving irrigation measures should be adopted in the middle reaches, and the irrigation area could not expand anymore. However, the basic conditions have changed significantly since the establishment of the water diversion scheme.

The hydrologic connectivity in the middle reaches of the Heihe River has changed significantly after the establishment of the water diversion scheme. Because the irrigation area in the tributary was small in the 1950s and 1960s, there was only one mountain reservoir, which supplied about 2-3 × 10^8 m^3 water to the mainstream. By the end of 1980's, due to the sustained development of the irrigation, the reservoirs had increased to 19, which only supplied about 0.7-0.9 × 10^8 m^3 water to the mainstream. By the end of 1990's, there were 23 tributary reservoirs. The inflow of the tributaries was effectively retained and consumed. Many of the main streams and tributaries completely lost surface hydraulic connections, which fundamentally caused changes in the water resources conditions from the tributaries to the mainstream. The basic conditions of synchronization between the tributaries and the mainstream are not held anymore.

The economic and social conditions in the middle reaches of the Heihe River have changed greatly since the construction of the water diversion scheme. The agriculture and economy in Zhangye have developed fast since 1980-1990's. Through water consumption analysis

in the mid-1980s and the end of 1990s, the population increased by 152.9 thousand, the cultivated land increased by 373.6 km^2, and the agricultural water consumption increased by 2.21×10^8 m^3. The annual water consumption was approximately 8.3×10^8 m^3, whereas the available amount confirmed in the current water allocation scheme was only 6.3×10^8 m^3.

The area of cultivated land in the middle and lower reaches of the Heihe River has increased greatly since the implementation of the '97' water diversion scheme. The cultivated land area in the middle reaches increased by 280 km^2, and the water consumption exceeded approximately 2×10^8 m^3. In Ejina Qi, the cultivated land area increased by 60 km^2, which caused more than 0.7×10^8 m^3 of the water used for agricultural activities.

Implementation of the '97' Water Diversion Scheme

The water dispatching of the Heihe River improved the downstream environment by reducing the middle irrigation water usage and increasing the water volume to the downstream. According to the principle of "full-scale closed, centralized discharge" during the key scheduling period, the water diversion modes were roughly divided into three stages. First, from 2000 to 2003, the measures of "full-scale closed" were at the trial stage; the water diversion mode had not been fixed. Second, when water division moved into the mature stage in 2004 to 2007, measures of "full-scale closed, centralized discharge" were conducted in mid-July, mid-August and early September till the end of October every year. The time table had been substantially fixed, which achieved good effects. Finally, ecological water dispatching has been implemented since 2008. In order to adapt to the change in the planting structure in the midstream and the ecological water requirement in the downstream, the time of closed spring scheduling was extended, which improved the water discharged in the spring of the Zhengyixia section. Satisfactory results have been achieved since the water division was implemented, and the total actual amount of discharged water in the Zhengyixia section was 132.04×10^8 m^3 (annual average 10.16×10^8 m^3), which has been increased significantly from the 1990s.

According to the analysis of the runoff data from 2000 to 2015, the Zhengyixia section suffered a decrease of 24.3×10^8 m^3 water volume annually and accounted for 10.9% of the water volume that should

have been discharged. Compared with the annual target amount of the discharged water, the actual amount of discharged water of the Zhengyixia section was lower.

Since the water diversion scheme has been implemented, most of the years were high flow years. The rationality to different inflows of the scheme cannot be evaluated because the water diversion scheme has not been tested over a long period of time. The implementation of the scheme under the different water requirements from 1954 to 2012 was simulated by a simulation model for water resources allocation in the middle and lower reaches of the Heihe River, and the rationality of the water diversion scheme was evaluated.

Methods

Global methods for water resources allocation can be mainly divided into three categories: optimization, simulation and a combination of both (You et al. 2006; Thevs et al. 2014). Generally, the result of an optimization method can be obtained by establishing a mathematical model, setting the target and determining the constraints. However, due to the complexity of the water resources system, it is difficult to construct a complete model with the objective function and constraints; moreover, the model may be too complicated to solve or the optimization results do not correspond to the actual situation. The simulation model emphasizes the description of the details. Through the simulation and control of each process of the water resources system, water resources were allocated under the pre-set rules or constraints. Compared to the optimization model, the simulation model is more flexible and adaptable, and it is easier to combine the experience of professionals.

Considering the characteristics of complex transformation between surface water and groundwater and the allocation of water resources mainly under artificial control, the paper generalized the water resources system using abstraction and generalization methods and proposed a set of simulation processes that are controlled by rules. Then, the simulation model for the water resources allocation in the middle and lower reaches of the Heihe River was established through the process of object-oriented programming.

Construction of the Model

The water resources system of the Heihe River Basin is a complex and complete system that consists of surface water and groundwater such as rivers, reservoirs and spring water. Therefore, the water transformation characteristics of the middle reaches of the Heihe River Basin and factors of water balance, such as the seepage of the river course, discharge of spring water, phreatic water evaporation and field infiltration of canal system, should be included in the water resources allocation model of the Heihe River to capture the water balance calculation under different scenarios of inflow and water consumption.

The water allocation models of the Heihe River mainstream mainly included a groundwater equilibrium model of the irrigation area in the middle reaches, a water resources balance model between supply and demand and a water resources allocation model. The groundwater equilibrium model was mainly used to calculate the groundwater replenishment under different water allocation schemes and releasing balances. The water resources balance model between supply and demand and the water resources allocation model were mainly used to analyze the water demand, supply and shortage in irrigation areas and to calculate the water resources. The framework of the water resources model is shown in Figure 3.

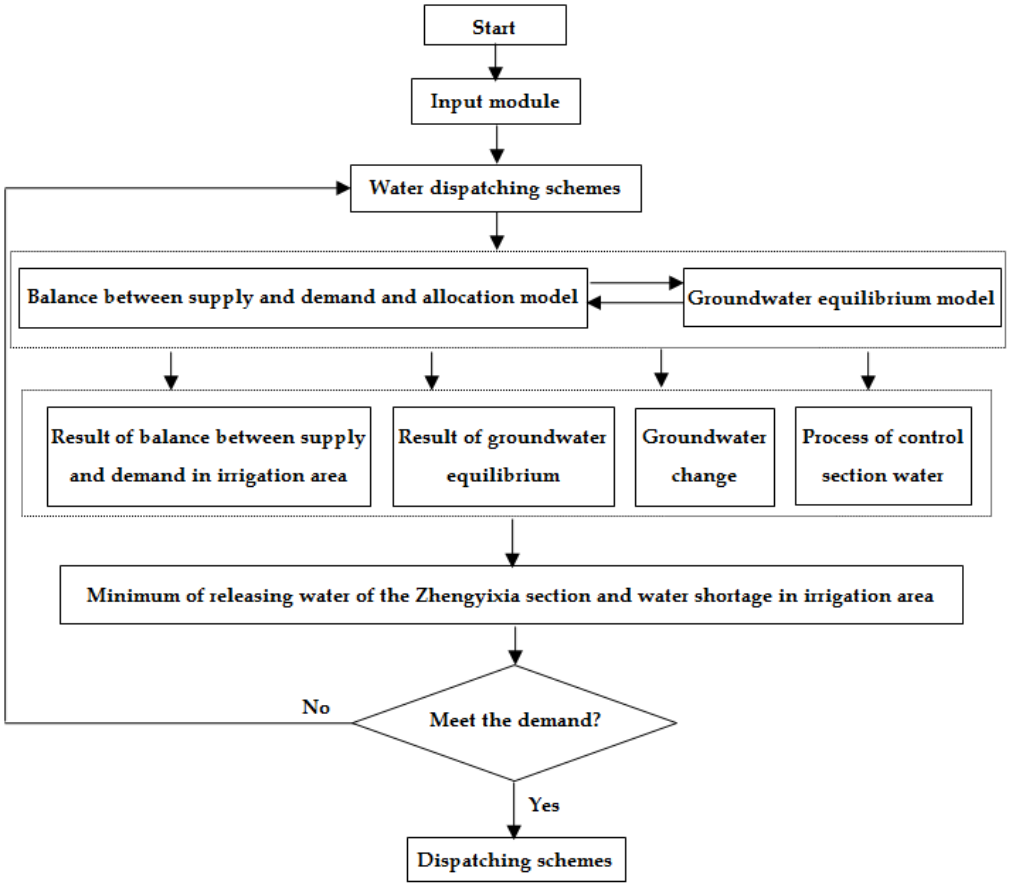

Figure 3. Frame of the water resources allocation model.

Groundwater Equilibrium Model in the Middle Reaches of the Heihe River

East of middle reaches of the Heihe River mainstream, the replenishment and drainage of groundwater were calculated using the scale of the irrigation unit. Replenishment comes from the aquifer of the calculated area of precipitation, surface water infiltration and groundwater runoff in per unit time under the conditions of a natural state or artificial exploitation, including Piedmont groundwater lateral replenishment, condensate rainfall infiltration replenishment, channel leakage replenishment, canal seepage replenishment, field infiltration, underground lateral runoff replenishment, and plain reservoir seepage replenishment. Based on the methods of drainage, the drainage was divided into potential water evaporation, groundwater exploitation, spring overflow, and underground lateral runoff drainage.

Tecnología y ciencias del agua, 10 (4), 66-87. DOI: 10.24850/j-tyca-2019-04-04

After considering replenishment and drainage, the water balance equation can be expressed as follows:

$$\Delta w = \left(q_{pl} + q_r + q_{li} + q_p + q_c + q_f + q_b\right) - (q_\varepsilon + q_{lo} + q_s + q_m)$$

Where Δw denotes the groundwater balance difference; q_{pl} is the piedmont lateral water infiltration amount; q_r represents the river infiltration amount; q_{li} denotes the section lateral inflows; q_p denotes the amount of precipitation and condensed water infiltration; q_c is the canal water infiltration capacity; q_f denotes the field water infiltration capacity; q_b denotes the urban and rural industrial water covering groundwater infiltration amount; q_ε stands for the potential water evaporation and plant transpiration; q_{lo} denotes the section lateral outflow, q_s denotes the amount of spring water overflow; and q_m denotes the artificial exploitation.

The Water Balance Model between Supply and Demand

According to the principle of water balance and based on the groundwater equilibrium pattern and using the irrigation areas as the unit, the model consisted of a calculation of the discharged flow and analysis of water balance between supply and demand and water shortage in the irrigation areas of the Zhengyixia control cross-section. The principle of the water resources allocation considered the priority of groundwater to supply industrial and domestic water in urban and rural areas and irrigation water with the use of high and new water-saving technologies. Agriculture water and other water utilization in the irrigation areas were supplied by surface water, and the insufficient portion was supplied by groundwater within the limit of groundwater exploitation.

The rationale of the water balance model between supply and demand could be described by the following mathematical model.

Water balance between supply and demand:

$$\mathrm{w}_p = \mathrm{w}_s + \mathrm{w}_\varepsilon$$

$$\mathrm{w}_l = \mathrm{w}_p - \mathrm{w}_n$$

Tecnología y ciencias del agua, 10 (4), 66-87. DOI: 10.24850/j-tyca-2019-04-04

Balance of surface water:

$$q_s = a_i g f_i$$

$$q_o = q_i + q_s - w_s - q_d$$

Balance of groundwater:

$$w_r = q_{pl} + q_r + q_{li} + q_p + q_c + q_f + q_b$$

$$w_d = q_\varepsilon + q_{lo} + q_s + q_m$$

$$\Delta w = w_r - w_d$$

Constraint:

$$w_\varepsilon \leq w_{max}$$

$$\Delta w \leq \beta$$

Where w_p denotes the total water supply in the irrigation areas, w_s represents the surface water supply in the irrigation areas, w_ε is groundwater exploitation in irrigation areas, q_d denotes the channel loss, w_l represents the strength of spring overflow, f_i denotes the area of spring overflow, q_i represents the surface influx in the irrigation areas, q_o is the surface outflow in the irrigation areas, w_r denotes the groundwater recharge of the boundary in the irrigation areas, w_d denotes the groundwater replenishment of the boundary in the irrigation areas, w_{max} denotes the limitation of groundwater exploitation in the irrigation areas, and β denotes the groundwater equilibrium constraints.

Generalization of the Water Resources System in the Heihe River

Tecnología y ciencias del agua, 10 (4), 66-87. DOI: 10.24850/j-tyca-2019-04-04

The principle of the water resources system generalization utilizes the water distribution unit as the center and the Heihe River as the main line on the basis of the entire basin, different calculation units, administrative regions (inter-provincial and inter-county) and the entrance of the water diversion (combined) of each calculation unit. The water control section was utilized as a water quantity control node. With consideration of the tributaries which have hydraulic connections with the Heihe River surface water, the calculating units were divided according to administrative divisions, which will not break the irrigation divisions.

According to the actual operating conditions and administrative subordination relations, the middle reach based on irrigation area, the lower reach based on the river trend, the scientific research base, the national defense base and the ecological oasis, the calculating units of the water allocation are divided into 24 sections. Based on the needs of the water resources allocation and to reflect the internal relations among each of the main factors that can affect the analysis of supply and demand, the frame of the water resources system in the Heihe River Basin was simplified by calculating the spatial relationship and hydraulic connections among units, surface drainage, groundwater, large or medium-sized and key hydraulic engineering, as shown in Figure 4.

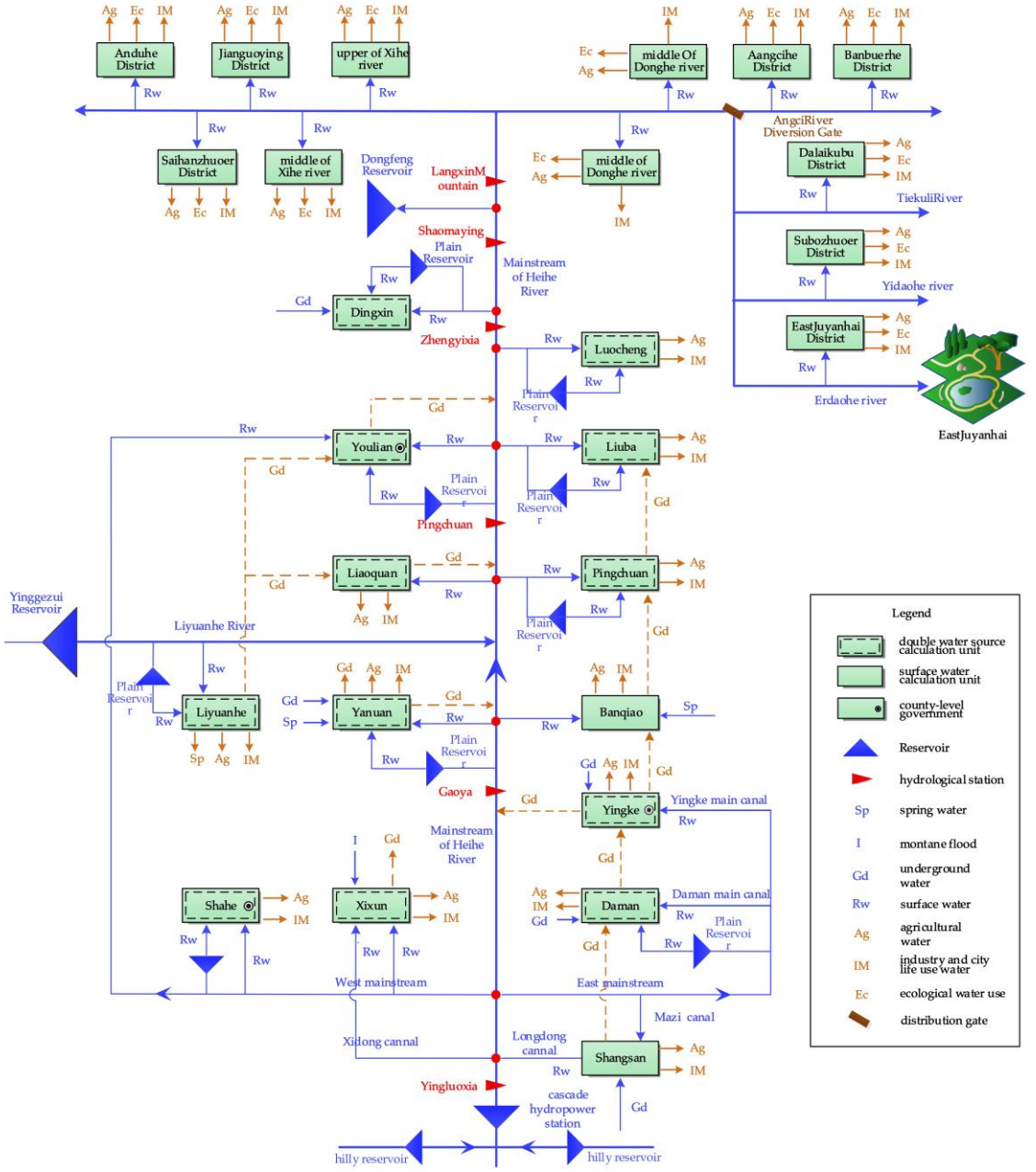

Figure 4. Water resources system frame in Heihe River Basin.

Model Verification

To examine the rationality of this model, the groundwater level of each irrigation area and the stream flow of each river section for the period from 2005 to 2010 were simulated, and the equilibrium relationships among the groundwater replenishment capacity, total water discharge

Tecnología y ciencias del agua, 10 (4), 66-87. DOI: 10.24850/j-tyca-2019-04-04

and groundwater storage variable of each irrigation area were analyzed. According to "The Supplementary Details of Groundwater Resources Amount and Allowable Groundwater Withdrawal", the absolute value of the relatively balanced error should be less than 10% for the computational accuracy of groundwater balance in the flat area. It can be seen from the simulation results that, the model can efficiently fit the water balance in the irrigation area, and the imitative effects of the cross-section streamflow were good.

Simulation Results under the Present Water Demand Condition

According to the water demand in the middle reaches of the Heihe River in an actual year, the completion of the water division scheme from 1954 to 2012 was obtained by calculating the model. Figure 5 shows the simulation results of water diversion scheme under the present water demand conditions from 1954 to 2012. Table 1 shows the simulation of the releasing indicator under present water demand conditions in different typical years. The irrigation guarantee rate was calculated as flows:

$$Irrigation\ guarantee\ rate = \frac{n}{N+1}$$

where *n* denotes the number of years when the irrigation was satisfied, *N* means the total years.

Tecnología y ciencias del agua, 10 (4), 66-87. DOI: 10.24850/j-tyca-2019-04-04

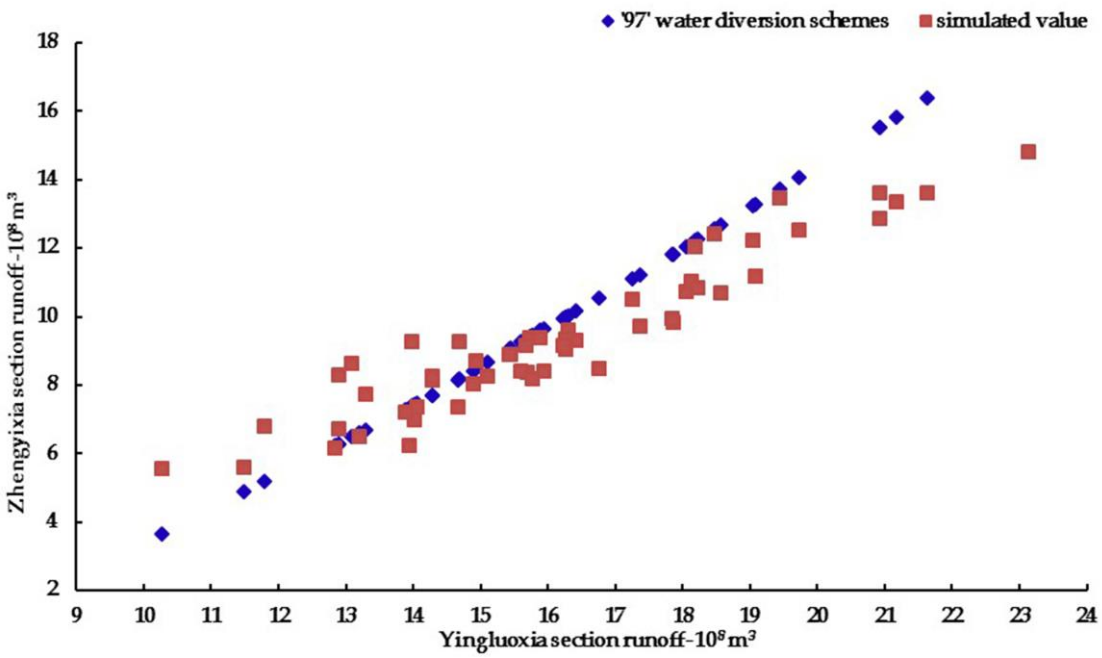

Figure 5. Simulation results of the water diversion scheme under present water demand conditions from 1954-2012.

Table 1. Simulation of the releasing indicator under present water demand in different typical years. Unit: 10^8 m^3.

Typical years	Yingluoxia section	Zhengyixia section			Groundwater exploitation	Irrigation guarantee rate	Simulated of Langxinshan section
		Releasing indicator	Simulated releasing	Water shortage			
Extreme high	20.27	14.73	13.10	-1.64	6.75	0.0%	7.05
Partial high	17.69	11.63	10.37	-1.26	6.92	0.0%	5.45
Normal	15.63	9.29	9.22	-0.07	7.30	0.0%	4.84
Partial low	14.56	8.10	7.80	-0.30	7.54	0.0%	4.00
Extreme low	12.79	6.19	7.06	0.87	7.88	0.0%	3.74
Average	16.16	9.95	9.39	-0.55	7.30	0.0%	4.94

The simulation of releasing water was less than the releasing indicator in the Zhengyixia section in high flow years, and the water volume discharged to the downstream section fell by 1.64 × 10^8 m^3 in extreme high flow years and 1.26 × 10^8 m^3 in partial high flow years. The releasing indicator can be completed in normal flow years and partial

low flow years. The water volume discharged to the downstream section increased by 0.87 × 10^8 m^3 in extreme low flow years. The average annual water volume discharged to the downstream section fell by 0.55 × 10^8 m^3, which was more than allowable deviation (0.5 × 10^8 m^3). The average annual groundwater exploitation was 7.3 × 10^8 m^3, which was far more than allowable groundwater exploitation (4.8 × 10^8 m^3). Hence, we can see from the results that, in the current water demand situation, the releasing indicator could not be completed, and long-term overexploitation of groundwater will worsen the ecological environment in the middle reaches.

Simulation Results under the Cultivated Land in the Midstream Decreased

The main reason that the releasing indicator cannot be achieved in high flow years was the increasing water demand in the midstream. The increase in cultivated land in the midstream was the main driving factor for the increase in water demand, and the reduction in water demand in the midstream was an important approach for reaching the releasing indicator in high flow years under the '97' water diversion scheme. There were two schemes for returning farmland in the midstream to the level in 2000 and to "The Planning of the Heihe River's Government in recent years", which aimed to accordingly calculate agricultural water demand and then simulate the completion of the releasing indicator under two water demand schemes from 1954 to 2012.

Figure 6 illustrates the simulation results of the water diversion scheme from 1954 to 2012 underwater demand level in 2000. Table 2 shows the simulation of the releasing indicator under the 2000 water demand in different typical years. As shown in Table 2, the Zhengyixia section still could not complete the releasing indicator in high flow years, and the water volume discharged to the downstream section decreased by 1.36 × 10^8 m^3 in extreme high flow years and 0.95 × 10^8 m^3 in partial high flow years. The releasing indicator can be completed in normal and low flow years. The average annual water volume discharged to the downstream section fell by 0.33 × 10^8 m^3, which was less than allowable deviation. The average annual groundwater exploitation was 6.28 × 10^8 m^3, less than the value under the present water demand condition, while it was still more than allowable groundwater exploitation.

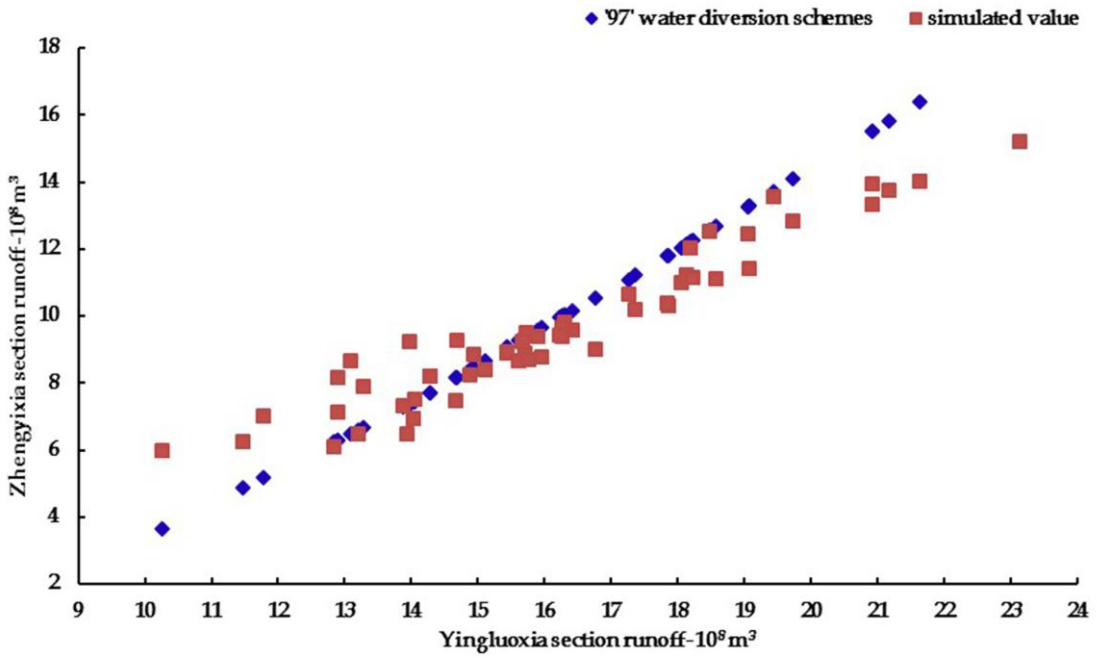

Figure 6. Simulation results of the water diversion scheme from 1954-2012 under the 2000 water demand.

Table 2. Simulation of the releasing indicator under the 2000 water demand in different typical years. Unit: 10^8 m^3.

Typical years	Yingluoxia section	Zhengyixia section	Groundwater exploitation	Irrigation guarantee rate	Simulated of Langxinshan section		
		Releasing indicator	Simulated releasing	Water shortage			
Extreme high	20.27	14.73	13.37	-1.36	5.75	20.0%	7.23
Partial high	17.69	11.63	10.68	-0.95	5.87	0.0%	5.88
Normal	15.63	9.29	9.35	0.06	6.29	11.1%	4.91
Partial low	14.10	7.62	7.83	0.21	6.64	25.0%	4.00
Extreme low	12.79	6.19	7.23	1.04	6.80	25.0%	3.79
Average	16.16	9.95	9.62	-0.33	6.28	14.5%	5.05

Figure 7 illustrates the simulated results of the water diversion scheme from 1954 to 2012 under the recent harnessing plan, and Table 3 shows the simulation of the releasing indicator under the recent harnessing

Tecnología y ciencias del agua, 10 (4), 66-87. DOI: 10.24850/j-tyca-2019-04-04

plan in different typical years. As displayed in Table 3, the average annual releasing indicator was accomplished when the arable land in the midstream returned farmland to the requirement in the recent harnessing plan underwater demand schemes. However, the water volume discharged to the downstream section fell by 0.61 × 10^8 m^3 in high flow years, and the water volume discharged to the downstream section increased by 1.4 × 10^8 m^3 in low flow years. Irrigation guarantee rate in the midstream was nearly 50%. However, the average annual overuse of groundwater in the midstream was nearly 1 × 10^8 m^3, whereas there was no extra water to supply groundwater or other environmental water, which might make the environment consistently worse in the midstream.

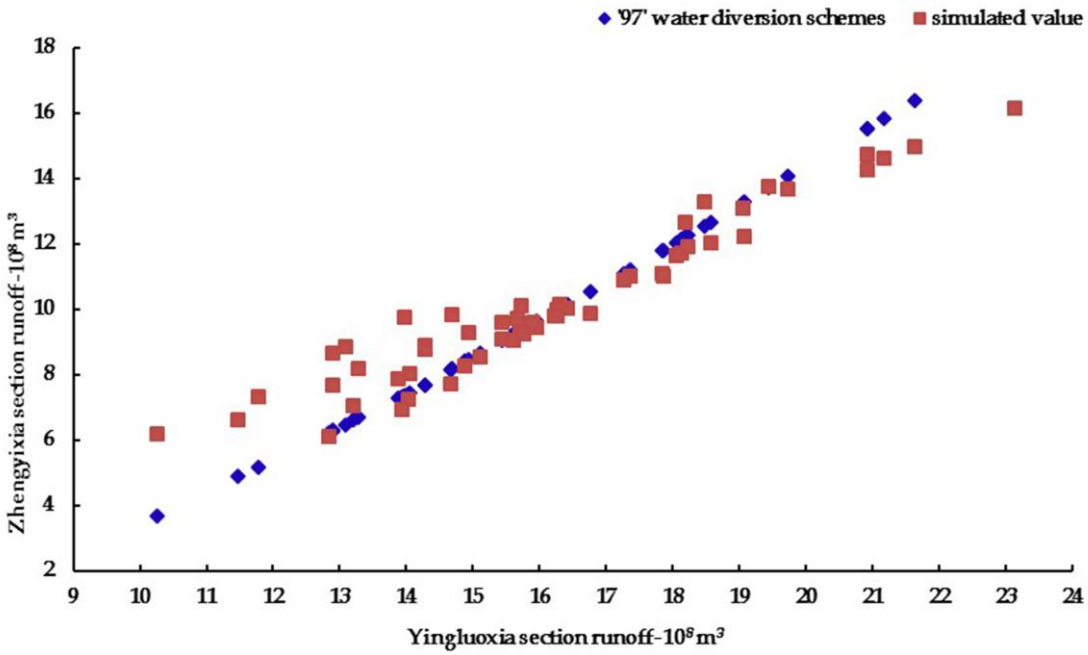

Figure 7. Simulation results of the water diversion scheme from 1954-2012 under the recent harnessing plan.

Table 3. Simulation of the releasing indicator under the recent harnessing plan in different typical years. Unit: 10^8 m^3.

Typical years	Yingluoxia section	Zhengyixia section			Groundwater exploitation	Irrigation guarantee rate	Simulated of Langxinshan section
		Releasing indicator	Simulated releasing	Water shortage			
Extreme high	20.27	14.73	14.12	-0.61	5.32	27.3%	7.65

Partial high	17.69	11.63	11.30	-0.33	5.41	42.9%	5.88
Normal	15.63	9.29	9.85	0.56	5.81	66.7%	5.12
Partial low	14.10	7.62	8.25	0.63	6.13	43.8%	4.16
Extreme low	12.79	6.19	7.61	1.41	6.26	25.0%	3.94
Average	16.16	9.95	10.14	0.19	5.79	49.1%	5.28

Rationality Analysis of the '97' Water Diversion Scheme

To sum up, in the current water demand situation, the releasing indicator of the '97' water diversion scheme could not be completed. The water diversion scheme could accomplish the releasing indicator when the farmland in the middle reaches returned to the level in 2000 and the harnessing plan in recent years, but the irrigation guarantee rate in the middle reaches is low and the situations of groundwater overuse are universal, which are caused by the great changes of economic and social conditions, as well as the hydrologic connectivity after the implementation of the water diversion scheme. Therefore, there is some irrationality between the '97' water diversion scheme based on economic, social and hydrologic conditions in the Heihe River in the mid-1980s and the current situation of the Heihe River Basin. Considering the actual need and the water resources status of the Heihe River Basin, it is deeply needed to find a new optimal water diversion scheme which can direct the water resources allocation in Heihe River Basin, and finally achieve the goals that ensure water usage in the middle reaches in low flow years, while allocating more water to the downstream in high flow years.

Potential Measures

Based on this situation, the potential measures that need to be adopted in the future were: 1) to decrease and control the cultivated land area; 2) to implement water saving measures; 3) to decrease and control the volume of groundwater exploitation to ensure an appropriate groundwater level; 4) to optimize the water diversion scheme to meet

the current situation of the Heihe River Basin; 5) to optimize the water resources allocation process to satisfy the irrigation and ecological water demand in the Heihe River Basin.

Conclusions

In this study, the water diversion based on the long-term data sets was simulated by the establishment of a water allocation model. In the current water demand situation, the releasing indicator cannot be satisfied in wet years because the economic, social and hydrological conditions have changed greatly before and after the diversion and the '97' water diversion scheme were suitable for the present situation of the Heihe River based on the socio-economic and hydrological conditions of the Heihe River in the mid-1980s.

When reducing the arable land of the middle reaches to the recent management planning requirements, the releasing indicator for the long-term data sets were successfully completed; in addition, the requirements of the water diversion scheme in the different typical years were mainly completed. This result indicates that according to the requirements of "Heihe River Recent Management Plan" to manage the land and water resources of the Heihe River, the '97' water diversion scheme could be achieved, but the irrigation guarantee rate in the middle reaches is low and the situations of groundwater overuse are universal. What's more, the scheme did not consider the environment water demand of the middle reaches, which may cause a deterioration of the environment of the middle reaches.

In summary, due to the environment changes, the '97' water diversion scheme of the Heihe River cannot complete the releasing indicator. There exist some irrationalities in the '97' water diversion scheme based on economic, social and hydrologic conditions in the Heihe River in the mid-1980s and the current situation of the Heihe River Basin. Although the implementation of the '97' water diversion scheme has effectively improved the utilization efficiency of water resources, ameliorated the environment of the lower reaches, and promoted the economic and social development in the Heihe River Basin, the irrationality of the '97' water diversion scheme under the background of changing environment results in some problems to water resources management in the Heihe River Basin. In order to ensure the sustainable development of regional resources development and utilization and the environment, the '97' water diversion scheme should

be optimized based on the present condition in the Heihe River, which is very necessary to promote the efficient utilization and scientific management of water resources.

Acknowledgments

This research was supported by the National Natural Science Foundation of China (grant number 91325201 and 51190093) and the National Department Public Benefit Research Foundation of Ministry of Water Resources (grant number 201501058). We greatly appreciate the professional comments and corrections from the editor and reviewers, which greatly improved the final version of this paper.

References

Guo, Q., Feng, Q. & Li, J. (2009). Environmental changes after ecological water conveyance in the lower reaches of Heihe River, northwest China. *Environmental Geology*, 58(7), 1387-1396.

Huang, S. Z., Huang, Q., Chang, J. X. & Leng, G. Y. (2016a). Linkages between hydrological drought, climate indices and human activities: a case study in the Columbia River basin. *International Journal of Climatology*, 36(1), 280-290.

Huang, S. Z., Huang, Q., Leng, G. Y. & Chang, J. X. (2016b). A hybrid index for characterizing drought based on a nonparametric kernel estimator. *Journal of Applied Meteorology and Climatology*, 55(6), 1377-1389.

Huang, S. Z., Huang, Q., Leng, G. Y. & Liu, S. Y. (2016c). A nonparametric multivariate standardized drought index for characterizing socioeconomic drought: A case study in the Heihe River Basin. *Journal of Hydrology*, 542 875-883.

Jiang, X. H. & Liu, C. M. (2009). The response of vegetation to water transport in the lower reaches of the Heihe River. *Acta Geographica Sinica*, 64(7), 791-797.

Kharrazi, A., Akiyama, T., Yu, Y. & Li, J. (2016). Evaluating the evolution of the Heihe River Basin using the ecological network analysis: Efficiency, resilience, and implications for water resource management policy. *Science of the Total Environment*, 572, 688-696.

Liu, X. L. & Wang, L. Z. (2012). Discussion of dispatching schemes and water transfer curves in Heihe River mainstream. *Gansu Water Resources and Hydropower Technology*, 48(10), 16-18.

Lu, Z. Y., Tang, D. S., Zheng, B. & Zhu, C. G. (2011). Post-evaluation of the ecological impact of water diversion and recent management in the downstream Heihe River. *Acta Scientiae Circumstantiae*, 31(7),

1556-1561.

Tang, D. S. & Jiang, X. H. (2009). *Transferring water and post-assessment of recent controlling in the Heihe River*. Beijing: China Water & Power Press.

Thevs, N., Peng, H. Y., Rozi, A., Zerbe, S. & Abdusalih, N. (2014). Water allocation and water consumption of irrigated agriculture and natural vegetation in the Aksu-Tarim river basin, Xinjiang, China. *Journal of Arid Environments*, 112, 87-97.

Wu, B., Zheng, Y. & Wu, X. (2015). Optimizing water resources management in large river basins with integrated surface water-groundwater modeling: A surrogate-based approach. *Water Resources Research*, 51(4), 2153-2173.

You, J. J., Wang, H. & Gan, H. (2006). Current status and prospect of study on simulation model of water resources system. *Advances in Water Science*, 17(3), 425-429.

Zhang, Y. C., Yu, J. J., Qiao, M. Y. & Yang, H. W. (2011). Effects of eco-water transfer on changes of vegetation in the lower Heihe River Basin. *Shuili Xuebao*, 42(7), 757-765.

Zhao, Q. & Huang, W. D. (2015). Analysis and evaluation on effect of water integrated regulation and comprehensive river basin management of the Heihe River. *Yellow River*, 37(8), 60-63.

DOI: 10.24850/j-tyca-2019-04-05
Special Article

Influence of Environmental Variables on Benthic Macroinvertebrate Communities in a Shallow Eutrophic Lowland Lake (Ge Lake, China)

Influencia de las variables ambientales en comunidades de macroinvertebrados bénticos en un lago poco profundo de tierras bajas eutróficas (lago Ge, China)

D. Li[1]
K. Cai[2]
X. Li[3]
J. P. Giesy[4]
Z. Niu[5]
Y. Cai[6]
J. Dai[7]
D. Xu[8]
X. Zhou[9]
H. Liu[10]
H. Yu[11]*

[1]State Key Laboratory of Pollution Control and Resource Reuse, School of the Environment, Nanjing University, Nanjing, Jiangsu, China

Jiangsu Environmental Monitoring Centre, Nanjing, Jiangsu, China, email: springli1229@163.com, ORCID 0000-0001-7126-3375

[2]Jiangsu Environmental Monitoring Centre, Nanjing, Jiangsu, China, email: 164519788@qq.com

[3]Jiangsu Environmental Monitoring Centre, Nanjing, Jiangsu, China, email: lwx241@163.com

[4]State Key Laboratory of Pollution Control and Resource Reuse, School of the Environment, Nanjing University, Nanjing, Jiangsu, China

Department of Veterinary Biomedical Sciences and Toxicology Centre, University of Saskatchewan, Saskatoon, Saskatchewan S7N5B3, Canada

Department of Zoology and Center for Integrative Toxicology, Michigan State University, East Lansing, Michigan 48824, United States of America

School of Biological Sciences, University of Hong Kong, Hong Kong, SAR China, email: john.giesy@usask.ca

[5]Jiangsu Environmental Monitoring Centre, Nanjing, Jiangsu, China, email: yaoyan@jshb.gov.cn

[6]Taihu Laboratory for Lake Ecosystem Research, State Key Laboratory of Lake Science and Environment, Nanjing Institute of Geography and Limnology, Chinese Academy of Sciences, Nanjing, PR China, email: 150293443@qq.com

[7]State Key Laboratory of Hydrology-Water Resources and Hydraulic Engineering, Nanjing Hydraulic Research Institute, Nanjing, 210029, P. R. China, email: 425627074@qq.com

[8]Changzhou Environmental Monitoring Centre, Changzhou, Jiangsu, China, email: 2689080494@qq.com

[9]Tianjin Environmental Monitoring Centre, Tianjin, China, email: 21233010@qq.com

[10]State Key Laboratory of Pollution Control and Resource Reuse, School of the Environment, Nanjing University, Nanjing, Jiangsu, China, email: hlliu@nju.edu.cn

[11]State Key Laboratory of Pollution Control and Resource Reuse, School of the Environment, Nanjing University, Nanjing, Jiangsu, China, email: yuhx@nju.edu.cn

*Corresponding author: Dr. Hongxia Yu, yuhx@nju.edu.cn

Abstract

Shallow lowland lakes are critical components of the water cycle, providing an essential service function. However, the impacts of microcystin from phytoplankton communities on benthic macroinvertebrate community diversity and structure have seldom been investigated. During 2008-2012, the impacts of water environmental variables on the diversity of macrobenthic communities, including water temperature, pH, dissolved oxygen, transparency, conductivity, the

permanganate index, Chlorophyll *a*, total phosphorus, total nitrogen, and microcystin-LR (L for leucine and R for arginine), were measured in a typical shallow lowland lake, Ge Lake. The results of the present study demonstrated that there were 31 benthic macroinvertebrate taxa in Ge Lake, including 7 oligochaetes, 7 Mollusca, 14 chironomids, and 3 other taxa. Among the macrobenthic taxa in the benthic community, opportunistic taxa such as *Limnodrilus hoffmeisteri* are present and can occur at greater densities in disturbed habitats. However, a significant reduction/disappearance of sensitive and clean taxa was observed among the benthic macroinvertebrates. Water temperature, dissolved oxygen, conductivity, ammonia nitrogen, transparency and total phosphorus were the main environmental variables influencing macrobenthic community structure, while water temperature, conductivity, ammonia nitrogen, Chlorophyll *a*, the permanganate index, total phosphorus and total nitrogen were the main factors that influenced macrobenthic community diversity indices (the numbers of taxa, Shannon's diversity index, Margalef's richness index, and Pielou's evenness index). Our results underscore the severity of the effects of human activity on Ge Lake and strongly suggest that restoring the benthic invertebrate community to previous conditions would require the control and reduction of environmental pollutants and nutrients in Ge Lake.

Keywords: Eutrophication, Diversity, Nutrients, Microcystin-LR.

Received: 18/12/2018

Accepted: 26/03/2019

Introduction

Macrobenthic invertebrates play important roles in the ecosystem functions of lakes through geochemical cycling of elements, including nutrients that limit overall productivity (Holker et al., 2016). Macrobenthic animals, spending all or most of their life on the bottom of a water body, exhibit a weak ability to migrate, making them good indicators of the ecological quality of aquatic environments worldwide (Wong et al., 2015; Dauer, 1993; Chainho et al., 2006). Furthermore,

they have been employed to monitor changes in environmental variables over decades (Resh, 2007). Because benthic invertebrates exhibit different abilities to adapt to changes in environmental conditions, fluctuations in their relative abundances can provide insights into the causes and severity of pollution (Wallace et al., 2015; Beck and Hatch, 2009; Richman and Somers, 2010; Marzin et al., 2012). Structural measures of macrobenthic assemblages, such as their community structures and diversity, can be used as integrative indicators of environmental quality. Macroinvertebrate communities are an important component in nutrient cycling and pollutant transformation (Signa et al., 2015; Lawrence et al., 2016). Because environmental pollution is harmful to native taxa and often encourages the intrusion of invasive taxa, human activity may affect macrobenthic communities (Gichana et al., 2015; Galil, 2000). Changes in environmental parameters (e.g., salinity, sedimentation and eutrophication) might also play a crucial role in these adverse effects (Broch et al., 2016; Nishijima et al., 2015; Lamptey and Armah, 2008; Yoon et al., 2017; Pereira et al., 2012; Mandal and Harkantra, 2013). Studies have demonstrated that seasonally varying conditions in terms of sediment parameters, such as pH, salinity and flow rate, are significant determiners influencing the distribution of macrobenthic communities in estuaries (Courtney and Clements, 1998; Kilgour et al., 2008; Feebarani et al., 2016; O'Brien and Keough, 2013). However, previous studies have mainly focused on estuaries, lagoons and marine areas (Marques et al., 2013; Romeo et al., 2015; Jordana et al., 2015; Gillett et al., 2015), and the relationships between macrobenthic indicators (structure and diversity) and environments have rarely been investigated in shallow freshwater lowland lakes (Cai et al., 2017; Li et al., 2016).

Shallow lowland lakes are critical components of the water cycle and provide essential service functions, including storing and purifying water, providing habitats for animals, protecting biodiversity, and irrigation. Because the water capacity is low and sediment interface processes are weak in shallow lakes, such lakes are seriously disturbed by bioenvironmental stressors, especially in lowland regions (Havens et al., 2007). Water quality deterioration leads to eutrophication in shallow lowland lakes. Consequently, shallow lowland lakes face a number of ecological problems, such as habitat destruction, the presence of invasive taxa, and reduction in the functional diversity of communities (Zhang et al., 2016; Rahel, 2002; Angeler and Johnson, 2013). Therefore, to better manage lake ecosystems, researchers and managers need to improve their understanding of the main factors that

influenced macrobenthic community diversity in lake ecosystems. Ge Lake (Ch: *Ge*), the largest lake in southern Jiangsu province in eastern China, is a representative shallow lowland lake. As an important component of the lakes in the vicinity of Tai Lake (Ch: *Tai*), Ge Lake gives play to a significant role of protecting ecological environments in Tai Lake. Ge Lake is used for commercial navigation, excursions, irrigation and aquaculture (Huang, 2001). Over the past three decades, Ge Lake has suffered anthropogenic pollution from industrial and domestic wastewater and agricultural runoff. The water quality in Ge Lake has been characterized by a decreasing ability to process and assimilate this waste. The proportions of plants in the community have changed, with a reduction in the absolute and relative numbers of aquatic macrophytes. Due to eutrophication and phytoplankton blooms in Ge Lake, the relative proportions of animals in communities, including benthic invertebrates, have been reduced (Guo, 2007). Monitoring of the status and trends of both abiotic and biotic indicators of environmental quality in Ge Lake is currently focused on total nitrogen (TN), total phosphorus (TP) (Xu et al., 2013), algal blooms (Tao et al., 2011; Duan et al., 2012) and technologies to control nutrients and biomass from blooms of a few dominant phytoplankton taxa (Zhang et al., 2011). However, ecological indicators of the aquatic benthic community, such as diversity and evenness have been seldom studied (Wang et al., 2012). Additionally, the relationship between cyanobacterial microcystins (MCs) and macrobenthic communities has rarely been researched in freshwater lakes (Li et al., 2016; Lance et al., 2010).

In this study, structure and diversity of macrobenthic communities as well as environmental variables in Ge Lake and catchments of its upstream tributaries were investigated to characterize the status of the benthic invertebrate communities, to establish a benchmark against which future changes can be interpreted, to ascertain the impacts of water environmental variables on ecological indicators, to distinguish factors influencing structure and diversity of macrobenthic communities, and to offer basic information for lake resource utilization and ecological protection in the future.

Materials and Methods

Study Area

Ge Lake (119°44’15” to 119°52’56”E and 31°43’04” to 31°28’19”N) is located at the southwest of Changzhou City, northeast of Tai Lake, and east of Changdang Lake, is situated in the upstream portion of the Tai Lake catchment. Ge Lake is 25 km long and 6.6 km wide, and it has a surface area of 164 km^2. The near-shore water depth in the lake is approximately 0.8 to 1.0 m, with an annual average water level of 3.27 m. However, the water level in Ge Lake has decreased due to excessive lake water use for human development since the 1990s. Water flows from Ge Lake into Zhushan Bay in Tai Lake through the Taige Canal.

There were six sampling sites in the study area (Fig 1): site S1 was located at the outlet of Changdang Lake; site S2 was located downstream of S1 on the Beigan River; sites S3 and S4 were located south of Ge Lake; site S5 was located north of Ge Lake, and site S6 flowed into Tai Lake. Sites S1 and S2 were upstream of Ge Lake, while sites S3, S4, S5, and S6 were in Ge Lake. Based on the study (Liu et al., 2005), the difference in macrobenthic community structure between the north and south of Ge Lake was insignificant. Thus, sites S4 and S5 were chosen.

Tecnología y ciencias del agua, 10 (4), 88-119. DOI: 10.24850/j-tyca-2019-04-05

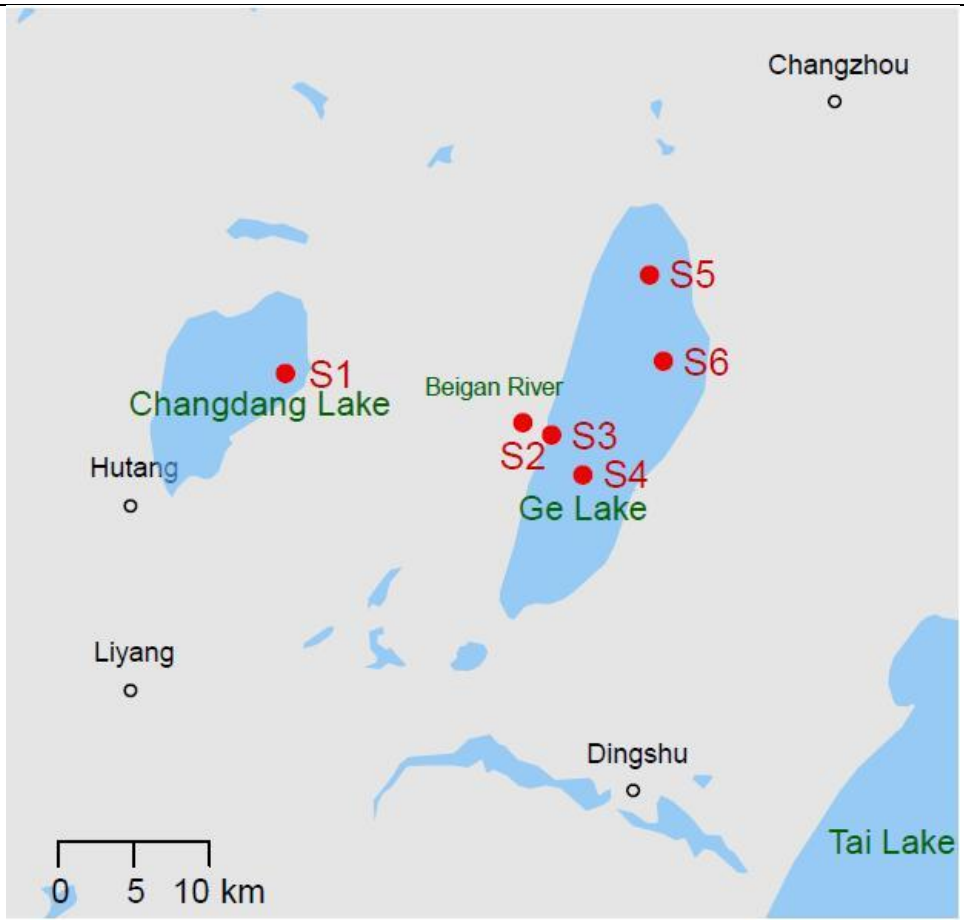

Figure 1. The Six Sampling Sites in Ge Lake and Its Surroundings.

Map of Ge Lake in eastern China and its surroundings. The sampling sites are labeled S1, S2, S3, S4, S5 and S6. Site S1 is located at the outlet of Changdang Lake and sites S3 and S6 are national control sites. According to a previous study (Liu et al., 2005), the difference in macrobenthic community structure between the north and south of Ge Lake was insignificant. Thus, sites S4 and S5 were chosen.

Sampling

Macroinvertebrate Sampling. A Peterson grab (0.0625 m^2 sample area) was used to collect sediment samples, including benthic

Tecnología y ciencias del agua, 10 (4), 88-119. DOI: 10.24850/j-tyca-2019-04-05

invertebrates. We collected substrate sludge samples in triplicate for the identification and enumeration of macroinvertebrates at each site during each sampling period. According to standard methods (State Environmental Protection Administration of China, 2002), each sediment sample was seriously filtered *in situ*, and the remainders were kept in 10% formalin and brought to the lab as soon as possible.

Water Sampling. Water samples were synchronously collected with microbenthic samples at the six sites during both May and September between 2008 and 2012. Water samples were collected 0.5 m below the surface into glass bottles for measurements of environmental variables at each site and each time point. YSI multi-water quality parameters were used to analyze water temperature (WT), pH, dissolved oxygen (DO), and conductivity *in situ*. A Secchi disk was used to examine water transparency (SD). To examine ammonia nitrogen (NH_4^+-N), the permanganate index (COD_{Mn}), Chlorophyll a (Chl *a*), total phosphorus (TP), total nitrogen (TN), and MC-LR, water were sampled and stored at 0-4 °C in the dark; and were then processed as soon as possible in the lab.

Analytical Procedures

Macrobenthic Communities. Macrobenthic community samples were washed, sorted out large taxon, appraised to the minimum groups, and recorded the information. Abundances were expressed as individuals m^{-2}. The numbers of taxa (S), Shannon's diversity index (H'), Margalef's richness index (D), and Pielou's evenness index (J) were analyzed using PRIMER Version 6.1.10 for each sample.

Environmental Variables. The concentrations of NH_4^+-N, TP, TN, COD_{Mn}, and Chl *a* in water samples were analyzed based on standard methods in the laboratory (State Environmental Protection Administration of China, 2002). Based on previous studies (Rivasseau et al., 1999; Jarkko et al., 2002), MC-LR was analyzed via enzyme-linked immunosorbent assays (ELISAs).

The synthesized trophic state index (STSI) was calculated as an indicator of the magnitude of eutrophication for each sample of water (Equation 1), based on SD, TP, TN, Chl *a*, and COD_{Mn}:

$$STSI = TSI(\sum) = \sum_{j=1}^{m}(\mathrm{Wj} \times \mathrm{TSIj}) \quad (1)$$

where m is the number of observations; W_j is entropy weight, and TSI_j is the trophic state index for variable j. The weight coefficient of each variable was calculated based on previously described methods (Zadeh, 1965; Mon et al., 1994; Qiu, 2001). The correlations between the synthesized trophic state index and lake water environmental quality measures are shown in Table 1.

Table 1. Correlations of the Synthesized Trophic State Index and Water Environmental Quality Classifications in Lakes (Zadeh, 1965; Mon et al., 1994; Qiu, 2001).

Trophic state	STSI	Water quality
Oligotrophication	0<STSI≤30	Excellence
Mesotrophication	30<STSI≤50	Good
Eutrophication	50<STSI≤60	Polluted
Supereutrophication	60<STSI≤70	Superpolluted
Hypereutrophication	70<STSI≤100	Hyperpolluted

STSI: synthesized trophic state index.

Data Analysis

Repeated measures using SPSS 19.0 was employed to test differences between macrobenthic community abundance among years. The spatial difference in the benthic community was analyzed using multivariate statistical analysis. According to the Bray-Curtis similarity matrix, macrobenthic community compositions were compared using a clustering analysis method. Taxon abundance data were log(x+1) transformed. Analysis of similarity (ANOSIM) was used to analyze the differences in macrobenthic community assemblages among sites were analyzed using (Clarke, 1993). According to the Bay-Curtis similarity matrix, non-metric multidimensional scaling (NMDS) was carried out;

and data of macroinvertebrate abundance were transformed using log(x+1). PRIMER Version 6.1.10 was used to perform these analyses.

A pairwise Pearson correlation analysis was used to analyze the correlations between environmental variables and macrobenthic indicators (S, H', D, and J) were analyzed using (Pfeifer et al., 1998; Peeters et al., 2004; Hosmani, 2012). A *p*-value of < 0.05 was a statistical importance threshold. SPSS 19.0 was used to perform these analyses.

The effect of environmental variables on macrobenthic communities was analyzed using canonical correspondence analysis (CCA). All environmental variables, as well as the T-RF peak area data, were log(x+1)-transformed. Based on 499 permutations under the reduced model and using the αvalue of 0.05, forward selection of the Monte Carlo test was used to discern the environmental variables, with. These analyses were conducted using the software CANOCO 4.5.

Environmental variables with significant multicollinearity (with variance inflation factor >10 and Pearson correlation coefficient $|r| >= 0.75$) were excluded. Due to their greater correlations (r=-0.761, r=0.790) with SD and COD_{Mn}, STSI was removed (Table S2) and the other 11 environmental variables were included in the following analyses. Based on Gaussian error distribution (McGullagh and Nelder, 1989), Generalized linear models (GLMs) were used to analyze the factors of macrobenthic community diversity indices (S, H', D and J). According to Akaike's information criterion (AIC) (Akaike, 1974), the best approximating model was selected. GLMs were performed with all environmental variables, except for STSI. R software version 3.3.3 was used to perform all these analyses.

Results

Macrobenthic Assemblage Composition

42 macrobenthic taxa were investigated in this study area during the survey, including 22 arthropods (1 gomphidae, 1 libellulidae, 3

crustaceans and 17 chironomids), 11 molluscs (4 bivalves and 7 gastropods), 7 oligochaetes, and 2 other taxa. Among the macrobenthic assemblages, the oligochaete worm *Limnodrilus hoffmeisteri* was observed most frequently (96.7%), followed by the gastropod *Bellamya purificata*, which occurred in 58.3% of samples. Site S2 exhibited the greatest abundance among macrobenthic communities, ranging from 256 to 8256 individuals m^{-2}; site S1 was second. Relatively low abundances were recorded at four sites in Ge Lake, S3, S4, S5, and S6, which ranged from 32 to 1728 individuals m^{-2}. There were 31 taxa of benthic macroinvertebrates observed in Ge Lake (see Table S1 in the SM), including 7 oligochaetes, 7 Mollusca, 14 chironomids, and 3 other taxa, while there were 37 macrobenthic taxa upstream of the lake. In most cases, *L. hoffmeisteri* exhibited the greatest density, presenting values as high as 1728 individuals m^{-2} among the macrobenthos.

Multivariate Analyses of Macrobenthic Invertebrates

Based on Bray-Curtis similarity coefficients (at the similarity level of 60%), spatial differences in microbenthic community structure between Ge Lake (sites S3, S4, S5, and S6) and upstream locations (sites S1 and S2) were significant using the non-metric multidimensional scaling (NMDS) analysis (Fig 2). Significant differences in the structure of macrobenthic communities between sampling sites in Ge Lake and upstream areas (R=0.335, p=0.001) were found by one-way ANOSIM. According to the SIMPER procedure, *L. hoffmeisteri*, *B. purificata*, the gastropod *Bellamya aeruginosa*, and the oligochaete *Branchiura sowerbyi* were the most common taxa at sites S1 and S2, upstream of Ge Lake, while *L. hoffmeisteri*, *B*. *sowerbyi*, and the chironomid *Tanypus punctipennis* were the primary contributing taxa at the four sites (S3, S4, S5, and S6) in Ge Lake.

Tecnología y ciencias del agua, 10 (4), 88-119. DOI: 10.24850/j-tyca-2019-04-05

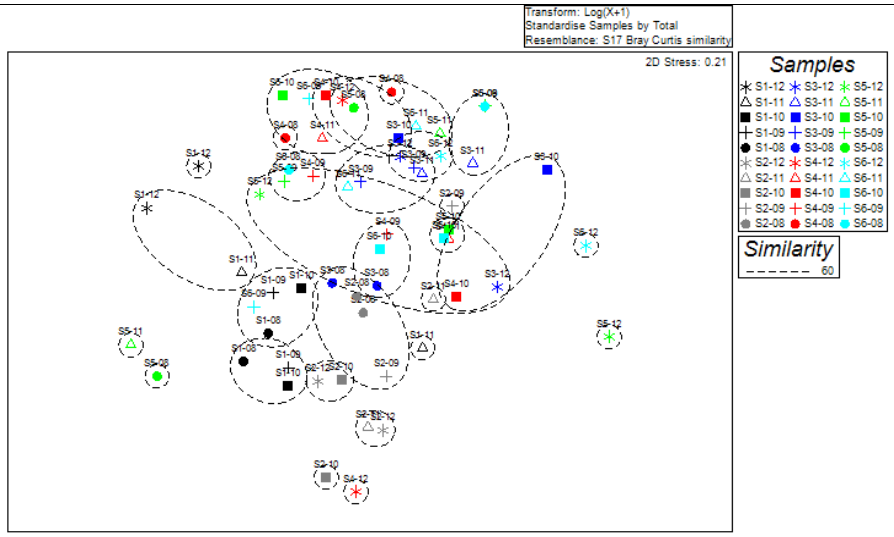

Figure 2. According to Bray-Curtis Similarity Coefficients, Non-metric Multidimensional Scaling (NMDS) among Macroinvertebrate Communities. Year labels: 8 (2008); 9 (2009); 10 (2010); 11 (2011); and 12 (2012).

Compared with the two upstream sampling sites, the four Ge Lake sites exhibited lower macrobenthic community diversity (Fig S1. in the SM). However, the mean Shannon-Wiener diversity index (H') of the macrobenthic communities in Ge Lake increased between 2008 and 2012, with the exception of 2009 (Fig S2. in the SM).

Environmental Variables

The environmental variables measured at the six sampling sites for the entire sampling period were shown in Table 2. There were statistically significant differences between the four sites in Ge Lake and its two upstream sites. The concentrations of pollutants (NH_4^+-N, COD_{Mn} and MC-LR) and nutrients (TP and TN) in Ge Lake were greater than in more upstream regions. Based on the correlations between STSI and lake water quality indicators (Table 1), Ge Lake was a supereutrophic lake, while the upstream area was a eutrophic lake.

Tecnología y ciencias del agua, 10 (4), 88-119. DOI: 10.24850/j-tyca-2019-04-05

Table 2. Summary of the Averaged Values from 5 Years of Field Measurements: n=10 Water Environmental Parameters at Ge Lake Sampling Sites.

Site	S1	S2	S3	S4	S5	S6	*p*
WT (°C)	22.6±2.5	23.3±4.0	22.4±3.4	22.2±3.4	22.4±3.3	21.5±3.6	n.s.
pH value	8.96±0.40	8.30±0.53	7.86±0.84	7.96±0.89	7.96±0.79	7.80±0.76	n.s.
DO (mg/L)	8.65±1.49	7.90±1.21	6.62±1.28	6.69±1.31	6.64±1.19	6.57±1.21	**
Conductivity (μs/cm)	620±54	605±39	672±92	643±100	660±104	665±89	n.s.
NH_4^+-N(mg/L)	0.46±0.12	0.43±0.07	0.67±0.17	0.62±0.16	0.69±0.17	0.70±0.19	**
Chl *a* (mg/m^3)	77.0±44.8	45.4±18.1	53.6±28.4	60.0±38.5	61.0±31.2	48.9±32.8	n.s.
SD (m)	0.40±0.06	0.48±0.05	0.26±0.08	0.26±0.09	0.30±0.13	0.26±0.07	***
COD_{Mn} (mg/L)	4.30±0.16	3.99±0.18	6.44±1.59	6.36±1.37	5.53±1.28	6.00±1.48	***
TP (mg/L)	0.070±0.009	0.059±0.010	0.188±0.091	0.141±0.033	0.148±0.072	0.116±0.049	***
TN (mg/L)	1.844±0.763	1.484±0.467	2.731±1.065	2.685±1.080	2.670±0.996	2.705±0.929	**
STSI	57.4±5.4	56.4±2.1	66.2±3.1	65.7±4.0	64.6±4.4	63.7±4.2	***
MC-LR (μg/L)	0.110±0.104	0.087±0.056	0274±0.126	0.256±0.142	0.243±0.106	0.224±0.112	**
Trophic status	Eutrophication	Eutrophication	Supereutrophication	Supereutrophication	Supereutrophication	Supereutrophication	/
Water Quality	Polluted	Polluted	Superpolluted	Superpolluted	Superpolluted	Superpolluted	/

*: $P<0.05$; **: $P<0.005$; ***: $P<0.0005$; n.s.: not significant.

WT: water temperature, DO: dissolved oxygen, Chl *a*: Chlorophyll a, COD_{Mn}: permanganate index, TP: total phosphorus, TN: total nitrogen, STSI: synthesized trophic state index.

Factors That Influenced Macrobenthic Community Structure and Diversity

According to pairwise Pearson correlation analyses, the relationships between environmental variables and macrobenthic community diversity (S, H', D and J) varied (Table 3). WT, DO and pH were significantly positively correlated with macrobenthic indicators (S, H' and D) ($p < 0.05$). H' and the Pielou Index (J) were significantly positively correlated with transparency (SD) (R=0.381, $p < 0.05$; R=0.699, $p < 0.05$). Conversely, COD_{Mn}, STSI and MC-LR were negatively correlated with macrobenthic community diversity indices (S, H', D and J) ($p < 0.05$). Meanwhile, H', D and J were negatively related to TN ($p < 0.05$).

Based on the CCA analysis, WT, DO, conductivity, NH_4^+-N, transparency and TP were the significant environmental variables that explained the macrobenthic community structure variance (Fig 3). Relationships between environmental variables and macrobenthic community diversity indices were analyzed using generalized linear models (GLMs). WT, conductivity, NH_4^+-N, Chl *a*, COD_{Mn}, TP and TN were the main factors that influenced macrobenthic community diversity indices (Table 4).

Table 3. Pearson Correlation Coefficients between Macrobenthic Indicators and Environmental Variables (n=60).

	S	H'	D	J
WT	**0.321***	**0.325***	**0.411****	0.117
pH	**0.362****	**0.329***	**0.463****	**0.340****
DO	**0.509****	**0.298***	**0.304***	**0.478****
Conductivity	**0.389***	**0.344***	**0.519****	0.227
NH_4^+-N	-0.024	0.125	-0.166	0.134
Chl *a*	-0.086	0.006	0.042	-0.227
SD	0.112	**0.381***	0.240	**0.699****
COD_{Mn}	**-0.501****	**-0.398****	**-0.502****	**-0.560****
TP	-0.098	-0.240	-0.175	**-0.373***
TN	-0.167	**-0.380***	**-0.400****	**-0.373***

Tecnología y ciencias del agua, 10 (4), 88-119. DOI: 10.24850/j-tyca-2019-04-05

STSI	**-0.350***	**-0.431****	**-0.409****	**-0.691****
MC-LR	**-0.414****	**-0.497****	**-0.378****	**-0.542****

*: $P<0.05$; **: $P<0.01$.

S: Number of taxa, H': Shannon-wiener diversity index, D: Margalef's richness, J: Pielou's evenness index.

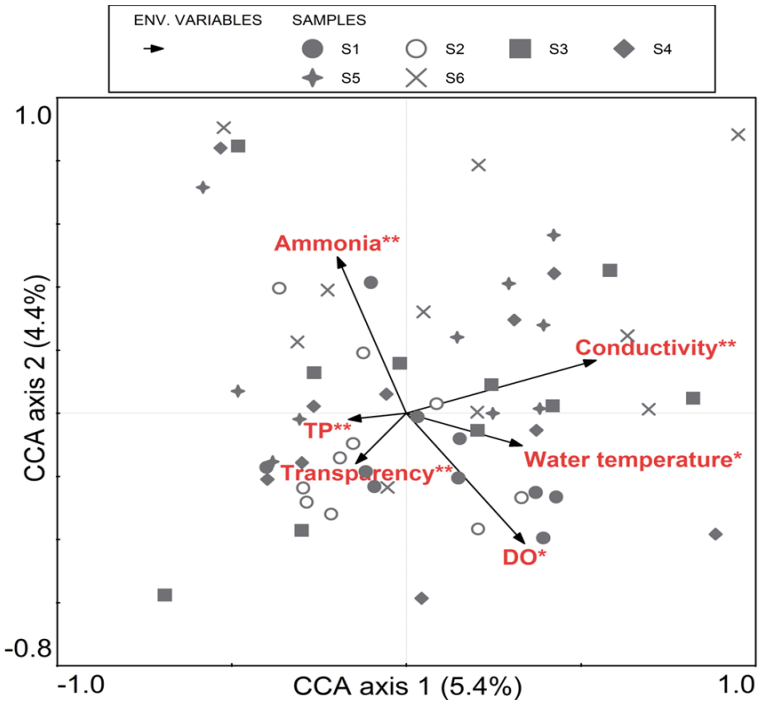

Figure 3. Canonical correspondence analysis (CCA) for Macrobenthic Communities and Environmental variable.

Table 4. Results of the generalized linear model (GLM). Selected variables, t values and AIC are given.

S	Variables	Intercept	DO	NH_4^+-N	COD_{Mn}		
	t value	2.410*	-1.534	-1.653	-3.302**		
	AIC	**254.44**					
H'	Variables	Intercept	WT	TN			
	t value	0.824	2.479*	-2.996**			
	AIC	**78.192**					
D	Variables	Intercept	pH	DO	Conductivity	Chl *a*	COD_{Mn}
	t value	-1.554	3.263**	-1.403	1.744	1.632	-4.016***

	AIC	**32.682**					
J	Variables	Intercept	Conductivity	NH_4^+-N	Chl *a*	TP	
	t value	2.442*	2.680**	2.412**	0.525*	-2.680**	
	AIC	**4.4466**					

*: $P<0.05$; **: $P<0.01$; ***: $P<0.001$.

Discussion

Changes in Ge Lake Macrobenthic Community

The macroinvertebrate assemblages in Ge Lake have changed significantly over recent decades, and the abundance of more sensitive taxa that require cleaner water has decreased. In general, the macrobenthic community structure is fairly stable, except when environmental variables change dramatically. Between 1991 and 1994, there were 47 macrobenthic animal taxa in Ge Lake, with Ephemeroptera, dragonflies and other sensitive taxa, such as molluscs, which are used as indicators of clean water, being observed in Ge Lake (Zhu et al., 1997). At that time, Ge Lake contained more aquatic macrophytes, with submerged plants covering 87.5% of the area. In addition, there were few fish net-pen cultures in Ge Lake during the 1990s (Zhu et al., 1997; Tao et al., 2010). Compared with the concentrations surveyed in this study (Table 2), the concentrations of TP (< 0.05 mg/L), COD_{Mn} (< 3.7 mg/L), and TN (< 1.0 mg/L) (Li and Song, 2013) were very low. During that time, agriculture and fisheries were the main human activity in the area of the Tai River Basin. Between 2002 and 2003, thirty-one taxa of benthic invertebrates were observed, but the number of taxa has decreased significantly. More sensitive taxa have decreased, while more tolerant taxa associated with polluted water have increased (Liu et al., 2005). The species number of mollusk decreased from 24 to 14, while the numbers of intolerant taxa aquatic insects, such as Ephemeroptera, Plecoptera, and Trichoptera (EPT), have decreased from 10 to 3, and the number of oligochaete taxa increased from 2 to 6 between 1995 and 2003. Between 2008 and

2012, there were thirty-one benthic invertebrates recorded, with *L. hoffmeisteri* being the predominant species in Ge Lake during the survey. Sensitive taxa that inhabit clean water and were observed in the 1990s, such as dragonflies, were rarely found in this study, with only one sensitive clean water taxon, *Sinictinogomphus* sp. of the Gomphidae family, being observed during the present study. Findings from this study and those of previous studies suggest that macrobenthic community structure and diversity in Ge Lake have been changed by deteriorating environmental conditions; activities associated with human population growth in the catchment of Ge Lake are the likely cause. With the rapid development of the regional population and associated economic activities, there have been greater amounts of pollutants flowing into Ge Lake since the 1990s (Li and Song, 2013). These environmental conditions have promoted phytoplankton growth, limited the absolute and relative numbers of taxa in macrobenthic communities, and promoted a large population increase of *L. hoffmeisteri*. Results from previous studies (Beghelli et al., 2012; Li et al., 2016; Zhou et al., 2014) have confirmed that oligochaetes such as *L. hoffmeisteri* and chironomids are widely recognized as indicators of eutrophic conditions in the Tai River Basin.

Diverse habitats are provided by macrophytes, where macrobenthic animals can survive and escape predation. Tews et al. (2004) found that it was necessary to protect macrophytes to protect benthic animal and fish biodiversity. The populations of submerged macrophytes in Ge Lake have rapidly deteriorated. Tao et al. (2010) found that the area covered by submerged plants has declined at an annual rate of more than 10% since 1995. In addition, benthic macroinvertebrates living among aquatic macrophytes were unable to survive (Kennedy et al., 2017; Beresford and Jones, 2010). The lack of plant cover could be the reason for the low number of gastropods found in this study. Previous studies have demonstrated that habitats characterized by gastropods occur in macrophyte-dominated regions (Hu et al., 2016; Jaschinski et al., 2011). In addition, fish net-pen cultures in Ge Lake could likely have contributed to the loss of macrobenthic community biodiversity due to loading of nutrients and habitat destruction, resulting in eutrophication and organic matter loading that has enriched sediments and resulted in decreased dissolved oxygen. Scalable fish net-pen cultures in Ge Lake had occurred since 1995 (Liu et al., 2005). Consequently, waste derived from the feed, including uneaten feed and fish excreta, was released into the water (Jones, 2010; Boaventura et al., 1997). Roberts et al (2009) found that sediment pollution from fish farms can have adverse

effects on benthic macroinvertebrates. An increase in suspended solids from fish farm effluents may cause a decrease in lake transparency (Guilpart et al., 2012). Previous studies (Wu et al., 2012; Silva et al., 2013; Karimi et al., 2016) have found that pollution of sediments by effluents from fish farms could have resulted in the reduction of macrobenthic community diversity.

However, the diversity (Shannon-Wiener diversity index) of the macrobenthic communities in Ge Lake had been increasing over the period during 2008 and 2012. Although the differences in macrobenthic community diversity between years were not statistically significant, benthic invertebrate diversity appears to be improving in response to efforts by the local government to reduce environmental pollutants in Ge Lake. In 2007, 2008, and 2009, the City of Changzhou implemented various phases of environmental mitigation following the drinking water crisis of 2007. These mitigations included reducing the scale of fish net-pen culture and ecological restoration projects. Based on the yearbook of the City of Changzhou in 2009, the area of fish net-pen cultures was reduced from 44.7 square kilometers, which represented 22.7 percent of the total area in Ge Lake in 2007, to 7.3 square kilometers in 2009. Water purification was found to be influenced by aquatic plant growth in the eastern section of Ge Lake during 2009 and 2010 (Wu et al., 2013). Furthermore, the water quality in Ge Lake was shown to be improved through the reconstruction of submerged macrophyte communities in the lake (Huang, 2011). The results of several studies (Scheffer, 1998; Jukka and Leena, 2003; Griffin et al., 2009) have indicated that macrophytes as an important component of lakes, absorb phosphorus in eutrophic lakes, restrain sediment to increase lake transparency, and supply complex habitats for macrobenthic communities. The periphyton layer covering macrophytes is probably a particularly important food source for benthic macroinvertebrates (Brönmark, 1989). Researchers (Lloret and Marin, 2009) have found that the benthic macroinvertebrate community and benthic macrophytes play a crucial role in absorbing surplus nutritive materials from water and keeping them in sediments.

Factors That Affected the Structure and Diversity of Macrobenthic Communities

Tecnología y ciencias del agua, 10 (4), 88-119. DOI: 10.24850/j-tyca-2019-04-05

The physical and chemical characteristics of water are important factors that can affect freshwater macrobenthic community structure and diversity (Nicola et al., 2010). In this study, WT, DO, conductivity, NH_4^+-N, transparency and TP were observed to be the primary environmental variables that affected macrobenthic community structure and diversity in Ge Lake. The abundance of food (Humpesch, 1979), the temperature can also affect the structures of communities of macrobenthos (Courtney and Clements, 1998; Joydas et al., 2016). Conductivity has been reported as another principal variable that influences the numbers and distribution of oligochaetes (Achurra et al., 2015). The study (Li et al., 2017) found a significant decline in diversity of the benthic invertebrate community of Tai Lake since 1980's, which could be associated to continuous exposure to ammonia over decades given different sensitivity of taxa to ammonia in Tai Lake, China. Transparency was found to affect Pielou's evenness index of the macrobenthic communities in the study area. Lower transparency likely results in lower primary productivity, resulting in less secondary growth of benthic macroinvertebrates. Increasing concentrations of TP and TN promoted phytoplankton growth, leading to phytoplankton blooms, resulting in lower transparency and lower concentrations of DO near the lake bottom (Zeng et al., 2013). In addition, the trophic state index, which is a synthetic parameter, was significantly negatively correlated with Pielou's evenness index (Table 3). The results obtained in Ge Lake confirmed results of previous studies showing that lower taxon diversity is often found in supereutrophic lakes, while greater diversity is found in mesotrophic lakes (Frouin, 2000). Trophic status is correlated with water chemistry and is an important factor influencing freshwater benthic macroinvertebrate communities (Nicola et al., 2010). Ge Lake was classified as a supereutrophic lake, and macrobenthic community diversity in the lake was determined to be low. Severe eutrophication exerts detrimental effects on macrobenthic assemblages due to greater nutrient concentrations, leading to increased phytoplankton growth and favoring cyanobacteria growth, resulting in hypoxia (Kilgour et al., 2008). The changes of the macrobenthic community assemblages in Ge Lake observed over the past several decades are consistent with increasing eutrophication of lakes. The dominant macrobenthic community taxa in Ge Lake shifted from bivalves in 1990 to the oligochaete *L. hoffmeisteri* at present. This shift is consistent with results from Dianchi and Tai Lakes in China (Wang et al., 2007; Cai et al., 2012). Furthermore, the water upstream of Ge Lake is eutrophic (Table 2), and the Beigan River is a tributary that flows into the lake. Therefore, it is necessary to control pollutants upstream of Ge Lake.

Previous studies have shown that MC-LR is a toxic derivative of cyanobacterial blooms (Qin et al., 2010; Freitas et al., 2014). Acute and subacute toxicity can be induced by MCs in freshwater ecological food webs (Ibelings and Chorus, 2007; Lahrouni et al., 2012). The present study demonstrated that MC-LR concentrations were higher at the four Ge Lake sites than at the Changdang Lake site (Table 2). MCs have an adverse effect on Mollusca and zooplankton (Chen et al., 2005; Krzton et al., 2017). Although the concentrations of MC-LR in Ge Lake did not exceed WHO standards (1.0 μg/L), their potential impact on aquatic animals and humans in the future cannot be ignored.

Due to the increasing impacts of anthropogenic activities on Ge Lake, its macrobenthic communities are threatened by environmental pollutants. The change in the macrobenthic community structure in Ge Lake since the 1990s has been enormous. Thus, strict control on water quality and the introduction of nutrients from rivers into Ge Lake is urgent and crucial for protecting water functions and biological diversity in the lake. Additionally, it is equally important to control cyanobacteria blooms in Ge Lake. Analyzing the factors affecting water quality and macrobenthic metrics and seeking methods for improving the water environment will be helpful for water quality management and ecological function recovery in Ge Lake.

Conclusions

The present study records new data on the structure and diversity of the macrobenthic community in Ge Lake from 2008 to 2012. Changes in the structure of macrobenthic communities in Ge Lake were huge. This present study found that the macrobenthic communities in Ge Lake exhibited much lower diversity than historical reports that could reflect the environmental conditions of the lake. WT, conductivity, $NH4^{+}$-N and TP were the main environmental variables that influenced the structure and diversity of macrobenthic communities in Ge Lake. The effects of fish net-pen cultures on macrobenthic community structure and diversity need to be furtherly studied. The present study should provide useful basic data for water environmental protection and ecological restoration in the shallow lowland lakes.

Acknowledgments

This work was financially supported by the National Major Science and Technology Program for Water Pollution Control and Treatment (2017ZX07302003-5) and by the general office of Lake Taihu Water Pollution Prevention and Control, Jiangsu Province in China (TH2018304). John P. Giesy was financed by the "Great Level Foreign Experts" program (#GDT20143200016) from the State Administration of Foreign Experts Affairs, the P.R. China to Nanjing University and the Einstein Professor Program of the Chinese Academy of Sciences. He was also financed by the Canada Research Chair program and a Distinguished Visiting Professorship in the School of Biological Sciences of the University of Hong Kong.

Supporting Information

Table S1. Macrobenthic Animals Collected in Ge Lake (Ch: *Gehu*). Occurrence (%) Represents the Percentage of Sites at Which the Species were Collected During Sampling.

Species	Occurrence (%)	Species	Occurrence (%)
Mollusca		*Procladius* sp.	2.5
Alocinma longicornis	5.0	*Cryptotendipes* sp.	5.0
Parafossarulus striatulus	2.5	*Tanytarsus* sp.	10.0
Bellamya aeruginosa	25.0	*Microchironomus* sp.	5.0
Bellamya purificata	45.0	*Glyptotendipes tokunagai*	2.5
Corbicula fluminea	5.0	*Dicrotendipes nervosus*	2.5
Anodonta angula	12.5	*Tanypus punctipennis*	40.0
Hyriopsis cumingii	2.5	*Microchironomus tener*	2.5
Oligochaeta		*Tanypus vilipennis*	2.5
Aulodrilus sp.	2.5	*Chironomus salinarius*	2.5
Tubifex sp.	5.0	*Chironomus riparius*	5.0
Limnodrilus	2.5	*Chironomus dorsalis*	2.5

grandisetosus			
Limnodrilus claparedianus	15.0	*Chironomus lugubris*	2.5
Limnodrilus hoffmeisteri	97.5	**Others**	
Limnodrilus udekemianus	2.5	*Sinictinogomphus* sp.	2.5
Branchiura sowerbyi	40.0	*Caridina* sp.	12.5
Chironomidae		*Gammarus* sp.	5.0
Chironomus attenuatus	15.0	/	/

Table S2. Pairwise Pearson correlations between environmental variables.

	WT	pH	DO	Conductivity	NH_4^+-N	Chl *a*	Transparency	COD_{Mn}	TP	TN	STSI
WT	1.000										
pH	0.332**	1.000									
DO	0.222	0.530**	1.000								
Conductivity	0.461**	0.524**	0.214	1.000							
NH_4^+-N	-0.262*	-0.340**	-0.467**	-0.241	1.000						
Chl *a*	0.198	-0.122	-0.266*	-0.012	0.050	1.000					
Transparency	0.120	0.271*	0.378**	-0.074	-0.458**	-0.147	1.000				
COD_{Mn}	-0.316*	-0.285*	-0.535**	0.039	0.274*	0.313*	-0.550***	1.000			
TP	-0.041	-0.129	-0.291*	0.180	0.323*	0.021	-0.562***	0.504	1.000		
TN	-0.101	-0.444**	-0.302*	0.046	0.084	0.307*	-0.510***	0.474	0.469	1.000	
STSI	-0.137	-0.321*	-0.510***	0.064	0.365**	0.523***	**-0.761****	**0.790****	0.692**	0.736***	1.000
MC-LR	-0.074	0.168	0.157	0.042	-0.023	0.412*	0.186	0.468*	0.375*	0.057	0.378*

*: $P<0.05$; **: $P<0.01$; ***: $P<0.001$. Note: STSI was excluded due to its higher correlations with Transparency and COD_{Mn} (bold numbers).

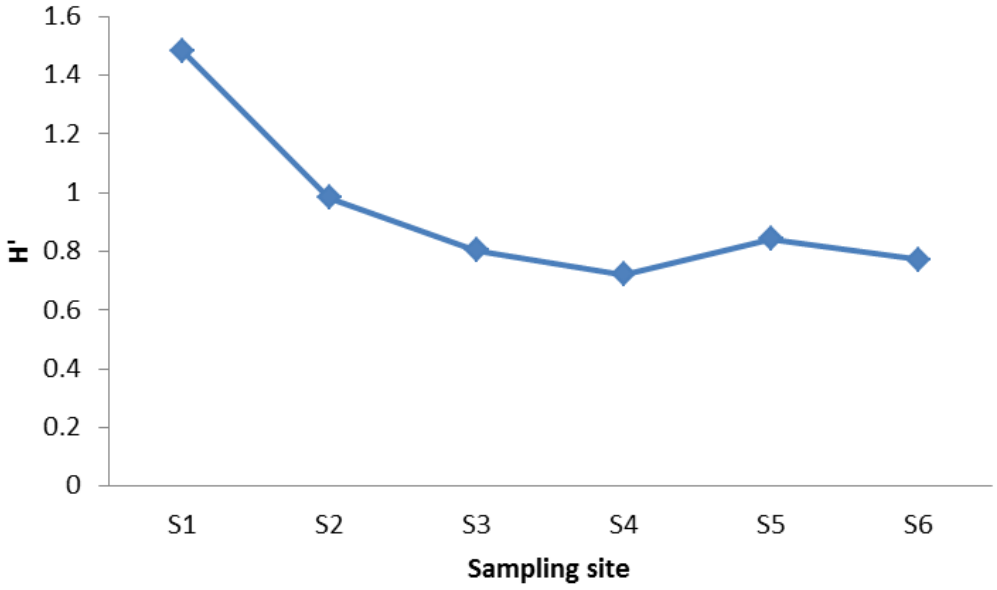

Figure S1. Mean Values (n=10) of the Shannon-wiener Diversity Index based on the Macrobenthic Communities at Six Sampling Sites (S1, S2, S3, S4, S5 and S6) in Ge Lake in Eastern China.

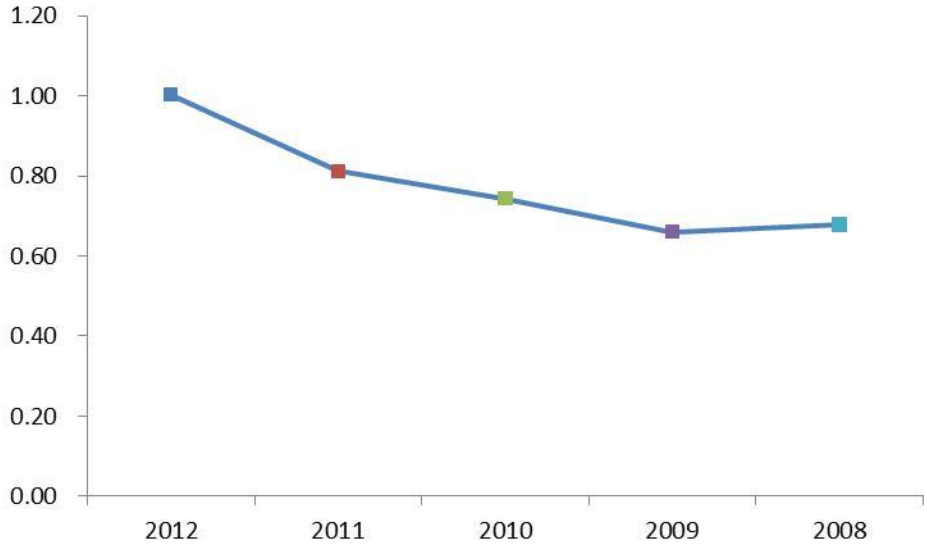

Figure S2. Mean Values of the Shannon-wiener Diversity Index at Four Sites in Ge Lake.

References

Tecnología y ciencias del agua, 10 (4), 88-119. DOI: 10.24850/j-tyca-2019-04-05

Achurra, A., Rodriguez, P. & Reynoldson, T. B. (2015). Is the Cantabrian region of northern Spain a biodiversity hotspot for obligate groundwater fauna? The case of oligochaetes (Annelida, Clitellata). Hydrobiologia, 745:151-166.

Angeler, D. G. & Johnson, R. K. (2013). Algal invasions, blooms and biodiversity in lakes: accounting for habitat-specific responses. *Harmful Algae*, 23:60-69.

Beck, M. W. & Hatch, L. K. (2009). A review of research on the development of lake indices of biotic integrity. *Environmental Reviews*, 17:21-44.

Beghelli, F. G. D. S., Santos, A. C. A. D., Ursoguimaraes, M. V. & Calijuri, M. D. C. (2012). Relationship between space distribution of the benthic macroinvertebrates community and traophic state in a Neotropical reservoir (Itupararanga, Brazil). *Biota Neotropica*, 12:1-11.

Beresford, A. L. & Jones, J. I. (2010). Weedbeds and big bugs: the importance of scale in detecting the influence of nutrients and predation on macroinvertebrates in plant-dominated shallow lakes. *Freshwater Biology*, 55:514-530.

Boaventura, R., Pedro, A. M., Coimbra, J. & Lencastre, E. (1997). Trout farm effluents: characterization and impact on the receiving streams. *Environmental Pollution*, 95:379-387.

Brock, T. C., Bas, D. A., Belgers, J. D., Bibbe, L., Boerwinkel, M. C., Crum, S. J. H., Diepens, N. J., Kraak, M. H. S., Vonk, J. A. & Roessink, I. (2016). Effects of sediment-spiked lufenuron on benthic macroinvertebrates in outdoor microcosms and single-species toxicity tests. *Aquatic Toxicology*, 177:464-475.

Brönmark, C. (1989). Interactions between epiphytes, macrophytes and freshwater snails: a review. *Journal of Molluscan Studies*, 55:299-311.

Cai, Y., Gong, Z. & Qin, B. (2012). Benthic macroinvertebrate community structure in lake Taihu, China: effects of trophic status, wind-induced disturbance and habitat complexity. *Journal of Great Lakes Research*, 38:39-48.

Cai, Y., Zhang, Y., Wu, Z., Chen, Y., Xu, J. & Gong, Z. (2017). Composition, diverstiy, and environmental correlates of benthic macroinvertebrate communities in the five largest freshwater lakes of China. *Hydrobiologia*, 788:85-98.

Camargo, J. A., Gonzalo, C. & Alonso, A. (2011). Assessing trout farm pollution by biological metrics and indices based on aquatic macrophytes

and benthic macroinvertebrates: a case study. *Ecological Indicators*, 11:911-917.

Chainho, P., Costa, J. L., Chaves, M. L., Lane, M. F., Dauer, D. M. & Costa, M. J. (2006). Seasonal and spatial patterns of distribution of subtidal benthic invertebrate communities in the Mondego river, Portugal-a poikilohaline estuary. *Hydrobiologia*, 555:59-74.

Chen, J., Xie, P., Guo, L., Zhen, G. L. & Ni, L. (2005). Tissue distributions and seasonal dynamics of the hepatotoxic microcystins-LR and-RR in a freshwater snail (Bellamya aeruginosa) from a large shallow, eutrophic lake of the subtropical China. *Environmental Pollution*. 134:423-430.

Clarke, K. (1993). Non-parametric multivariate analyses of changes in community structure. *Austral Ecology*, 18:117-143.

Courtney, L.A. & Clements, W. H. (1998). Effects of acidic pH on benthic macroinvertebrate communities in stream microcosms. *Hydrobiologia*, 379:135-145.

Dauer, D. M. (1993). Biological criteria, environmental health and estuarine macrobenthic community structure. Mar Pollut Bull. 26:249-257.

Duan, H., Ma, R. & Hu, C. (2012). Evaluation of remote sensing algorithms for cyanobacterial pigment retrievals during spring bloom formation in several lakes of East China. *Remote Sensing of Environment*, 126:126-135.

El, A. F., Zidane, H., Maanan, M., Tamsouri, M. & Errhif, A. (2015). Taxonomic diversity and structure of the molluscan fauna in Oualidia lagoon (Moroccan Atlantic coast). *Environmental Monitoring & Assessment*, 187:545. Doi:10.1007/s10661-015-4752-7.

Feebarani, J., Joydas, T. V., Damodaran, R. & Borja, A. (2016). Benthic quality assessment in a naturally- and human-stressed tropical estuary. Ecological Indicators 67:380-390.

Freitas, M., Azevedo, J., Carvalho, A. P., Campos, A. & Vasconcelos, V. (2014). Effects of storage, processing and proteolytic digestion on microcystin-LR concentration in edible clams. *Food & Chemical Toxicology*, 66:217-223.

Frouin, P. (2000). Effects of anthropogenic disturbances of tropical soft-bottom benthic communities. *Marine Ecology Progress*, 194:39-53.

Galil, B. S. (2000). A sea under siege-alien species in the Mediterranean. *Biological Invasions*, 2:177-186.

Gichana, Z., Njiru, M., Raburu, P. O. & Masese, F. O. (2015). Effects of human activities on benthic macroinvertebrate community composition and water quality in the upper catchment of the Mara River Basin, Kenya. *Lakes & Reservoirs Research & Management*, 20:128-137.

Gillett, D. J., Weisberg, S. B., Grayson, T., Hamilton, A., Hansen, V., Leppo, E. W., Pelletier, M. C., Borja, A., Cadien, D., Dauer, D., Diaz, R., Dutch, M., Hyland, J. L., Kellogg, M., Larsen, P. F., Levinton, J. S., Llanso, R., Lovell, L. L., Montagna, P. A., Pasko, D., Phillips, C. A., Rakocinski, C., Ranasinghe, J. A., Sanger, D. M., Teixeira, H., Dolah, R. F. V., Velarde, R. G. & Welch, K. T. (2015). Effect of ecological group classification schemes on performance of the AMBI benthic index in US coastal waters. *Ecological Indicators*, 50:99-107.

Griffin, J. N., Jenkins, S. R., Gamfeldt, L., Jones, D., Hawkins, S. J. & Thompson, R. C. (2009). Spatial heterogeneity increases the importance of species richness for an ecosystem process. *Oikos*, 118:1335-1342.

Guo, L. (2007). Doing battle with the green monster of Taihu lake. *Science*, 317: 1166.

Guilpart, A., Roussel, J-M., Aubin, J., Caquet, T., Marle, M. et al. (2012). The use of benthic invertebrate community and water quality analyses to assess ecological consequences of fish farm effluents in rivers. *Ecological Indicators*, 23:356-365.

Havens, K. E., Jin, K-R., Iricanin, N. & James, R. T. (2007). Phosphorus dynamics at multiple time scales in the pelagic zone of a large shallow lake in Florida, USA. *Hydrobiologia*, 581:25-42.

Holker, F., Vanni, M. J., Kuiper, J. J., Meile, C., Grossart, H. P., Stief, P., Adrian, R., Lorke, A., Dellwig, O., Brand, A., Hupfer, M., Mooij, W. M., Nutzmann, G. & Lewandowski, J. (2016). Tube-dwelling invertebrates: tiny ecosystem engineers have large effects in lake ecosystems. Ecological Monographs, 85:333-351.

Hosmani, S. (2012). Application of benthic diatom community in lake water quality monitoring. Online International Interdisciplinary *Research Journal*, II:21-34.

Huang, Y. (2001). Water environment and pollution control of Tai lake. Beijing: *Science Press* PP259-265.(in Chinese).

Huang, F. (2011). Reconstruction and water purification of submerged macrophytes community in Ge lake. Master Dissertation, *Suzhou University of Science and Technology*. (in Chinese).

Humpesch, U. (1979). Life cycle and growth fates of *Baetis* spp. (Ephemeroptera: Baetidae) in the laboratory and in two stone streams in Austria. *Freshwater Ecology*, 9:467-479.

Ibelings, B. W., Chorus, I. (2007). Accumulation of cyanobacterial toxins in freshwater "seafood" and its consequences for public health: a review. *Environmental Pollution*, 150:177-192.

Jarkko, R., Kirsti, E., Jaana, K., Kaarina, S. & Kirsti, L. (2002). Detection of Microcystins with protein phosphatase inhibition assay, high-performance liquid chromatography-UV detection and enzyme-linked immunosorbent assay comparison of methods. *Analytica Chimica Acta*. 466:213-231.

Jaschinski, S., Brepohl, D. C. & Sommer, U. (2011). The trophic immportance of epiphytic algae in a freshwater macrophyte system (Potamogeton perfoliatus L.): stable isotope and fatty acid analyses. *Aquatic Sciences*, 73:91-101.

Joel, A., Tocqueville, A. & Kaushik, S. J. (2011). Characterization of waste output from flow-through trout farms in France: comparison of nutrient mass-balance modelling and hydrological methods. *Aquatic Living Resources*, 24:63-70.

Jones, G. J. (2010). Pollution from fish farms. *Water & Environment Journal*, 4:14-18.

Jordana, E., Piendo, S. & Ballesteros, E. (2015). Macrobenthic assemblages, sediment characteristics and heavy metal concentrations in soft-bottom Ebre Delta bays (NW Mediterranean). *Environmental Monitoring & Assessment*, 187:71. Doi:10.1007/s10661-015-4315-y.

Joydas, T. V., Qurban, M., Krishnakumar P. K., Rabaoui, L., Kandan, M., Ashraf, T. T. M., Saji, A. P. & Lopes, M. (2016). Responses of macrobenthic communities to hypersaline and high temperature conditions: An example from the Arabian Gulf. International Marine Conservation Congress.

Jukka, H. & Leena, N. (2003). Effects of submerged macrophytes on sediment resuspension and internal phosphorus loading in lake Hiidenvesi (Southern Finland). *Water Research*, 37:4468-4474.

Karimi, J. M., Takami, G. A., Khara, H. & Abbaspour, R. (2016). Influence of trout farm effluents on water quality parameters and benthic macroinvertebrates. *Iranian Journal of Fisheries Sciences*, 15:133-143.

Kennedy, M. P., Lang, P., Grinaldo, J. T., Martins, S. V., Bruce, A. et al. (2017). Niche-breadth of freshwater macrophytes occurring in tropical southern African rivers predicts species global latitudinal range. *Aquatic Botany*, 136:21-30.

Kilgour, B., Clarkin, C., Morton, W. & Baldwin, R. (2008). Influence of nutrients in water and sediments on the spatial distributions of benthos in Lake Simcoe. *Journal of Great Lakes Research*, 34:365-376.

Krzton, W., Pudas, K., Pociecha, A., Strzesak, M., Kosiba, J., Walusiak, E., Szarek-Gwiazda, E. & Wilk-Wozniak, E. (2017). Microcystins affect zooplankton biodiversity in oxbow lakes. *Environmental Toxicology Chemistry*, DOI: 10.1002/etc.3519.

Lahrouni, M., Oufdou, K., Faghire, M., Peix, A., Ei, K. F., Vasconcelos, V. & Oudra, B. (2012). Cyanobacterial extracts containing microcystins affect the growth, nodulation process and nitrogen uptake of faba bean (*Vicia faba* L., Fabaceae). *Ecotoxicology*, 21:681-687.

Lamptey, E. & Armah, A. K. (2008). Factors affecting macrobenthic fauna in a tropical hypersaline coastal lagoon in Ghana, West Africa. *Estuaries Coasts*, 31:1006-1019.

Lance, E., Brient, L., Carpentier, A., Acou, A., Marion, L., Bormans, M. & Gerard, C. (2010). Impact of toxic cyanobacteria on gastropods and microcystin accumulation in a eutrophic lake (Grand-Lieu, France) with special reference to Physa (=Physella) acuta. *Science of the Total Environment*, 408:3560-3568.

Lawrence, B. A., Bourke, K., Lishawa, S. C. & Tuchman, N. C. (2016). Typha invasion associated with reduced aquatic macroinvertebrate abundance in nothern Lake Huron coastal wetlands. *Journal of Great Lakes Research*, 42:1412-1419.

Li, A. & Song, X. (2013). Eutrophication status of Ge lake and comprehensive control countermeasures. *Environmental Science & Management*, 38:85-92. (in Chinese).

Li, D., Erickson, R. A., Tang, S., Zhang, Y., Niu, Z., Liu, H. & Yu, H. (2016). Structure and spatial patterns of macrobenthic community in Tai lake, a large shallow lake, China. *Ecological Indicators*, 61:179-187.

Liu, Q., Kong, Y., Chen, L., Pu, Y. & Yan, W. (2005). Effect of pen aquaculture on community structure and species diversity of zoobenthos in Gehu Lake. *Chinese Journal of Applied & Environmental Biology*, 11:566-570. (in Chinese).

Li, Y., Xu, E. G., Liu, W., Chen, Y., Liu, H., Li, D., Liu, Z., Giesy, J. P. & Yu, H. (2017). Spatial and temporal ecological risk assessment of unionized ammonia nitrogen in Tai Lake, China (2004–2015). *Ecotoxicology and Environmental Safety*, 140:249-255.

Lloret, J. & Marin, A. (2009). The role of benthic macrophytes and their associated macroinvertebrate community in coastal lagoon resistance to eutrophication. *Marine Pollution Bulletin*, 58:1827-1834.

Loch, D. D., West, J. L. & Perlmutter, D. G. (1996). The effect of trout farm effluent on the taxa richness of benthic macroinvertebrates. *Aquaculture*, 147:37-55.

Mandal, S. & Harkantra, S. N. (2013). Changes in the soft-bottom macrobenthic diversity and community structure from the ports of Mumbai, India. *Environmental Monitoring & Assessment*, 185: 653-672.

Marques, L., Carrico, A., Bessa, F., Gaspar, R., Neto, J. M. & Patrício, J. (2013). Response of intertidal macrobenthic communities and primary producers to mitigation measures in a temperate estuary. *Ecological Indicators*, 25:10-22.

Marzin, A., Archaimbault, V., Belliard, J., Chauvin, C., Delmas, F. & Pont, D. (2012). Ecological assessment of running waters: do macrophytes, macroinvertebrates, diatoms and fish show similar responses to human pressures? *Ecological Indicators*, 23:56-65.

Mon, D-L., Cheng, C-H. & Lin, J-C. (1994). Evaluating weapon system using fuzzy analytic hierarchy process based on entropy weight. *Fuzzy Sets & Systems*, 62:127-134.

Munoz, I., Bueno, M. J. M., Aguera, A. & Fernandez-Alba, A. R. (2010). Environmental and human health risk assessment of organic micro-pollutants occurring in a Spanish marine fish farm. *Environmental Pollution*, 158:1809-1816.

Nicola, G. G., Almodóvar, A. & Elvira, B. (2010). Effects of environmental factors and predation on benthic communities in headwater streams. *Aquatic Sciences*, 72:419-429.

Nishijima, W., Umehara, A., Okuda, T. & Nakai, S. (2015). Variations in macrobenthic community structures in relation to environmental variables in the Seto Inland Sea, Japan. *Marine Pollution Bulletin*, 92:90-98.

O'Brien, A. L. & Keough, M. J. (2013). Detecting benthic community responses to pollution in estuaries: a field mesocosm approach. *Environmental Pollution*, 175:45-55.

Peeters, E. T., Gylstra, R. & Vos, J. H. (2004). Benthic macroinvertebrate community structure in relation to food and environmental variables. *Hydrobiologia*, 519:103-115.

Pereira, P., Carvalho, S., Pereira, F., de Pablo, H., Gaspar, M. B., Pacheco, M. & Vale, C. (2012). Environmental quality assessment combining sediment metal levels, biomarkers and macrobenthic communities: application to the Obidos coastal lagoon (Portugal). *Environmental Monitoring & Assessment*, 184:7141-7151.

Pfeifer, D., Bäumer, H-P., Dekker, R. & Schleier, U. (1998). Statistical tools for monitoring benthic communities. *Senckenbergiana Maritima*, 29:63-76.

Qin, W., Xu, L., Zhang, X., Wang, Y., Meng, X., Miao, A. & Yang, L. (2010). Endoplasmic reticulum stress in murine liver and kidney exposed to microcystin-LR. *Toxicon*, 56:1334-1341.

Qiu, W. (2001). *Management decision and applied entropy*. Beijing: China Machine Press. (in Chinese).

Rahel, F. J. (2002). Homogenization of freshwater faunas. *Annual Review of Ecology & Systematics*, 33:291-315.

Resh, V. H. (2007). Multinational, freshwater biomonitoring programs in the developing world: lessons learned from African and Southeast Asian river surveys. *Environmental Management*, 39:737-748.

Richman, L. A. & Somers, K. (2010). Monitoring metal and persistent organic contaminant trends through time using quagga mussels (Dreissena bugensis) collected from the Niagara River. *Journal of Great Lakes Research*, 36:28-36.

Rivasseau, A., Racaud, P., Deguin, A. & Hennion, M. (1999). Evaluation of an ELISA Kit for the monitoring of Microcystins (Cyanobacterial Toxins) in water and algae environmental samples. *Environmental Science & Technology*, 33:1520-1527.

Roberts, L., Boardman, G. & Voshell, R. (2009). Benthic macroinvertebrate susceptibility to trout farm effluents. *Water Environment Ressearch A Research Publication of the Water Environment Federation*, 81:150-159.

Romeo, T., D'Alessandro, M., Esposito, V., Scotti, G., Berto, D., Formalewicz, M., Noventa, S., Giuliani, S., Macchia, S., Sartori, D., Mazzola, A., Andaloro, F., Giacobbe, S., Deidun, A. & Renzi, M. (2015). Environmental quality assessment of grand harbour (Valletta, Maltese Islands): a case study of a busy harbour in the central Mediterranean

sea. *Environmental Monitoring & Assessment*, 187:747. Doi:10.1007/s10661-015-4950-3.

Scheffer, M. (1998). *Ecology of shallow lakes* Dordretcht: Kluwer Academic Press.

Signa, G., Mazzola, A., Costa, V. & Vizzini, S. (2015). Bottom-Up Control of Macrobenthic Communities in a Guanotrophic Coastal System. *Plos One* 10:e0117544.

Silva, C., Yanez, E., Martin-Diaz, M. L., Riba, I. & DelValls, T. A. (2013). Integrated ecotoxicological assessment of marine sediments affected by land-based marine fish farm effluents: physicochemical, acute toxicity and benthic community analyses. *Ecotoxicology*, 22:996-1011.

State Environmental Protection Administration of China. (2002). *Water and wastewater monitoring analysis method*. Beijing: China Environmental Science Press. (in Chinese).

Tao, H., Pan, J., Shen, Y., Li, W. & Huang, F. (2011). Effects of substrate character of Ge lake on the growth of *Potamogetoncripus* and *Elodea nattalii*. *Journal of Lake Science*, 23:383-388. (in Chinese).

Tao, H., Pan, J-Z., Shen, Y-L., Li, W-C. & Huang, F. (2010). Overview and degradation reasons of submerged macrophytes of Ge lake. *Environmental Science & Technology*, 5:64-68. (in Chinese).

Tews, J., Brose, U., Grimm, V., Tielbörger, K., Wichmann, M. C., Schwager, M. & Jeltsch, F. (2004). Animal species diversity driven by habitat heterogeneity/diversity: the importance of keystone structures. *Journal of Biogeography*, 31:79-92.

Wallace, J. B. & Eggert, S. L. (2015). Benthic invertebrate fauna, small streams. *Encyclopedia of Inland Waters*, 173-190.

Wang, L., Liu, Y., Chen, L., Xiao, B., Liu, J. & Wu, Q. (2007). Benthic macroinvertebrate communities in Dianchi lake Yunnan and assessment of its water. *Acta Hydrobiologica*, 11:232-239.

Wang, L., Wu, L., Zhang, R. & Zhang, Y. (2012). Spatiotemporal variation of zoobenthos community and bio-assessment of water quality in Ge lake. *Chinese Journal of Ecology*, 31:1990-1996. (in Chinese).

Wong, M. C. & Dowd, M. (2015). Patterns in Taxonomic and Functional Diversity of Macrobenthic Invertebrates Across Seagrass Habitats: a Case Study in Atlantic Canada. *Estuaries and Coasts*, 38:2323-2336.

Wu, P., Liu, S. & Liu, X. (2012). Composition and spatio-temporal changes of soil macroinvertebrates in the biodiversity hotspot of Northern Hengduanshan mountains, China. *Plant and Soil*, 357:321-338.

Wu, X., Pan, J., Li, W., Huang, F. & Zhao, H. (2013). Water purification effect in the eco-remediation zone in the east of Ge lake. *Journal of Ecology and Rural Environment*, 29:284-289.

Xu, L., Pan, J., Jiang, J., Zhao, H. & Liu, C. (2013). A history evaluation modelling and forecastation of water quality in shallow lake. *Water & Environment Journal*, 27:514-523.

Yoon, S. J., Hong, S., Kwon, B. O., Ryu, J., Lee, C. H., Nam, J. & Khim, J. S. (2017). Distributions of persistent organic contaminants in sediments and their potential impact on macrobenthic faunal community of the Geum River Estuary and Saemangeum Coast, Korea. *Chemosphere*, 173:216-226.

Zadeh, L. A. (1965). Fuzzy sets. *Information and Control*, 8:338-353.

Zeng, Q., Gu, X., Chen, X. & Mao, Z. (2013). The impact of Chinese mitten crab culture on water quality, sediment and the pelagic and macrobenthic community in the reclamation area of Guchenghu lake. *Fisheries Science*, 79:689-697.

Zhang, X., Mei, X. & Gulati, R. D. (2016). Effects of omnivorous tilapia on water turbidity and primary production dynamics in shallow lakes: implications for ecosystem management. *Reviews in Fish Biology & Fisheries*, 1-10.

Zhang, Y., Zhang, Y., Gao, Y., Zhang, H., Cao, J., Cai, J. & Kong, X. (2011). Water pollution control technology and strategy for river-lake systems: a case study in Gehu lake and Taige Canal. *Ecotoxicology*, 20:1154-1159.

Zhou, X., Zhang, N., Zhang, Y., Niu, Z., Liu, L. & Yu, H. (2014). Preliminary study on the relationship between the water quality and the aquatic biological health status of Tai lake. *Environmental Science*, 35, 272-279. (in Chinese).

Zhu, C., Wang, Y. & Yu, N. (1996). *Researches on benthic ecological distribution and its variation in GeLake*. Beijing: China Agriculture Press; PP149-155. (in Chinese).

Zhu, C., Wang, Y. & Yu, N. (1997). *Collections of studies on high fishery production model and ecological fishery in Ge Lake*. China Agriculture Press. PP149-155. (in Chinese).

Tecnología y Ciencias del Agua

DOI: 10.24850/j-tyca-2019-04-06
Special Article

Relationship between Gully Erosion and Agricultural Landscape Pattern in the Typical Black Soil Region of Northeast China

Relación entre la erosión de los barrancos y el modelo de paisaje agrícola en la región de suelo negro típico del noreste de China

Rongxin Deng[1]
Wenjuan Wang[2]*

[1]School of Resources and Environment, North China University of Water Resources and Electric Power, Zhengzhou 450045, China, email: ----------, ORCID 0000-0001-7350-0426

[2]College of Resources and Environment, Henan University of Economics and Law, Zhengzhou 450046, China, email: wenjuan110@163.com, ORCID 0000-0003-4029-5344

*Corresponding author: Wenjuan Wang, wenjuan110@163.com

Abstract

The black soil region of Northeast China is an important grain producing area that faces a serious erosion problem. We used SPOT5 remote sensing imagery from 2008 to establish the gully distribution in a typical black soil region located in the Wuyuer and Nemoer River basin, and Landsat Thematic Mapper imagery to designate landscape patterns. Ninety-three sub-basins were determined based on digital elevation model data using a hydrological analysis module for which landscape pattern metrics and gully density were obtained using FRAGSTATS software and the Geographic Information System (GIS) spatial analysis function, respectively. The results show a gully density of 4,219.2 m^2/km^2 with 10,149.5 ha of eroded dry land and 25,261.2 ha of destroyed dry land. Correlation analysis between gully density and the landscape percentage of dry land and forest, perimeter-area fractal dimension, contagion index, and Shannon's diversity index indicate that regulation of the proportion of forest, dry land, and grass, and reasonable optimization of landscape arrangement is very important for soil erosion management and control. Additionally, the findings indicate

that landscape differences between each sub-basin are not the principal reason for differences in gully erosion. Further research on gully formation should integrate the effect of natural forces and human activities.

Keywords: Gully erosion, gully density, black soil region of Northeast China, landscape metrics.

Received: 18/12/2018

Accepted: 28/03/2019

Introduction

The black soil region of Northeast China is an important and marketable grain production base, but local soil erosion poses a very serious concern. Erosion leads to decreased fertility of the black soil that directly affects its productivity. Within this context, the Chinese government, as well as scientists and farmers, have paid great attention to the erosion and degradation of the black soil region (Liu 2005). Since the 1990s, several studies have investigated local erosion (Zhang *et al.* 1992, 2006, 2008; Wang *et al*. 2008, 2012a; Fang *et al.* 2012), although most focused on hillslope erosion. Gully erosion also causes land degradation and is an important source of sediment. However, studies on gully erosion in the black soil area remain limited. Data collected around the world show that gully erosion represents between 10% and 94% of the total sediment yield caused by water erosion (Poesen *et al.* 2003), and both on-site and off-site effects can cause tremendous harm. Reasonable and effective schemes for the control and prevention of gully erosion are therefore very important for food production. Previous studies have been mostly small scale, monitoring <10 gullies over periods of 3–5 years, and using GPS to obtain gully parameters (Hu *et al.* 2007; Zhang *et al.* 2007; Wu *et al.* 2008; Hu *et al.* 2009; Dong & Wu 2010), while only a few studies have been conducted on a larger scale (Meng & Li 2009; Yan *et al.* 2010; Wang *et al*. 2012b).

Landscape ecology theory is a new application in the study of soil erosion. Land use and land cover change are important driving forces that lead to changes in landscape patterns. Furthermore, land use structures are closely related to soil and water loss, and different types of land use and structures within a landscape have a clear impact on

runoff and erosion processes (Trimble 1999; Fu *et al*. 2003). Understanding the relationship between landscape pattern and soil erosion is important for the management of land use structures required to improve the quantity and proportion of the different landscape types, and to optimize the composition of patches to effectively prevent and control erosion (Wei *et al.* 2006).

This study investigates the relationship between landscape patterns and gully erosion in a typical agricultural landscape of Northeast China's black soil region. Such landscapes have greater variability than natural landscapes because of the interplay between natural environmental factors and anthropogenic activities. The study of the agricultural landscape is important for understanding the relationships between landscape pattern, the environment, ecological processes, and socioeconomic activities, and is also important for the control and management of land resources and erosion.

Gully distribution data within the study area were obtained from Geographic Information System (GIS) and SPOT5 imagery. In addition, 93 sub-basins were extracted from a digital elevation model (DEM) using an ArcGIS hydrology analysis module. Gully density and corresponding landscape pattern metrics in each sub-basin were established based on the GIS spatial analysis function and FRAGSTATS software. Furthermore, correlation analysis was performed to evaluate the relationship between gully erosion and the agricultural landscape pattern. This study improves the understanding of the causes and effects, as well as laws controlling gully erosion in different land use types and landscape patterns. Furthermore, the results can be considered a basis for the development of land use planning schemes for the control and prevention of soil erosion and water loss.

Material and Methods

Study Area

The study area is located within the Wuyuer and Nemoer River basin and is typical of the black soil region of Northeast China. Situated in the middle of Heilongjiang Province, this area covers about 23,000 km^2. The cities of Wudalianchi and Beian lie to the north and east, and Mingshui and Fuyu counties lie to the south and west (Figure 1).

Geomorphologically, the region is in the transition area between the Songnen Plain and Lesser Hinggan Mountains. The landscape is characterized by rolling hills with gentle slopes of mostly <5°.

The major soil types of the study area include black soil, as well as meadow soil and bog soil found mainly in the low-lying wetland plains. Black soil is characterized by high organic matter content, loose texture, and large pore gaps, the latter two of which facilitate accelerated erosion. The elevation ranges from 150 to 600 m with the highest point in the northeast highlands, while the southwest comprises lower-lying rolling hills/plains. The study area has a temperate continental monsoon climate; its mean annual temperature is 0.2–1.5°C, mean annual rainfall is 550–600 mm, and mean depth of runoff is about 75 mm. The Wuyuer, Nemoer, Shuangyang, Laolai, and Runjin rivers constitute the principal waterways within this region, and the vegetation is characteristically interwoven forest and meadow plains of the Mongolia vegetation zone.

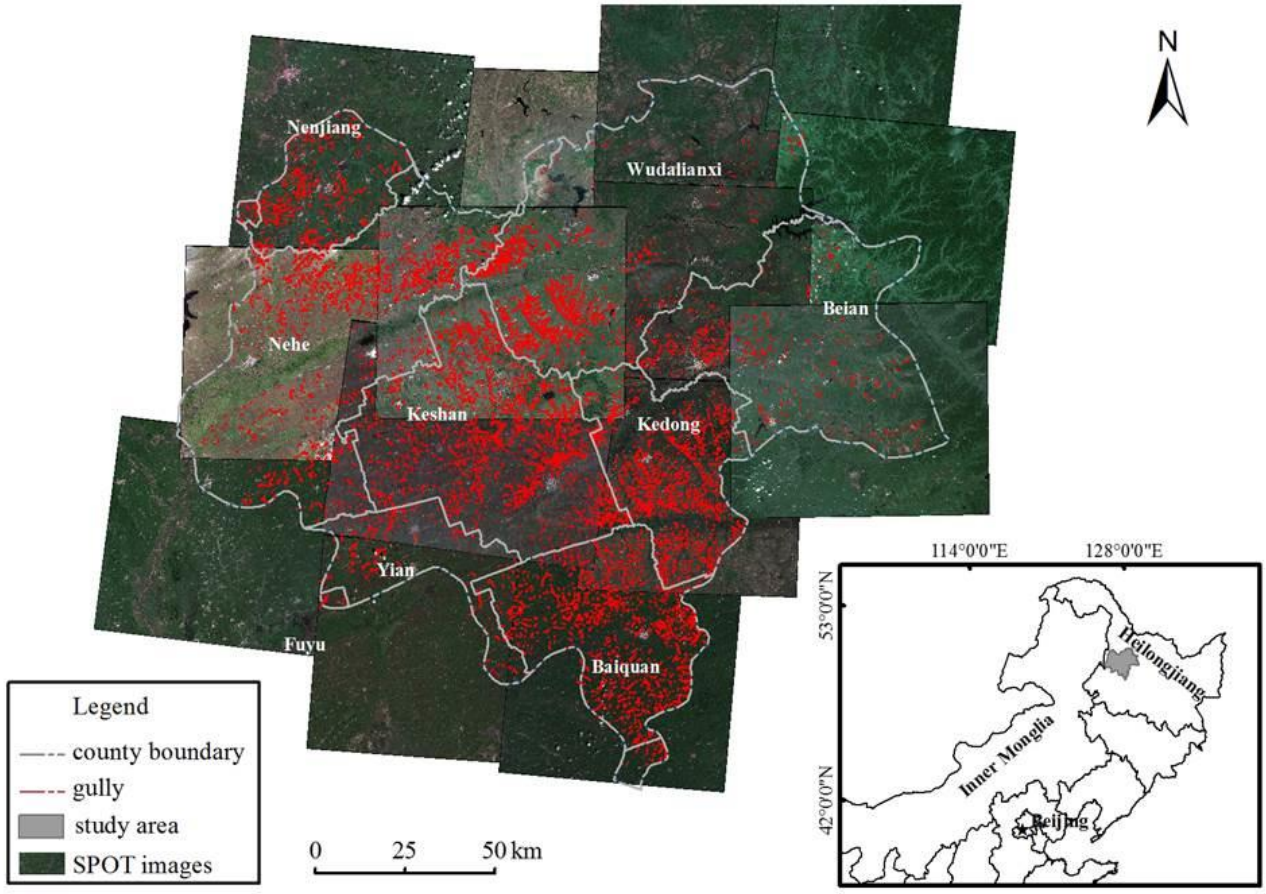

Figure 1. Location of the study area, SPOT5 images and gully data distribution map.

Gully Data

Fourteen cloud-free 2.5-m resolution simulated true color SPOT5 images from 2008 were used as the source from which the gully data were obtained. Field surveys were conducted over a period of about 20 days in 2008 and 2009. The gully width, length and deposit in the gully bottom were investigated, in addition to the lithology, agrotype, land use and vegetation both in and around the gullies. After completion of the field survey, gully interpretation signs were built following the theory of gully classification and growth (Yang 2001) and with support of expert knowledge. The primary method to discriminate the gullies is according to their spectral characteristics; gullies are light green on SPOT5 images and some segments on the gully bottoms appear white. There is a clear boundary between gully and slope, and a fundamental difference in slope, erosion form, land use, soil properties, and vegetation coverage. Gully distribution data were obtained using a combination of ArcGIS 9.3, expert experience, and topographic, geomorphologic, and soil maps. An additional six days were spent conducting validation work in 2009, following which the obtained gully data were updated and finalized (Figure 1). The precision of the gully data was determined to be >90%.

Landscape Pattern Data

Landsat/Thematic Mapper (TM) images from 2008 were used as the data source for assessing landscape patterns. Although SPOT5 images can also be used to obtain landscape pattern information, this source requires considerably more analysis time and is therefore unrealistic due to the large study area (>20,000 km^2). TM images are a more appropriate data source for large-scale studies. The necessary interpretation symbols were built based on imagery characteristics (e.g., color, shape, and texture), expert experience, field survey data, and other related geographical maps. ArcGIS 9.3 was then used to interpret the TM images and derive an agricultural landscape map using an interactive module. Compared with the field data, the overall precision of the interpretation was at least 95%. The landscape was classified into eight types: dry land, forest, paddy field, grass,

Tecnología y ciencias del agua, 10 (4), 120-134. DOI: 10.24850/j-tyca-2019-04-06

construction land, water area, bare land, and wetland (Figure 2) based on the land use classification system established by previous studies (Liu *et al.* 2005), Landsat/TM image data sources, and features of the study area.

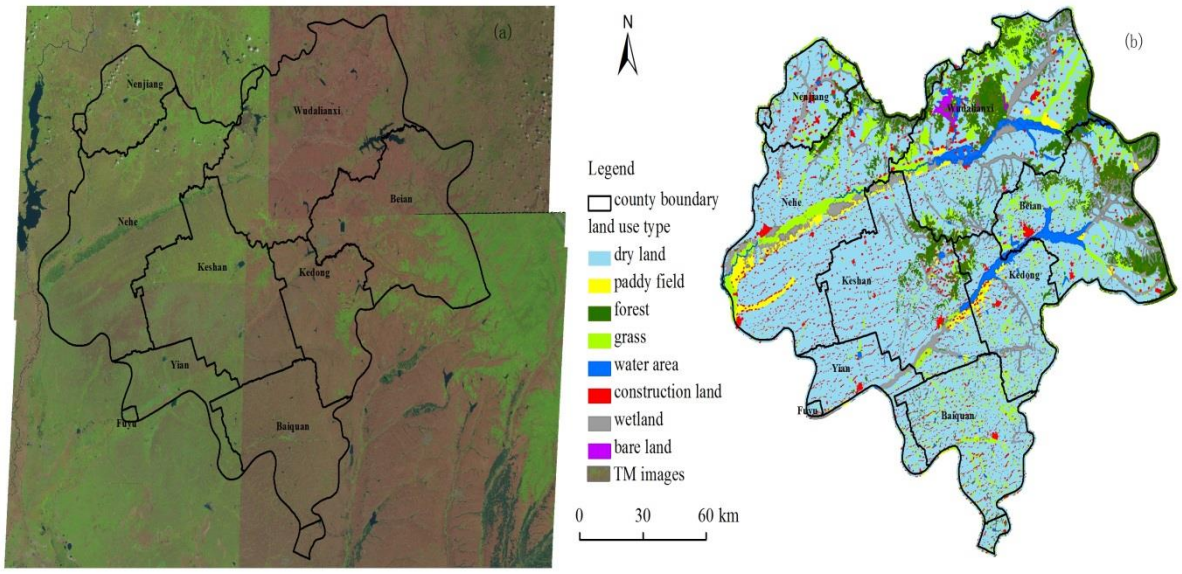

Figure 2. (a) Landsat Thematic Mapper images and (b) land use distribution map in 2008.

DEM and Sub-Basin Data

Contours and elevation points were obtained by vectorization using topographic maps. A 5-m resolution DEM was then built using the digital contours and elevation points in the TOPGRID module. The ArcGIS hydrology analysis module was used to extract 93 sub-basins from the DEM as the basic analysis units.

Landscape Pattern Analysis

The main quantitative method to study landscape patterns and dynamics is landscape pattern metrics (Guo *et al.* 1999). Accordingly, landscape pattern metrics were adopted in the present study to analyze

the landscape pattern and identify potential order within the disordered landscape. The percentage of landscape (PLAND) of different land use types was selected as the metric class level with regard to its effect on soil erosion. The perimeter-area fractal dimension (PAFRAC), contagion index (CONTAG), and Shannon's diversity index (SHDI) were selected as landscape metrics to assess the independence of individual metrics and information integration (Riitters *et al.*, 1995). The metrics above were calculated using FRAGSTATS 3.3 software. Formulas and implications of the metrics can be found in the help file of the FRAGSTATS 3.3 software (http://www.nefu.edu.cn/other/vip/eco-space/ecosoft.him). Single and multi-factor correlation analyses were performed using SPSS 15 software to analyze the relationship between gully erosion and landscape pattern. The methods and goals of the present study are summarized as a flowchart in Figure 3.

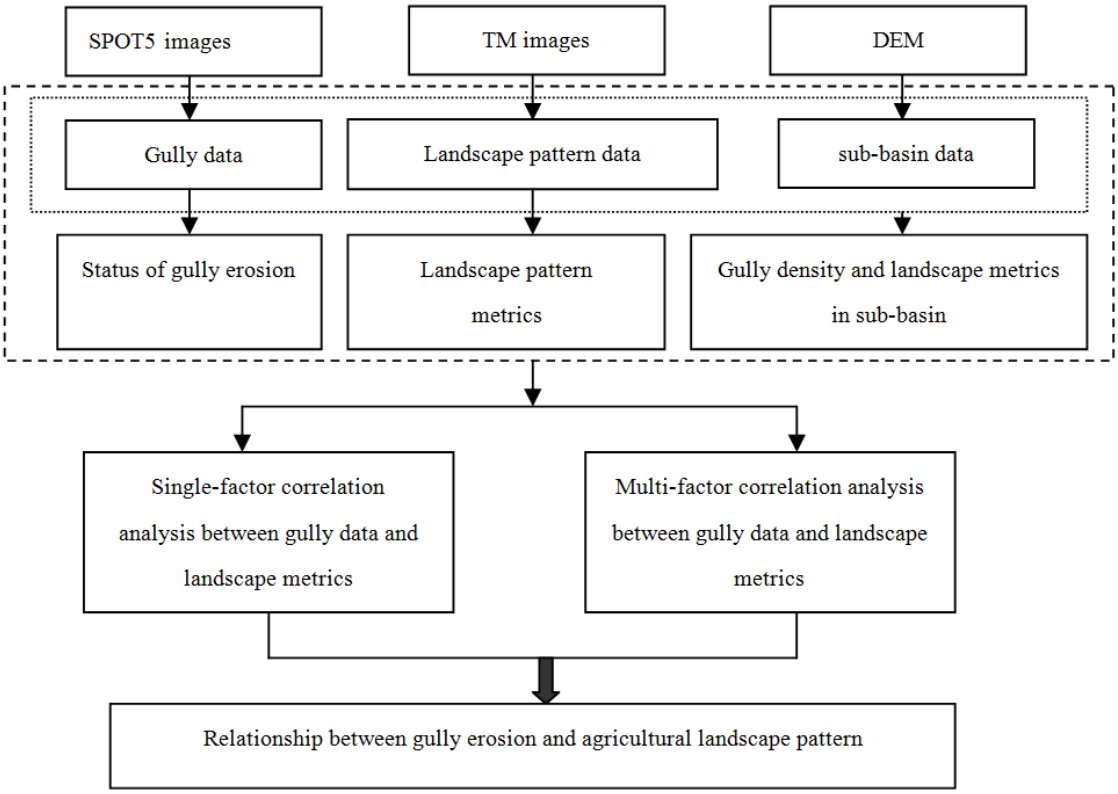

Figure 3. Flowchart of the approach and main goals of this work.

Results and Discussion

Tecnología y ciencias del agua, 10 (4), 120-134. DOI: 10.24850/j-tyca-2019-04-06

Status of Gully Erosion

The average gully density is 4,219.2 m^2/km^2 (Table 1). According to the classification and gradation of soil erosion by the Water Conservancy Department of China (Water and Soil Conservation Office of Water Conservancy Department of China, 1997), there is currently no standard to define damage to planar gully density even though gully degradation poses challenges to sustainable agriculture development and can be directly detected in field investigations. A reasonable standard for the degradation of planar gully density is therefore required.

The area of eroded dry land is 10,149.5 ha (Table 1), but field surveys and interviews with local farmers indicate that the land is unsuitable for cultivation within 10 m of a gully edge. Cultivation performed in such close proximity to a gully leads to accelerated erosion and an exacerbated rate of loss of cultivable land. Therefore, the analysis was performed using a 10-m buffer zone to estimate the eroded dry land (hereafter called destroyed dry land) yielding a total area of 25,261.2 ha (Table 1).

Gully erosion within the study area presents a very serious problem with grave consequences for local agricultural production. Land management schemes and policies must be adopted to prevent gully erosion and control agricultural practices. Gully volume was not measured in the present study but future efforts to derive this parameter may provide important estimates of sediment yield (Wang *et al*. 2011).

Table 1. Gully erosion data in the study area.

Gully density (m^2/km^2)	Eroded cultivated land area (ha)	Destroyed cultivated land area (ha)
4219.2	10149.5	25261.2

Landscape Patterns and Metrics of the Study Area

According to the class-level metric PLAND, the landscape distribution

Tecnología y ciencias del agua, 10 (4), 120-134. DOI: 10.24850/j-tyca-2019-04-06

includes 68.23% dry land, 1.92% paddy field, 9.38% forest, 7.25% grass, 6.57% wetland, 3.65% construction land, 2.63% water area, and 0.37% bare land. The landscape level metric CONTAG is 76.6364, PAFRAC is 1.4502, and SHDI is 1.2535. According to the values of metrics analysis, landscape types and distribution within the study area can be simplified. For example, dry land and forest form the matrix, while paddy field, grass, and construction land are present in mosaic patches, and the water area and wetland constitute corridors. Our results show that this region suffers high levels of artificial intervention, which concentrates areas of dry land and reduces diversity. The combination of these factors means that the region has evolved into an artificial agricultural ecology with low heterogeneity (Liu *et al*. 2002). This type of landscape has a great impact on soil erosion (Han *et al.* 2005).

Sub-Basin Gully Density and Landscape Metrics

A sub-basin is both an integrated unit, with runoff, erosive sediment yield, and delivery, and a basic unit over which comprehensive control of soil erosion and water loss can be implemented (Jia *et al.* 2005). Table 2 shows that the coefficient of variance (CV) of PAFRAC, CONTAG, and SHDI are similar (0.02, 0.82, and 0.12, respectively), which indicates that there is little difference between the landscape pattern configurations within each sub-basin. PAFRAC values range from 1.13 to 1.54 with an average of 1.28, which reveals a concerning level of human disturbance and regular shape of the sub-basins. However, SHDI values are much lower, which indicates a low degree of landscape diversity within each sub-basin. High CONTAG values imply extensive connectivity between batches of the study. The mainland use type was dry land (67.50%) followed by grass (9.74%) and forest (7.2%). All land use types showed that dry land forms the matrix with its simple shape and high levels of human disturbance.

Table 2. Extent of change of gully density and landscape metrics in sub-basins.

index	Gully density (m^2/km^2)	Dryland (%)	Grass (%)	Forest (%)	PAFRAC	CONTAG	SHDI
Minimum	32.76	3.60	0.00	0.00	1.13	61.98	0.24

(min)							
Maximum (max)	13789.93	94.93	81.37	60.35	1.54	93.15	1.55
Mean	3878.91	67.50	9.74	7.72	1.28	74.20	0.96
Coefficient of variance (CV)	3541.38	5.78	22.72	9.34	0.02	0.82	0.12

Single-Factor Correlation Analysis between Gully Density and Landscape Metrics

The relationship between gully density and landscape metrics are listed in Table 3. Our findings indicate a positive correlation between gully density and the PLAND of dry land, grass, PAFRAC, and CONTAG, while the PLAND of forest and SHDI show a negative correlation. The positive correlation of gully density with dry land suggests this land use type is a dominant factor in the generation of gully erosion. On the contrary, the negative correlation of forest with gully density implies that this land use type plays an important role in erosion prevention and control. However, in view of the centralized distribution of forest land in the northern and southeastern areas, its functionality in terms of soil and water conservation is limited. The lower correlation of grass might be related to its small coverage area.

Table 3. Correlation analysis between gully density and landscape metrics.

	Dry land (%)	Forest (%)	Grass (%)	PAFRAC	CONTAG	SHDI
R	0.58**	-0.43**	0.25*	0.515*	0.48*	-0.569**

*$P < 0.05$; **$P < 0.01$;

The positive correlations of PAFRAC and CONTAG indicate that lower PAFRAC and higher CONTAG values easily enable erosion. One possible explanation for this finding is the high level of human influence that is characteristic of an agricultural landscape. Correspondingly, the regular patch shapes and simple spatial landscape composition can also easily lead to soil erosion. The SHDI is considerably more sensitive to

landscape pattern type and can reflect landscape heterogeneity. The negative correlation of SHDI demonstrates that it can serve as an indicator of erosion control. The matrix composed of dry land indicates that patches are ductile with high connectivity and low diversity. Low SHDI values and high CONTAG values bring the potential risk of erosion.

Our findings indicate that the simplified and inhomogeneous landscape pattern found in the study area accelerates gully erosion. The deep analysis shows that regulation of the percentages of grass, dry land and forest, reasonable optimization of the landscape configuration, and an increase of the SHDI can enhance the capability of the landscape to control water erosion (Wei *et al*. 2005).

Multi-Factor Correlation Analysis between Gully Density and Landscape Metrics

The formation of gullies is dominated by many factors, and the integrated impact between gullies and landscape pattern is interpreted according to theory. Here, using gully density as the dependent variable *y* and the landscape pattern metrics as independent variables (PAFRAC as x_1, CONTAG as x_2, SHDI as x_3, percent of dry land as x_4, percent of forest as x_5, and percent of grass as x_6), a linear regression was determined using SPSS 15 software. The derived equation is given as:

$$y = 5.78 + 0.223x_1 + 0.19x_2 - 0.118x_3 + 0.233x_4$$

The results yield R = 0.534. Independent variables x_5 and x_6 were eliminated because these two metrics had little effect on the integrated analysis. The results also show that the integrated effect of multi-factors in gully formation is not particularly high. A given independent variable can only explain about 25% of the dependent variable and might be caused by small differences between the sub-basins. Therefore, landscape differences between sub-basins are not the principal reason for the observed differences in gully erosion. However, these results do suggest that flow hydraulics, rainfall, topography, soils, and land use have important effects on gully formation. The integrated effect of rainfall, land use, soil, vegetation, and landscape physiognomy on erosion needs to be determined in future work (Poesen *et al*. 2003; Valentin *et al.* 2005).

Conclusions

The average gully density within the study area is 4,219.2 m^2/km^2, and the areas of eroded dry land and destroyed dry land are 10,149.5 and 25,261.2 ha, respectively. These values indicate that the study area suffers from severe gully erosion, which is a threat to food production and requires strengthened control measures. The study area is typical of an agricultural landscape with dry land accounting for 68.23%, which constitutes the matrix landscape type, while other types constitute considerably smaller areas. This landscape pattern results in lower PAFRAC and SHDI values and higher CONTAG values, but the difference between the metrics in each sub-basin is insubstantial. This type of pattern accelerates erosion. Large areas of dry land are therefore the most important for concentrating soil and water conservation activities.

The gully erosion and agricultural landscape pattern show characteristic spatial heterogeneity with a range of relationships between different pattern characteristics and soil erosion. Correlation analysis between gully density and landscape pattern metrics indicates that dry land is the predominant landscape that causes gully erosion and forest plays an important part in its prevention. Based on the analysis of PAFRAC, SHDI and CONTAG, reasonable regulation of the landscape pattern configuration of dry land, forest, and grass can be effective in preventing erosion.

Acknowledgments

This work was supported by Training Plan for Young Backbone Teachers in Colleges and Universities of Henan Province in China, and NG Teng Fong / Sino Outstanding Youth Fund of HUEL.

References

Dong, Y. F. & Wu, Y. Q. (2010). Short-term gully erosion at different places of bottom of gully using virtual erosion pins. Scientia Geographica Sinicae, 30(6): 892-897.

Fang, H. Y., Li, Q. Y., Sun, L. Y. & Cai, Q. G. (2012). Using 137Cs to study spatial patterns of soil erosion and soil organic carbon (SOC) in an agricultural catchment of the typical black soil region, Northeast China. Journal of Environmental Radioactivity, 112: 125-132.

Fu, B. J., Chen, L. D. & Wang, J. (2003). Land use structure and ecological processes. Quaternary Sciences, 23(3): 247-255.

Guo, J. P., Yang, H. X. & Zhang, Y. X. (1999).Studies on spatial pattern and dynamics for landscape elements in Guandishan forest region, Shanxi, China. Acta Ecologica Sinica, 19(4): 468-473.

Hu, G., Wu, Y. Q., Liu, B. Y., Yu, Z. T., You, Z. M. & Zhang, Y. G. (2007). Short-term gully head retreat rates over rolling-hill areas in Black Soil of Northeast China. Catena, 71: 321-329.

Hu, G., Wu, Y. Q., Liu, B. Y., Zheng, Q. H., Zhang, Y. G. & Wei, X. (2009). Growth characteristics of ephemeral gully in rolling hills of black soils in Northeast China. Scientia Geographic Sinica, 29(4): 545-549.

Han, X. Z., Wang, S. Y. & Song, C. Y. (2005). Effects of land use and cover change on ecological environment in Mollisols Region. Scientia Geographica Sinica, 25(2): 203-208.

Jia, Y. Y., Zheng, F. L. & Yang, Q. K. (2005). Distributed water erosion prediction model for small watershed in loess plateau. Shui li Xue bao, 36(3): 328-332.

Liu, J. Y., Zhang, Z. X., Zhuang, D. F., Zhang, S. W. & Li, X. B. (2005). Study on RS' Spatial-temporal Information of Land Use Change in China 1990s'. Beijing, Science Press: 54-55.

Liu, X. T., He, Y. & Dang, W. (2002). Research on Comprehensive Development of Regional culture in Northeast China. Beijing, Sciences Press: 179-188.

Liu, X. Y. (2005). The loss of black soil and its rehabilitation. Research of Soil and Water Conservation, 12(5): 128-152.

Meng, L. Q. & Li, Y. (2009). The mechanism of gully development on sloping farmland in Black Soil Area, Northeast China, Journal of Soil and Water Conservation, 23(1): 7-11, 44.

Poesen, J., Nachtergaele, J., Verstraeten, G. & Valentin, C. (2003). Gully erosion and environmental change: importance and research needs. Catena, 50: 91-133.

Riitters, K. H., O'Neill, R. V., Hunsaker, C. T., Wickham, J. D., Yankee, D. H., Timmins, S. P., Jones, K. B. & Jackson, B. L. (1995). A factor analysis of landscape pattern and structure metrics. Landscape Ecology, 10: 23-39.

Trimble, S. W. (1999). Decreased rates of alluvial sediment storage in the Coon creek basin, Wisconsin, 1975-1993. Science, 285: 1244-1246.

Valentin, C., Poesen, J. & Yong, L. (2005). Gully erosion：Impacts，factors and control．Catena，63：132-153.

Wang, W. J., Zhang, S. W. & Deng, R. X. (2011). Gully status and

relationship between gully and Landscape Pattern in Black Soil Area of Northeast China. Transactions of the CSAE, 27(11):192-198.

Wang, W. J., Zhang, S. W., Li, Y. & Bu, K. (2008). Analysis of land use/cover change and soil erosion in different regions of Sanjiang plain during the past 50 years. Journal of the Graduate School of the Chinese Academy of Sciences, 25(4): 492-502.

Wang, W. J., Deng, R. X. & Zhang, S. W. (2012a). Spatial Pattern Change and Topographic Differentia of Gully Erosion in the type Black Soil Area of Northeast China during the past 40 Years, Geography and Geo Information Science, 28(3): 68-71.

Wang, W. J., Zhang, S. W. & Fang, H. Y. (2012b). Coupling mechanism of slope-gully system in Type Black Soil Area of Northeast. Journal of Natural Resources, 27(12): 2113-2122.

Water and Soil Conservation Office of Water Resource Minstry (1997). Specification for Soil Erosion Classification and Gradation. Beijing, China Water Conservancy and Water and Electricity Press.

Wei, J. B. & Xiao, D. N. (2005). Landscape pattern and its functioning after ecological reconstruction in Mollisols region of northeast China. Chinese Journal of Applied Ecology, 16(9): 1699-1705.

Wei, J. B., Xiao, D. N., Li, X. Z., Bu, R. C. & Zhang, C. S. (2006). Relationship between landscape pattern and soil erosion of an agricultural watershed in the Mollisols region of northeastern China. Acta Ecologica Sinica, 26(8): 2608-2615.

Wu, Y. Q., Zheng, Q. H., Zhang, Y. G., Liu, B. Y., Cheng, H. & Wang, Y. Z. (2008). Development of gullies and sediment production in the black soil region of northeastern China. Geomorphology, 101: 683-691.

Yan, Y. C., Zhang, S. W. & Yue, S. P. (2010). Dynamic change of hill slope and gully erosion in typical area of black soil region during the past 40 years. Transactions of the CSAE, 26(2):109-115.

Yang, H. (2001). Classification of gully in loess region of Jixian County, Shanxi Province. Journal of Beijing Forestry University, 23(1): 38-43.

Zhang, S. W., Wang, W. J., Li, Y., Bu, K. & Yan, Y.C. (2008). Dynamics of hillslope soil erosion in the Sanjiang Plain in the past 50 years. Resources Science, 30(6): 843-849.

Zhang, X. K., Xu, J. H., Lu, X. Q., Deng, Y. J. & Gao, D. W. (1992). A study on the Soil Loss Equation in Heilongjiang Province. Bulletin of Soil and Water Conservation, 12(4): 1-10.

Zhang, X. P., Liang, A. Z., Shen, Y., Li, W. F., Zhang, X. L. Wang, Y. X., Xie, Y. J., Liu, F. F. & Yang, X. M. (2006). Erosion characteristics of Black Soils in Northeast China. Scientia Geographic Sinica, 26(6): 687-692.

Zhang, Y. G., Wu, Y. Q., Liu, B. Y., Zheng, Q. H. & Yin, J. Y. (2007).

Characteristics and factors controlling the development of ephemeral gullies in cultivated catchments of black soil region, Northeast China. Soil & Tillage Research, 96: 28-41.

DOI: 10.24850/j-tyca-2019-04-07
Special Article

Response of Benthic Invertebrate Communities in River-Changed Ponds to River Habitat Modification in Water-Deficient Area

Respuesta de comunidades de invertebrados bentónicos en estanques cambiados por el río debido a la modificación del hábitat del río en áreas con deficiencia de agua

F. Liu[1]

B. Baoligao[2]*

Y. Wu[3]

W. Cui[4]

X. Mu[5]

[1]State Key Laboratory of Simulation and Regulation of Water Cycle in River Basin, China Institute of Water Resources and Hydropower Research, Beijing, China, email: liuf832@163.com, ORCID 0000-0002-1796-8590

[2]State Key Laboratory of Simulation and Regulation of Water Cycle in River Basin, China Institute of Water Resources and Hydropower Research, Beijing, China, email: baiyinblg@hotmail.com, ORCID 0000-0002-5408-6802

[3]State Key Laboratory of Simulation and Regulation of Water Cycle in River Basin, China Institute of Water Resources and Hydropower Research, Beijing, China, email: wuyih@iwhr.com, ORCID 0000-0001-5242-6482

[4]State Key Laboratory of Simulation and Regulation of Water Cycle in River Basin, China Institute of Water Resources and Hydropower Research, Beijing, China, email: joylife@126.com, ORCID 0000-0001-6542-5016

[5]State Key Laboratory of Simulation and Regulation of Water Cycle in River Basin, China Institute of Water Resources and Hydropower Research, Beijing, China, email: swood2002@163.com, ORCID 0000-0002-8067-8289

*Corresponding author: Baiyin Baoligao, baiyinblg@hotmail.com

Abstract

In the water-deficient area, river-changed ponds are common and vital for aquatic species. This paper studies the relationship between the environmental factors and the benthic invertebrate communities in varying ponds under river habitat modifications (RHM). For analysis, numerous samples are collected from river-changed ponds in Beijing, China. These ponds are classified into five types, including totally reinforced ponds, channel reinforced ponds, bank reinforced ponds, natural ponds, and restored ponds. Results indicate: 1) the biodiversity of benthic invertebrates is dependent strongly on the pond type; 2) habitat quality explains a considerable amount of variations in benthic invertebrate communities, and RHM show strong power in explaining variations in habitat quality; 3) RHM on the pond bank has stronger impact on the habitat quality than that on the pond bottom. These findings suggest that RHM can affect the benthic invertebrate community through changing habitat quality. And we suggest that ecological restoration of pond bank should be a useful way to improve invertebrate biodiversity for rive-changed ponds in Beijing.

Keywords: Benthic invertebrate community, River-changed ponds, Water-deficient area, Habitat quality, River habitat modification.

Received: 18/12/2018

Accepted: 01/04/2019

Introduction

Ponds are defined as small (1 m^2 to about 5 ha), man-made or natural shallow waterbodies, which permanently or temporarily hold water (Meester et al., 2005). In water-deficient areas, ponds are very common. For a long time, ponds have been ignored by freshwater biologists (Céréghino et al., 2008). Recently, there is growing evidence that ponds are species-rich (Williams et al., 2003) and important surrogate habitats for aquatic organisms (Peltzer et al., 2006) in water-deficient areas. With the rapid growth of the economy, the water quantity of rivers is strongly reduced as a result of water resources development for agricultural, industrial and domestic use. Many rivers are dried out for most of the year. Consequently, rivers are changed into some ponds with extremely low velocity. Such process can be observed in many water-deficient regions of the world (Céréghino et al., 2008;

Hale et al., 2015).

Managing river system often includes many river habitat modifications (RHM), such as flood protection works, water intake engineering, and ecological restoration projects (Pedersen, 2009; Szoszkiewicz et al., 2006). A number of habitat modification projects are done in river-changed ponds (Liu et al., 2009; Men et al., 2010) and obviously, these modifications have direct impacts on aquatic organisms (Albertson et al., 2011). Meanwhile, the alteration exerts on habitat quality features, such as water quality and bottom stability, have more effects in structuring aquatic communities (Petkovska & Urbanič, 2015). Benthic invertebrates play an important role (Duan et al., 2011) and changes of benthic invertebrate communities provide valuable information about the current status of aquatic systems (Mehler et al., 2015). Therefore, it is important to establish more precise links of invertebrate communities and environmental factors under the effect of RHM for river management.

Generally, the distribution of invertebrates in rivers appears to be mainly dependent on river discharge (Death & Zimmermann, 2005), water quality (Guilpart et al., 2012), and bottom stability (Duan et al., 2011). Most of these environmental drivers are associated with water flowing. In contrast, invertebrate assemblages seem to be primarily affected by various aspects of vegetation in lentic environments (Trigal-Dominguez et al. 2009). However, river-changed ponds in water-deficient areas are different from running rivers and totally lentic lakes. Few studies compared invertebrate communities in different types of ponds and tried to identify the main environmental drivers. Hale et al. (2015) compared the invertebrate community composition in natural stream ponds and man-made stock ponds watering domesticated animals and found that 81% of the taxa were exclusive to either stock ponds or natural ponds. Jurado et al. (2009) showed that the most important factors responsible for the differences in invertebrate community structures between natural stream ponds and wastewater treatment ponds were pH, vegetation structure and pollution levels. On the other hand, Oertli et al. (2008) suggested that connectivity was highly important in structuring the invertebrate assemblages in alpine ponds. Some other factors, such as the presence of bullfrog, are also discussed (Hale et al., 2015). Despite the important ecological role of river-changed ponds in the water-deficient area, there is a paucity of knowledge regarding whether there are differences for invertebrate communities in different types of river-changed ponds, and the factors determining such differences, including anthropogenic habitat modifications.

In this study, the main aims are to (i) compare community composition, abundance and biodiversity of benthic invertebrate

communities in different types of river-changed ponds, (ii) investigate the effect of RHM and habitat quality on invertebrate communities, and (iii) quantify the effect of RHM on habitat quality features and identify the main factors. The results will provide an important basic for enhancing freshwater biodiversity in river-changed ponds and be benefit for river management and rehabilitation.

Methods

Study Area

As composed by different types of ponds and have relatively good water quality in Beijing of China, Huaijiu River and Zhuan River are selected (Figure 1). Huaijiu River, with an area of 347.2 km^2, is located in the Huairou district which is one of the most important water sources in Beijing. With relatively less anthropogenic disturbance, it contains several ponds without any water projects. But segments across villages are embanked with nearly no floodplain. Some ponds are ecologically restored, including rehabilitation of natural riparian and hydrophytic vegetation. In contrast, Zhuan River, with a length of 3.7 km, is located in the central urban area and all of the channels are reinforced by concrete. But for some ponds, shallow waters with hydrophytes are created within the marginal area. During August 2014, a field investigation was conducted in Huaijiu River and Zhuan River.

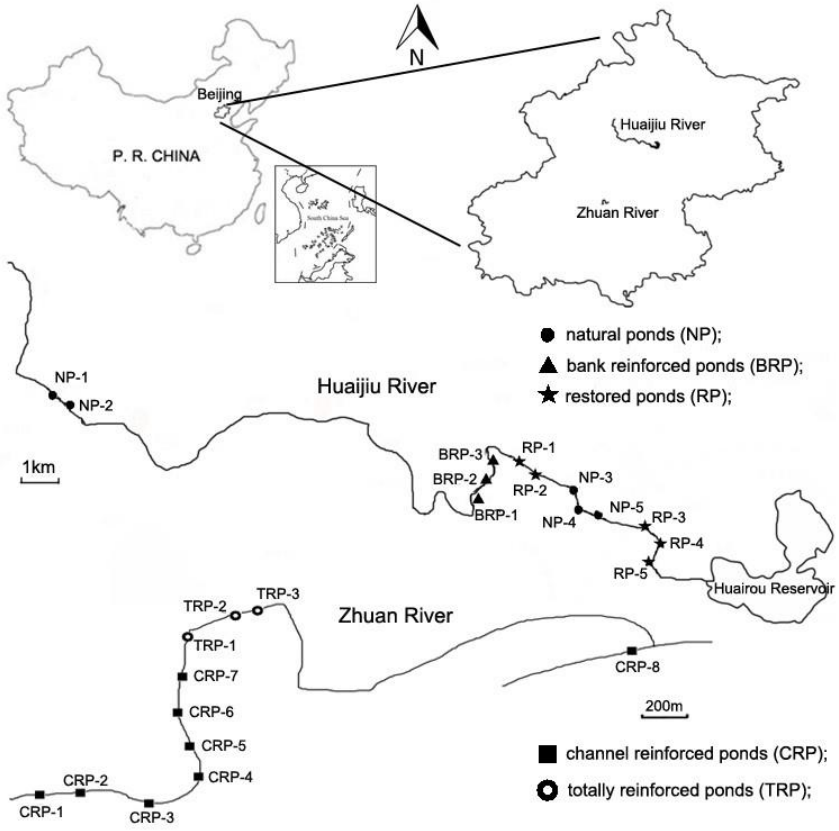

Figure 1. Sketch of study area and sampling sites.

Survey Design

Five types of ponds are defined here. Totally reinforced ponds (TRP) refer to the ponds with reinforced channel and vertical cement revetment (Figure 2a). Channel reinforced ponds (CRP) refer to the ponds with concrete channel underwater, but the vertical cement revetment above water are removed and shallow waters with hydrophytes are built in the marginal area (Figure 2b). Bank reinforced ponds (BRP) refer to the ponds with natural streambed, but vertical cement revetment and severely encroached flood plain (Figure 2c). Natural ponds (NP) refer to the fragmented habitats in rivers, without any artificial water utilization or restoration projects (Figure 2d). Cement revetment with slop in some ponds are covered with soils and ecologically restored by the rehabilitation of riparian and hydrophytic vegetation. Thus these ponds are defined as restored ponds (RP, Figure 2e).

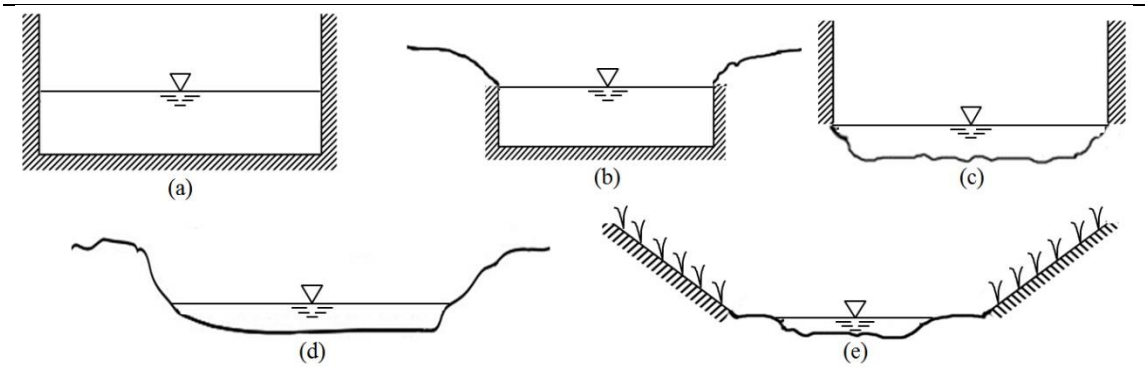

Figure 2. Sketch of five types of ponds in this research: totally reinforced ponds (a), channel reinforced ponds (b), bank reinforced ponds (c), natural ponds (d), and restored ponds (e).

A total of 24 sampling sites were chosen from the two rivers in Beijing, including 5 sites in NP, 3 sites in BRP, 5 sites in RP, 8 sites in CRP and 3 in TRP (Figure 1). All of the ponds contain water year round, with velocity lower than 0.3 m/s for most of the year.

Benthic Invertebrate Data Collecting

A D-frame dip net was used to sample along the substrates and in plant clusters. Replicate samples for each site were combined to form a composite sample, amounting to at least a minimum area of 1 m^2 (Duan et al., 2011). The samples were rinsed vigorously through a 300-μm sieve and the invertebrates were collected in plastic sample containers with 95% ethanol in the field. All invertebrates were identified and counted under a stereoscopic microscope in the laboratory. Invertebrates were identified to the finest taxonomic unit as possible, mostly to genus or species. For each sample, the total species number (S), individual density (N), and biomass density (W) were calculated or weighed.

Environmental Data Collecting

For each site, environmental data including bottom stability (BS), water quality (WQ), vegetation (Veg) and RHM were obtained, and the

specific environmental variables are listed in Table 1. Some environmental parameters including the water temperature, pH, dissolved oxygen (DO) were measured in situ using portable multiparameter water quality analyzer (YSI 6600). A water sample of approximately 1L was taken at each site to measure chemical oxygen demand (COD_{Mn}), five day's biochemical oxygen demand (BOD_5), total nitrogen (TN), ammonium (NH_3-N), and total phosphorus (TP) in laboratory, according to China's National Environmental Quality Standards for Surface Water (Chinese Research Academy of Environmental Sciences, 2003).

Table 1. Summary of environmental variables for the 24 sampling sites

	Abbreviation	unit	Variable group	Median (min-max)
pH	pH	-	WQ	7.79 (7.45-8.64)
dissolved oxygen	DO	mg/L	WQ	5.84 (4.14-13.44)
total nitrogen	TN	mg/L	WQ	1.45 (0.20-3.93)
ammonium	NH_3-N	mg/L	WQ	0.17 (0.03-1.60)
total phosphorus	TP	mg/L	WQ	0.11 (0.02-0.84)
chemical oxygen demand	COD_{Mn}	mg/L	WQ	2.30 (1.09-17.98)
five day's biochemical oxygen demand	BOD_5	mg/L	WQ	1.60 (0.36-16.92)
Rock angularity	Ra	Score [a]	BS	3 (1-4)
Brightness	Br	Score [a]	BS	1 (1-4)
Consolidation of particles	Cp	Score [a]	BS	4 (2-8)
Bottom size distribution	Bsd	Score [a]	BS	8 (4-12)
Scouring and deposition	Sd	Score [a]	BS	12 (6-24)
Aquatic vegetation	Av	Score [a]	BS	2 (1-4)

banktop vegetation structure	Btvs	Score [b]	Veg	0 (0-3)
banksurface vegetation structure	Bsvs	Score [b]	Veg	2 (0-3)
channel vegetation types	Cvt	Score [b]	Veg	11.0 (0.0-16.5)
Artificial bank material	Abm	Score [b]	RHM	0 (0-6)
bank modification	Bm	Score [b]	RHM	0 (0-7)
Artificial channel material	Acm	Score [b]	RHM	0 (0-6)
channel modification	Cm	Score [b]	RHM	0 (0-4)
Artificial bank profile	Abp	Score [b]	RHM	1.5 (0.0-6.5)
Bridge	Bri	Score [b]	RHM	1.5 (0.0-3.0)
Ford	For	Score [b]	RHM	0 (0-2)
Weir/sluice [c]	Ws	Score [b]	RHM	0 (0-3)
Outfalls	Ouf	Score [b]	RHM	0 (0-2)
water impoundment	Wi	Score [b]	RHM	0 (0-2)

[a] score of individual variable is calculated according to the bottom component of Pfankuch Stability Index (Pfankuch, 1975).

[b] score of individual variable is calculated according to the SIHM method (Tavzes & Urbanič, 2009).

[c] variables excluded from further analysis according to occurrence frequency lower than 10%.

Bed stability has significant effects on the composition of benthic invertebrate communities (Townsend et al., 1997). There are different approaches and techniques to quantify bed stability, such as the distance travelled by in-situ-marked tracer stones (Death, 2005), and the percentage of substrate that would move at bankfull discharge (Duncan et al., 1999). Schwendel et al. (2011) compared these

methods and found that the Pfankuch Index of bottom component was one of the most suitable measures for researching invertebrate communities. The Pfankuch Stability Index is a method for visual evaluation of streambed and bank stability (Pfankuch, 1975), and the bottom component of Pfankuch Stability Index (BCP) is used here to assess the bottom stability (Schwendel et al., 2011).

SIHM is a method for evaluating different categories of river features regarding their influence on benthic invertebrate communities, including the parts of Veg and RHM (Tavzes & Urbanič, 2009). Previous studies (Petkovska & Urbanič, 2015; Urbanič, 2014) showed a good explanatory power of SIHM linking to benthic invertebrates. Therefore, variables of Veg and RHM are used here and their scores are calculated according to the SIHM method (Tavzes & Urbanič, 2009).

Multivariate Data Analysis

For each invertebrate sample, the Margalef index (D), Pielou index (J) and Shannon-Wiener index (H) are calculated to determine the species richness (Margalef, 1958), evenness (Pielou, 1966) and diversity (Shannon & Wiener, 1949). Mean species number (S), individual density (N), biomass density (W), D, J, H, the percentages of phylum Mollusca (Mol), Annelida (Ann), and Arthropoda (Atr) individuals are compared among different types of ponds by using Mann-Whitney *U* test.

Ordination techniques are applied based on CANOCO 4.5. Benthic invertebrate data are ln(x+1) transformed to reduce the weights of rare taxa in all cases. Detrended Correspondence Analysis (DCA) on invertebrate data is used to analyze the relationship between invertebrate communities and environmental variables. Since the largest gradient length is 5.38, unimodal species responses are assumed, and thus the Canonical Correspondence Analysis (CCA) is applied. Firstly, CCA with forward selection on RHM are applied to identify the effect of RHM on invertebrate assemblages. Then the importance of the three habitat quality groups (WQ, BS and Veg) in explaining variability among benthic invertebrate assemblages is tested by CCA. Furthermore, DCA with forward selection is used to investigate the significance of RHM in explaining variations of habitat quality groups (WQ, BS and Veg) separately.

Results and Discussion

Invertebrate Communities in Different Types of Ponds

As shown in the appendix, a total of 82 invertebrate taxa (21 identified to species, 51 identified to genus, 10 identified to family) are identified, including 15 Mollusca, 9 Annelida and 58 Arthropoda. In Table 2, there are several statistically significant differences ($P < 0.05$) in invertebrate community variables between pairs of pond types through the Mann-Whitney *U* test. TRP have significant smaller species numbers (1~4) than CRP (4~18, $P = 0.018$), NP (6~22, $P = 0.025$) and RP (10~17, $P = 0.024$). TRP also have significant smaller individual density (6~94 ind./m^2) than NP (104~348 ind./m^2, $P = 0.025$) and RP (172~392 ind./m^2, $P = 0.025$). However, the biomass densities in TRP (11.20~79.79 g/m^2) are significantly higher than that in CRP (0.46~9.01 g/m^2, $P = 0.014$). The percentages of Mollusca in TRP (100%) are significantly higher ($P = 0.013$ to 0.037) than that in other ponds while the percentages of Arthropoda are significantly lower ($P = 0.013$ to 0.025).

Table 2. *P* values of Mann-Whitney *U* test between every two types of ponds.

Compared ponds	S	N	W	Mol	Ann	Art	D	J	H
TRP-CRP	0.018		0.014	0.013	0.013	0.028	0.025		0.014
TRP-SP	0.025	0.025		0.022		0.022	0.025		0.025
TRP-RSP	0.024	0.025		0.022		0.022	0.025		0.025
TRP-BRP				0.037	0.037	0.037			
CRP-SP			0.013					0.013	0.028
CRP-RSP				0.013		0.013			

CRP-BRP			0.025	0.041		0.024		0.014	0.041
SP-RSP									0.016
RSP-BRP									0.025

The Shannon-Wiener index is the most recognizable variable for different types of ponds. It is significantly highest in RP (2.36~3.66) and CRP (1.89~3.51), significantly lower in NP (1.96~2.41), and significantly lowest in BRP (1.11~2.27) and TRP (0.00~1.50). According to comparing TRP and RP, there is no significant difference (P = 0.770) in the Shannon-Wiener index, but significant differences (P = 0.013) in percentages of Mollusca and Arthropoda. Since all of these variables have no significant differences between NP and BRP, the results are not included in Table 2.

Although BRP and RP are modified by anthropogenic activities, they have similar community composition with NP. Such modified and river-changed ponds provide important surrogate habitat for some aquatic invertebrate taxa (Hale et al., 2015) in Beijing area. However, the species richness is rather low in TRP (only mollusk). Obviously, the channelization has given rise to strong changes of the habitat structure and reduced the integrity and complexity of the living environment, which is necessary to support diverse aquatic biota (Blann et al., 2009). On the other hand, the higher biomass in TRP is mainly caused by the existence of the large-sized gastropods (Pan et al., 2012).

A comparison between TRP and BRP reveals that there is no significant difference in species numbers, biodiversity, and biomass densities. However, the invertebrate assemblages in TRP are composed mainly of mollusks, while arthropods are observed in BRP. Since the two pond types have similar bank profiles but different bottom materials, the differences in the composition may be mainly owing to the substrate material and its stability (Duan et al., 2011).

For CRP, the vertical concrete bank above water has been removed, and slop bank with complex vegetation and riparian vegetation have been rebuilt, but the reinforced channel underwater is retained. Compared to TRP, CRP shows a significantly higher species richness and biodiversity, suggesting the importance of bank form and riparian vegetation (Demars et al., 2012). The relatively lower biodiversity in BRP confirms this point from the opposite angle.

The invertebrate fauna of urban rivers is often highly restricted when compared with non-urban watercourses in the same region (Davies &

Hawkes, 1981). However, compared to NP in the suburban area, CRP in the urban area has significantly higher biodiversity and a similar taxonomic composition, which prove the modification successful.

Comparing the Effects of RHM and Habitat Quality on Invertebrate Assemblages

The total variance in species data is 4.561, including 24 sampling sites and 82 invertebrate taxa. After forward selection only Abp (P = 0.004) and Out (P = 0.018) are selected. The total explained variance of RHM is 0.63 (13.9%), and the explanatory powers of Abp and Ouf were 7.4% and 6.5% (Figure 3).

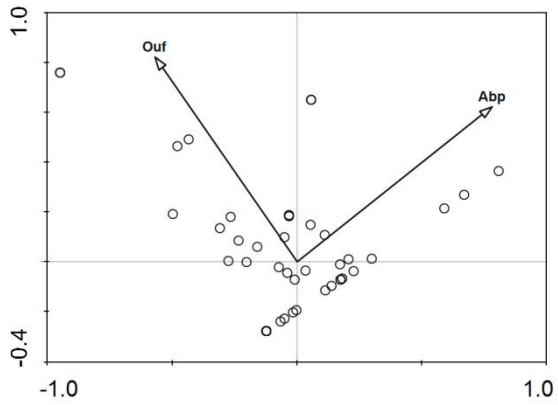

Figure 3. CCA ordination diagram of all species and the two forward-selected variables of RHM.

For detecting the effects of habitat quality on invertebrate communities, pH (P = 0.030), TP (P = 0.002), Br (P = 0.002), Av (P = 0.038), and Cvt (P = 0.002) are selected after forward selection. Testing the explanatory power of each variable group individually, each group comprises two or three variables after forward selection. From Figure 4, the highest explanatory power of variable groups is shown in bottom stability (23.0%), followed by the water quality (21.0%) and vegetation (20.5%).

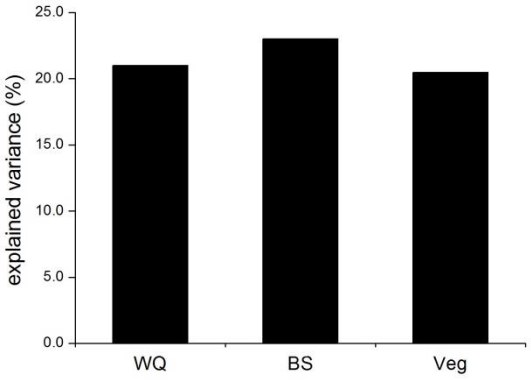

Figure 4. Explained variances of water quality (WQ), bottom stability (BS) and vegetation (Veg).

The RHM explains the least variation among the four variable groups. Thus the habitat quality has relatively more significant or direct impacts on invertebrate communities for river-changed ponds. That conforms to the conclusion that benthic invertebrate assemblages respond less to the physical alteration itself but more to the effect that the alteration exerts on habitat quality features (Petkovska & Urbanič, 2015).

Each habitat quality variable group is tested for its significance in structuring benthic invertebrate assemblages. Generally, approximate explanatory powers are shown among the WQ, BS and Veg. The importance of WQ, BS, and Veg to invertebrate assemblages has been reported from the previous researches (Duan et al., 2011; Demars et al., 2012), but studies on quantificationally comparing their effects are rare. Jurado et al. (2009) identified the main environmental factors structuring invertebrate community in natural and wastewater treatment ponds, and the results showed that WQ and the instream vegetation accounted for 26.53% and 17.69% of the explained variance. On the other hand, Petkovska & Urbanič (2015) found that the slope (20%) and the predominant flow (12%) were the most important in explaining invertebrate assemblage variances, while the Btvs (2%), Bsvs (1%) and Cvt (3%) were much less important. Moreover, Demars et al. (2012) found that the marginal and instream vegetation accounted for 60% of the total explained genus composition variance within the river and 26% between rivers. In fact, the natural substrate characteristics are the consequences of the interaction between the flowing water and the channels (Duan et al., 2011). Therefore the explanatory power of BS partly merges the influence of water flow on invertebrate assemblages. Compared to natural streams, all of the ponds in this study have similar low velocity and flow regimes. Consequently, the similarity reduces the importance of bottom stability and enhanced the importance of vegetation. Compared to totally lentic lakes, water in these ponds can flow and be connected in flood period or

by human manipulation. That may be why WQ, BS, and Veg revealed approximate significances in structuring benthic invertebrate assemblages of river-changed ponds in water-deficient areas.

Effects of RHM on Habitat Quality

DCA on WQ, BS, and Veg are performed, and the largest gradient lengths (0.37~1.48) are small. Thus RDA with forward selection is applied to detect the relationship between RHM and the other habitat quality variable groups (Table 3). RHM explains 43.59% of the variance in WQ with 3 statistically significant variables after forward selection, 60.85% of the variance in BS with 2 statistically significant variables, and 52.46% of the Veg variance with 2 statistically significant variables. The most explanatory RHM variable is the artificial bank profile (Abp), explaining 14.6%, 49.9% and 43.1% of the variance in WQ, BS and Veg, respectively. In addition, the artificial bank material (Abm) explained most of the variance in water quality (19.5%).

Table 3. Results of RDA with forward selection.

	RHM										
	Abp		Bm		Wi		Abm		For		total
	ƛ	*P*	ƛ	*P*	ƛ	*P*	ƛ	*P*	ƛ	*P*	ƛ
WQ	14.6	0.012			9.5	0.010	19.5	0.002			43.59
BS	49.9	0.002							10.9	0.002	60.85
Veg	43.1	0.002	9.3	0.014							52.46

Many changes in WQ, BS and Veg of the hydrosystems are directly or indirectly caused by anthropogenic habitat modification (Schlosser & Karr, 1981; Wyżga et al., 2012). Since rivers in Beijing area are highly disturbed by human activities, RHM explains a considerable amount (43.59% ~ 60.85%) of variations in habitat quality. RHM has relatively higher explanatory power for BS and Veg which are changed directly in many projects such as channelization works, alteration of the channel and bank materials. In contrast, water quality variance is relatively less explained because it is indirectly affected by channel materials, vegetation, water impoundment and so on (Marzin et al., 2012).

Variables for bank alteration (Abp, Bm, Abm) affect WQ (34.1%), BS (49.9%) and Veg (52.4%) significantly. Bank modification is also a

good explanatory variable for invertebrate assemblages in other studies (Stefania et al., 2006). It can be inferred that the bank system play an important role in maintaining the habitat quality and biodiversity for river-changed ponds. Thus the natural bank profile, material and vegetation should be modified carefully.

Conclusions

This study has proved that the river-changed ponds are important habitats for benthic invertebrates in Beijing for some of these modified ponds even supported higher biodiversity than natural stream pools. RHM can affect the benthic invertebrate community through changing the habitat quality, including WQ, BS, and Veg. Modification of river banks is the main human pressure affecting habitat quality in river-changed ponds. Moreover, the most important habitat quality variables for structuring benthic invertebrate assemblages are the bottom brightness, total phosphorus and vegetation types. Finally, we suggest that vegetation replanting in channels and riparian areas might be a useful way to improve invertebrate biodiversity in Beijing.

Acknowledgments

This work was financially supported by the IWHR Research & Development Support Program (HY0145C092014), and the Key Laboratory of Watershed Sciences and Health of Zhejiang Province (KFKT2016005).

Appendix

A total of 82 invertebrate taxa were identified and the list shown below.

Table A1. List of identified taxa.

NO.	Taxonomic group	NO.	Taxonomic group
	Mollusca		Gomphidae
	Gastropoda	35	*Sympetrum sp.*

	Melaniidae	36	*Sinictinogomphus sp.*
1	*Semisulcospira cancellata*	37	*Gomphidia sp. 1*
	Viviparidae	38	*Gomphidia sp. 2*
2	*Cipangopaludina chinensis*	39	*Stylogomphns sp.*
3	*Angulyagra polyzonata*		Libellulidae
4	*Bellamya purificata*	40	*Crocothemis sp.*
	Hydrobiidae	41	*Orthetrum sp.*
5	*Stenothyra glabra*	42	*Nannoph sp.*
6	*Bithynia misella*	43	*Tramea sp.*
7	*Bithynia fuchsiana*		Corduliidae
8	*Parafossarulus striatulus*	44	*Somatochlo sp.*
9	*Alocinma longicornis*		Coleoptera
	Lymnaeidae		Haliplidae
10	*Radix swinhoei*	45	*Peltodytes sp.*
11	*Radox plicatula*	46	*Haliplus sp.*
	Planorbidae	47	*Brychius sp.*
12	*Gyraulus convexiusculus*		Dytiscidae
13	*Hippeutis umbilicalis*	48	*Hydaticus sp.*
	Lamellibranchia	49	*Coelambus sp.*
	Sphaeriidae	50	*Platambus sp.*
14	*Sphaerium lacustre*	51	*Bidessus sp.*
	Corbiculidae	52	*Eretes sticticus*
15	*Corbicula largillierti*	53	*Noterus sp.*
	Annelida	54	Chrysomelidae sp. 1
	Hirudinea	55	Chrysomelidae sp. 2
	Glossiphoniidae		Hemiptera
16	*Glossiphonia sp.*	56	Corixidae sp.
	Erpobdellidae	57	*Micronecta sp.*
17	*Erpobdella sp.*	58	*Cymatia sp.*

	Hirudinidae	59	Pleidae sp
18	*Whitmania sp.*	60	*Paraple Esaki and China*
	Oligochaeta	61	*Naucoridae sp.*
	Tubificida		Nepidae
19	*Branchiura sp.*	62	*Ranatra sp.*
20	*Tubifex sp.*		Diptera (larva)
21	*Limnodrilus sp.*	63	Chironomidae sp.
	Lumbriculidae	64	*Chironomus sp.*
22	*Pachydrilus sp.*	65	*Parachironomus sp.*
	Naididae	66	*Thienemanniola sp.*
23	*Nais sp.*	67	*Einfeldia sp.*
	Platyhelminthes	68	*Polypedilum sp.*
24	Turbellaria sp.	69	*Rheotanytarsus sp.*
	Arthropoda		Tanypodinae
	Ephemerida (larva)	70	*Procladius sp.*
	Neoephemeridae	71	*Thalassomya sp.*
25	*Potamanthellus chinensis*		Orthocladiinae
	Baetidae	72	*Synorthocladius sp.*
26	*Cloeon sp.*		Culicidae
27	*Baetis sp.*	73	*Anopheles sp.*
	Caenidae	74	*Culex sp.*
28	*Caenis sinensis*	75	Stratiomyidae sp.
	Ephemeridae	76	Canaceidae sp.
29	*Ephemera sp.*	77	Athericidae sp.
	Potamanthidae		Tipulidae
30	*Rhoenanthus hunanensis*	78	*Holorusia sp.*
	Odonata (larva)		Lepidoptera
	Lestidae		Pyralidae
31	*Indolestes sp.*	79	*Nymphula sp.*
32	*Sympecma sp.*		Decapoda
	Platycnemididae		Palaemonidae

33	*Platycnemis sp.*	80	*Palaemon tokinnensis*
34	Calopterygide sp.	81	Grapsidae sp.
			Amphipoda
			Gammaridae
		82	*Gammarus sp.*

References

Albertson, L. K., Cardinate, B. J., Zeug, S. C., Harrison, L. R., Lenihan, H. S. & Wydzga, M. A. (2011). Impacts of channel reconstruction on invertebrate assemblages in a restored river. *Restoration Ecology*, 5, 627-638.

Blann, K. L., Anderson, J. L., Sands, G. R. & Vondracek, B. (2009). Effects of agricultural drainage on aquatic ecosystems: a review. *Critical Reviews in Environmental Science and Technology*, 39, 909-1001.

Céréghino, R., Biggs, J., Oertli, B. & Declerck, S. (2008). The ecology of European ponds: defining the characteristics of a neglected freshwater habitat. *Hydrobiologia*, 597, 1-6.

Davies, L. J. & Hawkes, H. A. (1981). Some effects of organic pollution on the distribution and seasonal incidence of Chironomidae in riffles in the River Colel. *Freshwater Biology*, 11, 549-559.

Death, R. G. & Zimmermann, E. M. (2005). Interaction between disturbance and primary productivity in determining stream invertebrate diversity. *Oikos*, 111, 392-402.

Demars, B. O. L., Kemp, J. L., Friberg, N., Usseglio-Polatera, P. & Harper, D. M. (2012). Linking biotopes to invertebrates in rivers: biological traits, taxonomic composition and diversity. *Ecological Indicators*, 23, 301-311.

De Meester, L., Declerck, S., Stoks, R., Louette, G., Van-De-Meutter, F., De-Bie, T., Michels, E. & Brendonck, L. (2005). Ponds and pools as model system in conservation biology, ecology and evolutionary biology. *Aquatic Conservation: Marine and Freshwater Ecosystems*, 15, 715-726.

Duan, X. H., Wang, Z. Y. & Xu, M. Z. (2011). Effects of fluvial processes and human activities on stream macro-invertebrates. *International Journal of Sediment Research*, 26, 416-430.

Duncan, M. J., Suren, A. M. & Brown, S. L. R. (1999). Assessment of streambed stability in steep, bouldery streams: development of a new analytical technique. *Journal of the North American Benthological Society*, 18, 445-456.

Guilpart, A., Roussel, J. M., Aubin, J., Caquet, T., Marle, M. & Bris, H. L. (2012). The use of benthic invertebrate community and water quality analyses to assess ecological consequences of fish farm effluents in rivers. *Ecological Indicators*, 23, 356-365.

Hale, J. R., Mims, M. C., Bogan, M. T. & Olden, J. D. (2015). Links between two interacting factors, novel habitats and non-native predators, and aquatic invertebrate communities in a dryland environment. *Hydrobiologia*, 746, 313-326.

Jurado, G. B., Callanan, M., Gioria, M., Baars, J.-R., Harrington, R. & Kelly-Quinn, M. (2009). Comparison of macroinvertebrate community structure and driving environmental factors in natural and wastewater treatment ponds. *Hydrobiologia*, 634, 153-165.

Liu, J. L., Ma, M. Y., Zhang, F. L., Yang, Z. F. & Domagalski, J. (2009). The ecohealth assessment and ecological restoration division of urban water system in Beijing. *Ecotoxicology*, 18, 759-767.

Margalef, D. R. (1958). Perspectives in Ecological Theory. Chicago: University of Chicago Press.

Marzin, A, Verdonschot, P. F. M. & Pont, D. (2012). The relative influence of catchment, riparian corridor, and reach-scale anthropogenic pressures on fish and macroinvertebrate assemblages in French rivers. *Hydrobiologia*, 704, 375-388.

Mehler, K., Acharya, K., Sada, D., Yu, Z. (2015). Factors affecting spatiotemporal benthic macroinvertebrate diversity and secondary production in a semi-arid watershed. *Journal of Freshwater Ecology*, 30, 197-214.

Men, B. H., Zhang, S. F. & Xia, J. (2010). The instream ecological water flow research at the lower reach of Guanting Reservoir on Yongding River, Beijing. *Journal of Resources and Ecology*, 1, 211-215.

Oertli, B., Indermuehle, N., Angelibert, S., Hinden, H. & Stoll, A. (2008). Macroinvertebrate assemblages in 25 high alpine ponds of Swiss National Park (Cirque of Macun) and relation to environmental variables. *Hydrobiologia*, 597, 29-41.

Pan, B. Z., Wang, Z. Y., Xu, M. Z. & Xing, L. H. (2012). Relation between stream habitat conditions and macroinvertebrate assemblages in three Chinese rivers. *Quaternary International*, 282, 178-183.

Pedersen, M. L. (2009). Effects of channelization, riparian structure and catchment area on physical habitat in small lowland streams. *Fundamental and Applied Limnology*, 174, 89-99.

Peltzer, M. P., Lajmanovich, R. C., Attademo, A. M. & Beltzer, A. H. (2006). Diversity of anurans across agricultural ponds in Argentina. *Biodiversity and Conservation*, 15, 3499-3513.

Petkovska, V. & Urbanič, G. (2015). The links between morphological parameters and benthic invertebrate assemblages, and general implications for hydromorphological river management. *Ecohydrology*, 8, 67-82.

Pfankuch, D. J. (1975). Stream reach inventory and channel stability evaluation. U. S. D. A. Forest Service, Region 1: Missoula, Montana.

Pielou, E. C. (1966). Species-diversity and pattern-diversity in the study of ecological succession. *Journal of Theoretical Biology*, 10, 370-383.

Schlosser, I. J. & Karr, J. R. (1981). Riparian vegetation and channel morphology impact on spatial patterns of water quality in agricultural watersheds. *Environmental Management*, 5, 233-243.

Schwendel, A. C., Death, R. G., Fuller, I. C. & Joy, M. K. (2011). Linking disturbance and stream invertebrate communities: how best to measure bed stability. *The North American Benthological Society*, 30, 11-24.

Shannon, C. E. & Wiener, W. (1949). The mathematical theory of communication. Urbana: University of Illinois Press.

Stefania, E., Andrea, B., Nigel, H., O'Hare, M., Scarlett, P. & Stenico, A. (2006). Preliminary testing of River Habitat Survey features for the aims of the WFD hydro-morphological assessment: an overview from the STAR Project. *Hydrobiologia*, 566, 281-296.

Szoszkiewicz, K., Buffagni, A., Davy-Bowker, J., Lesny, J., Chojnicki, B. H., Zbierska, J., Staniszewski R. & Zgola, T. (2006). Occurrence and variability of River Habitat Survey features across Europe and consequences for data collection and evaluation. *Hydrobiologia*, 566, 267-280.

Tavzes, B. & Urbanič, G. (2009). New indices for assessment of hydromorphological alteration of rivers and their evaluation with benthic invertebrate communities; Alpine case study. *Review of Hydrobiology*, 2, 133-161.

Townsend, C. R., Scarsbrook, M. R. & Doledec, S. (1997). The intermediate disturbance hypothesis, refugia, and biodiversity in streams. *Limnology and Oceanography*, 42, 938-949.

Trigal-Dominguez, C., Fernandez-Alaez, C. & Carcia-Criado, F. (2009). Habitat selection and sampling design for ecological assessment of heterogeneous ponds using macroinvertebrates. *Aquatic Conservation*, 19, 786-796.

Urbanič, G. (2014). Hydromorphological degradation impact on benthic invertebrates in large rivers in Slovenia. *Hydrobiologia*, 729, 191-207.

Williams, P., Whitfield, M., Biggs, J., Bray, S., Fox, G., Nicolet, P. & Sear,

D. (2003). Comparative biodiversity of rivers, streams, ditches and ponds in an agricultural landscape in Southern England. *Biological Conservation*, 115, 329-341.

Wyżga, B., Oglęcki, P., Pawlik, A. R., Skalski, T. & Zawiejska, J. (2012). Hydromorphological complexity as a driver of the diversity of benthic invertebrate communities in the Czarny Dunajec River, Polish Carpathians. *Hydrobiologia*, 696, 29-46.

DOI: 10.24850/j-tyca-2019-04-08
Special Article

Granulation Process and Mechanism of Aerobic Granular Sludge under Salt Stress in a Sequencing Batch Reactor

Proceso de granulación y mecanismo de lodo granular aeróbico bajo estrés salino en un reactor de secuenciación por lotes

Y. Chen[1]*

Z. Zhu[2]

W. Yu[3]

C. Zhang[4]

[1]Key Laboratory for Hydraulic and Water Transport Engineering of Ministry of Education, Chongqing Jiaotong University, Chongqing, China

School of River and Ocean Engineering, Chongqing Jiaotong University, Chongqing, China

National Inland Waterway Regulation Engineering Research Center, Chongqing Jiaotong University, Chongqing, China, email: cycquc@163.com, ORCID 0000-0002-1429-5247

[2]School of River and Ocean Engineering, Chongqing Jiaotong University, Chongqing, China, email: 972581492@qq.com, ORCID 0000-0002-2481-5111

[3]Key Laboratory for Hydraulic and Water Transport Engineering of Ministry of Education, Chongqing Jiaotong University, Chongqing, China

School of River and Ocean Engineering, Chongqing Jiaotong University, Chongqing, China

National Inland Waterway Regulation Engineering Research Center, Chongqing Jiaotong University, Chongqing, China, email: 605560236@qq.com, ORCID 0000-0003-3622-3436

[4]School of River and Ocean Engineering, Chongqing Jiaotong University, Chongqing, China, email: 635611270@qq.com, ORCID 0000-0001-9874-5972

*Corresponding author: Yao Chen, cycquc@163.com

Abstract

The formation and characteristics of aerobic granular sludge (AGS) under different operational conditions in a sequencing batch reactor (SBR), designed to treat Mustard tuber wastewater (MTW, characterized as saline wastewater), had been investigated in this study. Morphology and structure during granulation were determined using a microscope with a digital camera and scanning electron microscope (SEM). Granules formed in the reactors could be classified as zoogloea granules with a clear boundary outline and filamentous granules with mycelia bestrewing boundary. Zoogloea granules, cultivated in reactor R1 and R2, was with higher density than filamentous granules, cultivated in reactor R3, and consequently had a higher settling velocity. Results showed that divalent metal ions such as Ca^{2+} and Mg^{2+} with phosphate in inflow could transform into precipitates, serving as crystal nucleus and carriers for granulation. Moreover, appropriate organic loading, hydrodynamic shear and salt-stress selection can induce moderate growth of filamentous bacteria to act as granulation backbone and consequently granulation process under salt stress was a result together with crystal nucleus, filamentous bacteria, and extracellular polymeric substances (EPS), which could be affected by salinity-shifting strategies and dosage of aluminum salt coagulant.

Keywords: aerobic granular sludge (AGS), salt stress, sequencing batch reactor (SBR), filamentous, extracellular polymeric substances (EPS).

Received: 18/12/2018

Accepted: 03/04/2019

Introduction

The type of pollutants in wastewater can determine the selection of wastewater treatment technology. Wastewaters from industrial sources may contain both organic matter and inorganic pollutants. Saline wastewater, rich in salt (mainly known as NaCl) and nutrients, are often discharged from food-processing, leather and oil industry *(Lefebvre* and *Moletta 2006)*. Biological treatment of high salinity wastewater, if

feasible, would be relatively simple in processing flow, cost-effective in running and without farther pollution to the environment compared to physicochemical process. However, treating this wastewater can be more challenging, owing to plasmolysation of cells, inhibition of bioactivity, such as salt stress to microorganisms, and inhibition of some enzyme activity *(Rene et al. 2008)*. In spite of this, salt-tolerant activated sludge acclimation is accessible *(Aloui et al. 2009, Lefebvre and Moletta 2006)*. It has been reported that microbes attached growth have a higher tolerance capability than dispersed at high salt concentrations, and alternative bio-treatment systems for removing nutrients from saline effluents are increasingly the focus of research *(Aloui et al. 2009)*.

The aerobic granular sludge process, a promising prospect in the biological treatment, could cut the investment and operational costs as well as space requirements *(Liu et al. 2010, Zhu et al. 2013)*. Comparing with suspended activated sludge process, more outstanding advantages were confirmed, such as microbial community structure, favorable settling characteristics, high concentrations of biomass *(Chen and Lee 2015, Morales et al. 2012, Zhu et al. 2013)*, and tolerable to incoming shocks and medium toxic environment *(Adav et al. 2010, Zhu et al. 2013)*.

Besides, studies into applications of granular sludge technology in treating industrial wastewater have been advocated by some previous researchers *(Adav et al. 2008a, Rosman et al. 2014)*. These distinct characteristics approve that aerobic granular technology may become a promising alternative method for activated sludge process and has good applied prospects in treating saline and nutrients-rich wastewaters. Aerobic granules under high salt stress in SBR system exhibited a good stability and pollutants removal performance in treating saline wastewater *(Li et al. 2010, Moussavi et al. 2010, Taheria et al. 2012, Wan et al. 2014)*, and it is even observed that aerobic granules are more slippery and regular in appearance under high salinity *(Li and Wang 2008)*.

Mustard tuber wastewater (MTW) is a typical food-processing effluent, characterized by high-strength dissolved organic matters and high salinity *(Chai and Kang 2012)*. Many published studies treating saline effluent, mainly based on laboratory scale reactors, and focused on biofilm attached growth on surfaces of support materials and microbial fuel cells *(Chai and Kang 2012, Guo et al. 2013, Guo et al. 2015)*. Aerated granules sludge (AGS) could be regarded as a specific form of biofilm which is commonly developed by aggregation of a variety of microorganisms based on the microbiological point of view *(Ren et al. 2010)*. However, very few studies about the application of the AGS system for the treatment of MTW was reported.

The high concentration of divalent metal ions in MTW, such as Ca^{2+} and Mg^{2+} could enhance the granulation *(Jiang et al. 2003, Li et al. 2009, Yu et al. 2001)* and in the self-aggregation of microflora, since extracellular polymeric substances (EPS) are prone to link multi-valent metals *(Rudd et al. 1984)*. Furthermore, MTW has a high proportion of dissolved biodegradable substrate, which could promote the growth of filamentous organisms *(Liu* and *Liu 2006)*. In fact, filamentous organisms tend to exist in a variety of aerobic granular sludge, but at various levels *(Lee et al. 2010)*. It has been widely accepted that low-levels and moderate-levels growth of filamentous bacteria do not cause sludge bulking, on the contrary it could instead help entangle each other with mycelium under appropriate operational conditions, and thus build up the backbone of granules, which can stabilize the granule structure by binding material *(Lee et al. 2010, Liu* and *Liu 2006, Li et al. 2010)*. Therefore, maintaining moderate-filamentous growth might be supporting granulation but is unlikely to be the only key strategy to cultivate and maintain stable aerobic granular sludge.

Hence, aerobic granules appear to be an ideal process for MTW treatment. In this study, the granulation process of aerobic sludge in a sequencing batch reactor (SBR) operating with synthetic saline wastewater (salinity of 3%, calculated by NaCl) was studied. The research focused on the influence of salt-stress on the formation of AGS, the role of breeding filamentous involved in aerobic granulation by improving organic loading, and the strategy to induce filamentous microorganisms in moderate-levels growth. In addition, the variation of morphological structure in/on AGS and mechanism involved in their granulation under salt stress were investigated. A good understanding of the formation of AGS and its characterization would be helpful for developing rapid granulation strategy of activated sludge under high salt stress and thus promoting the application of aerobic granulation technology. Moreover, this study could contribute to the development of AGS-based systems for engineering application in treating MTW characterized by high-strength and high-salinity.

Materials and Methods

SBR System

Tecnología y ciencias del agua, 10 (4), 156-181. DOI: 10.24850/j-tyca-2019-04-08

Three duplicate column-type sequencing batch reactors (SBRs), labeled by R1, R2, and R3, respectively, were applied to granulate aerobic sludge in this study, where the effective volume, internal diameter and height of each reactor were 1.9 L, 0.048 m and 1.05 m, respectively. Bottom aeration of the reactor column was supplied by an air pump and microporous diffuser. The reactors were supplied with different airflow rate to meet the dissolved oxygen (DO) concentration and hydraulic shear force in a different experimental period during the aeration phase, and a gas flowmeter was used to control the air flow. The three columns were operated at the controlled temperature, and the water temperature was (30±1)°C. The reactor was operating for 12 or 24 h per cycle at a water drainage ratio of 50%, including 2 min influent (via the reactor top), 3 min discharge, aeration, and sedimentation for the remaining time, in which, the time of aeration and sedimentation was adjustable according to operating condition. The experiment included two stages, namely the stage without salt (Period I) and the stage of salinity lifting (Period II). Detailed information about reactor operation was shown in Table 1.

Table 1. Detailed experimental conditions of the reactor system.

Index	Period I	Period II					
Duration (d)	0-21	21-28	28-35	35-45	45-56	56-63	63-73
Running time per cycle (h)	12	12	12	12	12	12	24
Setting time (min)	5~10	5	5	5	5	5	5
Organic loading (kg COD m^{-3} d^{-1})	1.5	2.0	2.5	3.5	4.5	3.6	2.25
Airflow rate (L min^{-1})	3	4	5	7	8	9	9

Simulated saline wastewater was employed as the influent of reactors. Its compositions were as follow: 0-30 g of sodium chloride (0-3% as salinity), 1415-4245 mg of glucose (1500-4500 mg L^{-1} as chemical oxygen demand (COD) basis), 92.0-122.7 mg of KH_2PO_4 (21-28 mg L^{-1} as PO_4^{3-}-P basis), 381.6-858.8 mg of NH_4Cl (100-225 mg L^{-1} as NH_4^+-N basis), 225.7-1333.3 mg of $MgSO_4 \bullet 7H_2O$ (22-130 mg L^{-1} as Mg^{2+} basis), 49.9-277 mg of $CaCl_2$ (18-100 mg L^{-1} as Ca^{2+} basis) and 0.1 mL of trace elements solution (*Kishida et al. 2006*). The pH of influent before dosing was controlled below 6.0 to avoid the precipitation among multi-valent metals, phosphate, and ammonium. The pH of the reactor throughout

each initial stage of cycles was kept constant at 8.0 ± 0.5 by dosing a suitable amount of sodium bicarbonate ($NaHCO_3$). Meanwhile, poly aluminum chloride (PAC), as an aluminum salt coagulant, with a dosage of 20 mg L^{-1} as Al basis was added into the influent of reactor R1 and R2 during day 21 to 38 to investigate whether aluminum ions (Al^{3+}) can accelerate the granulation of aerobic sludge.

Inoculation of Aerobic Granules

Activated sludge with dark brownness and flocculent from sludge returning tank of Chongqing Wastewater Treatment Plant (with the A^2/O process), Chongqing, China, was used as inoculum sludge. Before inoculation, activated sludge was cultivated in aerobic condition without any substance feeding for several days to inhibit the activity of hydrophilic bacteria, which would be difficult to connect with sludge flocs in contrast with the hydrophobic counterpart *(Lee et al. 2010)*. Besides, hydrophobic bacteria were abundant in the inoculum sludge, which could accelerate aerobic granulation and then exhibit excellent settling property *(Wilen et al. 2004)*. After activated sludge pre-treated and experienced the endogenous respiration, the initial concentration of the mixed liquor suspended solids (MLSS) in the reactors was approximately 5000 mg L^{-1}, and the ration of mixed liquor volatile suspended solids (MLVSS) to MLSS for the seed sludge was 69.8 ± 0.2%. The pre-treated sludge had good settling property and poor bioactivity, sludge volume index (SVI) was 20 mL g^{-1} and dehydrogenase activity (DHA) was only 1.59 ug TF g^{-1} SS h^{-1} because of microbes in endogenous respiration without sufficient substrates.

Strategies to Increase Salinity

In this study, salt content in reactors was adjusted by feeding different salty influent to investigate the influence of the increasing salt stress on granulation and characteristic of sludge. The concentration of sodium chloride in each reactor was augmented stepwise by the added substrate as shown in Figure 1.

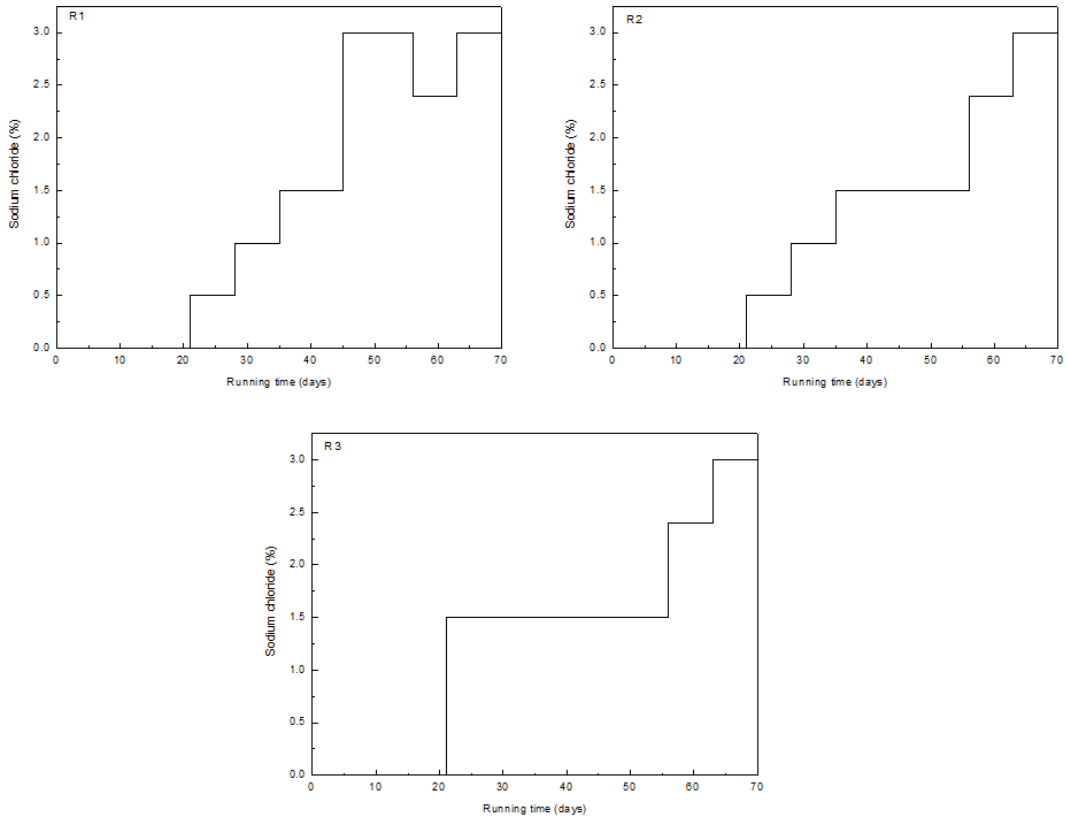

Figure 1. Augment of sodium chloride in the substrate of each reactor.

Analytical Methods

Morphologic Observation. Shape images of granular were attained using microscope BA210 (Nikon, Japan) and digital camera. Images of particles were randomly selected with a total particle number more than 500 and then measured in length and width for the size distribution analysis. The granules sub-sampled at -80°C were taken out from the refrigerator to thaw in room temperature for the subsequent analysis with a scanning electron microscope (SEM), and fixed in 2.5% glutaraldehyde for 4 h at 4°C, and then washed using phosphate buffer solution (PBS). Furthermore, the washed samples were stored in 1% osmic acid overnight at 4°C, and rewashed with PBS and then frozen using liquid nitrogen. Before SEM image taking (S3400N, Hitachi, Japan), the stored samples were dehydrated by placing in 30%, 50%, 70%, and 100% ethanol stepwise and then coated with gold.

Tecnología y ciencias del agua, 10 (4), 156-181. DOI: 10.24850/j-tyca-2019-04-08

Particle size distribution (PSD). The diameter of each particle was calculated by Sauter's Formula with length and width, as follows.

$$D = \frac{\sum(ab^2)^{\frac{1}{3}}}{n}$$

where, *D* means a diameter of each particle, calculated in mm; *n* means the number of particles; *a* and *b* mean the length and width of each particle respectively, calculated in mm. The results were then classified according to their particle size.

EPS. EPS was extracted from the granules by using cation exchange resin (CER) technique according to *Forlund et al. (1996)*. Granular samples were collected by centrifugation at 2000 rpm for 15 min, and then the compressed settling was washed twice with 0.1 M NaCl solution. Whereafter, the sludge settling was re-suspended to a prescribed volume and the solution was transferred to an extraction beaker, immediately adding the CER (strongly acidic styrene type-001×7, Na^+ form, pretreated with 0.1 M NaCl and 0.1 M NaOH for a pH of 7.0) with a dosage of 60 g g^{-1} SS. These CER/sludge suspensions were then mixed for 12 h at 500 rpm, and subsequently, the suspensions were standing for 3 min to separate CER and sludge suspensions. In the end, the EPS were harvested by centrifugation at 12000 rpm and 4°C for 30 min to eliminate residual sludge components. After centrifugation, the supernatants were filtrated through 0.22-mm acetate cellulose membranes and finally, the filtrates were collected for chemical analysis of the EPS fraction.

Extracellular proteins (PN) in the extracted EPS were adopted a modified Lowry method using folin-ciocalteau phenol reagent with bovine serum albumin as standard *(Forlund et al. 1996)*. Extracellular polysaccharides (PS) were determined by using the anthrone-sulfuric acid method with glucose as standard *(Laurentin* and *Edwards 2003)*.

Other Analyses. Sample analysis included COD, ammonium-N (NH_4^+-N), MLVSS and MLSS, all according to Standard Methods for the Examination of Water and Wastewater *(APHA 2005)*. MLSS content was measured by oven drying of the sample at 105°C for 1 h, whereas MLVSS was measured by ashing the dry sample at 550°C in a muffle for 15 min. DHA of AGS was determined according to the iodonitrotetrazolium chloride method *(Sebiomo et al. 2011)*. The oxygen content of mixed liquor was determined with a DO meter (HQ40d, HACH, USA). pH was measured by a pH meter (SENSION2, HACH, USA).

The physical characteristics of sludge (including SVI and granular strength) during granulation of activate sludge in the SBR columns

were analyzed. Settling performance of granules was evaluated in the aspect of SVI. The SVI was implemented according to the procedure described by *de Kreuk et al. (2005)*. The integrity coefficient (IC), which is defined as the ratio of residual particles to the total weight of granules after 5 min of shaking at 200 rpm on an orbital platform shaker *(Rosman et al. 2014)*, can be used to indirectly express as granular strength, and it also has an influence on granular compactness and bioactivity in the reactor.

Results and Discussion

Aerobic Granular Sludge Formation under Salt Stress and MorphologyCharacteristic

The morphology-evolution images of AGS, shown in Figure 2, during different formation stages were obtained by microscope and digital camera. Under microscopic examination, the morphology of initial seed sludge was fluffy, irregular and loose-structure. The sludge color gradually changed from dark brown to yellowish brown at the end of the experimental period.

In the initial stage of granulation (Period I), the loose flocs have easily broken into small pieces. After SBR reactors started, the sludge settling performance gradually became worse due to the high start-up loading and its poor activity, in where the DHA of inoculated sludge was only 1.59 ug TF g^{-1} SS h^{-1}. In the initial of operation, MLSS in the three reactors was 4952 mg L^{-1} and the SVI of inoculated sludge was 20 mL g^{-1}. Variations of MLSS and SVI are shown in Figure 3. Initially, the biomass was loose and bulked easily, and then flocs-like sludge gradually disappeared. MLSS decreased sharply with flocs washing out, and the SVI increased to around 200 mL g^{-1} in the first-week operation. During the next two weeks, the settling property of particles was improved gradually, and when the settling time was shortened to 5 min, the color of sludge appearance became from dark brown to yellowish brown. This is because that the washout of flocculated sludge can be commonly facilitated when settling time is shortened and small aggregates from the reactor and retained only well-settled granules *(Adav et al. 2008a, Long et al. 2014)*, which is often referred to hydrodynamic selection pressure for granulation. Meanwhile, we

occasionally observed that a few small particles appeared in all reactors and then gradually disappeared, and thus sampled some sludge to evaluate the granular strength. Results showed that IC value of samples was under than 10%, which indicated that the small particles were not strong enough to resist the mechanical collision and fluid shear stress resulting in the loss and disintegration of particles. The main components in EPS of all granules showed a similar trend, in where the extracellular proteins significantly increased, whereas the extracellular polysaccharides decreased, and thus the PN/PS ratio increased (Figure 4), which indicated the importance of the carbohydrates for promoting the cohesion and adhesion of cells during initial granules formed. Meanwhile, proteins existed in negative charge as pH of the reacting system controlled around 8.0, which can cross-bridge divalent metal ions (such as Ca^{2+} and Mg^{2+}) and EPS to promote microbes in cell-cell aggregation, causing the loose granules generally compacted and then accumulated. Furthermore, metal ions transferred to minerals with phosphate acting as a nucleus, which results in the accumulation of bacteria and the formation of biological mass. After 21-days continuous operation, the appearance of granular nuclei in each reactor have indicated the initial formation of AGS was achieved, meanwhile, the settling properties and biological activity of sludge were gradually improved, thereafter the granules considerably developed. After the end of Period-I experiments, The SVI of reactor R1, R2 and R3 decreased to 30.7, 30.2 and 27.8 mL g^{-1} respectively, and DHA were 50.91, 39.76 and 47.05 ug TF g^{-1} SS h^{-1} correspondingly. As aforementioned, the reactors were mainly dominated by flocculent sludge with good settling properties and some granules, but AGS were irregular in appearance (Figure 2b) and low granular strength (the IC values of granules in three reactors were only between 30% to 40%).

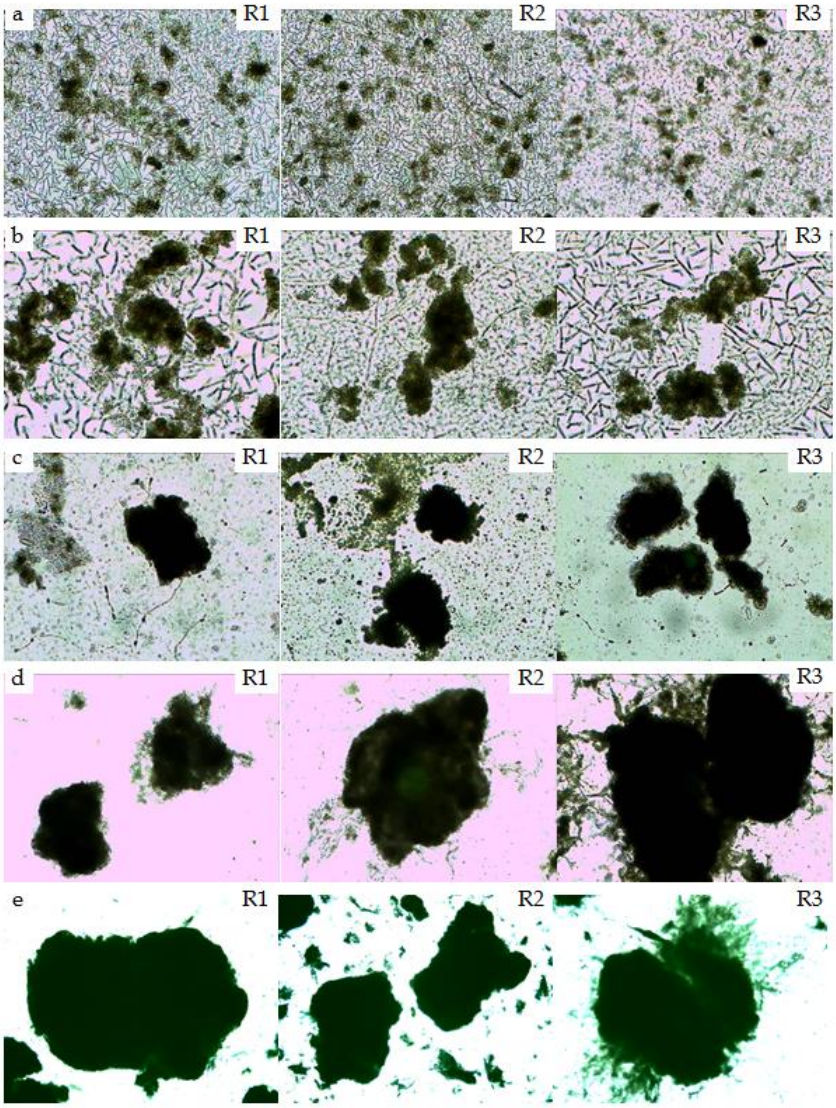

Figure 2. Photographs of the sludge after the following days in each SBRs: (a) 2 days (×100), (b) 19 days (×100), (c) 30 days (×100), (d) 47 days (×100), (e) 67 days (×40).

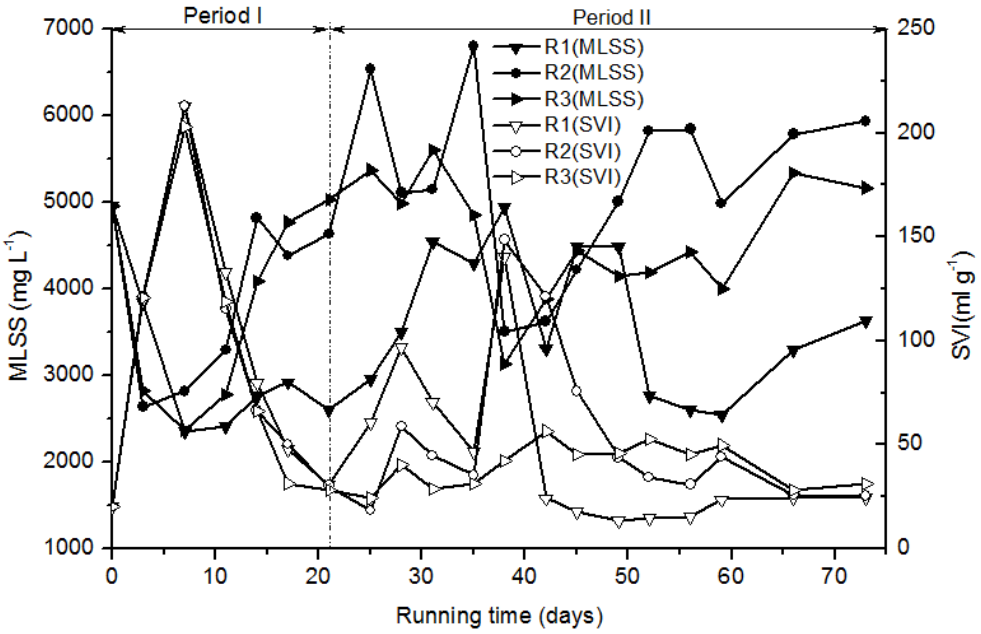

Figure 3. Variations of MLSS and SVI of the sludge in R1, R2, and R3.

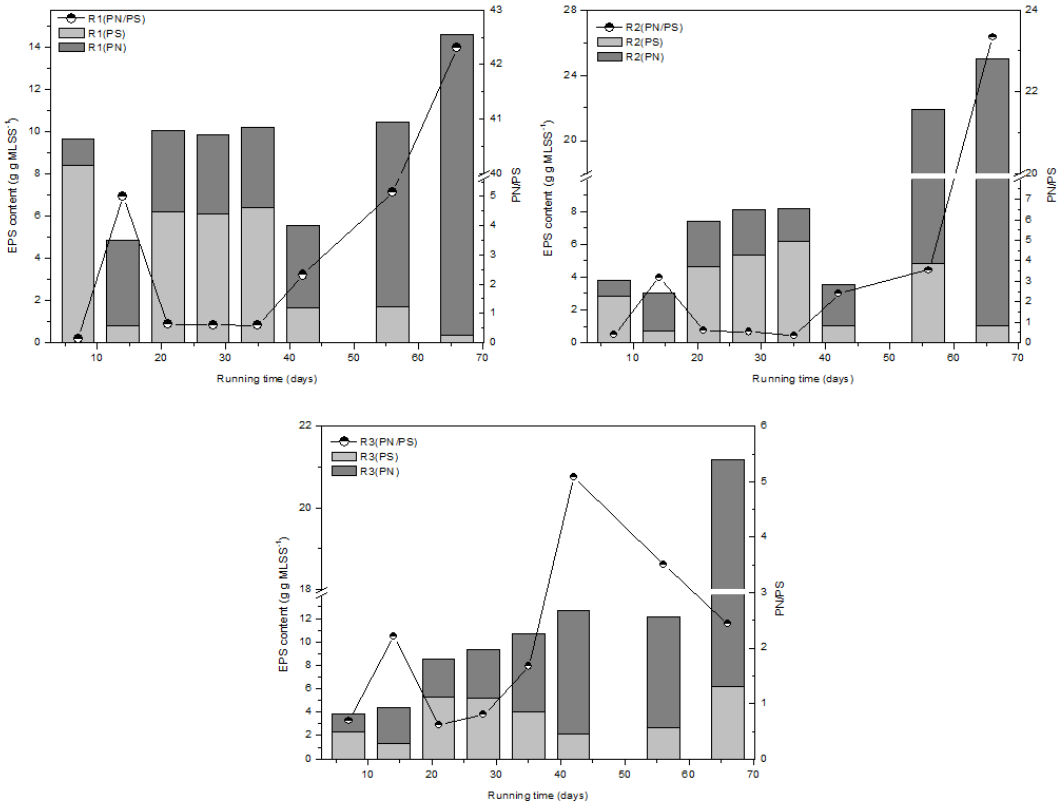

Figure 4. The variation of EPS content and ratio of PN to PS in granules.

In the subsequent Period II, the settling properties became worse gradually because of the adverse impact of a sudden increase of salinity on microbial species. Simultaneously, in a high and quick shifting sodium chloride content distributed system, granules were subjected to larger buoyancy, and the selection pressure was strengthened. Afterward, flocs-like sludge and granules with poor settling properties were continuously discharged from reactors, which result in the rise of SVI in reactor R1 and R2 to 96.9 and 58.7 mL g^{-1}, respectively (Figure 3). However, SVI in reactor R3 remained a relatively stable scale and biomass increased gradually, based on which can safely conclude that under initial high (1.5% of NaCl) and stable salinity, microbes had enough time to adapt and grow. It was reviewed that hydrodynamic shear would densify the granular sludge but have no impact on EPS content and compositions *(Di Iaconi et al. 2006)*, and the flocs would become compacter under a high shear force which induces the biomass aggregates to secrete more exopolysaccharides *(Dulekgurgen et al. 2008)*. Therefore, from 21st day, the aerating flux of reactors with the airflow rate of 3 L min^{-1} was raised to improve the hydrodynamic shear force. Under a higher airflow rate, exopolysaccharides contents rapidly increased in all granules, which means more polysaccharide contents were secreted by bio-aggregates. And PS contents sharply increased to 6.2, 4.6 and 5.3 g g^{-1} MLSS, respectively, while the PN contents remained small changes at the end of the 2nd cycle in the 21st day (Figure 4). Meanwhile, with a dosage of 20 mg L^{-1} PAC as Al basis added in the influent of reactor R1 and R2, the cross-bridging of Al^{3+} promoted bacterial self-immobilization to microbial aggregates, and then accelerated the granulation of aerobic sludge. Consequently, the settling properties of granules in reactor R1 and R2 were really not affected by the shocking of salinity in the following period, and the SVI values were under 30 mL g^{-1} (Figure 3). Also, as shown in Figure 4, the addition of PAC had no direct effect on the extracellular proteins but promoted the production of extracellular polysaccharides. It was proved that extracellular polysaccharides could improve both cohesion and adhesion of cells and play an important role in maintaining the structural integrity of biofilms and granular sludge *(Liu et al. 2004, Tay, Liu and Liu 2001)*. The formation and stability of AGS would be enforced by polysaccharides since it could constitute a strong and sticky configuration during activated sludge cultivation *(Liu et al. 2004, Ren et al. 2008)*, and IC of granules in reactor R2 and R3 can achieve around 75%, higher than reactor R1 with 58%. Therefore, PAC addition played an active effect in the aerobic granulation process.

It should be noted that for NaCl <5 g L^{-1}, most of the microbial community were environmentally resistant *(Salvado et al. 2001)*. Along with the adaptation of microorganisms on salinity and the continuous appearance of halophilic microbes, the increase of EPS contents under

higher salinity in the reactor played an important role in the granulation. And together with the impact of compressing the double electrode layer generated between the positively charged cationic ions, such as Ca^{2+}, Mg^{2+} and Na^{+}, and the negatively charged bacterial surface and EPS, acting as a bridge between bacteria, sludge flocs gradually became more dense and compact through bacterial self-immobilization and inter-granular binding, and then constantly grew up with filamentous twining.

By this time, it was considered that the evolution of inoculum sludge from flocculent to granular sludge was accomplished as a result of the interactions between inter-particle bridging process among EPS, bacterial cells and ion *(Sheng et al. 2010)*. Subsequently, the shape of small particles became more regular and its size gradually increased during the following weeks, whereas more flocs washed out from the reactor, resulting in the cumulation of the AGS with high settling rate. Some granules were sampled from each reactor and the morphology of which was observed on day 30. It was found that all particle size in reactors had increased, in which, the least granules in reactor R1, the most granules with uniform PSD in reactor R2, whereas irregularly shaped granules with maximum different PSD in reactor R3, and granular strength reached up to 80%. There was still a few flocs in each reactor, surrounding which a semitransparent floccule was EPS (Figure 2 c). The structure of EPS was yet loose, whereas the floccule was in a tendency of aggregating to the center of the flocs. Filamentous bulking broke out in reactor R1 and R2 on day 38, and the gradual disintegration of granules followed. The SVI of reactor R1 and R2 achieved up to 140 mL g^{-1}. In that case, it was reasonable to conclude that a dosage of Al^{3+} can clog the pore interior granules, which result in aggravating substrate transfer resistance and inhibiting heterotrophic bacteria activity in granules, and metabolic blocking of exopolysaccharide synthesis (showed as a decrease of PS contents in Figure 4) owing to the clogging of granular porous prevented microbial aggregation *(Yang et al. 2004)*. Furthermore, filamentous bulking or viscosity bulking occurred easily under the condition of high organic loading, and under such condition, the organisms residing in the granules would consume the matrix EPS excessively and slash the density of the granules, perhaps even leading to the cells' autolysis *(Zhang* and *Zhang 2013)*. Consequently, this would result in a loosened structure and bad settling ability. *Weissbodr et al. (2012)* asserted that washout was a selective process of microbial while zoogloea enriched in their dense particles and filamentous dominated in granules with a loose structure. Therefore, some measures, such as stopping the dosage of Al^{3+}, increasing hydrodynamic shear stress, and reducing organic loading gradually from day 56, were adopted to control the filamentous bulking, and then the bulking phenomenon of reactor R2

had been relieved. Under given conditions, high hydrodynamic stress could reduce substrate transfer resistance into the granules *(Lee et al. 2010)*, and enhance the activity of the inner microorganisms and avoid the cavities caused by cell autolysis. Meanwhile, maintaining high hydrodynamic shear stress can crush filamentous granules and then discharged from reactors. Additionally, it can induce microbes to secrete more EPS, which can work as a matrix for the granulation process at moderate levels, accelerating the granulation process of sludge, making the broken granules recover gradually, and finally making the granules evolve from fluffy inoculum to compact granules. With different salt stress selective pressure, mature and stable granules were achieved under salinity of 3% after 70-day cultivation. The yellowish-brown granules had good settling properties, with SVI of 24.8, 25.3, and 31.0 mL g^{-1}, respectively. In addition, the granules had a relatively higher value of biomass density and IC value was 95%, 98%, and 90%, respectively. It was observed that the granules in reactor R1 and R2 had a clear boundary outline in a round and a dense structure, with the maximum particle size of 3 and 2 mm respectively. While granules in reactor R3 manifested as filamentous granules with loose structure and filamentous mycelia bestrewing boundary due to the fast growth of particles and influence of mass transfer, and the maximum particle size of which can reach up to 6 mm, as shown in Figure 5.

Figure 5. Morphology of mature granules, R1 (a), R2 (b), R3 (c).

Comparing the bioactivity of granules in these reactors, the particle size of particles in reactor R1 was smaller than R2, but DHA in R2 was up to 48.91 ug TF g^{-1} SS h^{-1} was nearly double that figure in reactor R1 with 26.42 ug TF g^{-1} SS h^{-1} due to the more developed pore structure and the higher bioactivity. Moreover, the loosened granules in reactor R3 was covered with mycelia, and the bioactivity of which was the worst of the three reactors, and DHA was only 19.02 ug TF g^{-1} SS h^{-1}.

Although it is not the objective of this paper to discuss the treatment efficiency of granules, simple descriptive statistics of the concentrations of organic matter and ammonia nitrogen during the overall mature

granules period were conducted in order to allow a general view of the system's performance. Mean concentration of the influent COD and NH_4^+-N for the reactors was kept at 4500 and 225 mg L^{-1} during mature granules formation, and AGS showed high removal performance. The COD removal efficiencies of reactor R1, R2 and R3 can reach up to 92.5%, 95.1%, and 90.2%, and the corresponding removal rates of NH_4^+-N achieved to 59.8%, 67.1%, and 65.6%.

PSD and Average Particle Size

There was a vast difference in PSD of AGS cultivated under different operational conditions (Figure 6). The particle size of granules in reactor R2 was small, in which granules with the particle size less than 1 mm and the ranged between 1 to 2 mm occupied 58.4% and 39.7% respectively, and the average particle size was only 0.9 mm. In contrast, the particle size of granules in reactor R1 and R2, with an average diameter of 1.4 mm and 1.7 mm, was relatively larger, wherein with the diameter approximately 1-2 mm predominated, and occupied 70.5% and 64.4% respectively, and ranged between 2 to 3mm was 15.1% and 24.9% respectively. The PSD of granules in each reactor was fitted with normal distribution function, and it was found that the PSD of all reactors accorded with the normal distribution law, and fitting coefficient values (R^2) were all more than 0.9, especially which of reactor R1 was up to 0.96. At the same time, it was demonstrated that the average particle size of mature granules was positively correlated with dispersion. It can safely draw a conclusion that filamentous bacteria dominating in reactor R3 twined around each other to form fluffy filamentous granules surrounding with mycelium. And it was unlikely to maintain a stable structure and tend to expansion and even hydrolysis of aerobic granule core due to the poor stability. Thereafter, granules developed in dispersive growth, resulting in the maximum dispersion of 0.705 in reactor R3. By contrast, bacterial granules in reactor R2 predominated with zoogloea can aggregate with EPS, and manifested in good stability, resulting in a minimum dispersion of 0.377.

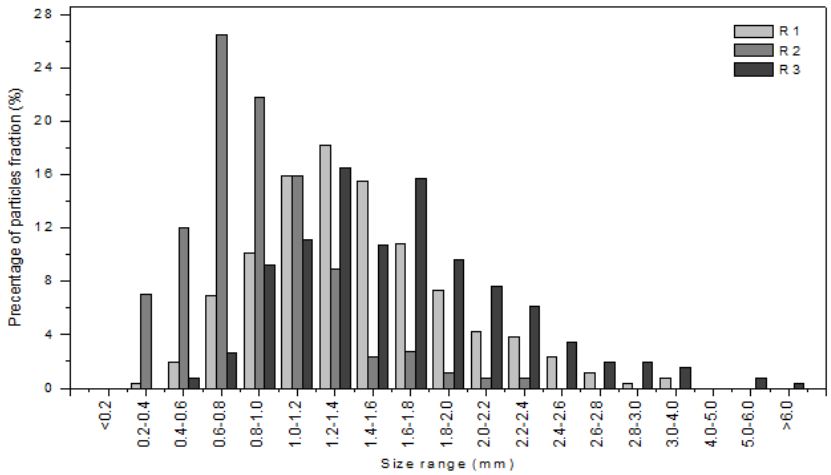

Figure 6. Size distributions of aerobic granules of each reactor.

Mechanism of Formation of Aerobic Granules under Salt Stress

Although there are many hypotheses for the formation of AGS, granulation mechanism of aerobic granules is still unclear. It is now widely accepted that the complex formation of AGS is the result of various mechanisms involved in cell-to-cell immobilization *(Qin et al. 2004)*, extracellular polymer *(Liu and Tay 2004)*, filamentous bacteria *(Beun and Hendriks 1999)*, cell surface hydrophobicity *(Liu and Tay 2004, Qin et al. 2004)* and nucleation hypothesis *(Liu and Tay 2004)*. However, there is no unified, reliable aerobic granules cultivation mode, because abundant factors can affect aerobic sludge granulation, which makes it difficult to control and predict the set-up process for AGS.

According to many researches, the formation of AGS, in fact, can be regarded as an aggregation of various microorganisms with cell-cell interaction from the microbial perspective *(Ren et al. 2010)*, a phenomenon denoted as quorum sensing (QS). QS is a means of intercellular communication, and it can affect gene expression and physiological behavior of an entire microflora to adjust the changing environment *(Shrout and Nerenberg 2012)*, and the involvement of QS in aerobic granulation has been well characterized and confirmed *(Li et al. 2014, Xiong and Liu 2012, Zhang et al. 2011)*. As aforementioned, it is reasonable to conclude that that variation of cultural conditions can directly affect the microbial attachment and composition of microbial community with different signaling molecules secreted by bacteria, and then result in aerobic granulation. The external morphological

characters and internal structures of the aerobic granules were further inspected using SEM. It showed that the mature granules in three reactors with the SEM had different morphology under cultural conditions of different strategies to augment salt stress and adding Al^{3+} or not. A carefully inspect revealed that intra-granules showed different microbial structure, as shown in Figure 7.

Granules in reactor R1 consisted of zoogloea, filamentous and bacillus bacteria adhering to the surface of filamentous bacteria. In contrast, granules in reactor R2 were mainly dominated by zoogloea, while filamentous predominated in granules of reactor R3. It was safely hypothesized that halotolerant and halophilic bacteria with high biological activity easily dominated in reactor under the condition of initial salt-stress selection at low concentration, and these preponderant microbes can secrete a relatively high quantity of EPS (Figure 4), which can bond bacterial cells and other particulates into an aggregation generating the precursor of a particle *(Liu et al. 2004)*. But excessive EPS can block inner cores of the granules which acting as mass transfer channels. And the resistance of mass transfer of granular sludge in reactor R1 could shape an anaerobic core to motivate bioactivities of anaerobic strains *(Zheng et al. 2006)*, which can cause the hydrolysis of anaerobic granule core, hence result in multiple cavities of intra-granules caused by cell autolysis (Figure 7 a). For organic loading rate, the higher the rate, the better to the growth of heterotrophic microbes, such as the breeding of filamentous bacteria, which conduced to irregular frames *(Moy et al. 2002)*, and further hindered the granulation. Whereas overgrowth of filamentous bacteria can be controlled by high hydrodynamic stress and reducing organic loading gradually at high salinity (2.4-3.0%), in particular, fluctuation of salinity could effectively induce moderate-levels of filamentous growth, which could play a role in intertwining and connection with zoogloea during granulation. Meanwhile, the wrapping and adherence of zoogloea can provide more stable and favorable ecological conditions for filamentous maintaining the structural integrity in granules formation. Therefore, filamentous and zoogloea formed a special symbiotic relationship in granular sludge of reactor R1 at appropriate cultivation conditions.

The dosage of Al^{3+} appeared to be a major cause of filamentous sludge bulking in aerobic granulation of reactor R2 and improved the aggregation of floc-like sludge through cell-cell bridging. However, Al^{3+} can transform to chemical precipitate with high content phosphate, which can result in a clogging of granular core and then affect the mass transfer, meanwhile filamentous cannot excess intra-granules to intertwine and connect aggregations, instead of outgrowth on the surface of particles freely, and finally caused filamentous granular bulking in reactor R2. After adopted some corresponding measures,

filamentous bacteria adhering to zoogloea and sediments clogging in granular cores were washed out from granules gradually. In addition, the high hydrodynamic shear force can drive microbes to secrete more EPS to promote granulation, improve microbial cell surface hydrophobicity *(Liu et al. 2003)*, and densify and compact the granules. The increase of EPS in Fig.4 from 56 days had confirmed the conclusion. Ultimately, the final matured aerobic granules dominated by zoogloea with a clear boundary outline and good settling properties were achieved. While filamentous microorganism appeared to be predominated microbes on high content initial salt-stress selection, result in a formation of filamentous granules. When the quantity of extracellular polysaccharides (decrease trend in Figure 4) was not sufficient to maintain granular structure, it will lead to a disintegration of filamentous particles and filamentous bulking.

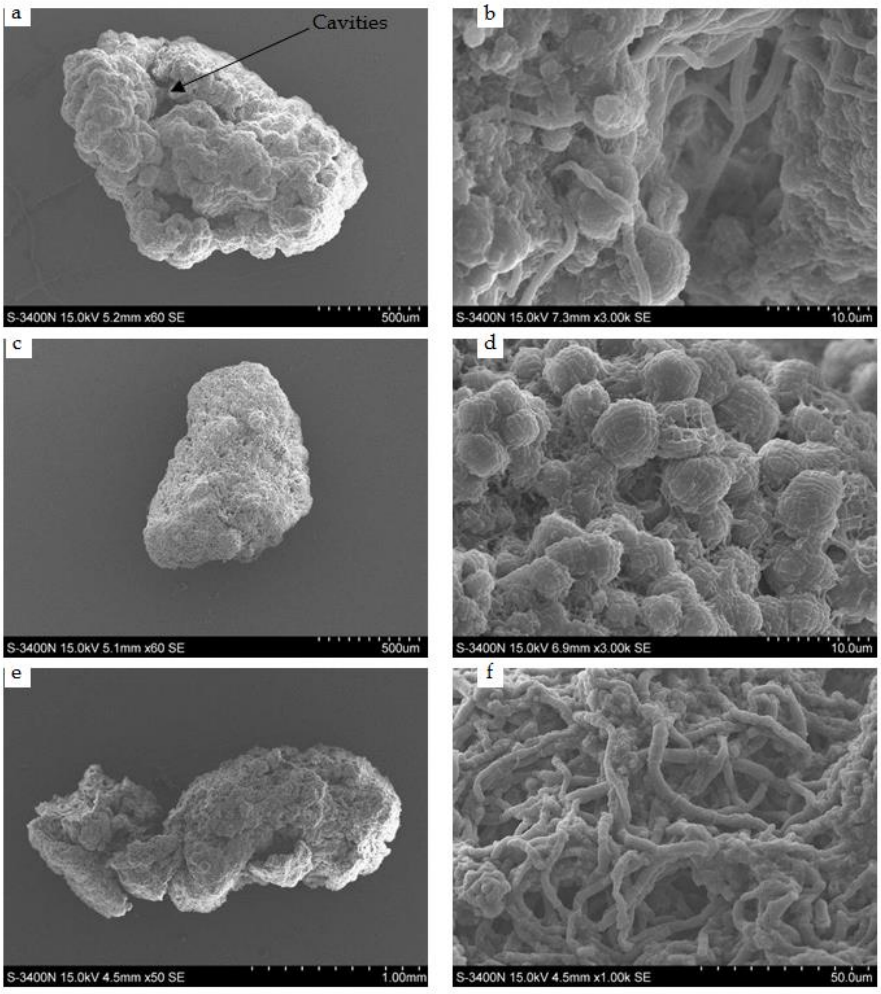

Figure 7. Image of granule, its surface, and inner part for each reactor, R1 (a, b), R2 (c, d), R3 (e, f).

Studies intend to examine the mechanisms that may involve in the granulation processes. In general, two models were proposed on granulation for AGS *(Li et al. 2010)*. The first model suggests that microbe-to-microbe contact form aggregates by physical forces, and initial attraction to shape into aggregates by physical, chemical or biochemical forces, and then EPS bind each other to make the aggregates become stronger, allowing physical enmeshment, consequently the final compact granules formed under hydrodynamic stress. The second model states that filamentous bacteria intertangle and thus form the backbone of particles. As in Figure 7, microbe-to-microbe adhered and aggregated by EPS binding in reactor R2, and granular backbone formed by filamentous microbes entangling each other in reactor R3. In contrast, how the inner granular structure found in reactor R1 formed could be proposed that filamentous bacteria accessed to inner granules and entangled with zoogloea to form granules based on cell-to-cell attachment through EPS enmeshing. Therefore, we can propose that in this research, two steps involved in the granulation under high salt stress were as follow:

1. Under unsalted condition, positive charged ions such as Ca^{2+} and Mg^{2+} combine with some bacteria as well as with negatively charged EPS to form high polymer bridged linkage biomacromolecule, which can provide crystal nucleus for aerobic granulation;

2. Under subsequent salt-shifting conditions, granules would develop mainly complied with the first model under low initial salt-stress selection, while the development of granules would comply with the second model under high initial salt-stress selection.

Conclusion

Inoculated with activated sludge when reactor adapted different operational conditions, aerobic granulation was realized within 70 days in three pilot scale SBRs fed with simulated saline wastewater. The reactors had good performance for COD and NH_4^+-N removal when the mean concentration of the influent COD and NH_4^+-N for the reactors was kept at 4500 and 225 mg L^{-1}. The COD removal efficiencies of reactor R1, R2, and R3 can reach up to 92.5%, 95.1%, and 90.2%, and the corresponding removal rates of NH_4^+-N achieved to 59.8%, 67.1%, and 65.6%.

Compact and stable aerobic granules dominated by zoogloea with an excellent settling ability and a clear boundary outline were successfully

cultivated in SBR system on low initial salinity, while filamentous granular sludge with irregular, loose structure and mycelia on outer layer was formed when given high initial salinity. Divalent metal ions such as Ca^{2+} and Mg^{2+} can transfer to minerals with phosphate in simulated MTW, then, it served as crystal nucleus and carriers for granulation. Appropriate organic loading, hydrodynamic shear, and salt-stress selection can induce filamentous bacteria on moderate growth to act as granulation backbone. Aerobic granulation process under salt stress was a result together with crystal nucleus, filamentous bacteria, and EPS, which can be affected by salinity-shifting strategies and dosage of aluminum salt coagulant. On low initial salt-stress selection, aerobic granules of reactor R1 cultivated were predominated by cell-to-cell aggregation with EPS bridging and filamentous intertwining and connection, and the average particle size was 1.4 mm without dosage of Al^{3+}, whereas adding coagulant can shorten granular shape on an average particle size of 0.9 mm without any filamentous microbes in granules of reactor R2, and then develop more pore structure with higher bioactivity of 26.42 ug TF g^{-1} SS h^{-1}, which compared to the double that figure in reactor R1. By contrast, moderate-level filamentous microorganisms induced can entangle each other acting as the backbone of granules and thus form filamentous granules in reactor R3 with average particle size of 1.7 mm and high bioactivity of 19.02 ug TF g^{-1} SS h^{-1} on high initial salt-stress selection.

Further researches are necessary with the focus on biological issues like how to control QS to reduce the EPS production and alter its component by bacteria under salt stress and to promote and maintain filamentous spatial structures.

Acknowledgment

This study was supported by the Science and Technology Research Program of Chongqing Municipal Education Commission (Grant No. KJ110403, KJ1400326, KJ1705140), the Science and Technology Research Program of Chongqing Science and Technology Commission (Grant No. cstc2017jcyjAX0292), Venture & Innovation Support Program for Chongqing Overseas Returnees (cx2017065), Natural Science Foundation of China (Grant No. 51608079) and Chinese Scholarship Council (CSC) (Grant No. 201508505098).

References

Adav, S. S., Lee, D. J., Show, K. Y. & Tay, J. H. (2008a). Aerobic granular sludge: Recent advances. *Biotechnology Advance* 26: 411-423.

Adav, S. S. & Lee, D. J. (2008b). Extraction of extracellular polymeric substances from aerobic granule with compact interior structure. *Journal of Hazardous Materials* 154: 1120-1126.

Adav, S. S., Lee, D. J. & Lai, J. Y. (2010). Aerobic granules with inhibitory strains and role of extracellular polymeric substances. *Journal of Hazardous Materials* 174(1-3): 424-428.

Aloui, F., Khoufi, S., Loukil, S. & Sayadi, S. (2009). Performances of an activated sludge process for the treatment of fish processing saline wastewater. *Desalination* 246: 389-396.

APHA: *Standard Methods for the Examination of Water and Wastewater*, 21st edn. (2005). Washington, DC: American Public Health Association.

Beun, J. J. & Hendriks, A. (1999). Aerobic granulation in a sequencing batch reactor. *Water Research* 33: 2283-2290.

Chai, H. X. & Kang, W. (2012). Influence of biofilm density on anaerobic sequencing batch biofilm reactor treating mustard tuber wastewater. *Applied Biochemistry and Biotechnology* 168(6): 1664-1671.

Chen, Y. Y. & Lee, D.J. (2015). Effective aerobic granulation: role of seed sludge. J*ournal of the Taiwan Institute of Chemical Engineers* 52: 118-119.

De Kreuk, M. K., Pronk, M. & van Loosdrecht, M.C.M. (2005). Formation of aerobic granules and conversion processes in anaerobic granular sludge reactor at moderate and low temperatures. *Water Research* 39: 4476-4484.

Di Iaconi, C., Ramadori, R., Lopez, A. & Passino, R. (2006). Influence of hydrodynamic shear forces on properties of granular biomass in a sequencing batch biofilter reactor. *Biochemical Engineering Journal* 30: 152-157.

Dulekgurgen, E., Artan, N., Orhon, D. & Wilderer, P. A. (2008). How does shear affect aggregation in granular sludge sequencing batch reactors? Relations between shear, hydrophobicity, and extracellular polymeric substances. *Water Science and Technology* 58: 267-276.

Frolund, B., Palmgren, R., Keiding, K. & Nielsen, P. H. (1996). Extraction of extracellular polymers from activated sludge using a cation exchange resin. *Water Research* 30: 1749-1758.

Guo, F., Fu, G. K., Zhang, Z. & Zhang, C. L. (2013). Mustard tuber wastewater treatment and simultaneous electricity generation using microbial fuel cells. *Bioresource Technology* 136: 425-430.

Guo, F., Fu, G. K. & Zhang, Z. (2015). Performance of mixed-species biocathode microbial fuel cells using saline mustard tuber wastewater as self-buffered catholyte. *Bioresource Technology* 180: 137-143.

Jiang, H. L., Tay, J. H., Liu, Y. & Tay, S. T. L. (2003). Ca^{2+} augmentation for enhancement of aerobically grown microbial granules in sludge blanket reactors. *Biotechnology Letters* 25: 95-99.

Kishida, N., Kim, J., Tsuneda, S. & Sudo, R. (2006). Anaerobic/oxic/anoxic granular sludge process as an effective nutrient removal process utilizing denitrifying polyphosphate-accumulating organisms. *Water Research* 40(12): 2303-2312.

Laurentin, A. & Edwards, C. A. (2003). A microtiter modification of the anthrone-sulfuric acid colorimetric assay for glucose-based carbohydrates. *Analytical Biochemistry* 315(1): 143-145.

Lee, D. J., Chen, Y. Y., Show, K. Y., Whiteley, C. G. & Tay, J. H. (2010). Advances in aerobic granule formation and granule stability in the course of storage and reactor operation. *Biotechnology Advances* 28: 919-934.

Lefebvre, O. & Moletta, R. (2006). Treatment of organic pollution in industrial saline wastewater: a literature review. *Water Research* 40(20): 3671-3682.

Li, X. M., Liu, Q. Q., Yang, Q., Guo, L., Zeng, G. M., Hu, J. M. & Zheng, W. (2009). Enhanced aerobic sludge granulation in sequencing batch reactor by Mg^{2+} augmentation. *Bioresource Technology* 100: 64-67.

Li, Y. C., Hao, W., Lv, J. P., Hao, W., Wang, Y. Q. & Zhu, J. R. (2014). The role of N-acyl homoserine lactones in maintaining the stability of aerobic granules. *Bioresource Technology* 159: 305-310.

Li, Z. H. & Wang, X.C. (2008). Effects of salinity on the morphological characteristics of aerobic granules. *Water Science and Technology* 58: 2421-2426.

Li, Z. H., Zhang, T., Li, N. & Wang, X.C. (2010). Granulation of filamentous microorganisms in a sequencing batch reactor with saline wastewater. *Journal of Environmental Sciences* 22(1): 62-67.

Liu, L., Gao, D. W., Zhang, M. & Fu, Y. A. (2010). Comparison of Ca^{2+} and Mg^{2+} enhancing aerobic granulation in SBR. *Journal of Hazardous Materials* 181(1-3): 382-387.

Liu, Y. & Liu, Q. S. (2006). Causes and control of filamentous growth in aerobic granular sludge sequencing batch reactors. *Biotechnology Advances* 24: 115-127.

Liu, Y. & Tay, J. H. (2004). State of the art of biogranulation technology for wastewater treatment. *Biotechnology Advances* 22(7): 533-563.

Liu, Y., Yang, S. F., Liu, Q. S. & Tay, J. H. (2003). The role of cell hydrophobicity in the formation of aerobic granules. *Current Microbiology* 46(4): 270-274.

Liu, Y., Yang, S. Y., Tay, J. H., Liu, Q. S., Qin, L. & Li, Y. (2004). Cell hydrophobicity is a triggering force of biogranulation. *Enzyme and Microbial Technology* 34: 371-379.

Liu, Y., Yang, S. F. & Tay, J. H. (2004). Improved stability of aerobic granules by selecting slow-growing nitrifying bacteria. *Journal of Biotechnology* 108: 161-169.

Long, B., Yang, C. Z., Pu, W. H., Yang, J. K., Jiang, G. S., Dan, J. F., Li, C. Y. & Liu F.B. (2014). Rapid cultivation of aerobic granular sludge in a pilot scale sequencing batch reactor. *Bioresource Technology* 166: 57-63.

Morales, N., Figueroa, M., Mosquera-Corral, A., Campos, J. L. & Méndez, R. (2012). Aerobic granular-type biomass development in a continuous stirred tank reactor. *Separation and Purification Technology* 89(3): 199-205.

Moussavi, G., Barikbin, B. & Mahmoudi, M. (2010). The removal of high concentrations of phenol from saline wastewater using aerobic granular SBR. *Chemical Engineering Journal* 158(3): 498-504.

Moy, B. Y. P., Tay, J. H., Toh, S. K., Liu, Y. & Tay, S. T. L. (2002). High organic loading influences the physical characteristics of aerobic sludge granules. *Letters in Applied Microbiology* 34(6): 407-412.

Qin, L., Tay, J. H. & Liu, Y. (2004). Selection pressure is a driving force of aerobic granulation in sequencing batch reactors. *Process Biochemistry* 39(5): 579-584.

Ren, T. T., Liu, L., Sheng, G. P., Liu, X. W. & Yu, H. Q. (2008). Calcium spatial distribution in aerobic granules and its effects on granule structure, strength and bioactivity. *Water Research* 42: 3343-3352.

Ren, T. T., Yu, H. Q. & Li, X. Y. (2010). The quorum-sensing effect of aerobic granules on bacterial adhesion, biofilm formation, and sludge granulation. *Applied Microbiology and Biotechnology* 88: 789-797.

Rene, E. R., Kim, S. J. & Park, H. S. (2008). Effect of COD/N ratio and salinity on the performance of sequencing batch reactors. *Bioresource Technology* 99(4): 839-846.

Rosman, N. H., Anuar, A. N., Chelliapan, S., Din, M. F. M. & Ujang, Z. (2014). Characteristics and performance of aerobic granular sludge treating rubber wastewater at different hydraulic retention time. *Bioresource Technology* 161: 155-161.

Rudd, T., Sterritt, R. M. & Lester, J. N. (1984). Complexation of heavy metals by extracellular polymers in the activated sludge process. *Journal Water Pollution Control Federation* 56: 1260-1268.

Salvado, H., Mas, M., Menendez, S. & Gracia, M. (2001). Effects of shock loads of salt on protozoan communities of activated sludge. *Acta Protozoologica* 40(3): 177-186.

Sebiomo, A., Ogundero, V. & Bankole, S. (2011). Effect of four herbicides on microbial population, soil organic matter and dehydrogenase activity. *African Journal of Biotechnology* 10(5): 770-778.

Sheng, G. P., Yu, H. Q. & Li, X. Y. (2010). Extracellular polymeric substances (EPS) of microbial aggregates in biological wastewater treatment systems: a review. *Biotechnology Advances* 28: 882-894.

Shrout, J. D. & Nerenberg, R. (2012). Monitoring bacterial twitter: does quorum sensing determine the behavior of water and wastewater treatment biofilms? *Environmental Science and Technology* 46(4): 1995-2005.

Taheria, E., Khiadani, M. H., Amina, M. M., Nikaeen, M. & Hassanzadeh, A. (2012). Treatment of saline wastewater by a sequencing batch reactor with emphasis on aerobic granule formation. *Bioresource Technology* 111: 21-26.

Tay, J. H., Liu, Q. S. & Liu, Y. (2001). The role of cellular polysaccharides in the formation and stability of aerobic granules. *Letters in Applied Microbiology* 33: 222-226.

Wan, C. L., Yang, X., Lee, D. J., Liu, X., Sun, S. P. & Chen, C. (2014). Partial nitrification of wastewaters with high NaCl concentration by aerobic granules in continuous-flow reactor. *Bioresource Technology* 152: 1-6.

Weissbrodr, D. G., Lochmatter, S., Ebrahimi, S., Rossi, P., Maillard, J. & Holliger, C. (2012). Bacterial selection during the formation of early-stage aerobic granules in wastewater treatment systems operated under wash-out dynamic. *Frontiers in Microbiology* 3: 332-354.

Wilen, B. M., Gapes, D. & Keller, J. (2004). Determination of external and internal mass transfer limitation in nitrifying microbial aggregates. *Biotechnology and Bioengineering* 86: 445-57.

Xiong, Y. H. & Liu, Y. (2012). Essential roles of eDNA and AI-2 in aerobic granulation in sequencing batch reactors operated at different settling times. *Applied Microbiology and Biotechnology* 93(16): 2645-2651.

Yang, S. F., Tay, J. H. & Liu, Y. (2004). Inhibition of free ammonia to the formation of aerobic granules. *Biochemical Engineering Journal* 17: 41-48.

Yu, H. Q., Tay, J. H. & Fang, H. P. (2001). The roles of calcium in sludge granulation during UASB reactor start-up. *Water Research* 35: 1052-1060.

Zhang, C. Y. & Zhang, H. M. (2013). Analysis of aerobic granular sludge formation based on grey system theory. *Journal of Environmental Sciences* 25(4): 710-716.

Zhang, S., Yu, X., Guo, F. & Wu, Z. Y. (2011). Effect of interspecies quorum sensing on the formation of aerobic granular sludge. *Water Science and Technology* 64: 1284-1290.

Zheng, Y. M., Yu, H. Q., Liu, S. J. & Liu, X. Z. (2006). Formation and instability of aerobic granules under high organic loading conditions. *Chemosphere* 63: 1791-800.

Zhu, L., Yu, Y. W., Dai, X., Xu, X. Y. & Qi, H. Y. (2013). Optimization of selective sludge discharge mode for enhancing the stability of aerobic granular sludge process. *Chemical Engineering Journal* 217: 442-446.

DOI: 10.24850/j-tyca-2019-04-09
Special Article

Multiple Spatial Scales Chaos Characterization in Runoff Series by the 0-1 Test Algorithm

Caracterización de escalas de caos espaciales múltiples en series de vertidos por el algoritmo de prueba 0-1

X. Li[1]*
T. Hu[2]
Y. Wang[3]
T. Li[4]
T. Wang[5]
Z. Ren[6]

[1]Yellow River Institute of Hydraulic Research, YRCC, Jinshui district of Zhengzhou city, Henan province, 450001, China, email: xin_wd@163.com, ORCID 0000-0002-1825-9673

[2]School of Water Resources and Hydropower Engineering, Wuhan University, Luo Jia Shan, Wuchang district, Wuhan city, Hubei province, 430072, China, email: tshu@whu.edu.cn

[3]Yellow River Institute of Hydraulic Research, YRCC, Jinshui district of Zhengzhou city, Henan province, 450001, China, email: wangyuanjian@hky.yrcc.gov.cn

[4]Yellow River Institute of Hydraulic Research, YRCC, Jinshui district of Zhengzhou city, Henan province, 450001, China, email: litao@hky.yrcc.gov.cn

[5]Yellow River Institute of Hydraulic Research, YRCC, Jinshui district of Zhengzhou city, Henan province, 450001, China, email: wangting@hky.yrcc.gov.cn

[6]Yellow River Institute of Hydraulic Research, YRCC, Jinshui district of Zhengzhou city, Henan province, 450001, China, email: renzhihui@hky.yrcc.gov.cn

*Corresponding author: Xinjie Li, xin_wd@163.com

Abstract

In order to study the spatial changes in the Yellow River basin, a new nonparametric method called the 0-1 test algorithm is introduced to detect the change rule between runoff and basin area. The test approach has the virtue of applying directly to the time series without phase-space reconstruction. This thesis takes the logistic map as an example, the numerical results demonstrate the advantages of the method. Then, the runoff time series (2002-2009) collected by the six hydrologic stations (Tangnaihai, Lanzhou, Toudaoguai, Longkou, Sanmenxia and Huayuankou) of Yellow River, are selected to analyze the laws of evolution in different spatial scales. The asymptotic growth rates of Kc are 0.8751, 0.8985, 0.9783, 0.9793, 0.9848 and 0.9976, respectively. Multiple spatial scales runoff data of Yellow River Basin shows chaotic characteristic. The minimum value of Kc is in the upper reaches of the Yellow River (Tangnaihai). The maximum value of Kc is in the lower reaches of the Yellow River (Huayuankou). The spatial runoff process changes greatly in temporal and spatial scales. And the drainage area is an important factor in causing chaos variation. The conclusion illustrates the feasibility of this method and provides scientific data for runoff prediction.

Keywords: 0-1 test, chaos, runoff, the asymptotic growth rate, spatial scales.

Received: 18/12/2018

Accepted: 03/04/2019

Introduction

Runoff process is the product of the interaction of factors such as the climate of the water basin, complex underlying surface conditions, natural environment and geographic condition (Cao et al. 2011; Sivapalan M et al. 2015). It is a special hydrographic phenomenon; it has such characteristics as multi-dimensional, multiple and hierarchy variability. The development of nonlinear characteristics and its multi-scale study method will become the key point in the current study (Deman G et al. 2016; Shao Q et al. 2017). During the past two decades or so, studies on the application of the concepts of nonlinear dynamics and chaos to hydrologic systems and processes have been on the rise (Sivakumar 2000, 2004, 2009; Hu Z et al. 2013). A variety

of techniques developed in the context of nonlinear and chaotic dynamics have been employed to hydrological processes to identify their dynamics (Sivakumar 2001; Dhanya et al. 2010; Li et al. 2014; Yan B et al. 2015).

Runoff is a key factor in the hydrographic phenomenon. The traditional methods for identifying chaos of runoff time series are correlation dimension, Lyapunov exponent, false nearest neighbor and Kolmogorov entropy, etc. (Shevchenko I I. 2016; Faggini M. 2014; Kamizawa T T. 2014; Faure P and A Lesne. 2015). All of these methods demand the reconstruction of phase space, by determining an optimum embedding dimension and delay time. However, reconstruction of chaotic phase space is a long existing problem as argued in some papers (Casdagli et al. 1991; Aguirre et al. 2014). For example, there are two opposite opinions regarding the relationship between the two parameters involved in the processes of reconstructed embedding phase space. One is that delay time is correlative with the embedding dimension (Kim et al. 1999); the other is that they are irrelevant to each other (Grassberger and Procaccia 1983a). These problems, in turn, result to some extent of uncertainty and subjectivity in determining the value of the two parameters. In addition, the lack of objective indicators which are required to measure the effect of phase space reconstruction may increase the uncertainty and subjectivity.

Recently, a straightforward and effective method called 0-1 test was proposed (Gottwald et al. 2009). The input is the time series of a relevant variable and the output is zero or one (Sun et al. 2010). The test capable of may provide a clear-cut response on the chaotic behaviour of time series are effectively applied to both on basic theoretical data from various dynamical systems and on observational data bypassing the need for phase-space reconstruction (Falconer 2007; Gottwald et al. 2004, 2005; Litak et al.2009; Xin 2015), such as hydrological data, rainfall, groundwater levels data and so on (Xiong et al. 2016; Li et al. 2012, 2014). In order to demonstrate the reliability and universality of the test, the chaotic character is proved by using a chaotic time series created by logistic map as an example, the monthly runoff time series with more than 8 years from eight hydrologic stations (Tangnaihai, Lanzhou, Toudaoguai, Longkou, Sanmenxia and Huayuankou) in Yellow River, China, are then selected to study the capability of the 0-1 algorithm to analyze the laws of evolution in different spatial scales. The space distribution characteristics of runoff from the Yellow River Basin are analyzed.

0-1 Test of Chaos

Tecnología y ciencias del agua, 10 (4), 182-194. DOI: 10.24850/j-tyca-2019-04-09

Based on the one-dimensional observational data set φ(n) at time n=1,2,…, N. A random number c is generated in the 0-2π range, we use the data φ(n) to drive the 2-dimensional system, one defines the translation variables $p_c(n)$ and $q_c(n)$ (Grassberger, P., Procaccia, I. (1983a,1983b; Gottwald, Georg A., Melbourne, I. 2002, 2004, 2005):

$$p_c(n) = \sum_{j-1}^{n} \varphi(j) \cos\big(\theta(j)\big), n = 1, 2, \mathrm{L},\ N \quad (1)$$

$$q_c(n) = \sum_{j-1}^{n} \varphi(j) \sin\big(\theta(j)\big), n = 1, 2, \mathrm{L},\ N \quad (2)$$

Where

$$\theta(j) = jc + \sum_{i-1}^{j} \varphi(i), j = 1, 2, L,\ N \quad (3)$$

The improved mean-square displacement of the translation variables $p_c(n)$ and $q_c(n)$ is defined as(Gottwald, Georg A., Melbourne, I. 2009; Litak, G., Syta, A., & Wiercigroch, M. 2009):

$$M\ (n) = M_c(n) - \big(E(\varphi)\big)^2 \left(\frac{1-\cos nc}{1-\cos c}\right) \quad (4)$$

Where

$$M_c\ (n) = \lim_{N\to\infty} \frac{1}{N} \sum_{j-1}^{N} \left[(P_c(j+n) - p_c(j))^2 - (q_c(j+n) - q_c(j))^2\right] \quad (5)$$

$$E(\varphi) = \lim_{N\to\infty} \frac{1}{N} \sum_{j-1}^{N} \varphi(j) \quad (6)$$

If the behavior of p versus q is Brownian, the results strongly show that the data set φ(n) have chaos property, then $M(n)$ increases with the increase of linear growth. If the trajectory of p versus q is limited the underlying characteristic of data set φ(n) is non-chaotic. Then the trajectory of M(n) is a limited(Sun K., Liu X., Zhu C. 2010; Xin, B. 2015; Xiong, X. Y., Li. W., and Lai. J. J. 2016):

The asymptotic growth rate K_c is given by the definition:

$$K_c = \lim_{n\to\infty} \log D_c(n) / \log n \quad (7)$$

The test function K_c close to 0 means stable periodic orbits and K_c close to 1 implies a complicated non-linear system (Gottwald and Melbourne. 2005). According to these test results, a simple and rapid

detection criterion is put forward to chaos identification.

An Example: The Logistic Map

To demonstrate the validity of the algorithm, the Logistic map is chosen as an example, which has been widely studied in nonlinear dynamics. The dynamics may be chaotic or non-chaotic, which is depends on the value of parameter *u*. The plots of the bifurcation diagram and the largest Lyapunov exponents versus *u* are shown in Figure 1 (Li et al. 2012).

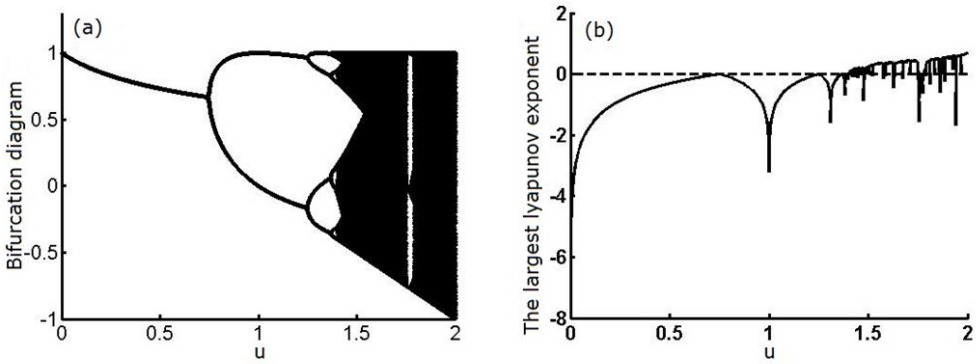

Figure 1. Logistic map $x_{n+1}=1-ux_n^2$. (a) Bifurcation diagram; (b) Lyapunov exponent

For the value of $u\in(0, 0.729)$, logistic map converges to an equivalence-point as *u* is increased beyond 0.729 the trajectory vacillate between 2 points, then 4 points, 8 points and so on, there exists period doubling bifurcation. When the parameter *u* greater than $u_{chaos}=1.399$, simulations show that the increase of the parameter *u* result in the appearance of chaotic gaits. The quasiperiodic interval $1.75<u<1.781$ is clearly visible. When $u=1.2$ the system is in the periodic state, then $u=1.6$, the system presents a chaotic state. Using the 0-1 test methods, the plot of *p* versus *q*, the mean square displacement $M(n)$ and the asymptotic growth rate K_c are shown in Figure 2 (Li, X. J., Hu, T. S. et al. 2012):

Tecnología y ciencias del agua, 10 (4), 182-194. DOI: 10.24850/j-tyca-2019-04-09

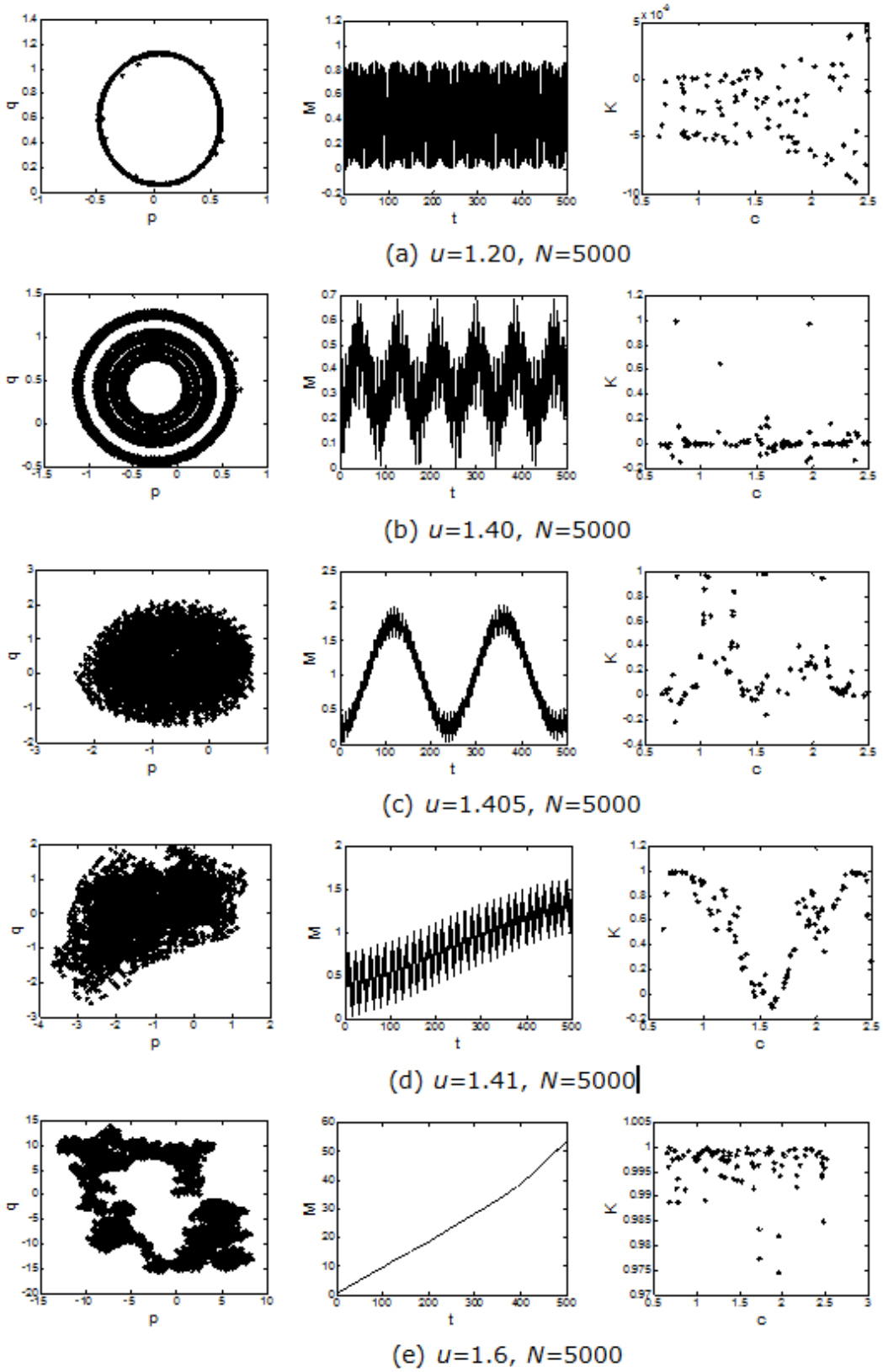

Figure 2. The test patterns of Logistic time series.

Tecnología y ciencias del agua, 10 (4), 182-194. DOI: 10.24850/j-tyca-2019-04-09

Using the data set φ(n) consists of N=5000, phase plots are experimentally obtained for different values of the parameter of u. For the parameters (u=1.2), trajectories in p versus q stay bounded (Figure. 2(a)), $M(n)$ is a limited and asymptotic growth rate (K_c =-0.003) implies that the underlying characteristic of Logistic time series (u=1.2) is cyclical.

For the parameters (u=1.40), trajectories in p versus q coordinates show bounded (Figure. 2(b)), $M(n)$ grows over time, the asymptotic growth rate is K_c =0, the underlying characteristic of Logistic time series (u=1.6) is 4-cyclical.

Table 1. The asymptotic growth rate of Logistic time series.

u	1.20	1.40	1.405	1.41	1.60
K_c	-0.003	0	0.123	0.669	0.998

For the parameters (u=1.405), trajectories in p versus q coordinates leap from periodic status to chaotic status, $M(n)$ increases with time, and the asymptotic growth rate K_c is 0.123, the underlying characteristic of Logistic time series (u=1.405) is under weak chaotic condition, as shown in Figure 2(c).

For the parameters (u=1.41), trajectories in p versus q coordinates leap from periodic status to chaotic status, $M(n)$ increases with time, the asymptotic growth rate K_c is 0.669, the underlying characteristic of Logistic time series (u=1.41) is under chaotic condition, as shown in Figure 2(d).

As shown in Figure 2(e), for the parameters (u=1.6), trajectories in p versus q coordinates show Brownian motion, $M(n)$ increases with time the asymptotic growth rate is K_c =0.998, K_c close to 1 means that the underlying characteristic of Logistic time series (u=1.6) is chaotic.

Compare Figure 1 and Figure 2, when Logistic time series is a periodic sequence, the asymptotic growth rate K_c is trending to zero when the time series is chaos time alignment, the asymptotic growth rate K_c is trending to one, the results of 0-1 test is consistent with the result of bifurcation graph. Figure 2 reveals that 0-1 test is an effective method to distinguish chaotic phenomenon in a specific range.

Case Studies

Tecnología y ciencias del agua, 10 (4), 182-194. DOI: 10.24850/j-tyca-2019-04-09

Data Used. Monthly runoff data of the Yellow River in China are analyzed in this study. A total of 8 years (January, 2002-December, 2009) of historic Monthly inflow data is used in the analysis, which is obtained by the Tangnaihai, Lanzhou, Toudaoguai, Longkou, Sanmenxia and Huayuankou, as shown in Figure 3. Tangnaihai hydrological station controls a drainage area of 121972 km^2. Lanzhou hydrological station is situated in the lower reaches of Tangnaihai, The valley area is 222551 km^2, the runoff is mainly supplied by mountains snowmelt and precipitations, there are no the effects of human activities, therefore, the runoff process at Tangnaihai and Lanzhou is in a basically natural status.

Toudaoguai, Longkou, Sanmenxia and Huayuankou are sited at the middle or lower reaches of the Yellow River. There are many water projects, reservoir hydro-constructions in the river. Hydrologic characteristics are often influenced severely by human activities.

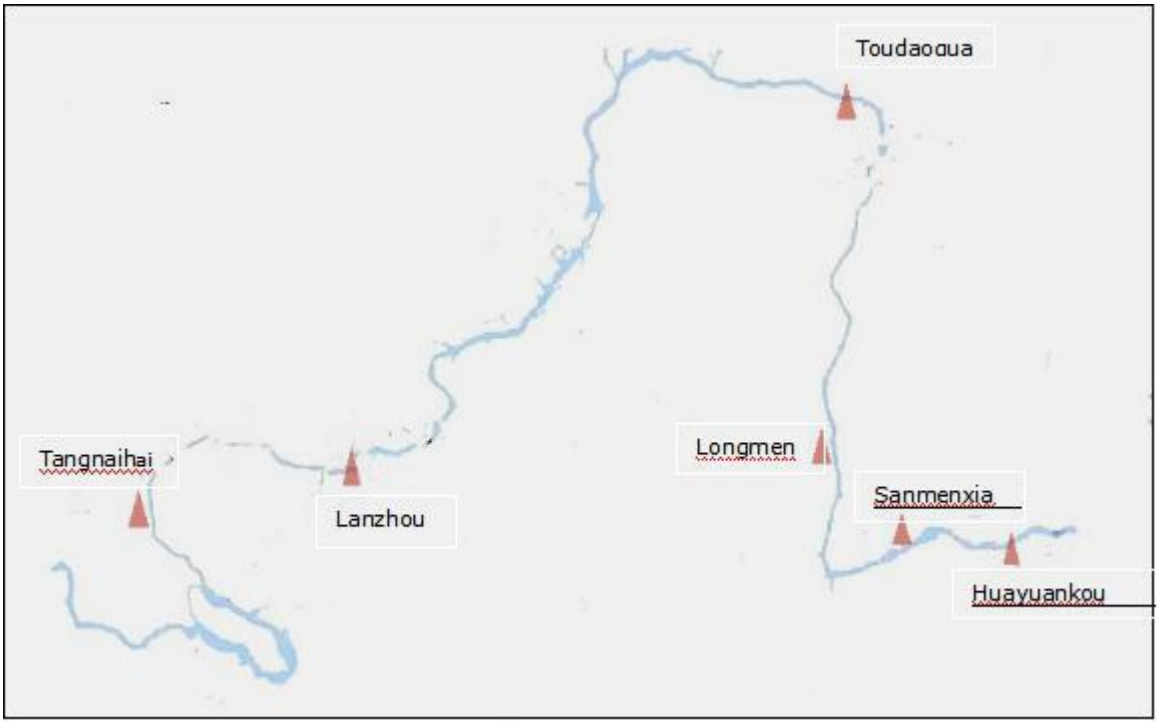

Figure 3. The hydrological station of Yellow River.

The statistical parameters of monthly runoff time series are shown in Table 2. The variation and skewness coefficients of runoff time series are high and these imply that the discharge data distribution is far from the normal distribution.

Table 2. The statistical tables.

Runoff series	Drainage area (km^2)	Runoff series					
		Min (billion m^3)	Max (billion m^3)	Mean (billion m^3)	Standard-D	Skewness	Kurtosis
Tangnaihai	121972	2.33	52.23	15.12	11.95	1.12	0.46
Lanzhou	222551	7.66	40.44	22.71	8.25	-0.012	-1.16
Toudaoguai	367898	2.00	29.03	12.64	6.19	0.79	-0.23
Longmen	497552	4.98	29.03	14.67	5.99	0.71	-0.30
Sanmenxia	688421	5.06	58.32	17.22	9.66	1.91	4.77
Huayuankou	730036	3.70	67.91	19.64	11.49	1.49	2.94

Chaotic Detection Results. The method is applied to the monthly runoff series of Yellow rivers. The plots of asymptotic growth rate Kc are shown in Figure 4. The minimum value of K_c is 0.8751 in the Tangnaihai hydrologic station, the maximum value of K_c is 0.9976 in the Huayuankou hydrologic station. Taking the data of Tangnaihai and Huayuankou hydrologic station as an example, trajectories in p versus q coordinates, the mean-square displacement $M(n)$ and the asymptotic growth rate K_c are shown in Figure 5 and Figure 6.

It is shown that the behavior of p versus q is asymptotically Brownian, the mean-square displacement $M(n)$ grows linearly in time, and the asymptotic growth rate K_c is near to 1 for monthly runoff time series of Tangnaihai and Huayuankou hydrologic station in Yellow River which clearly indicates the presence of chaotic behavior in the runoff time series. Results from Figure 7 suggest that Drainage area is an important factor in causing chaos variation.

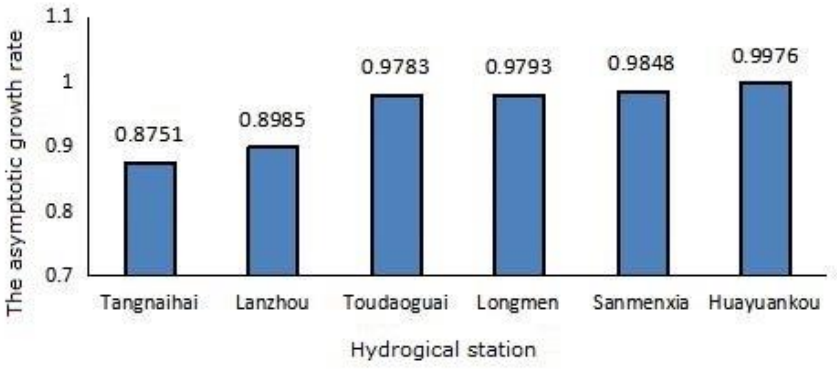

Figure 4. The hydrological station of Yellow River.

Tecnología y ciencias del agua, 10 (4), 182-194. DOI: 10.24850/j-tyca-2019-04-09

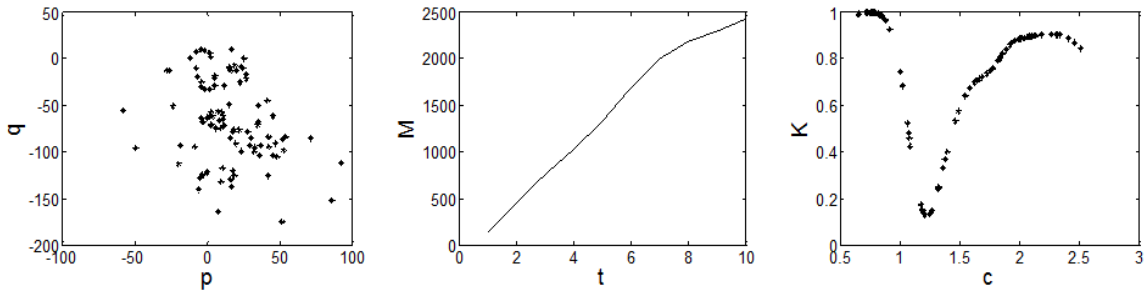

Figure 5. Monthly runoff time series of Tangnaihai hydrologic station.

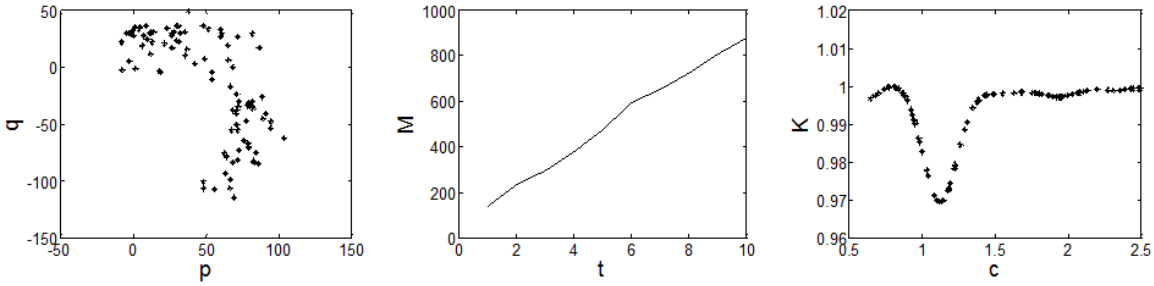

Figure 6. Monthly runoff time series of Huayuankou hydrologic station.

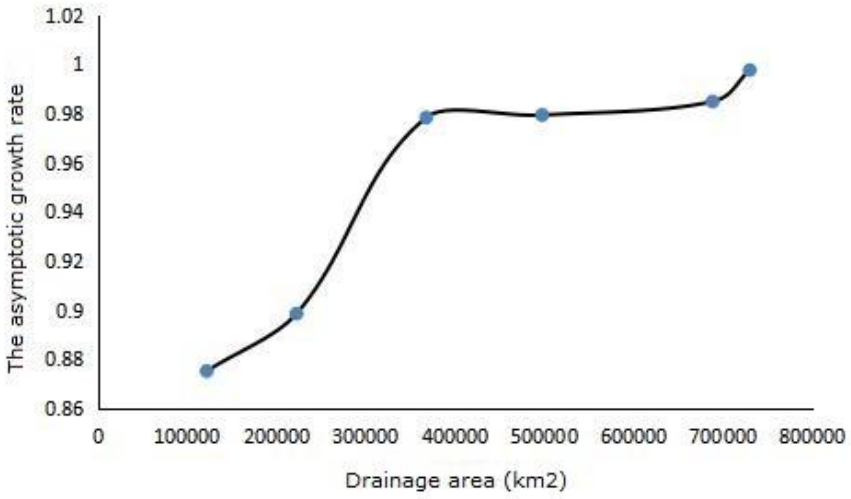

Figure 7. Relationship between Drainage area and the asymptotic growth rate.

Conclusions

Tecnología y ciencias del agua, 10 (4), 182-194. DOI: 10.24850/j-tyca-2019-04-09

(1) This paper attempts to have a thorough study of the spatial changes in the Yellow River basin from a new perspective. The dynamical behavior of runoff is identified by 0-1 test method. The research offered a new way for the varying regular research and modeling of time-space of runoff dynamical systems.

(2) Based on the testing result, the asymptotic growth rate K_c are 0.8751, 0.8985, 0.9783, 0.9793, 0.9848 and 0.9976 respectively, multiple spatial scales runoff data of Yellow River Basin shows chaotic characteristic. The runoff data in the lower Yellow River has strong characteristics of chaos, and the middle reaches of the yellow river secondly, then to the upper Yellow River. From the spatial scale, the paper analysis variation rules of runoff with drainage area. Results from the runoff data of different hydrologic station show that the chaos characteristic of runoff depends on the meteorology, terrain factors and so on, drainage area is an important factor in causing chaos variation.

Acknowledgments

This research obtained the financial support from two grants in China: (1) The National Natural Science Foundation of China (No. 51879115, 51509100, 51509102, 51679103); (2) The national Public projects Research Funding of in research institutions (No. HKY-JBYW-2016-26, HKY-JBYW-2016-10, HKY-JBYW-2017-19). The authors would like to thank the anonymous reviewers for their constructive comments.

References

Aguirre, L. A., Letellier, C. & Macau, E. E. N. (2014). Modeling nonlinear dynamics and chaos: a review. *Mathematical Problems in Engineering*, 2009(1024-123X), 266-287.

Aydin, A. C. & Cahit E. (2008). Effects of trend and periodicity on the correlation dimension and the lyapunov exponents. *International Journal of Bifurcation & Chaos, 18*(12), 3679-3687.

Broock, W. A., Scheinkman, J. A., Dechert, W. D. & LeBaron, B. (1996). A test for independence based on the correlation dimension. *Econom et. Rev.*, 15(3), 197-235.

Cao, L. J. Zhang. Y. & Zhi, Y. (2011). Climate change effect on hydrological processes over the Yangtze River basin. *Quaternary International*,211, 202-210.

Casdagli, M. S., Eubank, J., Farmer, D. & Gibson, J. (1991). State

space reconstruction in the presence of noise. Phys. D., 51, 52-98.

Deman, G., Konakli, K., Sudret, B., Kerrou, J., Perrochet, P. & Benabderrahmane, H. (2016). Using sparse polynomial chaos expansions for the global sensitivity analysis of groundwater lifetime expectancy in a multi-layered hydrogeological model. *Reliability Engineering & System Safety*, 147, 156-169.

Dhanya, C. T. & Nagesh, K. D. (2010). Nonlinear ensemble prediction of chaotic daily rainfall. *Adv. Water. Resour.*, *33*(3), 327-347.

Faggini, M. (2014). Chaotic time series analysis in economics: Balance and perspectives. *Chaos,* 24.4:042101.

Falconer, I., Gottwald, G. A., Melbourne, I. & Wormnes, K. (2007). Application of the 0-1 Test for Chaos to experimental data. *SIAM J. Appl. Dyn*., 6, 395-402.

Faure, P. & Lesne, A. (2015). Estimating Kolmogorov Entropy from Recurrence Plots. *Understanding Complex Systems* 45-63.

Gottwald, G. A. & Melbourne, I. (2002). A New Test for Chaos. *Physics*460.2042:603-611.

Gottwald, G. A. & Melbourne, I. (2004). A new test for chaos in deterministic systems. *Proc. Roy. Soc. A*., 460, 603–611.

Gottwald, G. A. & Melbourne, I. (2005). Testing for chaos in deterministic systems with noise. *Phys. D.*, 212, 100–110.

Gottwald, G. A. & Melbourne, I. (2009). On the Implementation of the 0-1 Test for Chaos. *SIAM J. Appl. Dyn*., 8, 129-145.

Grassberger, P. & Procaccia, I. (1983a). Measuring the strangeness of strange attractors. *Phys. D.*, 9, 189-208.

Grassberger, P. & Procaccia, I. (1983b). Estimation of the Kolmogorov entropy from a chaotic signal. *Phys. Rev. A., 28*(4), 2591-2593.

Hu, Z., Zhang, C., Luo, G., Teng, Z. & Jia, C. (2013). Characterizing cross-scale chaotic behaviors of the runoff time series in an inland river of central Asia. *Quaternary International*, 311(9), 132-139.

Kamizawa, T., Hara, T. & Ohya, M. (2014). On relations among the entropic chaos degree, the Kolmogorov-Sinai entropy and the Lyapunov exponent. *Journal of Mathematical Physics* 55.3:861-864.

Kennel, M. B., Brown, R. & Abarbanel, H. D. (1992). Determining embedding dimension for phase-space reconstruction using a geometrical construction. *Phys. rev. A.*, *45*(6), 3403.

Kim, H. S., Eykholt, R. & Sala, J. D. (1999). Nonlinear dynamics, delay times and embedding windows. *Phys. D.*, 127, 48-60.

Li, X., Gao, G., Hu, T., Ma, H. & Li, T. (2014). Multiple time scales analysis of runoff series based on the chaos theory. *Desalination &*

Water Treatment, 52(13-15), 2741-2749.

Li, X. J., Hu, T. S., Guo, X. N., Zeng, X. & Zhang, T. (2012). Application of the 0-1 test algorithm for chaos to runoff time series. *Advances in Water Science*, 23(6), 861-868.

Litak, G., Syta, A. & Wiercigroch, M. (2009). Identification of chaos in a cutting process by the 0–1 test. *Chaos Solitons & Fractals*, 40(5), 2095-2101.

Rosenstein, M. T., Collins, J. J. & Deluca, C. J. (1993). A practical method for the calculating largest Lyapunov exponents from small datasets. *Phys. D.,* 65, 117-134.

Shao, Q., Younes, A., Fahs, M., et al (2017). Bayesian sparse polynomial chaos expansion for global sensitivity analysis. *Computer Methods in Applied Mechanics & Engineering*, 318, 474-496.

Shevchenko, I. I. (2016). On the recurrence and Lyapunov time scales of the motion near the chaos border. *Physics Letters A,* 241:1-253-60.

Sivapalan, M. & Blöschl, G. (2015). Time scale interactions and the coevolution of humans and water. *Water Resources Research*, 51(9), 6988-7022.

Sivakumar, B. (2000). Chaos theory in hydrology: important issues and interpretations. *Journal of Hydrology*, 227(1), 1-20.

Sivakumar, B., Berndtsson, R. & Persson, M. (2001). Monthly runoff prediction using phase space reconstruction. *Hydrol. Sci J.*,46(3), 377-387.

Sivakumar, B. (2004). Chaos theory in geophysics: past, present and future. *Chaos Solitons & Fractals*, 19(2), 441-462.

Sivakumar, B. (2009). Nonlinear dynamics and chaos in hydrologic systems: latest developments and a look forward. *Stochastic Environmental Research and Risk Assessment*, 23(7), 1027-1036.

Sun, K., Liu, X. & Zhu, C. (2010). The 0-1 test algorithm for chaos and its applications. *Chin Phys. B*, 19(11):200-206.

Xin, B. (2015). Neimark–Sacker Bifurcation Analysis and 0–1 Chaos Test of an Interactions Model between Industrial Production and Environmental Quality in a Closed Area. *Sustainability* 7.8, 10191-10209.

Xiong, X. Y., Li. W. & Lai. J. J. (2016). Influence of amplitude on chaos sequence in the 0-1 test algorithm. *Journal of Hunan University of Arts & Science.,* 28(4):35-39.

Yan, B. Zh., Xiao, C. L., Qiao, Y., Liang, X. J. & Wei, R. C. (2015). Multiple timescale chaos identification of groundwater depth and subdivision of Jilin city based on 0-1 test [J].*Transactions of the Chinese Society for Agricultural Machinery*, 46(1):138-147.

DOI: 10.24850/j-tyca-2019-04-10

Special Article

Treatment of Nitrogen Heterocyclic Compounds (NHCs) in Coking Wastewater by White-Rot Fungi

Tratamiento de compuestos heterocíclicos de nitrógeno (NHC) en aguas residuales de coque por hongos de pudrición blanca

C. Huang[1]

D. Ren[2]*

C. Kang[3]

Z. Deng[4]

H. Guo[5]

S. Zhang[6]

X. Zhang[7]

[1]College of Resource and Environmental Engineering, Wuhan University of Science and Technology, Wuhan, China

Hubei Key Laboratory for Efficient Utilization and Agglomeration of metallurgic Mineral Resources, Wuhan University of Science and Technology, Wuhan, China, email: 740491866@qq.com, ORCID 0000-0003-1077-9444

[2]College of Resource and Environmental Engineering, Wuhan University of Science and Technology, Wuhan, China

Hubei Key Laboratory for Efficient Utilization and Agglomeration of metallurgic Mineral Resources, Wuhan University of Science and Technology, Wuhan, China, email: dj_ren@163.com, ORCID 0000-0003-0752-4184

[3]College of Resource and Environmental Engineering, Wuhan University of Science and Technology, Wuhan, China

Hubei Key Laboratory for Efficient Utilization and Agglomeration of metallurgic Mineral Resources, Wuhan University of Science and Technology, Wuhan, China, email: 914010147@qq.com, ORCID 0000-0002-0972-3286

[4]College of Resource and Environmental Engineering, Wuhan University of Science and Technology, Wuhan, China

Hubei Key Laboratory for Efficient Utilization and Agglomeration of metallurgic Mineral Resources, Wuhan University of Science and Technology, Wuhan, China, email: 1163909723@qq.com, ORCID 0000-0002-5459-1374

[5]College of Resource and Environmental Engineering, Wuhan University of Science and Technology, Wuhan, China

Hubei Key Laboratory for Efficient Utilization and Agglomeration of metallurgic Mineral Resources, Wuhan University of Science and Technology, Wuhan, China, email: 545645621@qq.com, ORCID 0000-0001-7481-8380

[6]College of Resource and Environmental Engineering, Wuhan University of Science and Technology, Wuhan, China

Hubei Key Laboratory for Efficient Utilization and Agglomeration of metallurgic Mineral Resources, Wuhan University of Science and Technology, Wuhan, China, email: zhangshuqin@wust.edu.com, ORCID 0000-0002-1572-308X

[7]College of Resource and Environmental Engineering, Wuhan University of Science and Technology, Wuhan, China

Hubei Key Laboratory for Efficient Utilization and Agglomeration of metallurgic Mineral Resources, Wuhan University of Science and Technology, Wuhan, China, email: zhangxiaoqing@wust.edu.com, ORCID 0000-0002-6456-0600

*Corresponding author: Dajun Ren, dj_ren@163.com

Abstract

In the present study the white-rot fungi BP was selected to study the degradation of nitrogen heterocyclic compounds in real and simulated coking wastewater. The study incorporated analysis of the degradation process, mechanism of action of white-rot fungi on nitrogen heterocyclic compounds, changes of enzyme activity and white-rot fungi biomass growth rate in coking wastewater (simulated and actual). The results showed that the addition of ammonia nitrogen and phenol in simulated wastewater had insignificant effects on the degradation of indole. Moreover, the promoting effect of phenol on quinoline degradation was greater than the inhibition effects of ammonia nitrogen. Degradation rates of quinoline, indole and pyridine are consistent with the zero-order kinetics equation. It was also found that the addition of Mg (II) and Mn (II) promotes the degradation of quinoline by white-rot fungi in the actual wastewater, while degradation of pyridine was inhibited by three ions, out of which the inhibition of Cu

(II) was the most obvious. Cu (II) was also found to have positive effects on the levels of activity of laccase enzyme secreted by the white-rot fungi as opposed to other metal ions tested. However, it was found to have inhibitory effects on the development of white-rot fungi, while Mg (II) and Mn (II) were found to promote the development of the white-rot fungi. The activity of the enzyme and the growth rate of the biomass of white-rot fungi first reached the maximum levels followed by a significant decline.

Keywords: White-rot fungi, Coking wastewater, Nitrogen heterocyclic compounds, Co-substrate, Laccase.

Received: 18/12/2018

Accepted: 05/04/2019

Introduction

Coking wastewater is the wastewater produced in the process of recovery of coal coking product. It is usually known to contain nitrogen heterocyclic compounds (NHCs) and polycyclic aromatic hydrocarbons (PAHs) that are difficult to biodegrade. It also contains a variety of other toxic substances that act as inhibitors of microbial activity. Therefore, the traditional biochemical treatment technology is difficult to meet the national emission standards for the removal effect of biological nitrogen is not obvious. NHCs account for 20-30% of the total organic components and are the main component of organic pollutants in coking wastewater (Joshi et al., 2016). The substitution of N and S makes these heterocyclic organic compounds more toxic than the corresponding non-heterocyclic organic compounds (Eisentraeger et al., 2008). It is, therefore, crucial to study the biodegradation of nitrogen heterocyclic compounds in coking wastewater in the coexistence of various other organic and inorganic pollutants.

In coking wastewater, quinoline (Q), indole (I), pyridine (Pd), phenol (P) and ammonia nitrogen (N) constitute a co-substrate system. Addition of a contaminant in the co-substrate system can either promote or inhibit the degradation of another one (Rasool et al., 2015; Martinez et al., 2015; Wen et al., 2011). *Phomopsis liquidambari*, *Brevundimonas sp.* and *Shinella zoogloeoides* have been identified to possess strong specificity for degrading indole, quinoline and pyridine, but not towards coking wastewater with a complex composition (Chen et al., 2013;

Wang et al., 2015; Bai et al., 2009). On the other hand, many studies have shown that white-rot fungi have a non-specific nature towards the degradation of the substrate and direct or indirect degradation ability for most aromatic compounds. Furthermore, white-rot fungi were also found to degrade a large number of single or mixed matrix contaminants (Pointing et al., 2001). The ability of degradation of multiple single substrate pollutants by white-rot fungi had also been demonstrated in some recently conducted studies (Ren et al., 2012; Stella et al., 2016). On the basis of these revelations, the degradation behavior and kinetic characteristics of four co-substrate systems in simulated coking wastewater were studied in this paper. Further study of the feasibility of degradation of nitrogenous heterocyclic compounds by white-rot fungi in the effect of metal ions in actual coking wastewater was also studied.

Materials and Methods

Reagent

Pyridine, quinoline and indole (AR, Sinopharm Group Chemical Reagent Co., Ltd., China); 2,2'-nitro-bis (3-ethylbenzothiazole-6-sulfonic acid) (ABTS) (Sigma-Aldrich); glacial acetic acid: AR; methanol: chromatographic pure; ammonium tartrate; glucose; ammonium sulfate ($(NH_4)_2SO_4$); monopotassium phosphate (KH_2PO_4); magnesium sulfate heptahydrate ($MgSO_4{\cdot}7H_2O$); manganese(II) sulfate monohydrate ($MnSO_4{\cdot}H_2O$); copper(II) sulfate pentahydrate ($CuSO_4{\cdot}5H_2O$) and microporous membrane (0.45μm).

Culture of White-Rot Fungi and Preparation of Medium

White-rot fungal strain (*Pleurotus sp.*) No. BP, selected and preserved by the Environmental Resources Microbiology Research Laboratory of Huazhong University of Science and Technology, China, was expanded

after 4 days as a spare bacterial fluid. The medium used in the experiment was a straw filtrate culture medium, consisting of water (1000 mL), corn stalk powder (30 g), bran (8 g) and cottonseed meal (1.2 g).

Preparation and Testing of Simulated and Actual Wastewater

10 mL bacterial fluid was inoculated into a 250 mL triangle flask containing 100 mL culture medium. A Pd+Q+I co-substrate degradation system was made up by adding certain amounts of pyridine (80 mg/L), quinoline (80 mg/L) and indole (80 mg/L) reserve solutions to the culture flask. The solution thus prepared was then added with phenol (150 mg/L) or ammonia nitrogen (290 mg/L) reserve solutions to simulate the presence of actual coking wastewater. The Erlenmeyer flask, which was inoculated with the bacteria and the substrate, was placed in a shaker (150 r/min) and subjected to a degradation test at 25°C.

The subsequent experimental setups that were carried on actual coking wastewater culture system contained 50mL actual wastewater obtained from Wuhan Iron and Steel Company coking plant (Table 1), and 50 mL of straw filtrate culture medium, which included four degradation systems: no metal system, Mg (II) system, Cu (II) system, Mn (II) system. The concentration of the metal ions in the culture medium was kept 1.0 mM/L and the experimental method followed was similar to that of simulated wastewater based experiment.

Table 1. Water quality of coking raw water in coking company.

Index	COD (mg/L)	Phenols (mg/L)	Ammonia nitrogen (mg/L)	Cyanide (mg/L)	Oils (mg/g)	pH
Concentration	≤3000	≤800	≤500	≤20	≤100	6.5-7.5

Determination

The concentration of quinoline, indole, pyridine and phenol were measured by using Hitachi HPLC (High Performance Liquid Chromatography) (Hitachi pump (L-7100), Hitachi dynamic mixers, UV-vis L-7420 detector and the Hypersil C-18 reverse column (250mm×4.6mmI.D., 5μm)). The standard curve of characteristic absorption peaks of organic compounds was used for conclusion could be got. The conditions for the determination of indole and phenol were as follows: the mobile phase was methanol and water (1% HAc), the volume ratio was 80:20, the flow rate was 0.6 mL/min, the detection wavelength was 270 nm, and the injection volume was 20 μL. The conditions for the determination of quinoline were as follows: the mobile phase was methanol and water (1% HAc), the volume ratio was 50:50, the flow rate was 0.6 mL/min, the detection wavelength was 313 nm, and the injection volume was 20 μL; and the conditions for the determination of pyridine were as follows: the mobile phase was methanol and water (1% HAc), the volume ratio is 70:30, the flow rate was 0.4 mL/min, the detection wavelength was 254 nm, and the injection volume was 20 μL.

The biomass dry weight of white-rot fungi was measured with the help of an electronic balance (FA2004). Ammonia nitrogen was analyzed by WT-1 portable ammonia nitrogen analyzer. The laccase activity levels were estimated using a UV-2550 UV spectrophotometer (SHIMADZU CORPORATION, Japan) by the method of Robert. One enzyme activity unit (U) was defined as the absorbance values of per mL degradable solution per minute increased by 0.001 (Bourbonnais et al., 1992).

Degradation of Simulated Coking Wastewater by White-Rot Fungi

Based on the Pd+Q+I co-substrate degradation system, ammonia nitrogen or phenol was added to the degradation system to form Pd+Q+I, N+Pd+Q+I, P+Pd+Q+I and N+P+Pd+Q+I. This was done to simulate coking wastewater for the purpose of analysis of the degradation behavior of white-rot fungi on various nitrogen heterocyclic compounds, ammonia and phenol.

Removal Effect and Reaction Kinetics

The degradation of quinoline by white-rot fungi in four co-substrate degradation systems is shown in Figure 1. After 15 days, the removal rates of quinoline in the four systems of Pd+Q+I, N+Pd+Q+I, P+Pd+Q+I and N+P+Pd+Q+I were, 66.2%, 62.5%, 70.0% and 68.7%, respectively. It is evident that the degradation rate of quinoline in the four systems was almost consistent.

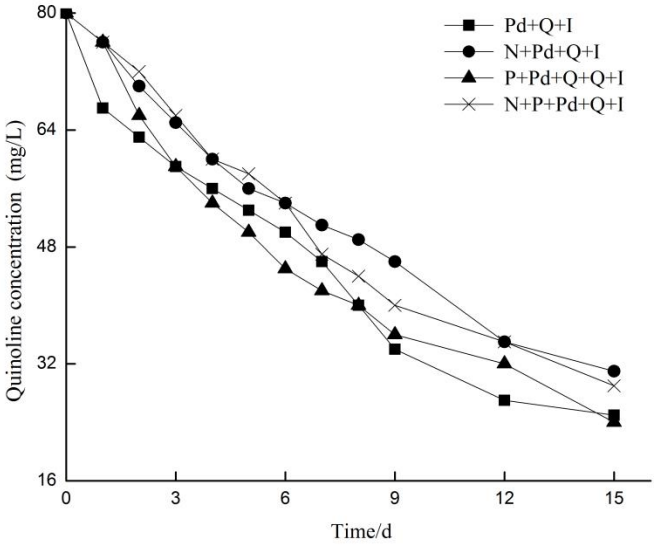

Figure 1. Time dependent changes in quinoline of the four systems.

The degradation data of quinoline in four different co-substrate degradation systems were linearly fitted in the zero-order kinetics equation (Table 2). From Table 2, it can be seen that the quinoline degradation rate constant (k_0) value in the four systems was about 3.5 mg/L·d, but with minor variations. Compared with Pd+Q+I, the value of k_0 of P+Pd+Q+I and N+P+Pd+Q+I was slightly increased, while for N+Pd+Q+I it was slightly decreased.

Table 2. Kinetic equations and parameters of quinoline degradation in different systems.

Co-substrate system	Kinetic equation	k_0 (mg/L·d)	r^2
Pd+Q+I	C=-3.5901t+71.541	3.5901	0.9443

N+Pd+Q+I	C=-3.3243t+75.279	3.3243	0.9687
P+Pd+Q+I	C=-3.7027t+72.633	3.7027	0.9294
N+P+Pd+Q+I	C=-3.6712t+77.110	3.6712	0.9705

The degradation of indole by white-rot fungi in four co-substrate degradation systems is also shown in Figure 2. The fungi could remove more than 99% of indole by the end of 3 days, and it was also found that the process of indole degradation rate was also consistent, with slight modifications.

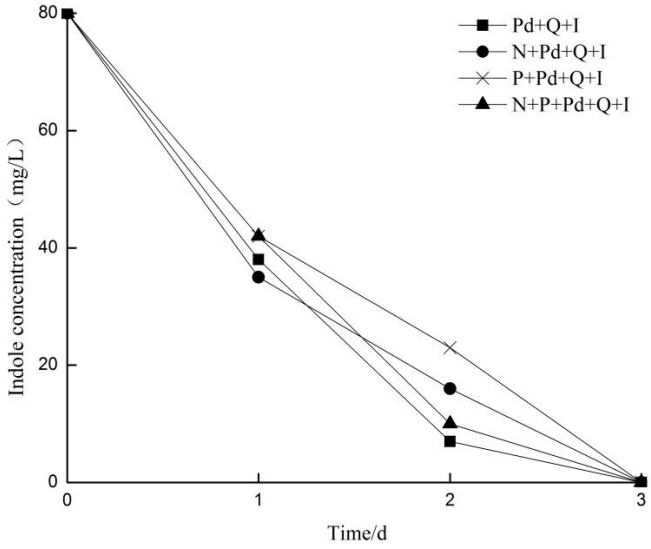

Figure 2. Time dependent changes in indole of the four systems.

The degradation data of indole in four different co-substrate degradation systems was found to fit in the zero-order kinetics equation. Table 3 clearly indicates that the average indole degradation rate constant (k_1) was about 26.5. Compared with Pd+Q+I, the degradation rate constants of the other three co-substrate degradation systems decreased slightly, but not obvious.

Table 3. Kinetic equations and parameters of indole degradation in different systems

Co-substrate system	Kinetic equation	k_1 (mg/L·d)	r^2
Pd+Q+I	C=-27.1t+71.9	27.1	0.9211

N+Pd+Q+I	C=-26.2t+71.8	26.2	0.9360
P+Pd+Q+I	C=-26.0t+75.0	26.0	0.9758
N+P+Pd+Q+I	C=-27.0t+73.5	27.0	0.9477

The degradation of pyridine by white-rot fungi in four co-substrate degradation systems are shown in Figure 3. After 15 days, the removal rates of pyridine in the four systems of Pd+Q+I, N+Pd+Q+I, P+Pd+Q+I and N+P+Pd+Q+I were 20%, 27%, 27.5%, 32.5%, respectively. It was found that the degradation rates of pyridine in the four degradation systems were affected by the co-substrate.

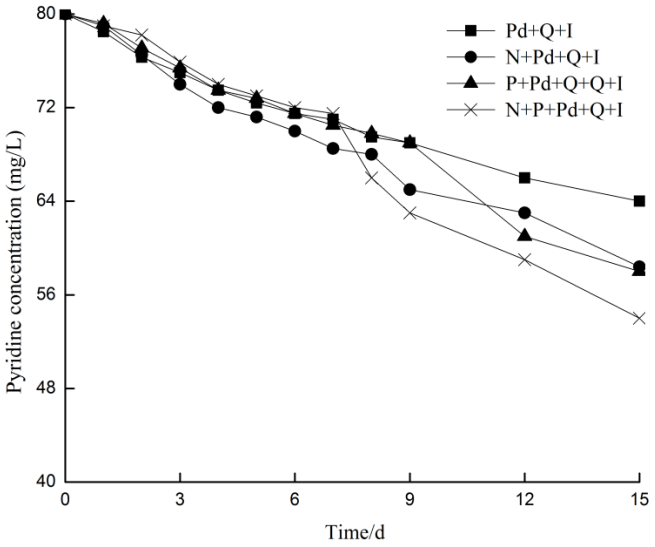

Figure 3. Time dependent changes in pyridine of the four systems.

The degradation data of pyridine in the degradation systems was also found to linearly fit in the zero-order kinetics equation. The data presented in table 4 shows that the pyridine degradation rate constant (k_2) was 1.05 in P+Q+I system. Compared with Pd+Q+I, the degradation rate constants were found to increase in the other three co-substrate degradation systems and the N+P+Pd+Q+I system was the most obvious.

Table 4. Kinetic equations and parameters of pyridine degradation in different systems.

Co-substrate	Kinetic equation	k_2	r^2

system		(mg/L·d)	
Pd+Q+I	C=-1.0500t+78.525	1.0500	0.9611
N+Pd+Q+I	C=-1.4194t+78.983	1.4194	0.9789
P+Pd+Q+I	C=-1.4653t+80.275	1.4653	0.9599
N+P+Pd+Q+I	C=-1.8198t+81.386	1.8198	0.9755

Effect of Co-Substrate on Pd+Q+I System

It could be seen from Figure 4 that the concentration curve of ammonia nitrogen and quinoline were basically the same in the first 3 days of the N+Pd+Q+I system. After 3 days, the indole concentration decreased to zero and the ammonia concentration began to rise. In Figure 5, it is shown that phenol and indole are the carbon sources that can be directly used by the white-rot fungi in the P+Pd+Q+I system. Hence, on the 3rd and 4th day, white-rot fungi removed more than 99% indole and phenol. Figure 6 further illustrates that indole and phenol in the N+P+Pd+Q+I system were completely removed by the fungi on 3rd and 5th day. The concentration of ammonia nitrogen was also found to be the lowest in these two days, 241 mg/L and 246 mg/L, respectively. From these three figures, it is clear that the effect of indole degradation was not obvious when ammonia nitrogen or phenol was used as a co-substrate. In addition, ammonia nitrogen was found to have inhibitory effects on quinoline degradation, but the promoting effects of phenol on quinoline degradation were greater than the inhibition effects of ammonia nitrogen.

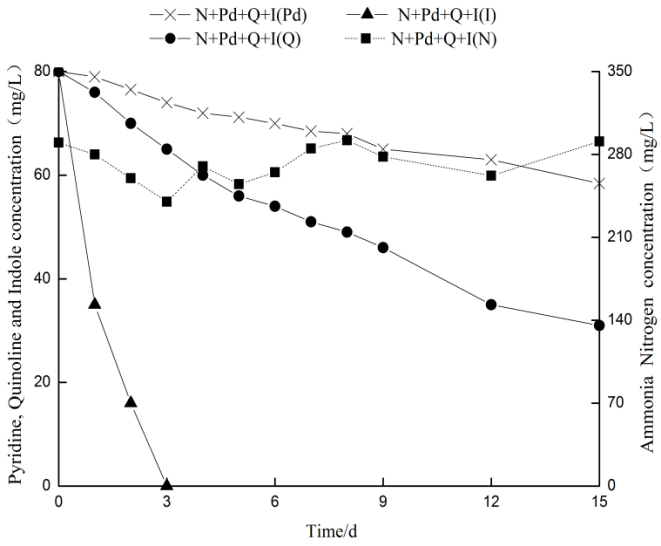

Figure 4. Concentrations of various substances in N+Pd+Q+I system.

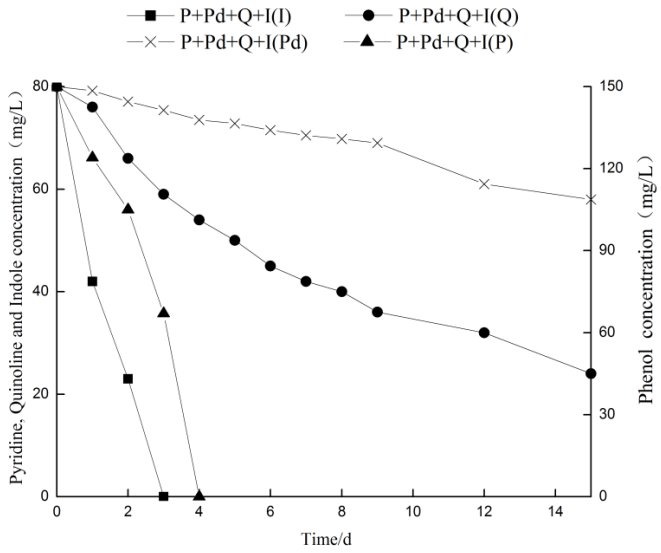

Figure 5. Concentrations of various substances in P+Pd+Q+I system.

Tecnología y ciencias del agua, 10 (4), 195-218. DOI: 10.24850/j-tyca-2019-04-10

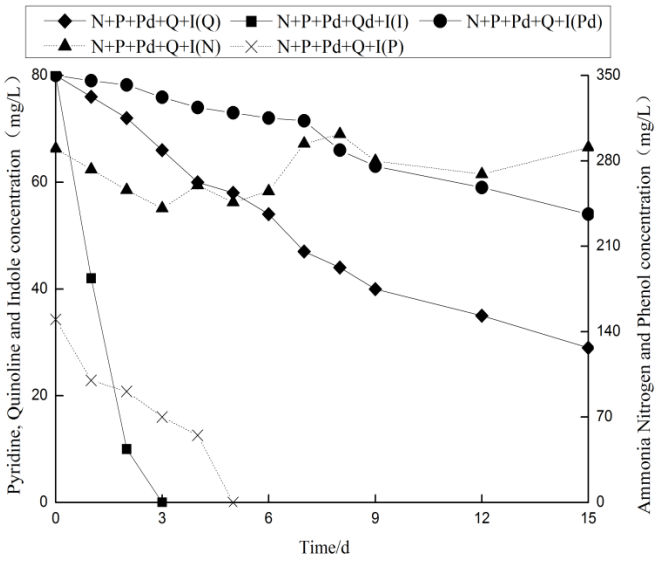

Figure 6. Concentrations of various substances in N+P+Pd+Q+I system.

Changes in Enzyme Activity, White-Rot Fungi Biomass and pH

As illustrated in Figure 7, on the 3rd day, the laccase activities of white-rot fungi in Pd+Q+I, N+Pd+Q+I, P+Pd+Q+I and N+P+Pd+Q+I reached the maximum levels of 366, 485, 401 and 411 U/mL, respectively. Compared with Pd+Q+I, the other three systems had even higher laccase activity peaks.

Tecnología y ciencias del agua, 10 (4), 195-218. DOI: 10.24850/j-tyca-2019-04-10

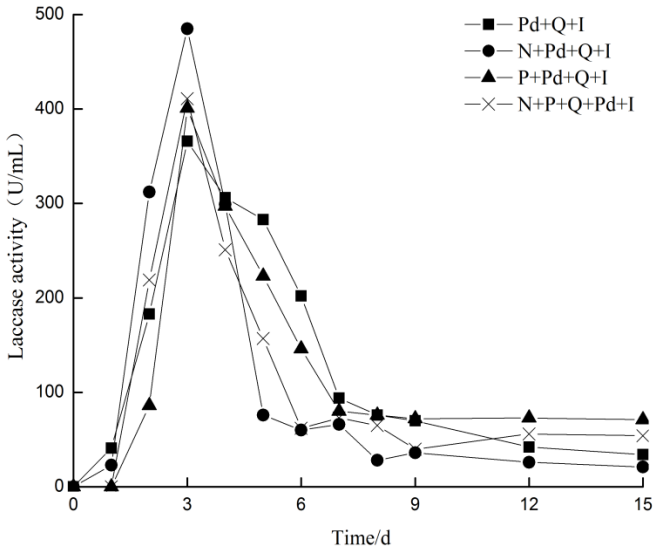

Figure 7. Changes of laccase activities of white-rot fungi.

As illustrated in Figure 8, the growth rates of the fungi in the Pd+Q+I, N+Pd+Q+I, P+Pd+Q+I and N+P+Pd+Q+I conditions reached the maximum values of 0.106, 0.102, 0.100 and 0.085 g/d on the 2nd, 2nd, 3rd and 2nd days, respectively.

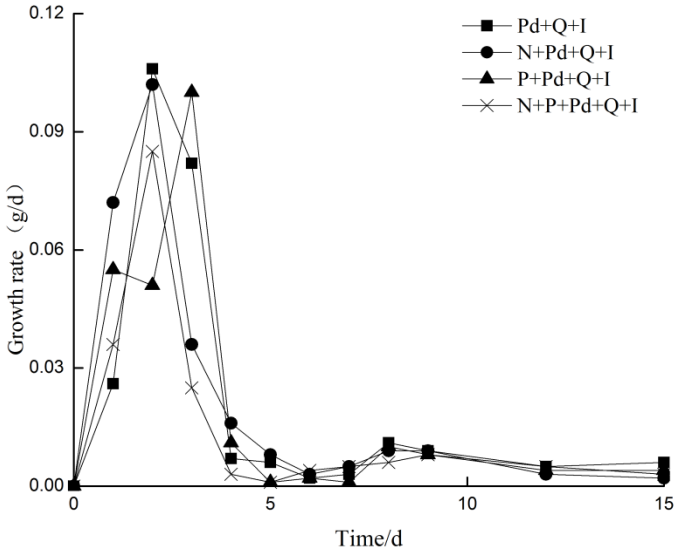

Figure 8. Growth rate of white-rot fungi biomass.

Figure 9 illustrates that the pH of the four systems in the first four days also changed similarly and then again reached the lowest values on the 4-5th day. This drop in pH can be attributed to the degradation of phenol and indole and their intermediates. However, other aromatic acid based compounds present (the degradation products of the cellulosic components of culture media) also play an important role. It was observed that the pH of N+Pd+Q+I and N+P+Pd+Q+I systems after four days was comparatively higher than that of the other two. This may be caused due to the presence of a stable buffer system formed between ammonia nitrogen and aromatic acids after the concentration of ammonia nitrogen was stable, and showed weak alkalinity.

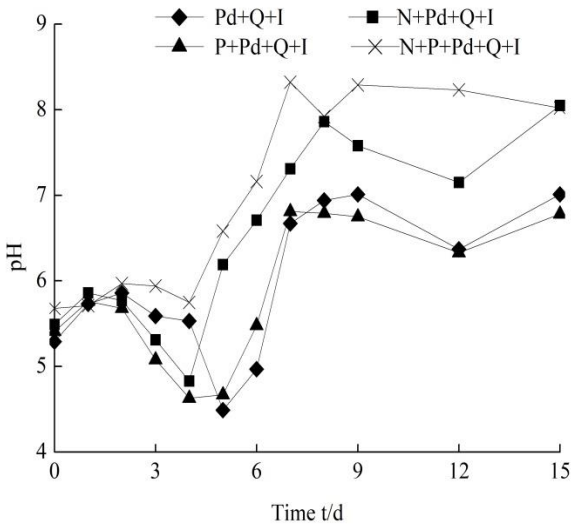

Figure 9. Time dependent changes in the pH of the four systems.

Treatment of Actual Coking Wastewater by White-Rot Fungi

The degradation of actual coking wastewater was mainly dependent upon the role of divalent metal ions in the degradation of nitrogen heterocyclic compounds. In addition, other factors that influenced the process of degradation included the concentration of other major pollutants in coking wastewater and the biological characteristics of white-rot fungi in the four degradation systems (no metal ions (CK) /

Mg (II) / Cu (II) / Mn (II)). The reason behind the selection of Cu (II), Mn (II) and Mg (II) in the present study was the fact that these divalent ions exist in the actual coking wastewater and it was intended to elucidate the effects that their changing concentration may imply on the biological properties of white rot fungi and hence on the rate of degradation of the wastewater. Since COD of the substrate in the culture medium was known to be very high, which in turn had a profound influence on the determination of the COD of the system; it was not considered for analysis in the experiment.

Effect of Divalent Metal Ion on the Removal of Nitrogen Heterocyclic Compounds

According to the Figure 10, white-rot fungi were cultured for 15 days on solid medium, and the removal rates of quinoline in the four degradation systems were 65%, 76%, 65% and 78%, respectively. It was found that the addition of Mg (II) and Mn (II) promoted the degradation of quinoline by white-rot fungi and even improved (slightly) the removal rate of quinoline. On the other hand, Cu (II) was not found to have any significant effects on the degradation of quinoline by white-rot fungi. It could be seen from Figure 11 that the removal rate of indole in the system of Mg (II), Cu (II) and Mn (II) could reach more than 99%, while Figure 12 illustrates that the removal rates of pyridine in the four systems were 38%, 32%, 24% and 31%, respectively. It was also found that the divalent metal ions inhibited the degradation of pyridine, out of which the inhibition effect of Cu (II) was the most obvious.

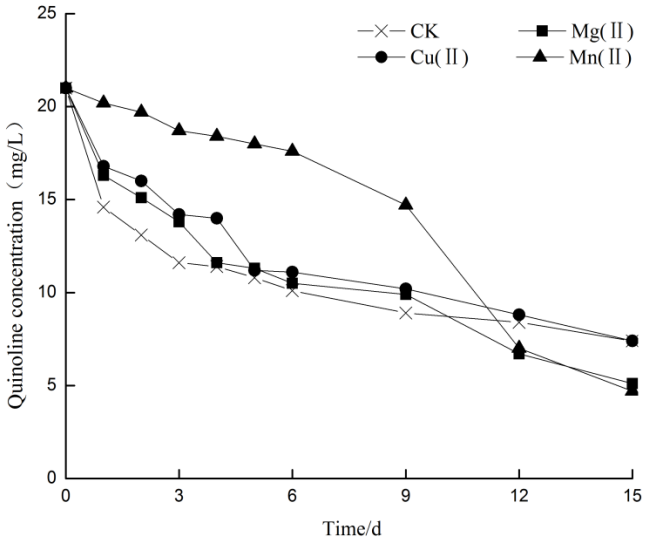

Figure 10. Time dependent changes in quinoline concentration.

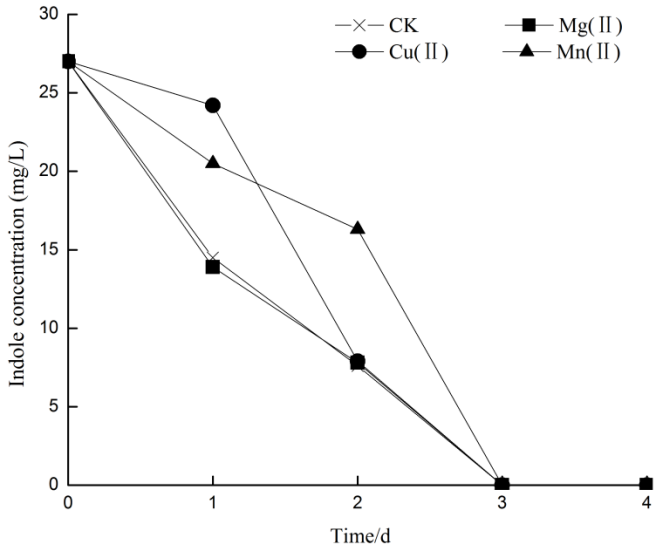

Figure 11. Time dependent changes of indole concentration.

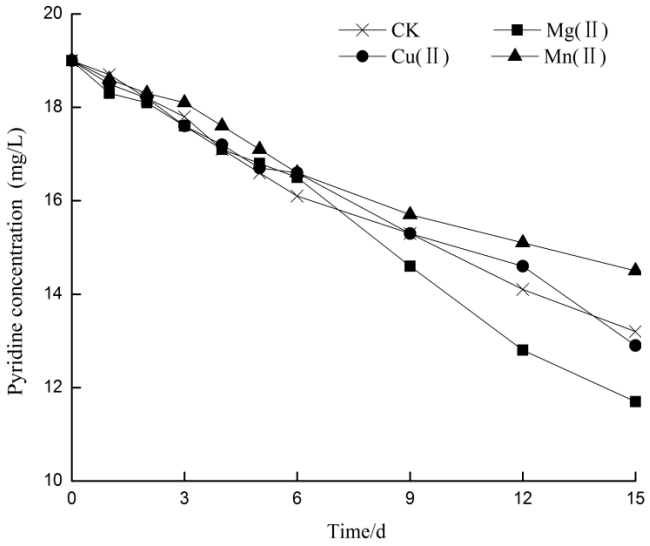

Figure 12. Time dependent changes of pyridine concentration.

It could be seen from Figure 13 and Figure 14 that the change in ammonia nitrogen concentration also followed a similar trend. The fluctuation range during the 0-6th days was very less and further decreased during the 6-12th days. An increase in fluctuation was observed during the 12-15th days. The changes in ammonia nitrogen concentration were also found to be similar to that of the simulated wastewater, both of which go through the process of declining first followed by a systematic rise in the values. Due to the high concentration of indole and phenol in the simulated wastewater, the overall change in ammonia nitrogen concentration was mainly brought about due to degradation of indole and phenol. In the actual coking wastewater, the change of ammonia concentration is mainly related to the removal of phenol (phenol concentration is 323 mg/L, and indole concentration is small in the actual coking wastewater). Figure 13 clearly demonstrates that phenol was removed significantly on the 6th day after which the ammonia concentration began to decrease. White-rot fungi were found to remove more than 99% of the phenol content in four of these systems. However, the initial degradation of phenol was slow, especially due to the inhibition of laccase secretion of white-rot fungi in the early stages, as the fungi were in its domestication stage. After five days, the fungi adapted to the actual coking wastewater environment, which led to an increase in the laccase enzymatic activity levels that further resulted in the rapid degradation of phenol.

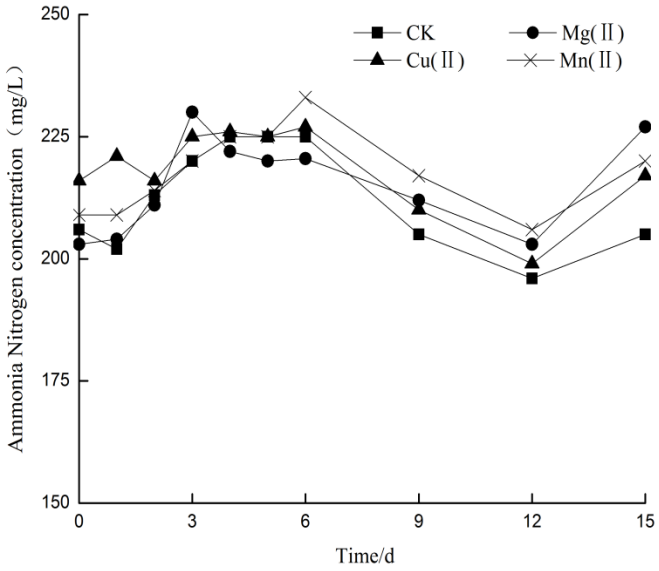

Figure 13. Time dependent changes of ammonia nitrogen concentration.

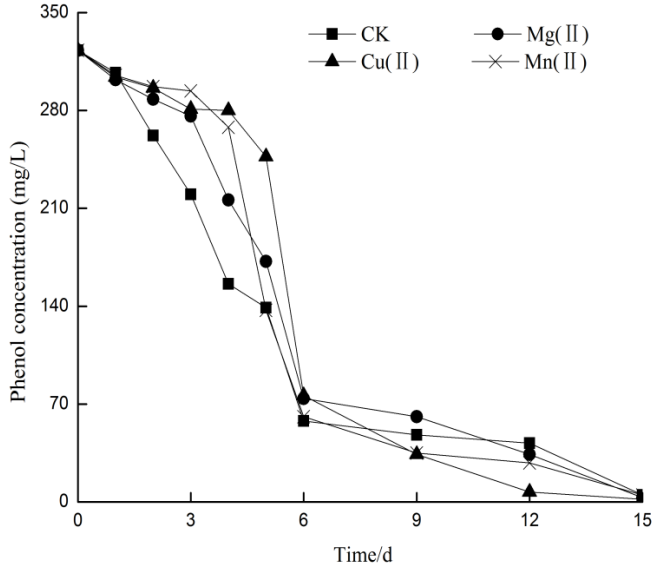

Figure 14. Time dependent changes of phenol concentration.

Change in Biomass and Enzyme Activity Levels of White-Rot Fungi

Tecnología y ciencias del agua, 10 (4), 195-218. DOI: 10.24850/j-tyca-2019-04-10

It can be seen from Figure 15, that on the first five days, the laccase secretion of white-rot fungi was inhibited. The laccase activity levels were maintained at about 10 U/mL, which is due to the simultaneous presence of a variety of other toxic and harmful substances in coking wastewater that may play significant roles in inhibition of enzyme secretion in white rot fungi (Asif et al., 2017). After five days of domestication, the white-rot fungi supposedly adapted to the actual coking wastewater culture environment which subsequently led to an increase in the enzyme activity levels. Results obtained from the present experiment demonstrated that the laccase secretion of white-rot fungi in the CK system was similar to Mg (II) system and Mn (II) system. This indicated that the addition of 1.0 mM/L of Mg (II) and Mn (II) had no significant effects on the laccase secretion activities of the fungi. Furthermore, the enzymatic activity of the white-rot fungi in the Cu (II) system was the same as that of the other three systems, especially in the first five days. On the 6-12th day, the activity of laccase was found to increase slowly and the laccase secretion was still inhibited. On the 12-15th day, the activity of laccase was found to increase rapidly and reached the level of 412 U/mL on the 15th day. It was thus concluded that the presence of 1.0 mM/L Cu (II) could promote laccase secretion.

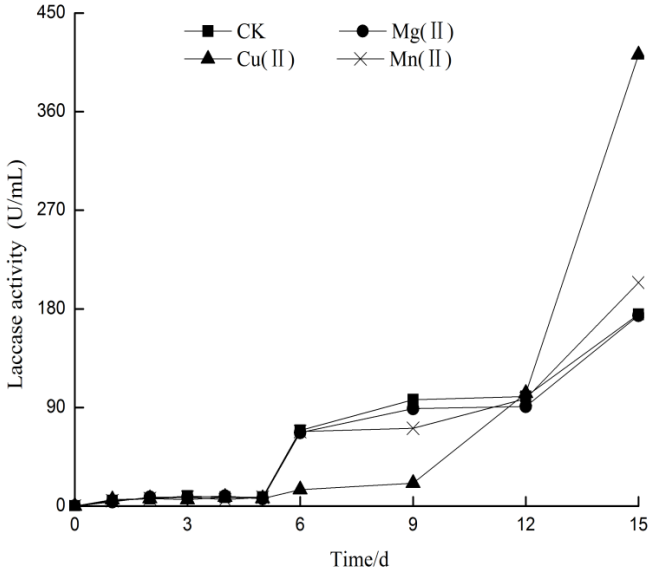

Figure 15. Time dependent changes of laccase activity of white-rot fungi.

As is shown in Figure 16, the growth rate of white-rot fungi biomass in CK, Mg (II), Cu (II) and Mn (II) in the actual coking wastewater reached a maximum of 0.0166, 0.0238, 0.0111 and 0.0373g/d on 2nd, 1st, 1st and 1st day, respectively. It was thus concluded that the presence of 1.0 mM/L Mg (II) and Mn (II) could promote the growth of white-rot fungi, due to which the fungi maintained a high biomass growth rate. In contrast to the influence on the laccase secretion of white-rot fungi, 1.0 mM/L Cu (II) inhibited the development of white-rot fungi strains, and the growth rate of white-rot fungi biomass was low during the whole experiment. The two peaks of biomass growth rate that were observed during the experiment corresponded to the 1st day and the 6th day in the degradation system.

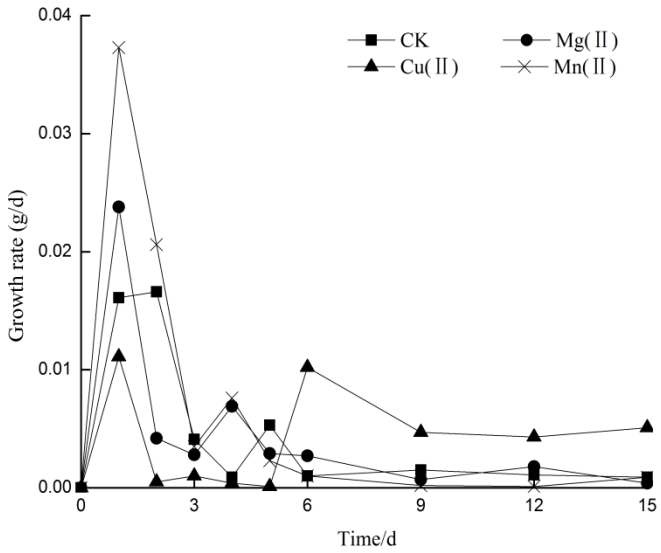

Figure 16. Time dependent changes in the growth rate of white-rot fungi biomass.

As that the straw filter medium was diluted twice caused the reduction of nutrient, while the actual coking wastewater composition is complex and toxic, in the actual coking wastewater culture environment, the growth rate of white-rot fungi biomass was found to be much lower than the simulated wastewater.

Discussion

In the simulated wastewater, the addition of ammonia nitrogen and phenol affected the enzyme secretion and enzyme activity of white-rot fungi, especially in the Pd+Q+I degradation system. The addition of ammonia nitrogen provided a nitrogen-rich culture environment to the white-rot fungi, and the phenol structure (with phenolic hydroxyl) induced the laccase secretion of the white-rot fungi. It was also found that quinoline could be better degraded in neutral or acidic environments while the degradation rate declined rapidly in an alkaline environment (Thomsen et al., 1998). The addition of ammonia nitrogen increased the pH of the system and thus inhibited the degradation rate of quinoline. However, the addition of phenol reduced the pH of the system to promote the degradation of quinoline. It was observed that OH plays a significant role in quinoline degradation due to the fact that phenolic hydroxyl groups on phenol are less stable (Camarero et al., 2010). They can thus attack the aromatic compounds, produce positive carbon ions and then induce a series of reactions that promotes the degradation of quinoline. On the other hand, the alcoholic hydroxyl groups on the ammonia nitrogen (ammonium tartrate) are relatively stable and have little effect on the degradation of quinoline.

In the actual coking wastewater, presence of moderate concentrations of Mg (II) and Mn (II) could promote the growth of white-rot fungi, so that more laccase was secreted and the removal rate of quinoline was slightly improved (Baldrian, 2003). The rate of initiation of the laccase secretion of white-rot fungi in the actual coking wastewater environment was much slower than simulated wastewater. Laccase activity was maintained at a low level on 0-12 days, but this is not due to the fact that some metal ions in the solution causes fungi in oxidative stress (Galhaup et al., 2001). The lower enzyme activity is mainly due to the complex composition of the actual coking wastewater. Such wastewater contains a lot of toxic and harmful substances which inhibit secretion of laccase (Asif et al., 2017). On 12-15th day, the laccase activity in the actual coking wastewater of Cu (II) system was twice as much as the laccase activity in other systems. It has already been established that the activity center of white-rot fungi laccase constitutes of four Cu ions constitute (Strong et al., 2011; Baldrian et al., 2006; Giardina et al., 2010). White-rot fungi allow direct passage of Cu (II) through its cell walls. Hence, the presence of Cu ions, even in concentrations of less than 1 mM/L can also act as an inducer and promote laccase secretion. Meanwhile, the presence of a variety of other aromatic and phenolic compounds induced continued maintenance of an activated state of the white-rot fungi which further promoted its laccase secretion activities (Tychanowicz et al., 2006). Cu

(II) can also directly activate the active site of extracellular laccase enzymes to improve its activity.

Conclusion

In simulated wastewater, ammonia nitrogen had an inhibitory effect on quinoline degradation, while the promoting effects of phenol on the same were even greater than the inhibition effect of ammonia nitrogen. White-rot fungi could remove more than 99% of indole only after three days. On the other hand, ammonia nitrogen and phenol had little effect on the degradation of indole, but they were beneficial for the degradation of pyridine and improving the peak of laccase activity. In actual coking wastewater, Mg (II) and Mn (II) promoted the degradation of quinoline and slightly improved the removal rate of quinoline. However, Cu (II) had no effect on the degradation of quinoline. It was concluded that the divalent metal ions had no significant effects on the degradation of indole, but they had a profound impact on the inhibition of the degradation of pyridine. Among all the metals studies, and the inhibition effect of Cu (II) was the most obvious. It is also important to note that though the addition of 1.0 mM/L Mg (II) and Mn (II) had no significant effects on the secretion of laccase, they could still promote the growth of white-rot fungi so that the fungi maintained high biomass growth rate. Conversely, 1.0 mM/L Cu (II) could promote the secretion of laccase, but inhibited the development of white-rot fungi.

Acknowledgments

This work was supported By the National Natural Science Foundation of China (Grant No 41571306) and State Key Laboratory of Biogeology and Environmental Geology (Grant No GBL21507).

Reference

Joshi, D. R., Zhang, Y., Tian, Z., Gao, Y. & Yang, M. (2015). Performance and microbial community composition in a long-term sequential anaerobic-aerobic bioreactor operation treating coking wastewater. *Applied Microbiology* & *Biotechnology,100* (18), 1-12. doi: 10.1007/s00253-016-7591-8.

Eisentraeger, A., Brinkmann, C., Hollert, H., Sagner, A., Tiehm, A. &

Neuwoehner, J. (2010). Heterocyclic compounds: toxic effects using algae, daphnids, and the salmonella/microsome test taking methodical quantitative aspects into account. *Environmental Toxicology* & *Chemistry, 27*(7), 1590-1596, doi: 10.1897/07-201.1.

Rasool, K., Mahmoud, K. A. & Lee, D. S. (2015). Influence of co-substrate on textile wastewater treatment and microbial community changes in the anaerobic biological sulfate reduction process. *journal of Hazardous Materials, 299*, 453-461, doi: 10.1016/j.jhazmat.2015.07.044.

Martinez, I., Santos, V. E., Alcon, A. & Garcia-Ochoa, F. (2015). Enhancement of the biodesulfurization capacity of Pseudomonas putida CECT5279 by co-substrate addition. *Process Biochemistry, 50*(1), 119-124, doi: 10.1016/j.procbio.2014.11.001.

Wen, J., Gao, D., Zhang, B. & Liang, H. (2011). Co-metabolic degradation of pyrene by indigenous white-rot fungus Pseudotrametes gibbosa from the northeast china. *International Biodeterioration* & *Biodegradation, 65*(4), 600-604, doi: 10.1016/j.ibiod.2011.03.003.

Chen, Y., Xie, X. G., Ren, C. G. & Dai, C. C. (2013). Degradation of n-heterocyclic indole by a novel endophytic fungus Phomopsis liquidambari. *Bioresource Technology, 129*(129C), 568-574, doi: 10.1016/j.biortech.2012.11.100.

Wang, C., Zhang, M., Cheng, F. & Geng, Q. (2015). Biodegradation characterization and immobilized strains' potential for quinoline degradation by Brevundimonas sp. K4 isolated from activated sludge of coking wastewater. *Bioscience Biotechnology* & *Biochemistry*, 79(1), 164-170, doi: 10.1080/09168451.2014.952615.

Bai, Y., Sun, Q., Cui, Z., Wen, D. & Tang, X. (2009). Aerobic degradation of pyridine by a new bacterial strain, Shinella zoogloeoides, BC026. *Journal of Industrial Microbiology* & *Biotechnology, 36*(11), 1391-1400, doi: 10.1007/s10295-009-0625-9.

Pointing, S. (2001). Feasibility of bioremediation by white-rot fungi. *Applied Microbiology* & *Biotechnology, 57*(1-2), 20, doi: 10.1007/s002530100745.

Ren, D., Zhou, S., Li, Q., Wang, C., Zhang, S. & Zhang, H. (2012). Enhanced electrokinetic remediation of quinoline-contaminated soils. *Toxicological* & *Environmental Chemistry Reviews, 98*(5-6), 585-600, doi: 10.1080/02772248.2015.1133383.

Stella, T., Covino, S., Čvančarová M, Filipová, A., Petruccioli, M. & D'Annibale, A., et al. (2016). Bioremediation of long-term pcb-contaminated soil by white-rot fungi. *Journal of Hazardous Materials, 324*, doi: 10.1016/j.jhazmat.2016.11.044.

Bourbonnais, R. & Paice, M. G. (1992). Demethylation and

delignification of kraft pulp by Trametes versicolor, laccase in the presence of 2,2'-azinobis-(3-ethylbenzthiazoline-6-sulphonate). *Applied Microbiology & Biotechnology, 36*(6), 823-827, doi: 10.1007/BF00172202.

Asif, M. B., Hai, F. I., Hou, J., Price, W. E. & Nghiem, L. D. (2017). Impact of wastewater derived dissolved interfering compounds on growth, enzymatic activity and trace organic contaminant removal of white rot fungi - a critical review. *Journal of Environmental Management, 201*, 89, doi: 10.1016/j.jenvman.2017.06.014.

Thomsen, A. B. (1998). Degradation of quinoline by wet oxidation - kinetic aspects and reaction mechanisms. *Water Research*, 32(1), 136-146, doi: 10.1016/S0043-1354(97)00200-5.

Cañas, A. I. & Camarero, S. (2010). Laccases and their natural mediators: biotechnological tools for sustainable eco-friendly processes. *Biotechnology Advances, 28*(6), 694-705, doi: 10.1016/j.biotechadv.2010.05.002.

Baldrian, P. (2003). Interactions of heavy metals with white-rot fungi. *Enzyme & Microbial Technology, 32*(1), 78-91, doi: 10.1016/S0141-0229(02)00245-4.

Galhaup, C. & Haltrich, D. (2001). Enhanced formation of laccase activity by the white-rot fungus Trametes pubescens in the presence of copper. *Applied Microbiology & Biotechnology, 56*(1-2), 225, doi: 10.1007/s002530100636.

Strong, P. J. & Claus, H. (2011). Laccase: a review of its past and its future in bioremediation. *Critical Reviews in Environmental Science & Technology, 41*(4), 373-434, doi: 10.1080/10643380902945706.

Baldrian, P. (2006). Fungal laccases - occurrence and properties. *Fems Microbiology Reviews, 30*(2), 215–242, doi: 10.1111/j.1574-4976.2005.00010.x.

Giardina, P., Faraco, V., Pezzella, C., Piscitelli, A., Vanhulle, S. & Sannia, G. (2010). Laccases: a never-ending story. *Cellular & Molecular Life Sciences Cmls, 67*(3), 369-385, doi: 10.1007/s00018-009-0169-1.

Tychanowicz, G. K., Souza, D. F. D., Souza, C. G. M., Kadowaki, M. K. & Peralta, R. M. (2006). Copper improves the production of laccase by the white-rot fungus Pleurotus pulmonarius in solid state fermentation. *Brazilian Archives of Biology & Technology, 49*(5), 699-704, doi: 10.1590/S1516-89132006000600002.

DOI: 10.24850/j-tyca-2019-04-11

Special Article

Impact of Water Allocation on Soil Desalination and Groundwater Hydro-chemical Characteristics: A Temporal and Spatial Analysis of a Case Study Region in China

Impacto de agua distribuida en tierra desalinizada y características hidroquímicas de aguas subterráneas: análisis temporal y espacial de un estudio de caso regional en China

P. Li[1]*

N. Magzum[2]

X. Qi[3]*

Y. Zhang[4]

Z. Du[5]

Z. Liang[6]

Z. Huang[7]

[1]Chinese Academy of Agricultural Sciences, Farmland Irrigation Research Institute, Xinxiang, China, email: firilp@163.com, ORCID 0000-0001-8322-2327

[2]Chinese Academy of Agricultural Sciences, Agriculture Water and Soil Environmental Field Science Research Station of Xinxiang City, Xinxiang, China, email: lpaska7979@sina.com, ORCID 0000-0002-6454-6323

[3]Chinese Academy of Agricultural Sciences, Farmland Irrigation Research Institute, Xinxiang, China, email: qxb6301@sina.cn, ORCID 0000-0002-4931-3089

[4]Chinese Academy of Agricultural Sciences, Key laboratory of high-efficient and safe utilization of agriculture water resources, Xinxiang, China, email: 15136479128@163.com, ORCID 0000-0002-8797-7708

[5]Chinese Academy of Agricultural Sciences, Agriculture Water and Soil Environmental Field Science Research Station of Xinxiang City, Xinxiang, China, email: imdzj11@163.com, ORCID 0000-0002-0510-9537

[6]Chinese Academy of Agricultural Sciences, Agriculture Water and Soil Environmental Field Science Research Station of Xinxiang City, Xinxiang, China, email: liang_zhj@163.com, ORCID 0000-0001-6373-9804

[7]Chinese Academy of Agricultural Sciences, Key laboratory of high-efficient and safe utilization of agriculture water resources, Xinxiang, China, email: zdhuang@126.com, ORCID 0000-0002-1639-4820

*Corresponding author: Ping Li, firilp@163.com and Xuebin Qi, *qxb6301@sina.cn*

Novelty Statement

The negative effect of water allocation has been rarely evaluated for improving water resources use efficiency in canal well combined irrigation district. The results showed that more surface water irrigation could drive salinity leaching to the lower soil horizons while average TDS concentration of groundwater has been increased by 18.66% in the study area. We found that combined well canal irrigation could be of water allocation method due mainly to temporal and spatial regulation water resources and root layer soil desalination, however, the possible increasing of TDS in the groundwater may cause potential risk after long term implementing water allocation in a semi-arid area

Abstract

The influence of water resources allocation patterns on root layers soil desalination and groundwater quality were investigated by monitoring different irrigation area from People's Victory Canal irrigation district in Huang Huai Hai plain China that had been conducted well canal combined irrigation patterns from 1954. A typical area was chosen belong to the People's Victory Canal irrigation district from 2013 to 2015. Precipitation of the area, surface water irrigation amount, groundwater consumption amount, salinity content in 0 to 100 cm soil layer and total dissolved solids in groundwater were monitored, the ratio of canal-well water (the ratio of surface water to groundwater irrigation amount, CWWR), soil salinity spatial dynamic, desalinization rate in 0 to 100 cm soil layer and sodium adsorption ratio (SAR) of groundwater were analyzed in the area. CWWR of Branch 1, Branch 2, and Branch 3 ranged from 0.72 to 1.03, 2.50 to 2.63, and 0.65 to 1.26 in 2013 to 2015, respectively. The soil salinity contents for the top 100 cm horizons in the Branch 2 irrigation area decreased slightly by 1.63% to 8.90% compared with the values in the Branch 1 and Branch 3 irrigation districts while the water resources allocation patterns were conducted two years later. Compared with the area in the hydrological period in 2013, the area of average soil salinity exceeded 0.32 mS/cm for the top 20 cm horizons has decreased notably in 2014 and 2015. Compared with the values in 2014, the average TDS concentration of groundwater increased by 18.66% in the study

area in 2015, whereas the sodium adsorption ratio (SAR) values in the above-mentioned irrigation areas decreased by 23.58%, 36.82%, and 53.37% in the normal period in 2015. The combined well-canal irrigation pattern could represent a useful water allocation method mainly because of the temporal and spatial regulation of water resources and root layer soil desalination; however, possible increases of TDS in the groundwater may cause potential ecosystem degradation risks after long-term water allocation in semi-arid areas. Thus, water allocation should be emphasized to maintain a healthy groundwater environment and sustainable stable yields of grain in combined canal-well irrigation districts.

Keywords: Combined well canal irrigation, Water allocation, Soil salinity, Desalinization rate, Hydro-chemical characteristics, Sodium adsorption ratio.

Received: 18/12/2018

Accepted: 09/04/2019

Introduction

Excessive soil salinity can inhibit or restrain crop growth, irrigation results in the accumulation of salt to above-normal concentrations in the rooting zone of arable land because high rates of evaporation and transpiration draw soluble salts from deeper layers of the soil profile in arid and semiarid climatic zones (Rozema *et al*. 2008). According to the National Agricultural Sustainable Development Planning (2015-2030), Huang Huai Hai plain is one of the important agricultural optimization development areas in China, although its environmental resource-carrying capacity does not meet the planning requirements (Yang *et al*. 2016). Water resources allocation technology was initiated in Huang Huai Hai plain starting in the 1950s in China, and it included the comprehensive management of the groundwater depth and crop growth to increase crop yields (Shi *et al*. 2013). The early water and salt balance estimation results of the plain showed that 25.7% of the water consumption entered the sea, and the majority of water consumption occurred via evaporation and transpiration. For example, 0.04 ‰ to 0.4 ‰ salinity levels were found in the precipitation and Yellow river water, respectively, and they may enrich the soil salinity by 0.04 billion tons per year (Wei. 1995), which corresponds to 0.16 million tons per year of salinity accumulating in the soil horizon in the People's Victory Canal irrigation district. In recent years, the ratio of agricultural water to water consumption in the Huang

Huai Hai Plain has declined each year regardless of the advantages of various practices to promote the safe use of limited water resources for agriculture (Yang *et al*. 2016, Yang *et al*. 2013). As a result of the decreased agricultural water consumption, the gap of agricultural water demand in the Huang Huai Hai plain exceeded 10 billion m^3 (Yang *et al*. 2015), and many questions have been raised with regard to changes in groundwater depth and accumulation of salt in soil profiles, which may consequently degrade the soil quality and crop yield. For instance, the sliding average precipitation value of 3 years was reduced by 2.92 mm/an according to a regression analysis, and the agricultural water consumption in the past 5 years was nearly 75% of the annual average value of agricultural water consumption in the People's Victory Canal irrigation district (Li *et al*. 2017), however, the topsoil salinity was elevated (Han *et al*. 2016, Mora *et al*. 2017).

Most studies on agricultural water management have focused on developing optimal algorithms for allocation models and determining the water availability and water resource carrying capacity in arid and semi-arid irrigation areas (Wang *et al*. 2016, Fulazzaky *et al*. 2014, Bekchanov *et al*. 2010, Sadati *et al*. 2014, Wu *et al*. 2014, Parna *et al*. 2014, Esmaeili *et al*. 2015, Al-Omari A *et al*. 2009), where excessive groundwater exploitation would lead to a sharp drop in groundwater level and raise the groundwater salinity (Mo *et al*. 2016), and inappropriate water management would improve root layer soil salinity and soil secondary salinization (Singh *et al*. 2012). Additionally, decreases in precipitation in arid and semi-arid areas have led to excessive groundwater exploitation and basin closure (Molden *et al*. 2007, Molle *et al*. 2010).

This study was conducted to estimate the effect of water allocation on soil profiles salinity, groundwater depth and groundwater hydro-chemical characteristics in western 3rd main canal area using location monitoring methodology. Although researchers mentioned above tried to determined water allocation patterns in well canal combined irrigation district, the highlight of the paper over the other in that in our methodology, we imposed soil profiles desalination and groundwater hydro-chemical characteristics, and the suitable water allocation pattern was put forward for well canal combined irrigation district.

The Study Area

General Description. The western 3rd main canal irrigation area lies in the center of the People's Victory canal irrigation district, the area of which is about 800 hm^2, the average annual precipitation is about 580 mm with about 70% of

the precipitation occurring from June to September, while the average annual water surface evaporation is about 1860 mm, with most of the irrigation events occurring in January, March, May and June. The western 3rd main canal irrigation area, shown in Figure 1 includes three branch canals. The research area is a typical intensive combined well-canal irrigation area in the People's Victory Canal irrigation district, which is characterized by an equipped foundation and a complete system of distribution canals, and three branch canals belong to the 3rd western main canal. The irrigation areas of the Branch 1, Branch 2, and Branch 3 are 300, 213.3 and 286.7 hm^2, respectively. Additionally, approximate indexes of cropping rotational system, water use habits and irrigation technology in the research area are available for the research area, and the irrigation schedule employed is the traditional border irrigation schedule that occurs in winter, the green stage of winter wheat, and the summer maize seeding stage with surface water and groundwater in the normal hydrological year, 1200 to 1800 m^3/hm^2 irrigation amount applied per time. The water allocation practices of branch canals operations are shown in Table 1. The total dissolved solids content of surface water and groundwater employed is 390 to 452, 762 to 1464 mg/L, respectively.

$$\mathrm{CWWR} = \frac{SWIM}{GWIM} \tag{1}$$

where CWWR represents the canal-well water ratio, which is the ratio of SWIM to GWIM, SWIM represents the surface water irrigation amount, and GWIM represents the groundwater irrigation amount.

Table 1. Irrigation amounts from surface water and groundwater for the branch canal areas in 2013-2015.

Year	Branch 1			Branch 2			Branch 3		
	SWIM ($\times 10^4$ m^3)	***GWIM*** ($\times 10^4$ m^3)	***CWWR***	***SWIM*** ($\times 10^4$ m^3)	***GWIM*** ($\times 10^4$ m^3)	***CWWR***	***SWIM*** ($\times 10^4$ m^3)	***GWIM*** ($\times 10^4$ m^3)	***CWWR***
2013	207.87	201.67	1.03	208.44	79.11	2.63	213.69	169.01	1.26
2014	140.11	161.33	0.87	158.06	63.29	2.50	129.83	135.21	0.96
2015	128.08	177.00	0.72	181.13	70.40	2.57	121.33	186.33	0.65

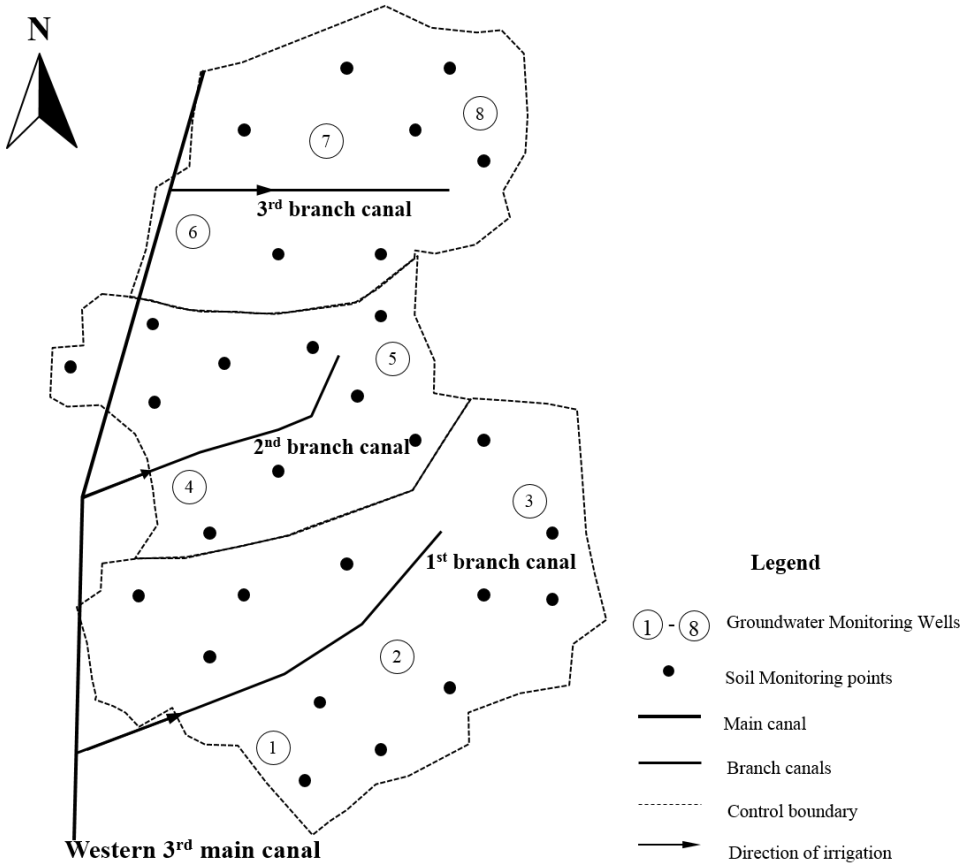

Figure 1. The layout of western 3rd main canal in the People's Victory Canal irrigation district.

Soil Sampling. Soils were sampled at fixed locations at winter wheat seeding stage (approximate 15th Oct. per year). Soil samples were collected at depth of 0 to 10cm, 10 to 20cm, 20 to 30cm, 30 to 40cm, 40 to 60cm, 60 to 80cm and 80 to 100cm with a standard 3.5 cm Ø soil auger, 5 samples were collected per plot and stored at room temperature before analyzing for electrical conductivity (EC). The EC was measured in extracts of soil pastes (1:5 soil to water ratio). Soil samples locations are shown in Figure 1.

Groundwater Monitoring. Groundwater sampled at 20th per month, depth-setting sampler (Solinst 425, Solinst, Canada) was employed below 20 cm of groundwater depth (phreatic aquifer). The pH was measured in pH meter method (PHSJ-5, Leici, Shanghai). The EC was measured in conductivity meter method (DDSJ-308A, Leici, Shanghai). K^+, Na^+, Ca^{2+}, Mg^{2+} concentration in the groundwater was determined using atomic absorption method (AA-7000, SHIMADZU, Japan), CO_3^{2-}, HCO_3^-, SO_4^{2-}, Cl^- concentration in the groundwater

was determined using ion chromatography method (ICS-1500, Dionex, USA). Groundwater samples locations are shown in Figure 1.

Soil Desalination Rate Calculation.

$$DR = \frac{N^{th}SS - (N+1)^{th}SS}{N^{th}SS} \times 100\% \quad (2)$$

where *DR* represents the soil desalination rate (%) [22], $N^{th}SS$ represents the soil horizons salinity in winter wheat seeding stage of N^{th} year, $(N+1)^{th}SS$ represents the soil horizons salinity in winter wheat seeding stage of $(N+1)^{th}$ year, *N* represents the number of the natural years.

Results and Discussion

Characteristic of Precipitation and Irrigation Implementation

Characteristic of precipitation and irrigation implementation was shown in Figure 2. The average annual precipitation is about 574 mm in the study area, while the yearly precipitation in 2013, 2014 and 2015 was 466.9, 558.5 and 569.6 mm, respectively. Additionally, precipitation occurred in major flood period accounted for 67.08%, 73.36% and 51.74% in 2013, 2014 and 2015, respectively. According to seasonal period, precipitation occurred in spring season was 135.0 mm, increased by 20.11% compared with the average annual seasonal precipitation, while precipitation occurred in summer, autumn and winter season was 306.2, 111.0, 17.4 mm, respectively, increased by -10.57%, 10.89%, -8.90% compared with the average annual seasonal precipitation in 2015, respectively.

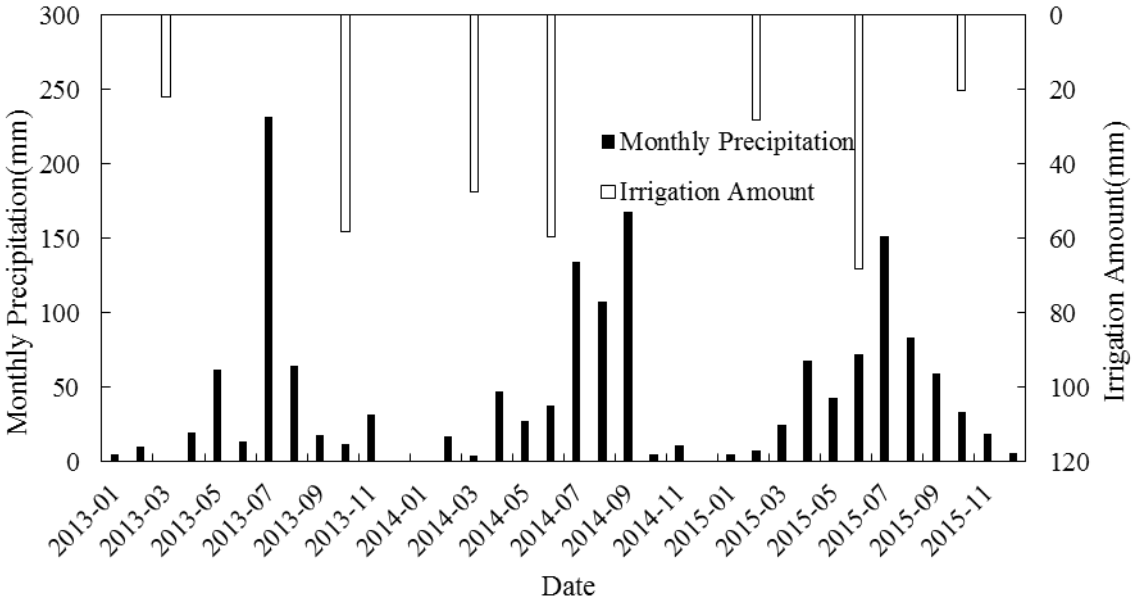

Figure 2. Distribution of monthly precipitation and irrigation amounts from 2013 to 2015.

Irrigation was employed in the seeding stage and green up stage of winter wheat in 2013, irrigation amount was 22.2, 58.2 mm, respectively. While irrigation was employed in green up stage of winter wheat and seeding stage of summer maize in 2014, irrigation amount was 47.6, 59.8 mm, respectively. And irrigation was employed in green up stage of winter wheat, seeding stage of winter wheat and summer maize in 2015, irrigation amount was 28.3, 68.2, 20.3 mm, respectively.

Dynamic of Root Layer Salinity

The dynamics of soil layer salinity by date in the study area are shown in Figure 3. It may be observed that soil salinity accumulated in the soil profile (0-10 cm) in the seeding stage of winter wheat in 2013-2015, varied from 0.2839 to 0.4129 mS/cm. The dynamic of soil salinity in examined soil profiles had similar distribution trends in soil horizons in 2013 to 2015, with the salinity of the top 10 cm layer in the irrigation area presenting higher values compared with the content in other soil profiles. At a lower depth of 30 cm, lower salinity was found in the soil profiles from 2013 to 2015. Compared with the values in the same period in 2013, the average soil salinity in the seeding stage decreased by 9.04 to 26.18%, 9.78 to 33.28%, and 4.56 to 36.35% in the soil profiles (0-100 cm) in

the irrigation area of the Branch 1, Branch 2, and Branch 3, respectively, in 2014, whereas the average soil salinity in 2015 was reduced by 1.05 to 31.26%, 8.34 to 27.18%, and 9.72 to 18.06% in the soil profiles (0-100 cm) in the irrigation area of the Branch 1, Branch 2 and Branch 3, respectively.

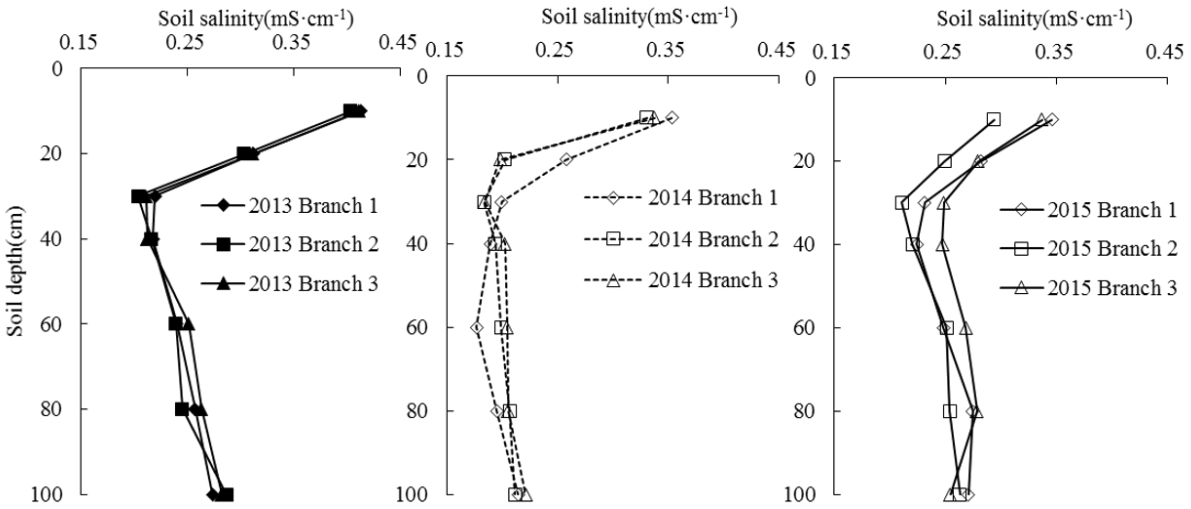

Figure 3. Soil salinity dynamics with soil depth in branch canal irrigation areas from 2013 to 2015.

In the irrigation areas of Branch 1, Branch 2, Branch 3, the ratio of surface water to groundwater irrigation ranged from 0.72-1.03, 2.50-2.63, 0.65-1.26 in 2013, 2014, and 2015, respectively (Table 2). The accumulation salinity for the top 100 cm horizons in Branch 2 irrigation area decreased slightly compared with the values in Branch 1, Branch 3 irrigation district by 1.63% to 8.90%, which might be caused by salts in the surface water as well as a preponderance of downward water movement and subsequent leaching to subsoil and groundwater (Molle *et al*. 2010). The standard deviation of soil salinity calculated from 2013 to 2015 in the study area and the crops tolerances to salinity (Turkan *et al*. 2009) indicate that the accumulated salinity in the root soil layer will likely represent a serious problem as long as water allocation method increases the soluble salt input levels in the study area (Gao *et al*. 2015). In addition, compared with the concentration in 2014, the average TDS concentration of groundwater in 2015 increased by 18.66% in the study area. Under certain conditions, soil salinity may be significantly reduced after the irrigation because under the high rates of irrigation with surface water of low salinity, continual leaching of salts to lower horizons will occur (Daou *et al*. 2016).

Tecnología y Ciencias del Agua

Table 2. Salinity and salinity desalination rate in different soil layers.

Soil Horizons (cm)	Irrigation Area	2013—2014			2014—2015			Desalination rate in 2013-2015 (%)
		Initial soil salinity ($mS \cdot cm^{-1}$)	Final soil salinity ($mS \cdot cm^{-1}$)	Desalination rate (%)	Initial soil salinity ($mS \cdot cm^{-1}$)	Final soil salinity ($mS \cdot cm^{-1}$)	Desalination rate (%)	
0-10	Branch 1	0.4129	0.3535	14.40	0.3535	0.3459	2.15	16.24
	Branch 2	0.4034	0.3308	17.99	0.3308	0.2938	11.20	27.18
	Branch 3	0.4111	0.3375	17.90	0.3375	0.3368	0.20	18.06
10-20	Branch 1	0.3114	0.2578	17.21	0.2578	0.2819	-9.34	9.48
	Branch 2	0.3034	0.2024	33.28	0.2024	0.2494	-23.21	17.80
	Branch 3	0.3111	0.1980	36.35	0.1980	0.2794	-41.13	10.18
20-30	Branch 1	0.2194	0.1996	9.04	0.1996	0.2316	-16.04	-5.55
	Branch 2	0.2034	0.1835	9.78	0.1835	0.2107	-14.81	-3.59
	Branch 3	0.2111	0.1843	12.66	0.1843	0.2485	-34.82	-17.75
30-40	Branch 1	0.2178	0.1895	12.98	0.1895	0.2245	-18.46	-3.09
	Branch 2	0.2162	0.1938	10.33	0.1938	0.2206	-13.80	-2.05
	Branch 3	0.2122	0.2025	4.56	0.2025	0.2472	-22.09	-16.53
40-60	Branch 1	0.2399	0.1771	26.18	0.1771	0.2484	-40.30	-3.58
	Branch 2	0.2392	0.1989	16.83	0.1989	0.2513	-26.33	-5.07
	Branch 3	0.2512	0.2043	18.68	0.2043	0.2682	-31.27	-6.74
60-80	Branch 1	0.2569	0.1950	24.09	0.1950	0.2746	-40.83	-6.90
	Branch 2	0.2452	0.2070	15.57	0.2070	0.2542	-22.80	-3.67
	Branch 3	0.2633	0.2055	21.95	0.2055	0.2784	-35.49	-5.76
80-100	Branch 1	0.2737	0.2144	21.67	0.2144	0.2709	-26.32	1.05
	Branch 2	0.2868	0.2117	26.20	0.2117	0.2629	-24.19	8.34
	Branch 3	0.2819	0.2213	21.49	0.2213	0.2545	-14.99	9.72

Spatial Dynamic of Soil Salinity with Irrigation Area

The spatial dynamics of soil salinity in 20 cm profile in 2013 to 2015 are shown in Figure 4. The EC values averaged for the top 20 cm horizons in 2013, 2014, and 2015 were 0.3456, 0.2820 and 0.2991 mS/cm in the study area, respectively, whereas the standard deviations of the EC values were 0.071, 0.058 and 0.029. For the whole examined soil profile (0-20 cm), the area of EC value exceeded 0.32 mS/cm (equal to 1.50 g/kg soil salinity) was calculated by Sufer 13.0 (Golden Software, LLC), 60.38%, 59.61% and 84.40% were presented respectively from Branch 1, Branch 2 and Branch 3 irrigation area in 2013. To 2014, 25.99%, 0.94% and 41.87% were presented respectively from the above mentioned irrigation area, in comparison with 2013, the area of EC value exceeded 0.32 mS/cm from Branch 1, Branch 2 and Branch 3 irrigation district has been decreased by 56.95%, 98.42% and 50.39%, respectively. In addition, 41.16%, 8.81% and 52.49% were obtained respectively from above mentioned irrigation area, in comparison with 2013, the area of EC value exceeded 0.32 mS/cm from above mentioned irrigation district has been decreased by 31.83%, 85.22% and 37.81%, respectively.

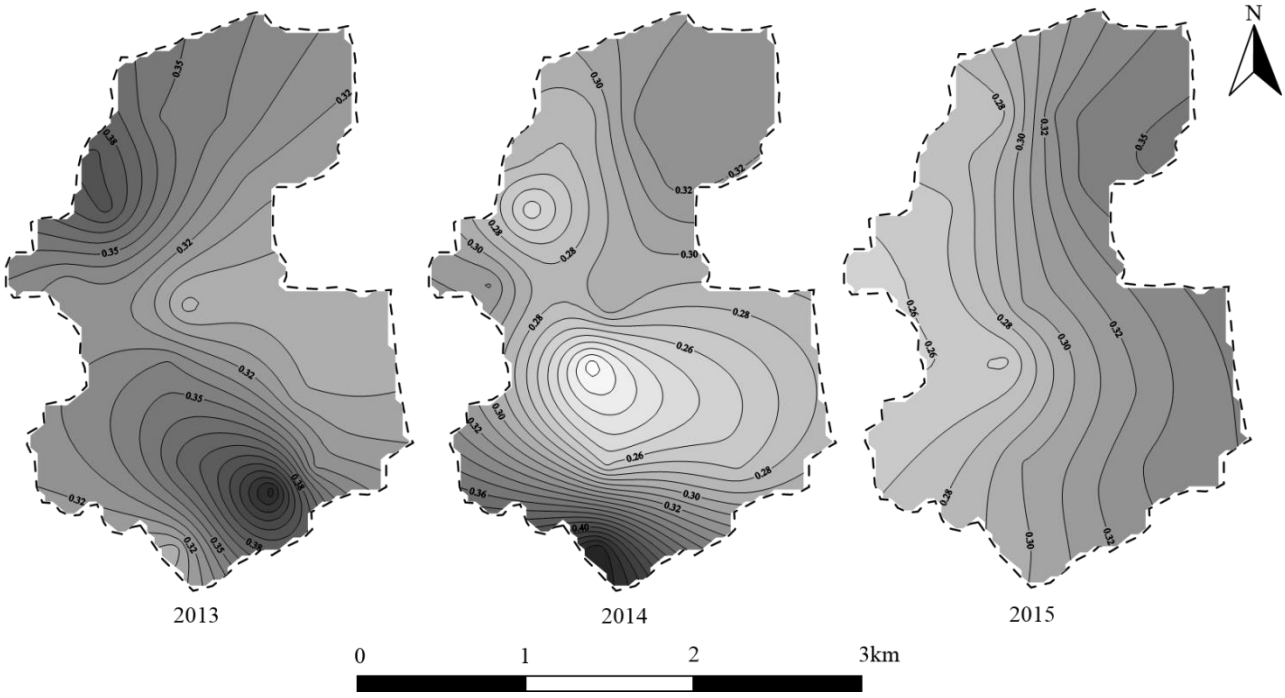

Figure 4. Distribution of average soil salinity of 0 to 20 cm soil layer in research areas from 2013 to 2015.

Compared with the area in the hydrological period in 2013, the area of average soil salinity exceeded 0.32 mS/cm for the top 20 cm horizons decreased notably

due to low salt precipitation leaching caused by the high rate of medium concentration water employed for irrigation in the study area (Li *et al*. 2016). In the present study, the area of average soil salinity exceeded 0.32 mS/cm for the top 20 cm horizons was a negative relationship with canal well water ratio, that is, on top 20 cm layers, average soil salinity content in higher CWWR irrigation area was lower as compared to content in soil from lower CWWR irrigation area (Ghazaryan *et al*. 2016). The results for the soil desalination rate for the top 100 cm horizons showed that areas with higher CWWRs presented increased values at all sampled depths of the profile and the EC values declined with increasing CWWRs because under the high CWWRs, continual leaching of salts to lower layers occurs. In addition, irrigation with low-salt water caused a drop in the root layer salinity. No doubt, surface water application caused an appreciated decrease in soil salinity, which may eliminate the risk of crop salt stress (Dai *et al*. 2015).

Effect of Soil Profile Desalination with Branch Canal Irrigation Area

The results from soil horizon desalination calculations of the branch canal irrigation area showed that irrigation by the water allocation patterns caused increases in salinity levels in the lower layer (20-80 cm), and decreased in salinity levels in the top layer (0-20 cm). It was observed that average EC value at all sampled depths of the profile in 2014 was lower than that of 2013, by 9.04% to 36.35%, while average EC value at examined soil profile (0-10, 10-20 and 80-100 cm) in 2015 was lower than that of 2013, by 1.05% to 27.18%. Additionally, compared with Branch 1, Branch 3 irrigation district, soil desalination rate for top 20cm horizons in 2013 to 2015 in Branch 2 was 23.15%, increased by 73.65%, 57.86%, respectively. Furthermore, in comparison with 2013, average EC values for 20-30, 30-40, 40-60 and 60-80 cm layer in 2015 has slightly accumulated, meaningfully, for the examined soil profiles (20-80cm), soil desalination in the Branch 2 irrigation area was -5.78%, which was higher than that in the Branch 1, Branch 3 irrigation area by 21.84% and 60.99%, respectively.

Effect of Groundwater Hydro-Chemical Characteristics with

Tecnología y Ciencias del Agua

Branch Canal Irrigation Area

The hydro-chemical characteristics of examined groundwater in Branch 1, Branch 2, Branch 3 irrigation areas are shown in table 3. The water types are generally distinct zones in which the cation and anion concentrations are described within the defined composition categories, and the dominant anion species of water changes systematically from HCO_3^-, Cl^- to SO_4^{2-} along groundwater flow direction from the irrigation area (Wang *et al*. 2014, Reddy *et al*. 2012). The Piper diagram (Wen *et al*. 2005) in Figure 5 shows that the water type in above-mentioned irrigation areas had similar change trends as groundwater. That is, during the dry period (December, January and February), normal period (March, April, May, October and November), wet period (June, July, August and September), the cation types were Ca^{2+}/Na^+, Na^+/Ca^{2+}, Ca^{2+}/Na^+, respectively. This result indicates that groundwater type had an obvious alkaline trend because of cation change of Ca^{2+}/Na^+ in the dry period to Na^+/Ca^{2+} in the normal period. Under certain conditions, groundwater hydro-chemical characteristics may be significantly impacted during winter wheat growth stage because under the high rates of phreatic evapotranspiration with unsuitable water allocation there would concentrate groundwater TDS (Rozema *et al*. 2008, Karmegam *et al*. 2011, Brunner *et al*. 2008). Additionally, in comparison with the dry period in 2014, average TDS concentrations of groundwater in 2015 were increased by 30.28%, 21.83%, 33.95% in Branch 1, Branch 2, Branch 3 irrigation area, respectively. While the normal period in 2014, average TDS concentrations of groundwater in 2015 were increased by 13.35%, 27.88%, 5.17%, and wet period, the increasing values of TDS in 2015 was 0.81%, 18.29% and 16.43% in the above mentioned area, respectively. It was observed that compared with 2014, average TDS concentration has been increased by 1.28, 1.15, 1.12 fold in the dry period, normal period and wet period with study area. From normal period groundwater with Branch 2 irrigation area, in comparison with Branch 1 and Branch 3 irrigation area, value added of TDS was improved by 1.23, 3.48 fold, respectively. No doubt, water allocation employed in the study area caused appreciable increased TDS in groundwater, which may improve the risk of groundwater irrigation occurring normal period.

Table 3. Annual dynamics of groundwater hydrochemical characteristics of a typical branch canal irrigation area.

Year	Irrigation	Water	Ca^{2+}	Mg^{2+}	Na^+	K^+	CO_3^{2-}	HCO_3^-	Cl^-	SO_4^{2-}	TDS	SAR

	Area	period	(mg·L^{-1})	(mg·L^{-1})	(mg·L^{-1})	(mg·L^{-1})	(mg·L^{-1})	(mg·L^{-1})	(mg·L^{-1})	(mg·L^{-1})	(mg·L^{-1})	
2014	Branch 1	Dry period	112.88	11.67	129.25	0.00	0.00	403.72	126.37	131.80	895.63	16.38
		Normal period	83.56	23.38	167.18	0.00	0.00	412.91	126.38	156.55	947.41	22.86
		Wet period	187.18	43.96	194.63	0.00	0.00	485.28	126.38	145.93	868.49	18.10
	Branch 2	Dry period	140.40	28.70	167.70	0.00	0.00	555.78	136.18	178.53	1113.43	18.24
		Normal period	82.93	39.98	201.12	0.00	0.00	511.53	126.33	186.85	1009.83	25.66
		Wet period	212.19	58.14	230.06	0.00	0.00	576.53	142.73	205.05	838.24	19.79
	Branch 3	Dry period	91.20	32.30	162.00	0.00	0.00	373.30	135.10	188.10	981.20	20.62
		Normal period	101.87	45.17	259.13	0.00	0.00	519.83	165.57	330.20	1214.30	30.22
		Wet period	222.68	75.13	233.50	0.00	0.00	647.05	174.33	234.73	814.67	19.14
2015	Branch 1	Dry period	130.86	18.71	149.25	0.00	0.00	488.97	133.55	209.33	1166.82	21.44
		Normal period	111.35	34.58	185.41	0.00	0.00	496.35	119.46	162.86	1073.85	17.47
		Wet period	234.12	33.74	182.68	0.00	0.00	371.11	140.07	112.28	875.51	15.79
	Branch 2	Dry period	135.42	28.47	157.24	0.00	0.00	609.87	151.12	211.70	1356.47	24.29
		Normal period	138.31	49.90	219.89	0.00	0.00	630.44	128.03	187.46	1291.38	16.21
		Wet period	233.45	41.55	208.41	0.00	0.00	416.89	166.13	123.40	991.53	17.77
	Branch 3	Dry period	144.00	32.52	143.09	0.00	0.00	564.11	156.13	223.53	1314.34	20.66
		Normal period	166.28	39.88	194.06	0.00	0.00	642.88	177.58	187.43	1277.11	14.09

		Wet period	239.48	48.45	207.63	0.00	0.00	456.63	178.60	117.13	948.48	17.30

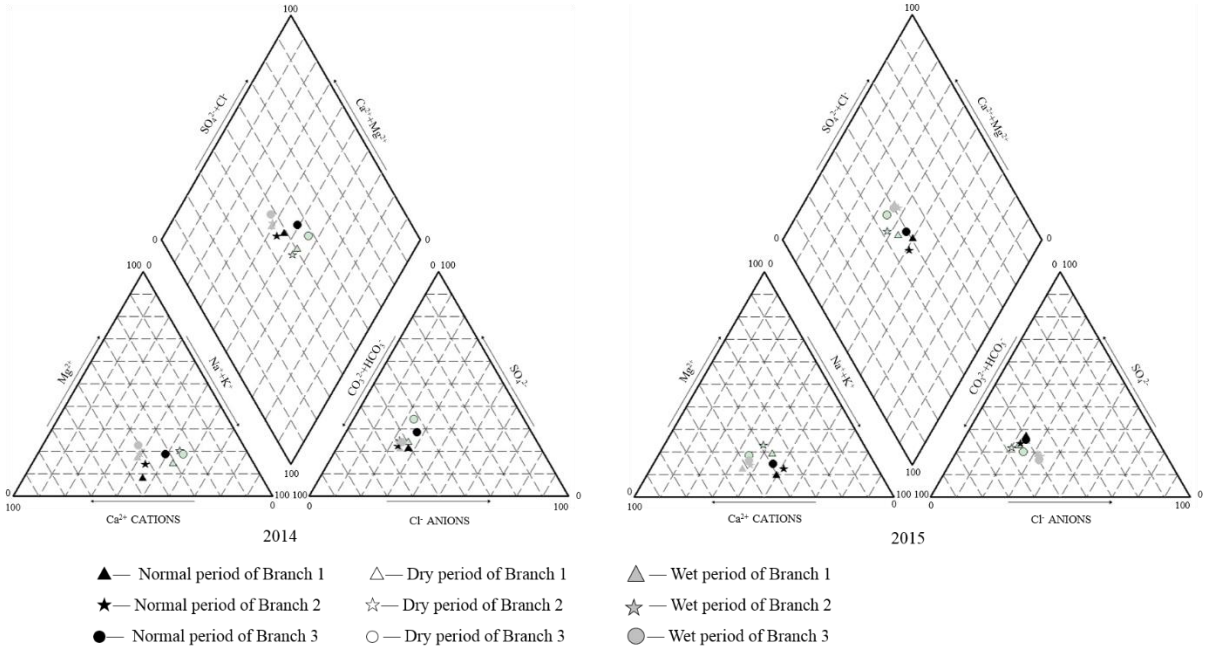

Figure 5. Dynamics of groundwater hydrochemistry of typical areas under CWWs from 2013 to 2015.

In comparison with that in the hydrological period in 2014, the average groundwater TDS concentration in 2015 was increased by 22.67% in the study area, which might be due to groundwater exploration as well as a preponderance of phreatic evaporation and subsequent irrigation leaching (Rao *et al*. 2008). In the present study, SARs of groundwater from Branch 1, Branch 2, Branch 3 irrigation area in the normal period were greater than 18. According to the agricultural irrigation water alkalization classification standard (Li *et al*. 2013, Vasanthavigar *et al*. 2010), if SAR values of groundwater were exceeded 18, then it is not fit for irrigation. Additionally, compared with the values in 2014, the SAR values in the above-mentioned irrigation area decreased by 23.58%, 36.82%, 53.37% in normal period, respectively. Furthermore, the SAR values in the above mentioned irrigation area were less than 18 in 2015. The groundwater SAR dynamics occurred largely as a result of the input of ions by surface irrigation, the leaching of ions by precipitation, or the evaporation of ions from groundwater. The decrease of groundwater SAR values in 2015 may have increased agricultural water resources and ensured the positive effect of water allocation (Chaudhuri *et al*. 2014, Huang *et al*. 2013).

Conclusions

Larger CWWRs modify the accumulation of salinity in topsoil. Additionally, in comparison with areas exceeded 0.32 mS/cm in 0-20 cm soil profile in a lower ratio of canal well water irrigation district, the results showed that canal water irrigation caused decreased soil salinity to the depths of 20 cm in the study area. Compared with rates in the hydrological period in 2013, soil desalination rate to the depths of 20cm in 2014 and 2015 was notably increased, and the rates improved with the CWWR. For soil desalination to the depths of 100cm from 2013 to 2015, larger CWWRs promoted salinity leaching to lower soil profiles and groundwater. Thus, water allocation employed in the study area might increase groundwater TDS concentration, which can result in alkalization trend of cation types in the normal period. A decrease in the sodium adsorption ratio was observed in the normal and wet period in 2015 compared with the value in 2014 because of irrigation water recharge to groundwater caused by water with low TDS concentrations employed for irrigation in the study area. However, possible increases of TDS in the groundwater may cause potential risks after long term water allocation in the study area. Therefore, water allocation should be emphasized to maintain a healthy groundwater environment and sustainable stable yields of grain in combined canal-well irrigation areas.

Acknowledgments

The research was financially supported by the Chinese Academy of Agricultural Sciences Basal Scientific Research Fund (FIRI2017-10) and the Agricultural Science and Technology Innovation Program of Chinese Academy of Agricultural Sciences (CAAS-ASTIP-FIRI-03).

References

Rozema, J. & Flowers, T. (2008). Crops for a salinized world. *Science*, 322: 1478–1480.

Yang, B., Zhang, Y. C., Qian, Y., Tang, J. & Liu, D. Q. (2016). Climatic effects of irrigation over the Huang-Huai-Hai Plain in China simulated by the weather research and forecasting model. *Journal of Geophysical Research-Atmospheres,* 121: 2246–2264.

Shi, W. J., Tao, F. L. & Liu, J. Y. (2013). Changes in quantity and quality of cropland and the implications for grain production in the Huang-Huai-Hai Plain of China. *Food Security*, 5, 69–82.

Wei, Y. Q. (1995). Soil salinization present and future from water and salt balance of Huang-Huai-Hai Plain. *Progress in Soil Sciences*, 23(2), 18–25. (in Chinese).

Yang, X. L., Gao, W. S., Shi, Q. H., Chen, F. & Chu, Q. Q. (2013). Impact of climate change on the water requirement of summer maize in the Huang-Huai-Hai farming region. *Agricultural Water Management*, 124, 20–27.

Yang, J. Y., Mei, X. R., Huo, Z. G., Yan, C. R., Ju, H., Zhao, F. H. & Liu, Q. (2015). Water consumption in summer maize and winter wheat cropping system based on SEBAL model in Huang-Huai-Hai Plain, China. *Journal of Integrative Agriculture*, 14, 2065–2076.

Li, P., Magzum, N., Liang, Z. J., Huang, Z. D. & Qi, X. B. (2017). Effects of canal well water ratios on root layer soil desalination and groundwater hydrochemical characteristics. Scientia Agricultura Sinica, 50(3), 526-536. (in Chinese).

Han, D. R., Sun, Z. G., Li, F. D., Hou, R. X., Li, J., Ouyang, Z., Li, B. B. & Cao, C. W. (2016). Changes and controlling factors of cropland soil organic carbon in North China Plain over a 30-year period. *Plant and Soil*, 403, 437–453.

Mora, J. L., Herrero, J. & Weindorf, D. C. (2017). Multivariate analysis of soil salination-desalination in a semi-arid irrigated district of Spain. *Geoderma*, 291, 1–10.

Wang, J. H., Hou, B. D., Jiang, D. C., Xiao, W. H., Wu, Y. X., Zhao, Y., Zhou, Y. Y., Guo, C. S. & Wang, G. X. (2016). Optimal Allocation of Water Resources Based on Water Supply Security. *Water*, 8, 237.

Fulazzaky, M. A. (2014). Challenges of Integrated Water Resources Management in Indonesia. *Water*, 6, 2000-2020.

Bekchanov, M., Karimov, A. & Lamers, J. P. A. (2010). Impact of Water Availability on Land and Water Productivity: A Temporal and Spatial Analysis of the Case Study Region Khorezm, Uzbekistan. *Water*, 2, 668–684.

Sadati, S. K., Speelman, S., Sabouhi, M., Gitizadeh, M. & Ghahraman, B. (2014). Optimal Irrigation Water Allocation Using a Genetic Algorithm under Various Weather Conditions. *Water*, 6, 3068–3084.

Wu, X., Zheng, Y., Wu, B., Tian, Y., Han, F. & Zheng, C. (2016). Optimizing conjunctive use of surface water and groundwater for irrigation to address human-nature water conflicts: A surrogate modeling approach. *Agricultural Water Management*, 163, 380–392.

Parna, P., Armaghan, A. & Reza, K. (2015). A heuristic evolutionary game theoretic methodology for conjunctive use of surface and groundwater resources. *Water Resources Management*, 29, 3905–3918.

Esmaeili, A. & Shahsavari, Z. (2015). Water allocation for agriculture in southwestern Iran using a programming model. *Appl. Water Sci.*5, 305–310.

Al-Omari, A., Al-Quraan, S., Al-Salihi, A. & Abdulla, F. (2009). A Water Management Support System for Amman Zarqa Basin in Jordan. *Water Resour. Manage*, 23, 3165–3189.

Mo, X., Wu, J. J., Wang, Q. & Zhou, H. (2016). Variations in water storage in China over recent decades from GRACE observations and GLDAS. *Natural Hazards and Earth System Sciences*, 16, 469–482.

Singh, A., Panda, S.N., Flugel, W.A. & Krause, P. (2012). Waterlogging and farmland salinization: causes and remedial measures in an irrigated semi-arid region of India. *Irrigation and Drainage*, 61, 357–365.

Molden, D., De Fraiture, C. & Rijsberman, F. (2007). Water scarcity - The food factor. *Issues in Science and Technology*, 23, 39–48.

Molle, F., Wester, P. & Hirsch, P. (2010). River basin closure: Processes, implications and responses. *Agricultural Water Management*, 97, 569–577.

Wang, H. J., Shi, J. C., Zhang, H. L., Sheng, J. D. & Ma, X. W. (2014). Soil salinity dynamic change and desalting effect under different improvement measures in severe salinity soil in Xinjiang. *Transactions of the Chinese Society of Agricultural Engineering*, 30, 102–111. (in Chinese).

Reddy, A. G. S., Saibaba, B. & Sudarshan, G. (2012). Hydrogeochemical characterization of contaminated groundwater in Patancheru Industrial Area, Southern India. *Environ. Monit. Assess*, 184, 3557–3576.

Wen X., Wu Y., Su J., Zhang Y. & Liu F. (2005). Hydrochemical Characteristics and Salinity of Groundwater in the Ejina Basin, Northwestern China. *Environ. Geol.* 48, 665–675.

Karmegam, U., Chidambaram, S., Prasanna, M. V., Sasidhar, P., Manikandan, S., Johnsonbabu, G., Dheivanayaki, V., Paramaguru, P., Manivannan, R., Srinivasamoorthy, K. & Anandhan, P. (2011). A study on the mixing proportion in groundwater samples by using piper diagram and phreeqc model. *Chin. J. Geochem.*30, 490–495.

Brunner, P., Li, H. T., Kinzelbach, W., Li, W. P. & Dong, X. G. (2008). Extracting phreatic evaporation from remotely sensed maps of evapotranspiration. *Water Resources Research*, 44, W08428.

Turkan, I. & Demiral, T. (2009). Recent developments in understanding salinity tolerance. *Environmental and Experimental Botany*, 67, 2–9.

Gao, X. Y., Huo, Z. L., Bai, Y. N., Feng, S. Y., Huang, G. H., Shi, H. B. & Qu, Z. Y. (2015). Soil salt and groundwater change in flood irrigation field and uncultivated land: a case study based on 4-year field observations. *Environmental Earth Sciences*, 73, 2127–2139.

Daou, C., Nabbout, R. & Kassouf, A. (2016). Spatial and temporal assessment of surface water quality in the Arka River, Akkar, Lebanon. *Environmental Monitoring and Assessment*, 188, 684.

Li, P., Qi, X.B., Magzum, N., Huang, Z.D., Liang, Z.J. & Qiao, D.M. (2016). Effect of Water Resources Allocation on Groundwater Environment and Soil Salinity Accumulation under Climate Change. *Journal of Earth Science and Engineering*, 6, 73–82.

Ghazaryan, K. & Chen, Y. N. (2016). Hydrochemical assessment of surface water for irrigation purposes and its influence on soil salinity in Tikanlik oasis, China. *Environmental Earth Sciences*, 75, 383.

Dai, Y., Senge, M., Ito, K., Onishi, T. & Yoshiyam, K. (2015). Experimental evaluation of irrigation methods for soil desalinization. *Paddy and Water Environment*, 13, 159–165.

Rao, N.S. (2008). Factors controlling the salinity in groundwater in parts of Guntur district, Andhra Pradesh, India. *Environmental Monitoring and Assessment*, 138, 327–341.

Li, P. Y., Wu, J. H. & Qian, H. (2013). Assessment of groundwater quality for irrigation purposes and identification of hydrogeochemical evolution mechanisms in Pengyang County, China. *Environmental Earth Sciences*, 69, 2211-2225.

Vasanthavigar, M., Srinivasamoorthy, K., Vijayaragavan, K., Ganthi, R. R., Chidambaram, S., Anandhan, P., Manivannan, R. & Vasudevan, S. (2010). Application of water quality index for groundwater quality assessment: Thirumanimuttar sub-basin, Tamilnadu, India. *Environmental Monitoring and Assessment*, 171, 595–609.

Chaudhuri, S. & Ale, S. (2014). Long term (1960-2010) trends in groundwater contamination and salinization in the Ogallala aquifer in Texas. *Journal of Hydrology*, 513, 376–390.

Huang, T. M., Pang, Z. H., Chen, Y. N. & Kong, Y. L. (2013). Groundwater circulation relative to water quality and vegetation in an arid transitional zone linking oasis, desert and river. *Chinese Science Bulletin*, 58, 3088–3097.

DOI: 10.24850/j-tyca-2019-04-12

Special Article

Denitrification in Simulated Groundwater Using Lignite as a Solid-Phase Organic Carbon Source

Desnitrificación en simulación de agua subterránea usando lignito como fuente de carbono orgánico en fase sólida

L. Jing[1]

Y. Sun[2]

H. Wang[3]*

W. Liu[4]

D. Wang[5]

[1]Department of Water Environmental Planning, Chinese Academy for Environmental Planning, China, email: jinglx@caep.org.cn, ORCID 0000-0003-2497-9105

[2]China Ordnance Industry Survey and Geotechnical Institute, China North Industries Group Corporation, China, email: 413626949@qq.com, ORCID 0000-0002-1440-0465

[3]College of Water Resource and Environment, China University of Geoscience (Beijing), China, email: wangheli@cugb.edu.cn, ORCID 0000-0001-5916-5297

[4]Department of Water Environmental Planning, Chinese Academy for Environmental Planning, China, email: liuwj@caep.org.cn, ORCID 0000-0002-1547-4976

[5]Department of Water Environmental Planning, Chinese Academy for Environmental Planning, China, email: wangdong@caep.org.cn, ORCID 0000-0002-8468-4889

*Corresponding author: Heli Wang, wangheli@cugb.edu.cn

Abstract

To ensure safety standards of drinking water, it is essential to perform NO_3 remediation in groundwater. Owing to the lack of organic carbon in groundwater, heterotrophic denitrification is not quite effective in groundwater. Few studies have reported how Chinese lignite can be

used as an organic carbon source for denitrification. In simulated conditions of groundwater, we determined whether the four lignite types (Lignite was obtained from Sanjitun, Lingshi, Wangniutan, and Zhaotong in China.) could be used as a solid-phase organic carbon source for denitrification; the analyses were performed in a test water column. For denitrification, the most effective carbon source was the lignite obtained from Wangniutan. It showed the highest efficacy of 34% in nitrate (NO_3) removal for an influent NO_3-N concentration of 30 mg· L^{-1}. The effluent NO_3-N concentrations below 20 mg L^{-1} and the water samples showed no acute toxicity when they were subjected to luminescent bacteria test. We performed static carbon release test and infrared spectral analysis on all the four lignite types, and we found that there was a direct relation between NO_3 removal and the lignite's ability for static carbon release. When NO_3 concentrations were high and the rate of static carbon release was low, the efficacy of denitrification was greater. This effect was achieved when the molecular structure of lignite contained small molecular organic compounds in free states; these compounds primarily included the following functional groups: alcohols, phenols, and organic acids. These compounds were primarily used by the denitrifying bacteria.

Keywords: Carbon source, denitrification, groundwater, lignite, nitrate (NO_3).

Received: 18/12/2018

Accepted: 11/04/2019

Introduction

The concentration of nitrate (NO_3) has increased tremendously in groundwater, causing incessant water pollution in China (Bi et al. 2010). In some regions, nitrate concentrations have soared to several hundred milligrams per liter (Zhang et al. 2012) in groundwater; such precarious concentrations are ten times greater than the Class III standards of Groundwater Quality Standards (GB/T 14848-93). Groundwater is one of the most important sources of drinking water in China; therefore, healthy humans would be adversely affected when they consume groundwater containing high levels of NO_3, which is a major contaminant. In a chemically reductive environment, nitrate (NO_3) compounds get easily converted into nitrite (NO_2) compounds. Furthermore, NO_3 and NO_2 are important functional groups in various

nitrogenous organic compounds. In particular, NO_3 and NO_2 participate in various chemical reactions and form the following categories of toxic compounds: carcinogenic, and/or mutagenic N-nitroso compounds (Zhang et al. 2008; Li C et al. 2013). According to statistical data, it is dangerous to consume NO_3 contaminated drinking water because it is closely linked to cancers of the stomach, intestine, skin, bone, and nervous system (Nathan S. Bryan et al. 2013; Yan 2013). To ensure the safety standards of drinking water, we need to carry out nitrate (NO_3) remediation in groundwater.

For NO_3 remediation in groundwater, biological denitrification is one of the most suitable methods. Anaerobic denitrification is the most widely used process in the biological environment. In this process, heterotrophic denitrifying bacteria metabolize organic compounds, which are primarily carbon compounds. In such metabolic reactions, the NO_3 radical is reduced and converted into free nitrogen under anaerobic conditions (Miso et al. 2014). Since groundwater lacks organic carbon, heterotrophic denitrification is not really effective in removing NO_3 contaminants from groundwater. Several previous studies have reported that acetic acid, ethanol, wood chips, compost, cotton, wheat straw, and paper scraps are not adequate carbon sources for heterotrophic denitrification (S. Israel et al. 2009; Jin and Liu 2011; Jian et al. 2013; Li et al. 2014). In 2010, some scholars found that Canadian lignite can be a suitable source for solid-phase organic carbon, which would apparently achieve NO_3 removal (Li 2010) more effectively. In another study, scholars reported that luminescent bacteria acute toxicity of Canadian lignite was low (Jiang et al. 2014). Lignite resources are abundant in China (Fu 2012). However, because of low grade coalification, the industrial application value of such lignite is poor (Shen et al. 2012). Therefore, scientific studies must be carried out to determine whether Chinese lignite can be used as an organic carbon source for denitrification of groundwater. Since very few studies have investigated the suitability of Chinese lignite for denitrification, we are not really sure whether Chinese lignite can be considered as a solid-phase organic carbon source. Moreover, very few studies have investigated the impact of Chinese lignite on human health; therefore, we cannot guarantee the safety standards of denitrification achieved by Chinese lignite. In this study, denitrification was performed on groundwater in simulated conditions using Chinese lignite as the organic carbon source. Lignite was obtained from the following places in China: Sanjitun, Lingshi, Wangniutan, and Zhaotong. The lignite samples of Wangniutan showed the highest efficacy (34%) in NO_3 removal process. By performing an acute toxicity test, we found that there was no toxicity in the lignite samples of Wangniutan. Furthermore, we investigated the preliminary mechanism through which lignite (the carbon source) initiated the denitrification process. For effective NO_3

removal, the organic compounds must have the ability to release static carbon easily; moreover, small molecule organic compounds were used as the main carbon sources for denitrification.

Materials and Methods

Test System

Polyvinyl chloride (PVC) columns (6.0 cm in internal diameter and 60 cm length) were set up with the following components: a water distribution zone, a reaction zone, and catchment areas of 5, 50, and 5 cm thickness, respectively. While designing the columns, we evenly spaced out four sampling ports along each column (Figure 1). The ports were installed at the following points: 15 (P1), 25 (P2), 35 (P3), and 45 cm (P4) from the base of the column. They were fitted with a rubber septum, which enabled sampling through a syringe.

Artificial wastewater was pumped into the column by a peristaltic pump (Figure 1), and samples were obtained from the sampling ports and catchment areas. These samples were subsequently analyzed with standardized techniques.

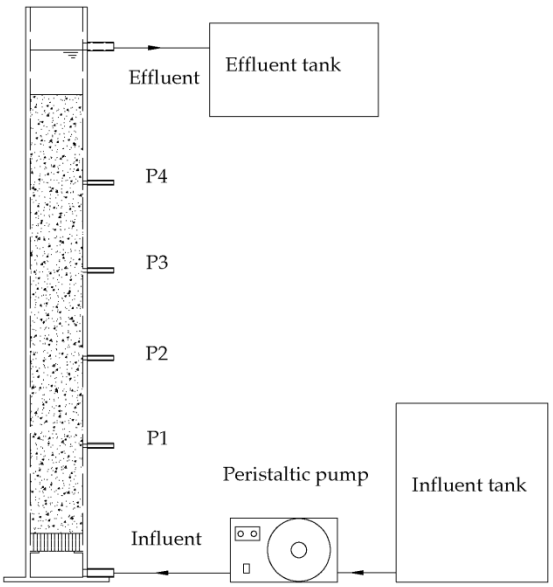

Figure 1. Scheme of the column setup.

Fillers

Fillers were prepared from various lignite types, which were obtained from the following places in China: Sanjitun (Heilongjiang Province), Lingshi (Shanxi Province), Wangniutan (Hebei Province), and Zhaotong (Yunnan Province). Typically, lignite material was dark brown in color. After grinding the lignite, we obtained rough, porous particles, with a particle size of 1–2 mm.

Simulated Groundwater

To prepare simulated groundwater containing NO_3, we mixed 216 mg of KNO_3 (AR, Xilong chemical plant, Guangdong, China) with 1 L of deionized water. The influent NO_3-N concentration was 30 $mg \cdot L^{-1}$. By adding Na_2CO_3 into the simulated groundwater, we adjusted the pH to 6.5–7.0. A UV/visible spectrophotometer (UV-1200, Mapada, Shanghai, China) was used to analyze the NO_3-N and NO_2-N concentrations in groundwater.

In the reaction chamber, we controlled the water temperature with a cooling liquid circulating system. As shown in Figure 2, the system included a plastic cooling hose and DLSB-10 (Low temperature cooling liquid circulating pump). During the experiment, the water temperature was in the range 12.0–16.0 °C in the column.

The following parameters were measured primarily: NO_3-N, permanganate index (COD_{Mn}), pH, water temperature, and microbial toxicity; the measurements were carried out using the methods described in the following reference books: *Water and Wastewater Monitoring Analysis Method (fourth edition, 2002)* and *Water quality - Determination of acute toxicity - Luminescent bacteria test (GB/T 15441-1995)*.

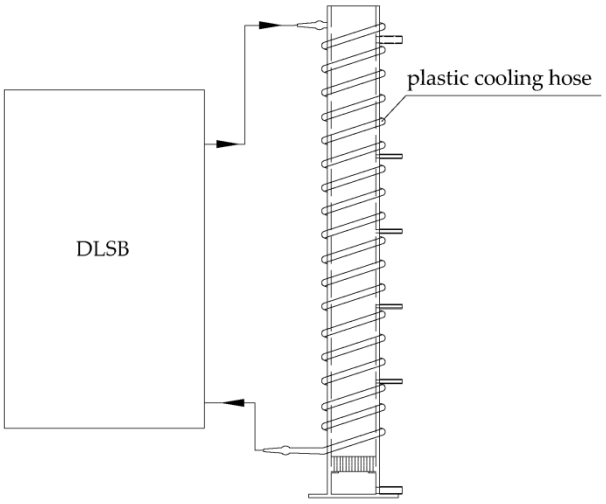

Figure 2. Scheme of the water temperature control system.

Test Method

Start and Operation of the Reactor. The lignite was washed with distilled water and dried naturally. The column was filled with a suspension, which was obtained from the denitrification segment of a sewage treatment plant in Beijing (Gaobeidian plant). Denitrifying bacteria were then introduced into the column. In the beginning, the column reactor was operated for initial hydraulic retention time (HRT) of 24 hours, with a flow rate of 0.5 $m \cdot d^{-1}$. Table 1 presents the operational parameters of the column reactor. The NO_3 removal rate and other

Tecnología y ciencias del agua, 10 (4), 238-255. DOI: 10.24850/j-tyca-2019-04-12

related indicators were detected periodically. The porosity of the columns was detected by mercury intrusion porosimetry.

Table 1. Operation parameters of the column reactor.

Number	Filler	Filling volume (cm^3)	Porosity (%)	Initial influent NO_3 concentration (mg L^{-1})	Initial hydraulic retention time (h)
R1	Sanjitun lignite	1.41×10^3	64.5	30	24
R2	Lingshi lignite	1.41×10^3	64.9	30	24
R3	Wangniutan lignite	1.41×10^3	63.8	30	24
R4	Zhaotong lignite	1.41×10^3	64.6	30	24

Static Carbon Release Test. After washing and drying all the lignite samples, we added 3.0, 7.0, and 12.0 g of lignite to three different conical flasks of 500 ml capacity. Then, 300 ml of deionized water was added into each conical flask, resulting in lignite concentrations of 10.0, 23.3, and 40.0 g L^{-1}. The lignite samples were soaked in the deionized water for 24 hours. For the analysis of COD_{Mn}, water samples from the conical flasks were taken after 0, 2, 6, 10, 16, and 24 hours. For COD_{Mn} analysis, water sampling was done every 3 hours. Finally, COD_{Mn} analysis was stopped when a stable value of COD_{Mn} was observed in water samples. To perform this test, the column water temperature was maintained in the range 13.0–15.0°C.

To describe the release of static carbon, Higuchi model (Brazel and Peppas 2000) was used. In the test solution, the carbon emission was described by COD_{Mn}.

$$M_t / M = k\, t^n \qquad (1)$$

where M (mg O_2 L^{-1}) is the total carbon released theoretically; M_t (mg O_2 L^{-1}) is the carbon released at time t; k (mg mg^{-1} h^{-n}) is the coefficient of carbon release rate; t is the carbon release time, and n is the characteristic parameter for carbon release.

After taking the logarithm of the equation, we found a linear relationship between $\ln(M_t)$ and $\ln(t)$. The parameter n represented the slope of the line, and $\ln(k)$ was the linear intercept. For $n < 0.45$, the carbon release mechanism was Fick diffusion. For $0.45 < n < 0.89$, it was a combination of diffusion and structure dissolution, and for $n >$

0.89, it was structure dissolution (Zhang et al. 2009).

Analysis of the Lignite Molecular Structure. Lignite samples (2.0 g) were taken, washed, and radiosterilized by an ultraviolet radiator (TUV 16W FA, Philips, Shanghai, China). After the treatment, lignite samples were air-dried. Then, the samples were ground to micron-sized particles with an agate mortar; these particles were tested by infrared microspectrometry (NICOLET iN10 MX, ThermoFisher, New York, USA). Table 2 presents the parameters of infrared microspectrometry.

Table 2. Parameters of the infrared microspectrometry.

Type	Test range (cm^{-1})	Detector	Beam splitter	Scan times	Resolution (cm^{-1})
NICOLET iN10 MX	4000–600	MCT/A	KBr/Ge	64	8

Results and Discussion

Nitrate Removal

At the beginning of the operation, the removal rate of NO_3 compounds was unstable because of the following factors: microorganism growth and adsorption of the filler. The NO_3-N removal rate became stable only after 15 days. Figure 3 illustrates the NO_3-N removal rate in the column reactor average (R1–R4) during the period of stable operation. Figure 4 illustrates the average concentration of NO_2 effluents under similar conditions.

Tecnología y ciencias del agua, 10 (4), 238-255. DOI: 10.24850/j-tyca-2019-04-12

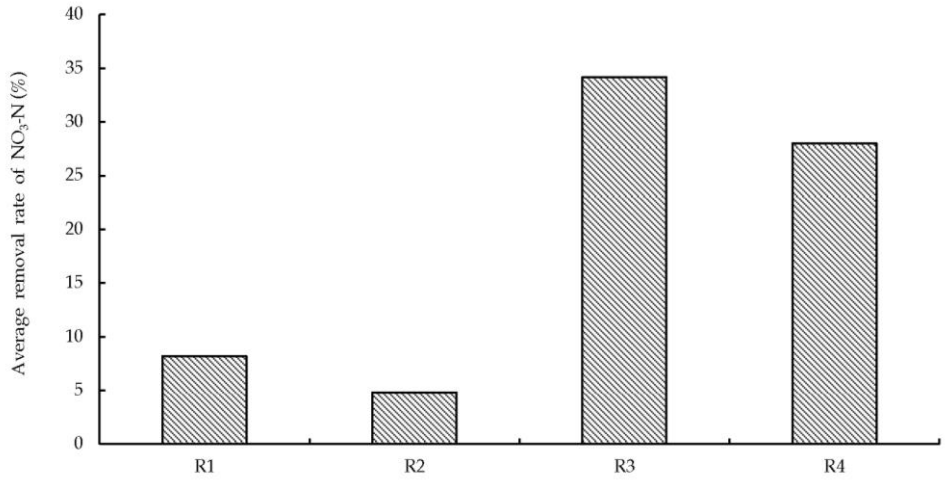

Figure 3. Column reactor average (R1–R4) of the NO_3-N removal rate during stable operation conditions.

As shown in Figure 3 and Figure 4, R3 had the highest NO_3 removal efficacy (34%), with the effluent NO_3 concentration being below 20 mg·L^{-1}. The NO_3 removal rate of R4 was 28%. The NO_3 removal rate was below 10% in other reactors: R_1 and R_2. Therefore, NO_3 removal efficacies were significant in the reactors R3 and R4, which contained lignite from Wangniutan and Zhaotong, respectively.

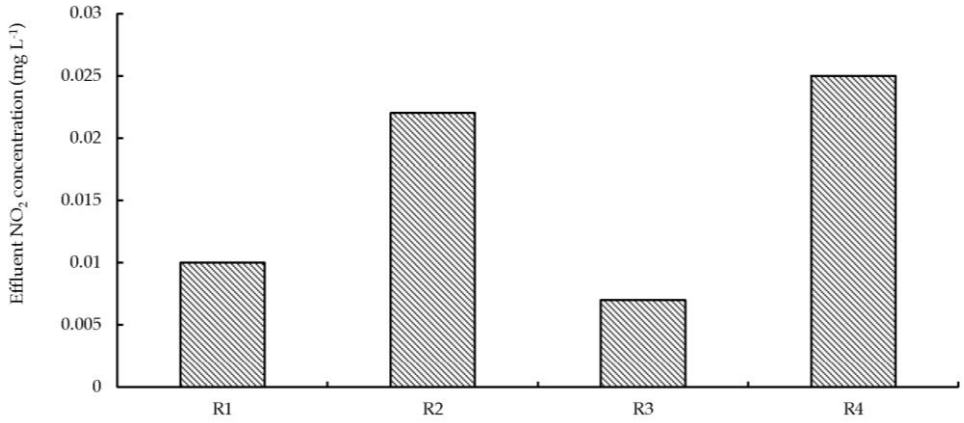

Figure 4. Column reactor average (R1–R4) of the effluent NO_2 concentration during stable operation conditions.

In R1 and R3, the effluent NO_2 concentrations were below 0.01 mg· L^{-1}. In R2 and R4, the effluent NO_2 concentrations were above 0.02 mg· L^{-1}. This indicates that denitrification reaction was almost complete when we used Chinese lignite obtained from Sanjitun and Wangniutan.

The water samples of R1 and R3 showed no-toxicity when we performed an acute toxicity test; however, the water samples of R2 and R4 showed low-toxicity. This implies that lignite obtained from Sanjitun and Wangniutan is far more superior. They can be effectively used as organic carbon sources for reducing NO_3 levels in groundwater (Tables 3 and 4).

Table 3. Acute toxicity evaluation standards of the luminescent bacteria test.

Cytotoxical grade	Relative luminance L (%)	Results
0	L > 90	No-toxicity
I	70 < L ≤ 90	Low-toxicity
II	50 < L ≤ 70	Middle-toxicity
III	30 < L ≤ 50	Low-high toxicity
IV	0 < L ≤ 30	Mid-high toxicity
V	L = 0	High-toxicity

Table 4. Acute toxicity results of the luminescent bacteria test

Water samples	Relative luminance L (%)	Results
R1	93–95	No-toxicity
R2	85–89	Low-toxicity
R3	96–99	No-toxicity
R4	75–80	Low-toxicity

Static Carbon Release

Figure 5 shows that the net carbon release was highest for the lignite obtained from Wangniutan; the COD_{Mn} values represented the net carbon release of various lignite types. When the lignite concentration was increased steadily, the net carbon release also increased proportionately. For lignite concentrations of 40.0 $g \cdot L^{-1}$, the net carbon release was 22.71 and 18.41 mg O_2 L^{-1} for lignite obtained from Wandniutan and Zhaotong, respectively.

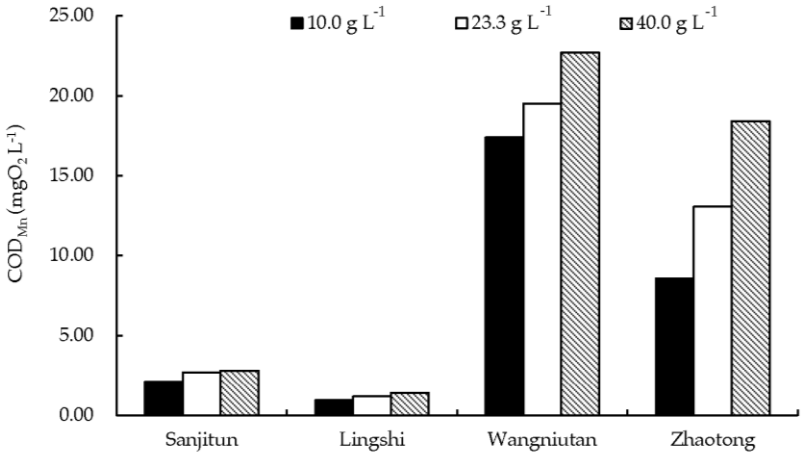

Figure 5. Net carbon release for the different lignite types.

The carbon release mechanism of all lignites was structure dissolution (Table 5). For lignite concentrations of 10.0 g L^{-1}, the coefficient of carbon release rate (k) was the highest for the lignite obtained from Sanjitun, followed by lignite obtained from Zhaotong, Lingshi, and Wangniutan. For lignite concentrations of 23.3 and 40.0 g L^{-1}, the sequence was as follows: Sanjitun > Lingshi > Zhaotong > Wangniutan.

Table 5. Results of the dynamic equation fitting for the carbon release.

Type	Concentration (g L^{-1})	Linear fitting parameters				Mechanism
		R^2	n	ln(k)	k	
Sanjitun	10.0	0.9963	1.0220	−3.4429	0.0320	structure dissolution
	23.3	0.9936	0.9725	−3.4121	0.0330	
	40.0	0.9971	0.9214	−3.0814	0.0459	
Lingshi	10.0	0.9983	1.0808	−3.7804	0.0228	structure dissolution
	23.3	0.9977	1.0952	−3.6801	0.0252	
	40.0	0.9965	1.0231	−3.3479	0.0352	
Wangniutan	10.0	0.9972	1.6764	−5.5486	0.0039	structure dissolution
	23.3	0.9931	1.5468	−5.0687	0.0063	
	40.0	0.994	1.4954	−4.8584	0.0078	

		8				
Zhaotong	10.0	0.9956	1.1332	−3.7684	0.0231	structure dissolution
	23.3	0.9934	1.2125	−3.9289	0.0197	
	40.0	0.9941	1.1324	−3.7349	0.0239	

Lignite Molecular Structure

For the lignite obtained from Sanjitun, Lingshi, Wangniutan, and Zhaotong, the infrared spectrum showed absorption peaks at 3600–3200, 3000–2800, 1600 and 1440, and 1320–1210 cm^{-1}, respectively (Figure 6). The absorption peaks at 3600–3200 cm^{-1} were produced by alcohol or phenolic hydroxyl groups, while those observed at 3000–2800 cm^{-1} were attributed to alkane-CH groups. The absorption peaks at 1600 and 1440 cm^{-1} resulted from the vibration of the aromatic ring and carboxylic acid-CO group, respectively, while the peaks that appeared between 1320–1210 cm^{-1} were attributed to the carboxylic acid-OH group. For the lignite obtained from Lingshi, the infrared spectrum showed some characteristic absorption peaks at 3000–2800 and 1600 cm^{-1}; however, absorption peaks were not observed at 3600–3200 and 1320–1210 cm^{-1}. For the lignite obtained from Lingshi, Wangniutan, and Zhaotong, an absorption peak appeared at 1038 cm^{-1}. This peak was probably generated from the vibration of the following functional groups: vibration of alkane-CH and anhydride-COC, the stretching vibration of sulfoxide-S=O, or a combination of the three.

Tecnología y ciencias del agua, 10 (4), 238-255. DOI: 10.24850/j-tyca-2019-04-12

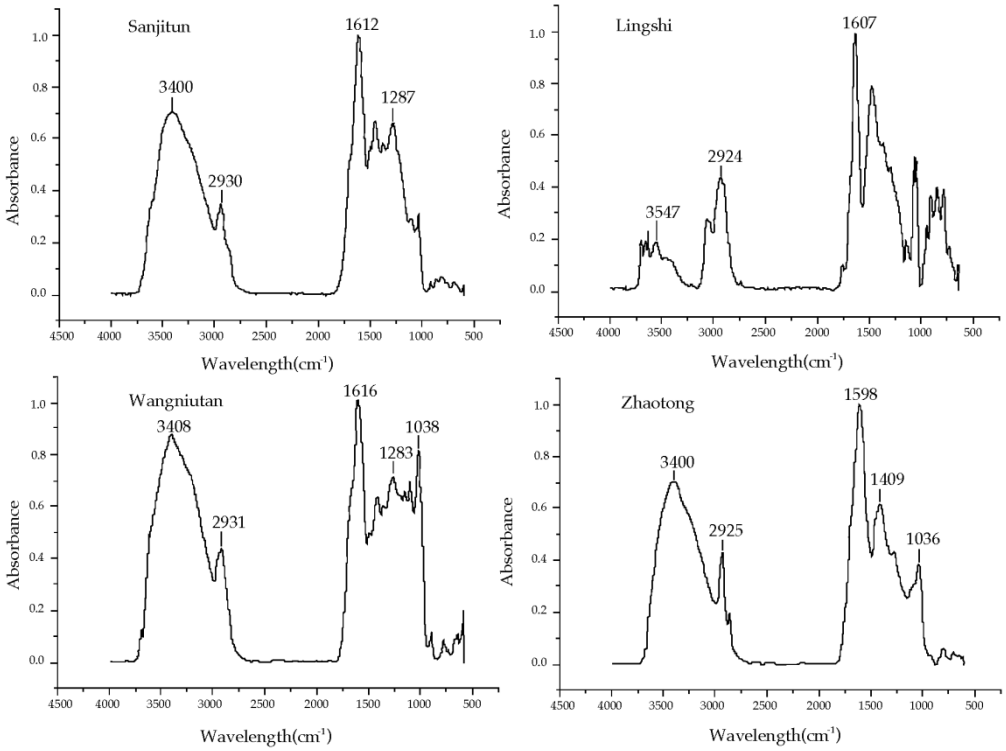

Figure 6. Infrared spectra of the Sanjitun, Lingshi, Wangniutan, and Zhaotong lignite.

Denitrification Effect

Greatest amounts of NO_3 were removed successfully when denitrification reaction was carried out using Chinese lignite obtained from Wangniutan and Zhaotong. For the lignite obtained from Wangniutan, the NO_3 concentration was below 20 mg·L^{-1} in the column effluent; the corresponding NO_2 concentration was below 0.01 mg·L^{-1}. Thus, the NO_3 and NO_2 concentrations completely complied with the Class III water standards of the Groundwater Quality Standards (GB/T 14848-93). For the lignite obtained from Wangniutan and Zhaotong, the net carbon release was high but the rate of static carbon release was low. This indicates that compared with the lignite obtained from Sanjitun and Lingshi, a slower rate of carbon release led to high NO_3 removal efficacy. By performing acute toxicity analysis, we found that there was low-toxicity in the effluent of the lignite obtained from Zhaotong. Moreover, there was no-toxicity in the effluent of the lignite obtained from Wangniutan. Therefore, the lignite obtained from Wangniutan was the best solid-phase organic carbon source for

denitrification in this study.

Denitrification Mechanism

While using lignite as a solid-phase organic carbon source, we found that NO_3 removal was related to the carbon emission and the rate of static carbon release (Zhang et al. 2009). When the net carbon release was high and the rate of static carbon release was low, the denitrification process was more effective (Shao et al. 2011; Wang 2013; Xie et al. 2013). For the lignite obtained from Sanjitun and Lingshi, the net carbon release was low and the rate of static carbon release was high. Therefore, there was a lack of total carbon release and excessive energy was released in a short time (Wang 2013). For the lignite obtained from Wangniutan and Zhaotong, the trend was completely opposite: the net carbon release was high but the rate of static carbon release was low. Thus, these lignite types showed a high NO_3 removal rate.

For the lignite obtained from Wangniutan and Zhaotong, we determined the molecular structure. Numerous small organic compounds, such as alcohols, phenols, and carboxylic acid, were detected in the molecular structure of these lignite types. These small organic compounds were the main carbon sources for denitrification, significantly improving NO_3 removal. Although numerous small organic compounds were detected in the molecular structure of lignite obtained from Sanjitun, the efficacy of NO_3 removal was poor with this lignite type. This must have happened due to the existing form of small organic compounds. In the main molecular structure of the lignite obtained from Sanjitun, there were small molecule organic compounds, such as hydrocarbons and oxygen-containing compounds; these compounds existed in a microporous embedded state or network embedded states. Free organic compounds are released easily by lignite. However, it is difficult to release embedded organic compounds from the molecular structure of lignite because of various reasons, such as physical adsorption, van der Waals forces, hydrogen bonding, and weak complexing (Chen et al. 2011; Han et al. 2014; Zhou et al. 2012). The small molecule organic compounds were mainly embedded in the molecular structure of the lignite obtained from Sanjitun. On the other hand, they were mainly in a free state in the lignite obtained from Wangniutan. As shown in Figure 7, denitrifying bacteria are more likely to use small molecule organic compounds in free states; these bacteria are present on the lignite surface or in an aqueous solution.

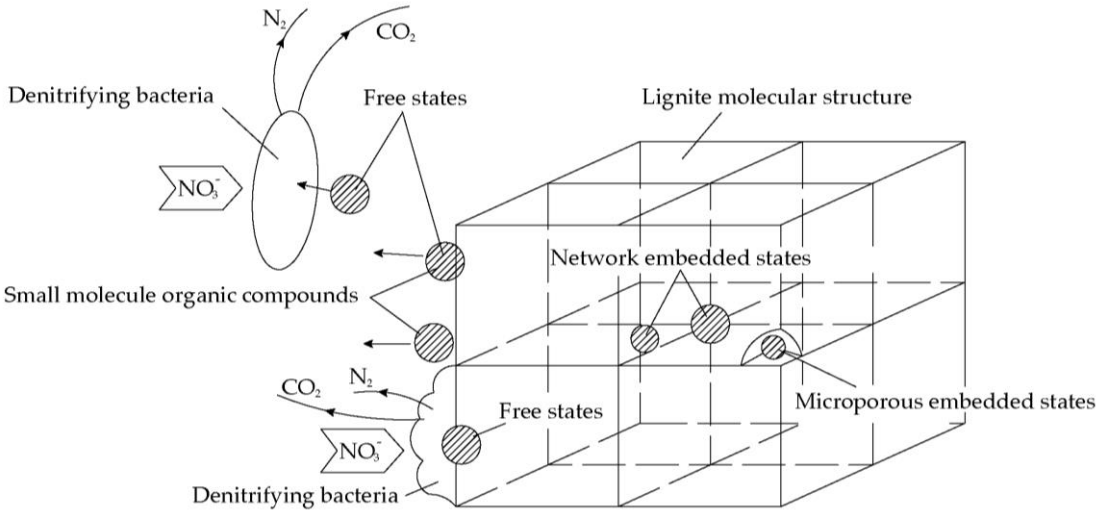

Figure 7. Scheme of the biological denitrification mechanism using lignite as an organic carbon source.

Conclusion

We obtained four different lignite types from Sanjitun, Lingshi, Wangniutan, and Zhaotong in China. These four lignite types were used as the solid-phase organic carbon sources for denitrification. Compared to the three lignite types, the lignite obtained from Wangniutan was superior in terms of its efficacy in NO_3 removal; it showed the highest efficacy (34%) in NO_3 removal, with the following characteristic accomplishments: the effluent NO_3 concentration was below 20 $mg \cdot L^{-1}$ and the effluent NO_2 concentration was below 0.01 $mg \cdot L^{-1}$; moreover, no-toxicity was observed in this lignite type when it was subjected to an acute toxicity test. Thus, the lignite obtained from Wangniutan is a safe organic carbon source for denitrification.

While using lignite as a solid-phase organic carbon source, we observed that NO_3 removal was related to the static carbon release from lignite. If the net carbon release was high and the rate of static carbon release was low, the denitrification process was better. From the lignite obtained from Wangniutan and Zhaotong, organic carbon was probably released to the groundwater at a slower rate; therefore, the NO_3 removal rates were much higher with these lignite types.

Small molecule organic compounds are the main carbon sources for denitrification. By determining the molecular structure of the lignite

obtained from Wangniutan and Zhaotong, we observed numerous small molecule organic compounds, such as alcohols, phenols, and carboxylic acid, in the molecular structure. These small molecule organic compounds were more likely to be used by bacteria when they were in a free state.

Acknowledgments

This work was financially supported by the Survey and Assessment of the National Groundwater-based Environmental Project (1441100022) and the Study of Groundwater Pollution Prevention and Control Technology System in the North China Plain (201309004).

References

Bi, J. J., Peng, C. S. & Xu, H. Z. (2010). Review of Research on Groundwater Nitrate Pollution and Its Removal. *Ground water*, 32(01), 97-102.

Brazel, C. S. & Peppas, N. A. (2000). Modeling of drug release from swellable polymers. *European Journal of Pharmaceutics and Biopharmaceutics*, 49 (1), 47-58.

Chen, D. R., Qin, Z. H., Chen, J., Hua, Z. Q. & Chen, D. M. (2011). Study on the model of coal structure and its prospects. *Coal Chemical Industry*, 39(04), 28-31.

Fu, X. H., Lu, L., Ge, Y. Y., Tian, J. J. & Luo, P. P. (2012). China Lignite Resources and Physical Features. *Coal Science and Technology*, 40(10), 104-107.

Han, F., Zhang, Y. G., Meng, A. H. & Li, Q. H. (2014). FTIR analysis of Yunnan Lignite. *Journal of China Coal Society*, 39(11), 2293-2299.

Jian, M. Z., Chuan, P. F., Si, Q. H. & Hui, L. H. (2013). Enhanced Heterotrophic Denitrification for the Treatment of Nitrate Contaminated Groundwater by Wheat Straw. *Applied Mechanics and Materials*, 316-317, 625-628., doi:10.4028/www.scientific.net/AMM.316-317.625.

Jiang, T. L., Li, D. & Wang, H. L. (2014). Study on the Selected Lignite Using as Organic Carbon in the Treatment of Nitrate Contaminated Groundwater. *Applied Mechanics and Materials*, 522-524, 652-655., doi: 10.4028/www.scientific.net/AMM.522-524.652.

Jin, H. & Liu, H. (2011). Carbon Source Study on Biological Denitrification in Groundwater. *Journal of Jilin Institute of Chemical Technology*, 28(09), 97-99.

Li, C., Zhang, J. & Liang, S. (2013). Nitrous oxide generation in denitrifying phosphoru s removal process: main causes and control

measures. *Environmental Science and Pollution Research*, 20 (8), 5353-5360.

Li, D. (September, 2010). *1st Conference on Environmental Pollution and Public Health*. In Scientific Research. Denitrification of Groundwater Using Hat Creek Lignite as Solid Phase Organic Carbon Source. Engineering Information Institute, Wuhan.

Li, X. L., Chen, Y. D. & Lin, P. (2014). The influence factors research of groundwater nitrate pollution removal with ethanol. *Pearl River*, 35(03), 112-115.

Miso, A., Ralf, K., Jože, U. & Frank, W. (2014). Determination of nitrogen reduction levels necessary to reach groundwater quality targets in Slovenia. *Journal of Environmental Sciences*, 26(9), 1806-1817.

Bryan, N. S. & Grinsven, H. V. (2013). The Role of Nitrate in Human Health. *Advances in Agronomy*, 119(119), 153-182.

Shao, L., Xu, Z. X., Wang, S., Jin, W. & Yin, H. L. (2011): Performance of New Solid Carbon Source Materials for Denitrification. *Environmental Science*, 32(08), 2323-2327.

Shen, J., Chen, P. N., Li, M. & Guan, W. L. (2012). Lignite utilization in our country and the economic analysis. *Henan Chemical Industry*, 29(Z5), 6-8.

Israel, S., Engelbrecht, P., Tredoux, G. & Fey, M. V. (2009). In Situ Batch Denitrification of Nitrate-Rich Groundwater Using Sawdust as a Carbon Source—Marydale, South Africa. *Water, Air, and Soil Pollution*, 204 (1), 177-194.

Wang, J. J. (2013). *Slow-release carbon source carrier carbon of the regular and denitrification characteristics*. Tang Shan: Hebei United University.

Xie, L. H., Ding, S. L., Chen, X. J. & Wang, M. (2013). Study on releasing carbon performance of agricultural waste shells as solid carbon sources. *Journal of Shanxi University of Science & Technology*, 31(05), 39-44.

Yan, L. J. (2013). The water nitrate pollution status, harm and removal technology. *Energy Environmental Protection*, 27(03), 39-42.

Zhang, D. Y., Li, G. H., Wang, Y., Zhou, G. Z. & Zhang, W. J. (2009). Model and effect of slow-release organic carbon-source materials on carbon release and denitrification. *Journal of Tsinghua University (Science and Technology)*, 49(09), 1507-1511.

Zhang, Q. Y., Wang, H., Zhang, L. Q., Li, J. & Tang, X. Q. (2008). Influence on Nitrate Nitrogen Pollution to Health in the Drinkable Water. *Ground water*, 30(1), 57-60.

Zhang, Z. J., Fei, Y. H., Guo, C. Y., Qian, Y. & Li, Y. S. (2012). Regional Groundwater Contamination Assessment in the North China Plain.

Journal of Jilin University (Earth Science Edition), 42(05), 1456-1461.

Zhou, J. L., Zhang, S., Wang, Y. G., Lin, X. C., Wang, C. H. & Xu, D. P. (2012). Study on Analysis Method of Lignite Carbon Structure and Oxygen Functional Groups. *Coal Science and Technology*, 40(10), 116-119.